SUPRAMOLECULAR CHEMISTRY OF 12-METALLACROWN-3 COMPLEXES

THÈSE N^{O} 3669 (2006)

PRÉSENTÉE LE 10 NOVEMBRE 2006

À LA FACULTÉ DES SCIENCES DE BASE

Laboratoire de chimie supramoléculaire

SECTION DE CHIMIE ET GÉNIE CHIMIQUE

ÉCOLE POLYTECHNIQUE FÉDÉRALE DE LAUSANNE

POUR L'OBTENTION DU GRADE DE DOCTEUR ÈS SCIENCES

PAR

Zacharias GROTE

chimiste diplômé de l'Université de Regensburg, Allemagne
de nationalité allemande

acceptée sur proposition du jury:

Prof. P. Vogel, président du jury
Prof. K. Severin, directeur de thèse
Prof. E. Dalcanale, rapporteur
Prof. P. J. Dyson, rapporteur
Dr J. Nitschke, rapporteur

ÉCOLE POLYTECHNIQUE
FÉDÉRALE DE LAUSANNE

Lausanne, EPFL
2006

“Der Mensch muß bei dem Glauben verharren, daß das Unbegreifliche begreiflich sei; er würde sonst nicht forschen.”

“Man has to persist in the faith that the incomprehensible is comprehensible; if not he wouldn’t do research.”

Johann Wolfgang von Goethe

Abstract

12-Metallacrown-3 complexes were formed by self-assembly of organometallic half-sandwich complexes $[(\pi\text{-ligand})MCl_2]_2$ (M = Ru, Rh, Ir) and 3-hydroxy-2-pyridone ligands in the presence of Cs_2CO_3 as base. Upon mixing of different macrocycles, reversible metal fragment exchange occured, resulting in the generation of small dynamic combinatorial libraries. Investigation of their adaptive behaviour revealed a strong bias for the amplification of hetero-assemblies, and especially of the member whose composition reflects the overall composition of the library. As a consequence, it is not necessarily the thermodynamically most stable member (e.g. the assembly with the highest affinity to a given target) that is amplified the most. Dynamic exchange processes of this kind have also been used to synthesise mixed-metal macrocycles by controlled desymmetrisation of sterically hindered 12-metallacrown-3 complexes.

Using amino-substituted 3-hydroxy-2-pyridone ligands, monomeric O,O'-chelate complexes were formed in aqueous solution. Self-assembly into trimeric metallamacrocycles was observed upon addition of base and in phosphate buffer solution, as evidenced by NMR spectroscopy and single crystal X-ray analyses. The macrocycles were able to act as highly selective receptors for lithium ions. The binding constants depend on the nature of the halfsandwich complex, the ligand, and the pH. With a commercially available $[(\text{cymene})RuCl_2]_2$ complex and 4-(N-methylpiperazine)-3-hydroxy-2-pyridone, a receptor with a Li^+ binding constant of $K_a = (5.8\pm1.0) \times 10^4\ M^{-1}$ and a Li^+ to Na^+ selectivity of 10000:1 has been obtained. The fact that the assembly process of the receptor is pH dependant has been used to detect the presence of lithium ions by a simple pH measurement. Furthermore, it was possible to transduce the binding of Li^+ into a change of color by means of a chemical reaction with $FeCl_3$. This allowed the detection of Li^+ in the pharmacologically relevant concentration range of 0.5–1.5 mM by the 'naked eye'. Modifications of the bridging ligand allowed the design of a potential fluorescent PET sensor for Li^+ ions in water.

$^7Li/^6Li$ isotope separation was achieved by complexation of LiCl with 12-metallacrown-3 complexes having sterically very demanding π-ligands. An enrichment of ^7Li of 5.4 % was observed. Using ligands in which two 3-hydroxy-2-pyridone units were connected by a linker, hexanuclear structures of up to 2.8 nm have been obtained. These assemblies can be regarded as expanded triple-stranded helicates.

Keywords

halfsandwich complexes $[(\pi\text{-ligand})MCl_2]_2$ (M = Ru, Rh, Ir) ◆ 3-hydroxy-2-pyridone ligands ◆ 12-metallacrown-3 complexes ◆ dynamic combinatorial chemistry ◆ pH dependant self-assembly ◆ lithium ionophores ◆ $^7Li/^6Li$ isotope separation ◆ expanded triple stranded helicates

Version Abrégée

Des complexes 12-metallacrown-3 ont été realisés par auto-assemblage de complexes demi-sandwich $[(\pi\text{-ligand})MCl_2]_2$ (M = Ru, Rh, Ir) et de ligands 3-hydroxy-2-pyridone en présence de Cs_2CO_3 agissant comme base. L'échange réversible des sous-unités métalliques des différents macrocycles a été observé. Ceci a été utilisé pour la formation de bibliothèques combinatoires dynamiques. L'investigation de leur comportement adaptatif a révélé que l'amplification des assemblages mixtes est favorisées. Spécialement le membre qui possède la même composition que la bibliothèque est amplifiée. En conséquence, le membre le plus stable thermo-dynamiquement (par example l'assemblage avec l'affinité la plus élévée pour une certaine molécule cible) n'est pas forcement le plus amplifié. Les processus d'échanges réversibles ont été exploités pour la synthèse de complexes comportant deux fragments métalliques différents par la désymmétrisation contrôlée de complexes 12-metallacrown-3 stériquement encombrés

Dans l'eau, des complexes monomériques ont été obtenus en utilisant des ligands 3-hydroxy-2-pyridones auxquelles un groupement amino a été attaché. Les deux atomes d'oxygène du ligand se coordinant au métal. Dans une solution tampon phosphate ou après addition de base, l'auto-assemblage de trimers métallamacrocycliques a été observé. Ceci a été vérifé par spectroscopie RMN et par l'analyse de monocristaux par rayons X. Les macrocycles obtenus sont des récepteurs sélectifs pour Li^+ dans l'eau. La constante d'association dépend de la nature des complexes demi-sandwich, du ligand et du pH. En utilisant le complexe commercial $[(\text{cymène})RuCl_2]_2$ et le ligand 4-(N-methylpiperazine)-3-hydroxy-2-pyridone, un récepteur avec une constante d'association de $K_a = (5.8 \pm 1.0) \times 10^4\ M^{-1}$ et une sélectivité de Li^+ sur Na^+ de 10000:1 a été obtenu. Grâce à l'auto-assemblage en fonction du pH, la présence du Li^+ a pu être détectée par une simple mesure du pH. La complexation de Li^+ a été visualisée par un changement de la couleur. Ceci a été atteint par réaction chimique du récepteur complexé avec $FeCl_3$. Il était ainsi possible de détecté le Li^+ dans la gamme pharmacologique important de 0.5–1.5 mM 'à l'œil nu'. La modification du ligand pontant a permis de proposer la structure d'un senseur PET fluorescent pour Li^+ dans l'eau.

Les isotopes ^6Li et ^7Li ont été séparés par complexation de LiCl en utilisant des complexes 12-metallacrown-3 stériquement très encombrés. Une augmentation de ^7Li de 5.4 % a été observée. Si deux unités de 3-hydroxy-2-pyridone sont connectées, des complexes hexanucléaires avec une longeur maximale de 2.8 nm ont été obtenus. Ils peuvent être décrits comme des hélicates élargis à trois branches.

Mots Clés

complexes demi-sandwich $[(\pi\text{-ligand})MCl_2]_2$ (M = Ru, Rh, Ir) ◆ ligands 3-hydroxy-2-pyridones ◆ complexes 12-metallacrown-3 ◆ chimie combinatoire dynamique ◆ auto-assemblage en fonction du pH ◆ ionophores du lithium ◆ séparation isotopique de ^6Li et ^7Li ◆ hélicates élargis à trois branches

Zusammenfassung

12-Metallakrone-3 Komplexe wurden durch Selbstanordnung von metallorganischen Halbsandwich Komplexen $[(\pi\text{-Ligand})MCl_2]_2$ (M = Ru, Rh, Ir) und 3-Hydroxy-2-pyridon-Liganden in Anwesenheit von Cs_2CO_3 als Base dargestellt. Beim Mischen verschiedener Makrozyklen wurde der reversible Austausch von Metallfragmentuntereinheiten beobachtet. So konnten kleine dynamische kombinatorische Bibliotheken erstellt werden. Untersuchung des adaptiven Verhaltens der Bibliotheken zeigte, daß diese eine starke Neigung zur Bildung von Heteroassoziaten aufwiesen. Vor allem der Komplex, der die Zusammensetzung der Bibliothek wiederspiegelt, wurde bevorzugt gebildet. Daraus kann gefolgert werden, daß der thermodynamisch stabilste Komplex (z. B. der Komplex mit der höchsten Affinität für ein Targetmolekül) nicht zwingenderweise am stärksten angereichert wird. Dieser dynamische Austauschprozeß ermöglichte die kontrollierte Aufhebung der Symmetrie von sterisch gehinderten 12-Metallakrone-3 Komplexen. Es wurden gemischte Metallamakrozyklen, d. h., Komplexe die zwei unterschiedliche Metallfragmente aufweisen, erhalten.

Bei der Verwendung von amino substituierten 3-Hydroxy-2-pyridon-Liganden in wässriger Lösung, bildeten sich einkernige O,O'-Chelatkomplexe. Bei Zugabe von Base oder in Phosphatpufferlösung fand Selbst-Assoziation in dreikernige Metallamakrozyklen statt. Dies wurde durch NMR Spektroskopie und Röntgenstrukturanalyse an Einzelkristallen gezeigt. Diese Makrozyklen sind hochselektive Rezeptoren für Li^+ Ionen. Die Stärke der Li^+-Bindungskonstante hing von der Natur des Halbsandwich Komplexes, des Liganden und des pH-Wertes ab. Die höchste Li^+-Affinität zeigte eine Mischung des kommerziell erhältlichen $[(\text{cymol})RuCl_2]_2$ Komplexes und des Liganden 4-(N-Methylpiperazin)-3-hydroxy-2-pyridon. Die Bindungskonstante betrug $K_a = (5.8 \pm 1.0) \times 10^4\ M^{-1}$ und der Komplex zeigte eine Li^+ Selektivität von 10000 : 1 im Vergleich zu Na^+. Die pH-Abhängigkeit der Bindungskonstante wurde genutzt, um die Anwesenheit von Lithium Ionen durch eine Messung des pH-Wertes nachzuweisen. Desweiteren konnte der Grad der Li^+-Komplexierung durch einen Farbtest visualisiert werden. Dies erlaubte den Nachweis im pharmakologisch relevanten Bereich (0.5–1.5 mM) durch das bloße Auge. Die Derivatisierung des verbrückenden Liganden erlaubte das Design eines potentiellen fluoreszierenden PET-Sensor für Li^+ Ionen in Wasser.

Eine Trennung der Isotope ^6Li und ^7Li wurde durch Komplexierung von LiCl mit 12-Metallakrone-3 Komplexen mit sterisch anspruchsvollen π-Liganden erreicht. ^7Li wurde zu 5.4 % angereichert. Sechskernige Metallkomplexe mit einer Länge von bis zu 2.8 nm wurden durch Verbrückung zweier 3-Hydroxy-2-pyridon-Liganden erhalten.

Schlüsselwörter

Halbsandwich Komplexe $[(\pi\text{-Ligand})MCl_2]_2$ (M = Ru, Rh, Ir) ◆ 3-Hydroxy-2-pyridon-Liganden ◆ 12-Metallacrown-3 Komplexe ◆ Dynamische kombinatorische Chemie ◆ pH-abhängige Selbstanordnung ◆ Lithium-Ionophore ◆ $^7Li/^6Li$-Isotopentrennung ◆ Erweiterte dreisträngige Helikate

Acknowledgement

I would like to thank…

Professor Kay Severin for the opportunity to work under his supervision, his confidence, his suggestions and that he kept his door always open.

The members of the jury: Professors Pierre Vogel, Paul Dyson, Enrico Dalcanale and Jonathan Nitschke who have invested the time to read and evaluate my thesis work.

Dr. Rosario Scopelliti who performed all X-ray crystallographic analyses and Dr. Euro Solari for his skill to find single crystals between all the others.

All the people who make research an almost smooth thing: Professeur Lothar Helm and Dr. Martial Rey for all their help concerning NMR spectroscopy, Alain Razaname for measuring all the mass spectra, Patrick Favre and Luc Patiny for an excellent electronic and IT service, Gil Corbaz and Yves Morier for their mechanical skills, Anita Schori and Christina Zamanos-Epremian for all the administrative work and finally Giovanni Petrucci, Glady Pache and Jaques Gremaud for running the best chemical store I have ever seen.

Sven Adolph for his precious help with the HPLC and Dr. Carsten Vock and Christopher Flowers for proof reading the manuscript.

All the friends and comrades who made every moment – good or bad – at Lausanne a memorable thing: Adrian, Alex, Alex, Alexandre, Ana, Andrey, Anke, Annabelle, Barnali, Burcak, Carsten, Celine F., Céline O., Charles, Chris, Christian, Christoph, Christophe, Christopher, Claudia, Corinne, Cyrille, Davinia, Edina, Elaine, Elvira, Enrico, Estelle, Evita, Fabien, Fidi, Frédéric, Gaëlle, Guillaume, Gustavo, J.-P., John, Hans-Christoph, India, Isabelle, Jérémy, Katrin, Kate, Kelly, Laurent, Luc, Lutz, Mang, Marie-Line, Markus, Matthew, Michel, Nathalie, Nelly, Nicolas A., Nicolas C., Nicole, Olimpia, Pascal, Petra, Philipp, Seb, Sébastian, Semia, Silke, Simon, Simone, Spyros, Sven, Theresa, Tilmann, Thomas B., Thomas G., Tobias, Wee-Han and Yvonne.

And of course my family Rosi, Christian, Rafael, Dominik, Olivia and David, my godfather Claus-Jürgen and especially Alexandra simply for alway being there.

Table of Contents

Chapter I
Introduction

I.I Molecular Architecture

Human beings have always been fascinated by symmetry. This fascination originates from the paradoxal combination of simplicity and complexity in symmetric objects. Symmetry is perceived as pure aesthetics, and symmetry is omnipresent.

The highest degree of symmetry is expressed in the sphere. Highly symmetric, convex polyhedra approximating a spherical shell are the Platonic (Figure I.1) and Archimedean solids. The faces of the five Platonic solids consist of only one regular polygon, and those of the 13 Archimedean solids of two or three regular polygons.[1] Spherical shells are important motifs in nature due to their low surface-to-volume ratios; an illustrative example is the icosahedral or dodecahedral shape of the capsids of most viruses.[2]

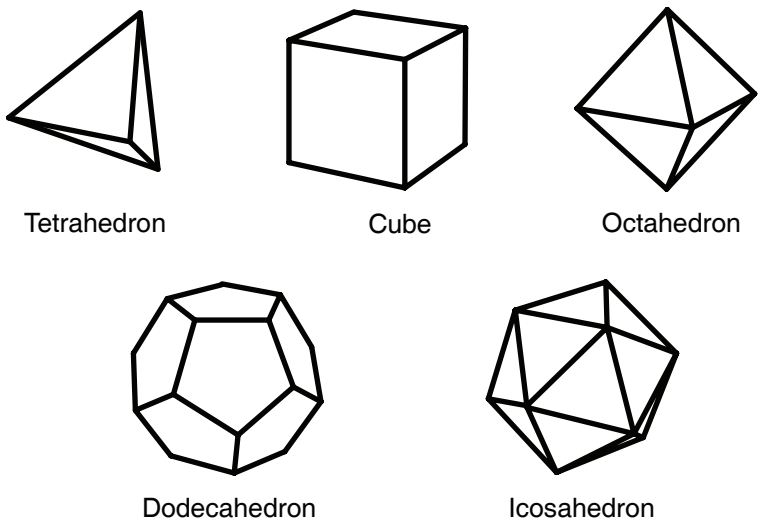

Figure I.1 The five Platonic solids: the faces of the tetrahedron, octahedron and icosahedron consist of regular triangles, those of the cube of squares and the faces of the dodecahedron of pentagons.

The imitation of such symmetric objects on the molecular level has always been a special challenge in synthetic chemistry. But although classical covalent hydrocarbon chemistry has a large collection of reliable reactions at their disposal, the synthesis of such objects has been proven to be extremely difficult. Nonetheless, three Platonic solids, tetra(tert-butyl)tetrahedrone,[3] cubane,[4, 5] and dodecahedrane[6, 7] have been synthesised after much effort. The remaining two Platonic solids, the icosahedron and the octahedron, are unlikely to be synthesised by classical organic means: first, because of the limited number of bonds a carbon atom can form, and second, because of the restriction to a tetrahedral, trigonal or linear geometry. Two more carbon-based highly symmetric structures are worthwhile to mention: adamantane,[8–10] which displays a tetrahedral symmetry, and fullerenes, with its best known member, C_{60}, representing the Archimedean solid of a truncated icosahedron (12 pentagonal and 20 hexagonal faces).[11–13]

Especially the restriction to certain angles provoked Fujita and coworkers to incorporate transition metal fragments into the organic framework. In 1990, they presented the formation of a *metallasupramolecular square*.[14–16] Complex **E1**, readily self-assembles from [(en)Pd(II)$(NO_3)_2$] and 4,4'-bipyridine in aqueous alcoholic solution. The preferred coordination geometry of the metal centre is square planar, with two coordination sites in *cis* position to each other blocked by the chelate ligand, so that the two bridging ligands can only coordinate by opening an angle of 90°. The strength of the metal–ligand interaction of the monodentate bridging ligand allows replacement of the weakly bound NO_3^- groups, but not of the chelate ligand. The ditopic bridging ligand itself is linear and rigid, with one coordination group at each side, so that upon coordination of four ligands and four metal centres only a square planar geometry can be formed. The self-assembly occurs under *thermodynamic control*, and results in almost *quantitative* product formation. Although metal organic frameworks have been reported before,[17–19] the power of Fujita's approach launched a completely new research domain: transition metal based self-assembly of discrete nanoscopic supramolecular species with predetermined size and shape such as molecular cycles, boxes and cages, so called molecular architecture.[20] The general synthetic approach has been extended to the formation of infinite networks and grids.[21]

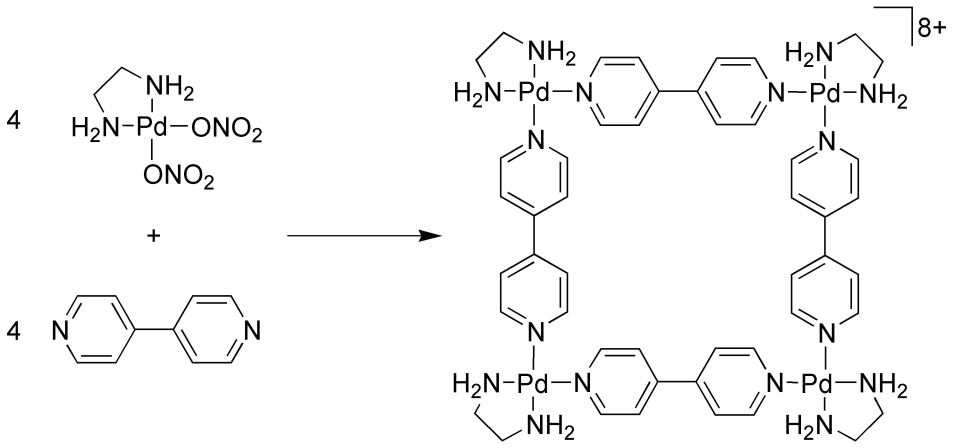

E1

Scheme I.1 Self-assembly of a molecular square presented by Fujita.[14]

Whereas in the beginning most structures were obtained by serendipity or 'trial and error', three different rational synthetic design strategies have been emerged over the last decade: the directional bonding approach,[22, 23] the symmetry interaction approach[24–26] and the weak-link approach.[27, 28] All three use metal centres with predetermined coordination geometry and angles as structural building blocks in combination with multibranched organic ligands possessing heteroatoms as coordination groups.

A large variety of different topologies has been synthesised up to now. Size, shape and internal cavity dimensions are now predictable features, but the interest in the field is far from ceasing. The driving force behind is the ease with which large and complex structures can be obtained. Nevertheless, the focus turns now from ‘structure to function’, and the new challenge is to transform aesthetic structures into functional constructs. Envisioned functional properties are cavity-directed synthesis, homo- and heterogeneous catalysis and photo- and electrochemical sensing. Host-guest chemistry, redox activity and magnetic behaviour of metallasupramolecular architecture are likewise in the focus of research.[29–32]

There are some intrinsic difficulties towards this aim. Typically, the metal centres are coordinatively inert, acting solely as corner stones of the supramolecular assemblies. Likewise, properties inherent to the ligands are often turned off, due to their proximity to the metal ions, e.g. quenching of the luminescence of ligands by the nearby metal centres has been observed.[33, 34] Moreover, chemistry confined to a small space inside supramolecular architecture behaves often quite different to what is expected, being at the same time strain and opportunity.

I.II Transition Metal Based Self-Assembly

In transition metal based self-assembly the building blocks are held together by metal–ligand coordinative interactions. The building blocks contain all necessary information to assemble selectively into discrete complex aggregates. The assembly process occurs generally under thermodynamic control, and the formed species have unique features different from their building blocks. *Self-correction* is an intrinsic feature of the synthetic strategy.[35]

Non-covalent metal–ligand bonds are considered as 'weak', though this assumption is probably more due to their inherent reversibility than their bond strength. Their bond strength of 40–120 kJ/bond is in between 'classical' non-covalent weak interactions such as hydrogen bonds, van der Waals, Coulombic and dipole-dipole interactions and covalent bonds. Weak interactions are usually associated with many different reaction pathways and poor selectivity. But this 'lack of control' turns out to be the intrinsic advantage, as it is synonymous with 'error correction'.

Non-covalent interactions are *kinetically labile*. Typically, a *fast thermodynamic equilibrium* exists between the starting materials and all potential products. An 'improperly' connected bond can simply 'go back' on the reaction pathway to be reconnected in another fashion. Due to this inherent reversibility, a self-correction process can take place, leading ideally to the thermodynamically favoured product in high yields. However, to single out one product, the thermodynamic advantage over all other possible species has to be sufficiently large. For many metallasupramolecular systems no clear thermodynamic preference is given, and several species are in equilibrium with each other.[29]

In contrast, the often observed formation of cyclic species in metal-directed self-assembly is no coincidence, but a consequence of thermodynamics. Cyclic structures are intrinsically favoured over oligomeric structures for the simple reason that the average number of metal–ligand interactions per building block is higher, thus displaying an higher relative enthalpic gain. If ligand structure and coordination geometry of the metal centre are purposely designed for cyclic structures, this behaviour is enhanced. Small assemblies are preferred over large assemblies due to entropic reasons: less building blocks are necessary to form the same amount of assemblies. Ercolani [36, 37] has examined the macrocyclisation process from a theoretical point of view. Cyclic species are in equilibrium with the monomeric building blocks and polymeric species and exist only in a certain concentration range. Below the so called lower self-assembly concentration (lsac), the equilibrium is in favour for the monomeric building blocks, whereas, above the effective molarity (EM) formation of polymeric species is preferred instead of further macrocyclisation.

In general, enthalpic reasons rule over entropic reasons due to the large gain of energy upon metal–ligand bond formation,[29] but entropy becomes the decisive factor if the enthalpies of two or more potential topologies are very close. An example is the competition between squares and triangles. Rigid linear bridging ligands and metal centres with square planar geometry should lead to the formation of molecular squares. However, some deviations from the ideal geometry are tolerated by both building blocks. Whereas enthalpy favours the formation of squares due to less strained systems, entropy favours triangles. Typically, both topologies co-exist in an equilibrium with each other. This is the case even for very rigid ligands such as tetraphenoxy-substituted diazadibenzoperylene bridging ligands and perfectly preorganised (dppp)Pd^{II} or (dppp)Pt^{II} units, as shown by Würthner and coworkers (Scheme I.2).[38]

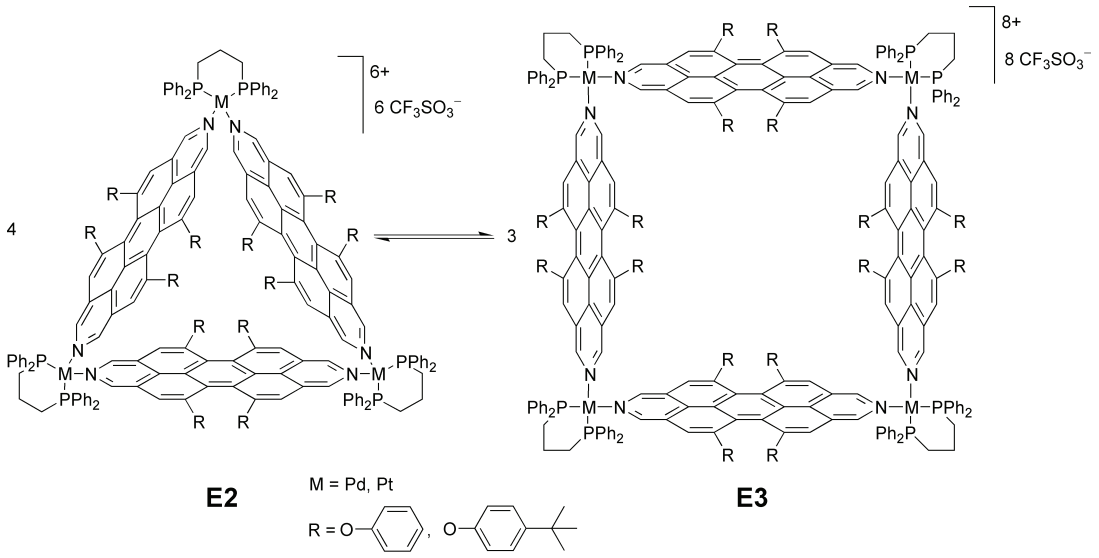

Scheme I.2 Equilibrium between square planar and triangular topology.[38]

As a result, bridging ligands are mostly very rigid with structurally predisposed coordination groups. Nitrogen is the most employed heteroatom for coordination to the metal centre, as the metal–nitrogen bond strength is strong enough to replace weakly bound ligands. The combination of metal ions having a geometric coordination preference and strongly bound directing ligands is most common. Directing ligands block certain coordination sites and direct the incoming ligands into a certain angle to each other. Generally, phosphine-metal bonds are strong enough to guarantee slow exchange kinetics; moreover chelate ligands are often used. Typical experimental concentrations are in the millimolar range in order to favour cyclic products over monomeric and polymeric species.

Metal-directed self-assembly targets primarily symmetric topologies.

One has to keep in mind, that metal-directed self-assembly targets primarily symmetric topologies. It is therefore suited to mimic size and shape of biological entities in order to

obtain similar structural properties, a goal difficult to achieve by organic means. Classical organic chemistry is specialized to form typically one new bond at the time, revealing a major drawback: the synthesis of large and complex molecular assemblies. Moreover, covalent bond formation is usually carried out under kinetic control, and improperly connected bonds are therefore hard to fix.

To summarise: self-assembly has several advantages compared to covalent chemistry when the synthesis of *large* and *symmetric* structures is concerned. The assembly of building blocks into supramolecular assemblies represents a highly convergent synthetic protocol with the simultaneous formation of a multitude of interaction. These interactions establish usually very fast in an almost defect-free fashion due to an inherent error correction process. Transition metal based self-assembly provides even more advantages as it combines the benefits of error correction with a certain stability of the metal–ligand bonds. Furthermore, classical weak interactions are *non-directional*, whereas transition metals and heterocycles provide some *directionality*.[39] Structural versatility is given due to a large number of transition metal complexes and bridging ligands.

I.III Design Strategies

Molecular architecture represents polygons and polyhedra on a molecular basis. Typically, the metal centres are located on the vertices, whereas the ligands outline the edges. But polyhedra can also be designed by covering the faces with ligands. This second way to depict polyhedra, is called molecular panelling and was particularly developed by Fujita.[16, 40, 41] Three different design strategies based on metal-directed self-assembly will be discussed. The directional bonding and the symmetry interaction approach target both the thermodynamic product. Ligands have several coordination groups. The directional bonding approach employs generally very rigid monodentate ligands, and the symmetry interaction approach chelating ligands (but assemblies with monodentate ligands have also been reported). Despite the availability of several atoms able to coordinate to metal ions, most often, nitrogen-to-metal coordination is employed. This leads commonly to charged assemblies. The main difference between these two methods is how to control the incoming ligands into their correct coordination position. Whereas the directional bonding approach makes use of directing ligands, which block certain coordination sites of the metal centre, the symmetry interaction approach takes advantages of the preferred coordination geometry of the 'naked' metal ion. The weak-link approach is a relatively new manner to access more flexible assemblies. Often, the kinetic product instead of the thermodynamic product is obtained. Ligands coordinate with two different coordination groups of different strength. Typically phosphines and ethers are used.

Molecular architecture was probably most often generated according to the directional bonding approach. The principle has been elaborated by Fujita[42, 43] since the beginning of the 90s and then been systematized by Stang in 1997.[22, 23] Since then, reviews have been appeared on a regular basis.[16, 20, 27, 35, 40, 44] The symmetry interaction model has extensively been used by Saalfrank,[45, 46] Lehn[47, 48] and Raymond.[24–26] Especially, definitions introduced by Raymond[25] describing the geometric relationship between the ligand and the metal centre facilitated the rational design and helped to evolve this rather complex approach. The symmetry interaction approach has been reviewed several times by Raymond[24–26] and others.[27, 35, 44] The weak-link approach has been developed in particular by Mirkin and was first demonstrated in 1998.[49] Two reviews on this topic have appeared so far.[27, 28] Worthwhile to mention is also a publication outlining the most important rules of ligand design by Steel.[50]

I.III.1 The Weak-Link Approach

The weak-link approach is not only conceptually different from the directional bonding and the symmetry interaction approach, but targets also another type of complexes containing more *flexible* ligands and metal centres with *free coordination sites*. Therefore, hemilabile ligands[51, 52] are used, which are in general chelate ligands, but with two

coordination groups of different affinity towards the metal ion. Upon coordination, one of the two metal–ligand bonds is much weaker than the other – the so called weak-link – and can be cleaved selectively while maintaining the overall supramolecular structure.

The employed hemilabile ligands are the core of the weak-link approach. Typically, they contain arenes as central bridging units, to which two bidentate coordination sites are attached. This bidentate coordination site is composed of a phosphine group and a second coordination group X, typically an ether. The general synthetic scheme of the weak-link approach is shown in Scheme I.3. Coordination of a hemilabile ligand to a metal ion such as Rh^I provides a *condensed intermediate* **B** with two metal–ligand bonds of different strength: a very strong metal–phosphine bond and a much weaker metal–X bond. The target molecule **C**, the *open* and much more *flexible* macrocyclic structure, is obtained by selectively cleaving the weak metal–X bond by addition of so called ancillary ligands **L**, which show a stronger affinity for the metal ion.

In further contrast to the directional bonding and the symmetry interaction approach, reactions of the weak-link approach occur under kinetic rather than thermodynamic control, and there is evidence that the mononuclear complex **A** is the thermodynamically favoured product.[53] But once the condensed intermediate **B** is formed, it seems to be metastable, and transition into **A** is hampered by large activation barriers. The kinetic control displays also the major disadvantage of the weak-link approach, as an error correction is not longer possible. However, use of flexible ligands and 'naked' transition metals ions allows the access to flexible structures and metal centres with free coordination sites, which are available for further chemistry. Both features are intrinsic advantages for the 'transition from structure to function'.

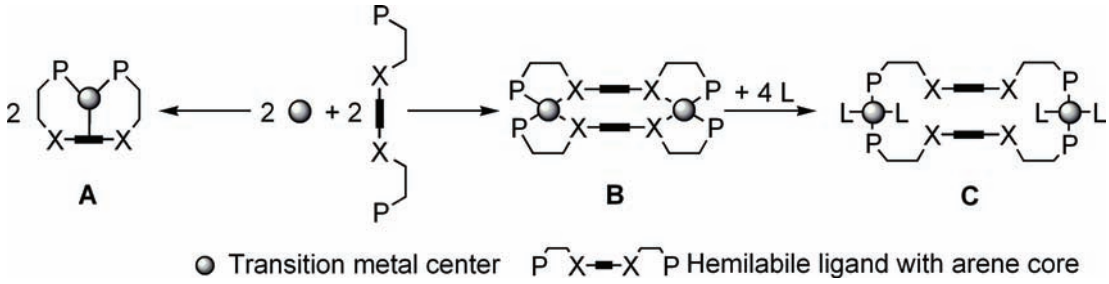

Scheme I.3 General synthetic scheme of the weak-link approach.

This strategy was first demonstrated by Mirkin in 1998, using the hemilabile bis(bidentate) ligand **E4** in combination with a Rh^I starting material in a 1:1 ratio to generate the condensed intermediate **E5**, in which both – the phosphine as well as the ether group – are coordinated to the metal ion. The open 26-membered macrocycle **E6** was obtained by breaking the weak Rh–O bond via coordination of ligands with higher affinity such as CO, CH_3CN or both to the metal centre (Scheme I.4).[49]

Generally, the weak-link consist of a ether-based hemilabile oxygen-metal bond, but thioethers and amines have also been used. As the strength of the metal–X bond increases from ethers to amines to thioethers, cleaving requires ancillary ligands with stronger affinity. Rh^{I} is most commonly used as transition metal, but other d^8 square planar metals such as Pd^{II} and Ir^{I} have likewise been used. Examples exist also for the d^{10} tetrahedral metal centre Cu^{I} and the d^6 octahedral metal centre Ru^{II}. Among the most used ancillary ligands are CO, acetonitrile and isocyanides, but ring opening can also be achieved by using anions, pyridines or diamines.[27, 28]

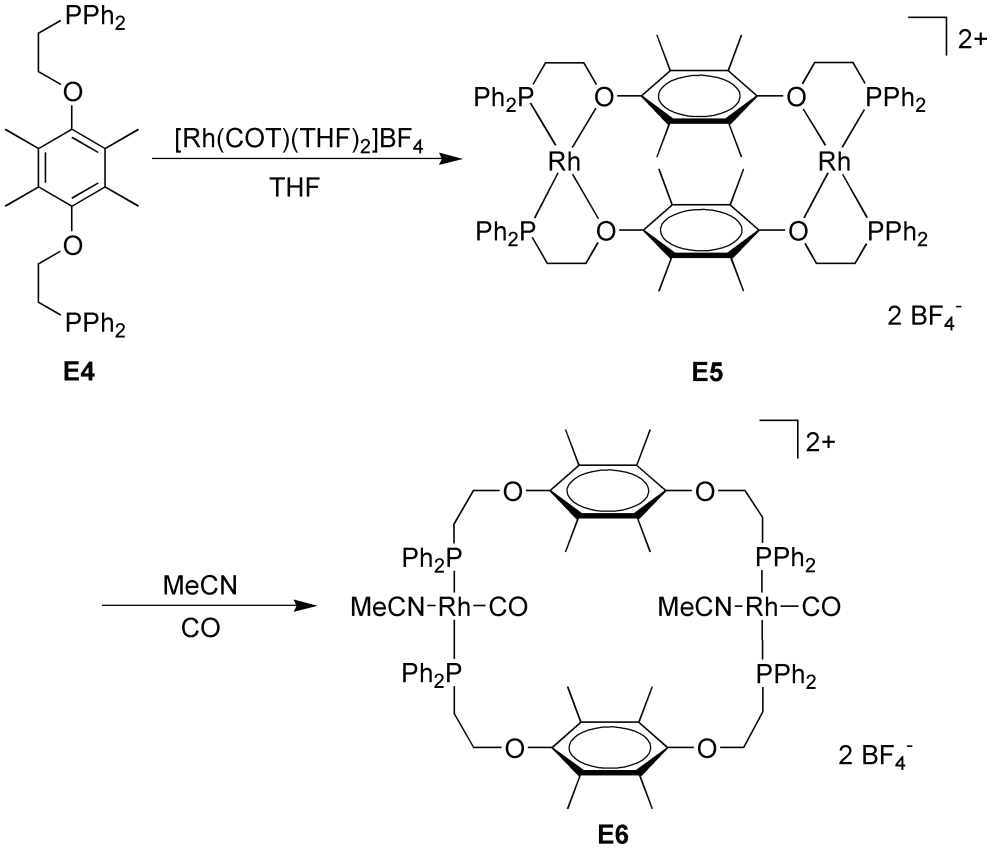

Scheme I.4 Synthesis of a flexible macrocyclic structures employing the weak-link approach.[49]

I.III.2 The Symmetry Interaction Approach

The symmetry interaction approach is the most sophisticated of the three design strategies, as the coordination geometry of the metal, the ligand orientation and the ligand-ligand steric interactions have to be considered. Preorganised multibranched chelate ligands in combination with transition or main group metals assemble into supramolecular structures, mainly driven by the preferred coordination geometry of the metal centre.

Generally, *chelate ligands*, providing stronger binding of the ligand to the metal,[54] and 'naked' metals ions, i.e., metals free of any strongly coordinating blocking ligands, are used. The first complexes synthesised according to the symmetry interaction approach have been presented in the mid 80s by Maverick (Figure I.2), even though unintentionally and without recognition of the underlying priniples.[18, 19]

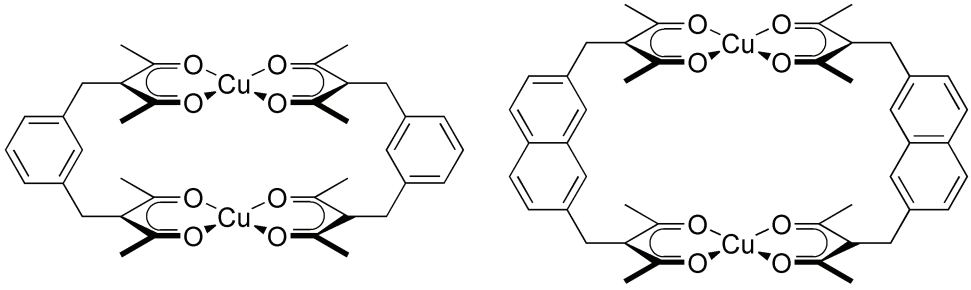

E7 **E8**

Figure I.2 First metallamacrocyclic structure employing the symmetry interaction approach.

Nowadays, numerous examples of discrete structures employing the symmetry interaction approach can be found in the literature, especially macrocyclic systems presented by the groups of Lehn,[47, 48] Saalfrank[45, 55–58] and Raymond.[24–26] But these topologies were often discovered by serendipity or by systematic variation of the ligand and metal components.[25, 27, 35] The complexity of the approach is both, its strength and limitation.

The development into a rational synthetic scheme was driven especially by Raymond and Caulder.[24–26] Their definition of terms which specify the geometrical relationship between the ligand and the metal centre are now essential for the description of high symmetry coordination clusters and facilitate their rational design.

The Coordinate Vector The coordinate vector is defined as the vector directed from the ligand to the metal centre. Monodentate and bidentate ligands are the two most important cases to consider. In the first case, the coordinate vector is simply the vector from the coordinating atom directed to the metal ion. In the second case, the coordinate vector is the vector which bisects the bidentate chelating group and is headed towards the metal ion.

The Chelate Plane The chelate plane is a plane orthogonal to the major symmetry axis of the metal complex. In the case of coordination of bidentate ligands to an octahedral metal centre, the chelate plane is spanned by the coordinate vectors of all coordinated ligands. Most importantly, any symmetric coordination complex can be described by the relationship between the chelate planes.

The Approach Angle The approach angle is the angle between the vector connecting the two coordinating atoms and the major symmetry axis of the metal centre.

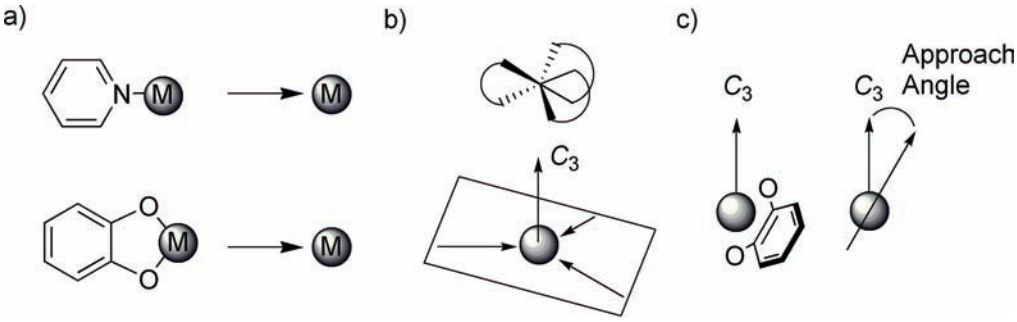

Figure I.3 Definitions for the symmetry interaction model. a) Coordinate vector for a bidentate ligand. b) Chelate plane defined by the plane orthogonal to the major metal symmetry axis. c) Approach angle for bidentate chelator.[24, 25]

In principle, coordination complexes of any symmetry can be formed. The symmetry elements of the point group corresponding to the target molecule have to be provided by the building blocks. Among the most widely reported topologies are helical and tetrahedral structures. These two topologies are an interesting examples of the complexity of the symmetry interaction approach, as they are both assembled from building blocks with the same inherent symmetry. But providing the symmetry elements is only a necessary requirement, the actual topology will be determined by the relative orientation of the symmetry axes one to another. For example, a M_2L_3 triple helicate belongs to the point group D_3,[59] consisting of a C_2 and C_3 axis. A tetrahedron owns likewise C_2 and C_3 axes. Thus, in both cases, one of the building blocks must possess a C_2 axis, whereas the other must have a C_3 axis. The three-fold axis can be provided by a metal centre with pseudo-octahedral coordination, and a two-fold axis by a C_2-symmetric bis(bidentate) ligand. If the symmetry axes span an angle of 90°, a triple helicate is formed, but if they span an angle of ~55°, a M_4L_6 adamantoid structure is obtained (Figure I.4).[26, 45, 55–58, 60, 61]

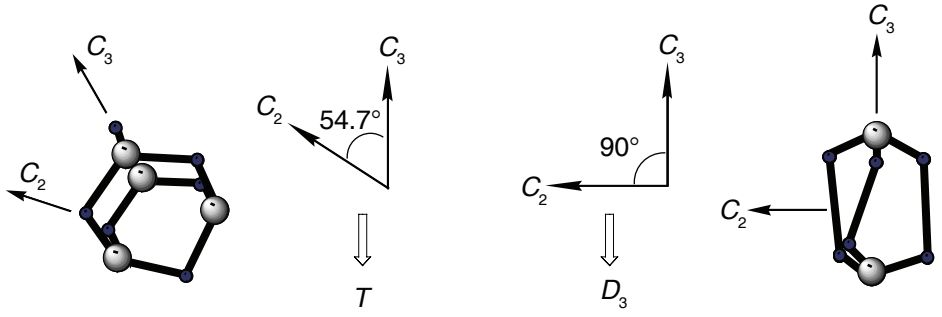

Figure I.4 Symmetry determination according to the orientation of the C_2 and C_3 axes. Reproduced by permission of The Royal Society of Chemistry from ref. [25].

I.III.3 The Directional Bonding Approach

The directional bonding approach is probably the most used design strategy for molecular architecture. First examples in the literature employing this approach are tetranuclear metal complexes from Verkade[17] and the quantitative synthesis of a molecular square by Fujita in 1990 (Scheme I.1).[14–16] The underlying principles were formulated for the first time by Stang in 1997,[22, 23] initially named 'molecular library approach'.[22] But this term didn't gain general acceptance and was replaced four years later with 'directional bonding approach' by Mirkin.[27]

The directional bonding approach employs highly directional metal fragments in combination with multibranched *monodentate* rigid ligands to gain structural access to polygons and polyhedra. Coordination in a directional fashion is ensured by the rigidity of the ligands and the coordination geometry of the metal centres in combination with large blocking ligands. These so called blocking or directing ligands are coordinatively inert, meaning that their kinetic exchange is so slow compared to those of the incoming bridging ligands and weakly bound ligands occupying the 'free' coordination sites of the metal that they can be seen as kinetically stable. Consequently, the angle spanned by the two incoming ligands is given and upon further coordination of metal centres and bridging ligands a 'closed' aggregate of predetermined symmetry will be obtained.[22, 23]

The design principle is illustrated in Scheme I.5 for several two-dimensional structures. Four metal centres with an 90° angle and four linear ditopic ligands will result in the formation of a molecular square, whereas a triangular macrocycle would be assembled from three linear ligands in combination with three metal fragments with an 60° angle.[22, 23]

In more general terms, a polygon or polyhedra is split into two different subunits, either both angular or into a linear and an angular one. Joined together in the correct ratio, the building blocks should theoretically assemble only in a predetermined geometrical form. Although this strategy has been developed for transition metal based self-assembly, the design principle should be applicable universally, as long as two requirements are fulfilled:

1. The building blocks are rigid, have predefined angles between the different coordination sites and are complementary to each other.

2. The building blocks are mixed in the appropriate ratio.

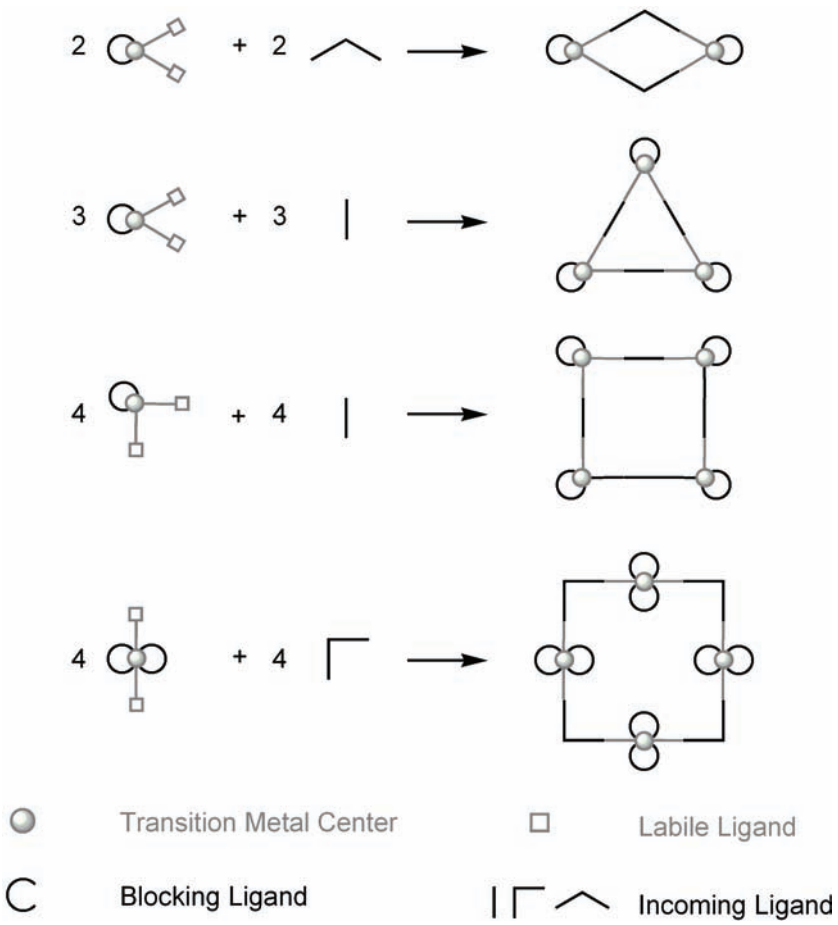

Scheme I.5 Design principle of the directional bonding approach for selected two-dimensional structures.[22, 23, 35]

However, things are more complicated and often not so straightforward as described here. The metal centres and the bridging ligands tolerate some deviations from their ideal geometry, and the self-assembly process itself is governed by more factors than the predetermination of building blocks. Thus, unexpected results are often obtained. Frequently, metallasupramolecular self-assembly reactions display no clear thermodynamic preference and two or more species are found in equilibrium. Many more topologies than those here presented have been obtained, among those prismatic, anti prismatic and non-symmetrical structures. Since the first systematic description in 1997,[22, 23] the topic has been reviewed several times by Stang,[20, 35] Mirkin,[27] Fujita[16, 42, 43] and others.[44] Whereas most researchers described molecular analogues of symmetric polyhedra, in which the ligands were located on the edges, Fujita did so by panelling the faces of polyhedra.[16, 40, 41] Several reviews with special emphasis on molecular squares[16, 29, 62] have been appeared and molecular architecture employing nucleobases as ligands has been intensively studied and reviewed by Navarro and Lippert.[39, 63] Jones paid special attention at the construction of molecular containers.[64]

The underlying design principles are also the major limitations of the approach. Rigid ligands favour the formation of supramolecular topologies but flexibility is important for functional features. The metal centres are coordinatively inert and no free coordination sites are available. They act solely as building blocks of the structure. Especially the perturbation of the physical properties of both, metal centres and ligands, hampers the development from structure to function. The largest potential lies probably in their application as reaction vessels[31] and containers for the stabilisation of guests which are difficult to study otherwise.[65–68]

I.III.3.a Assembly of Polygons

An overview of different polygons accessible by the combination of typical building blocks with different geometry is given in Figure I.5. Among these structures, tetranuclear molecular squares are most widely reported. Especially the emphasis of Fujita and Stang pushed molecular squares into a independent topic of metal-directed self-assembly.[22, 23, 35, 43, 62] The formation of squares starting from angular units displaying an 90° angle and linear building blocks is favoured, as the formation of a rectangular shape is almost strain free. Only few triangles have been reported, maybe due to the fact that angles of 60° are quite uncommon in transition metal complexes.[23] Nonetheless, triangles are often reported as side products from the formation of molecular squares (see chapter I.II).

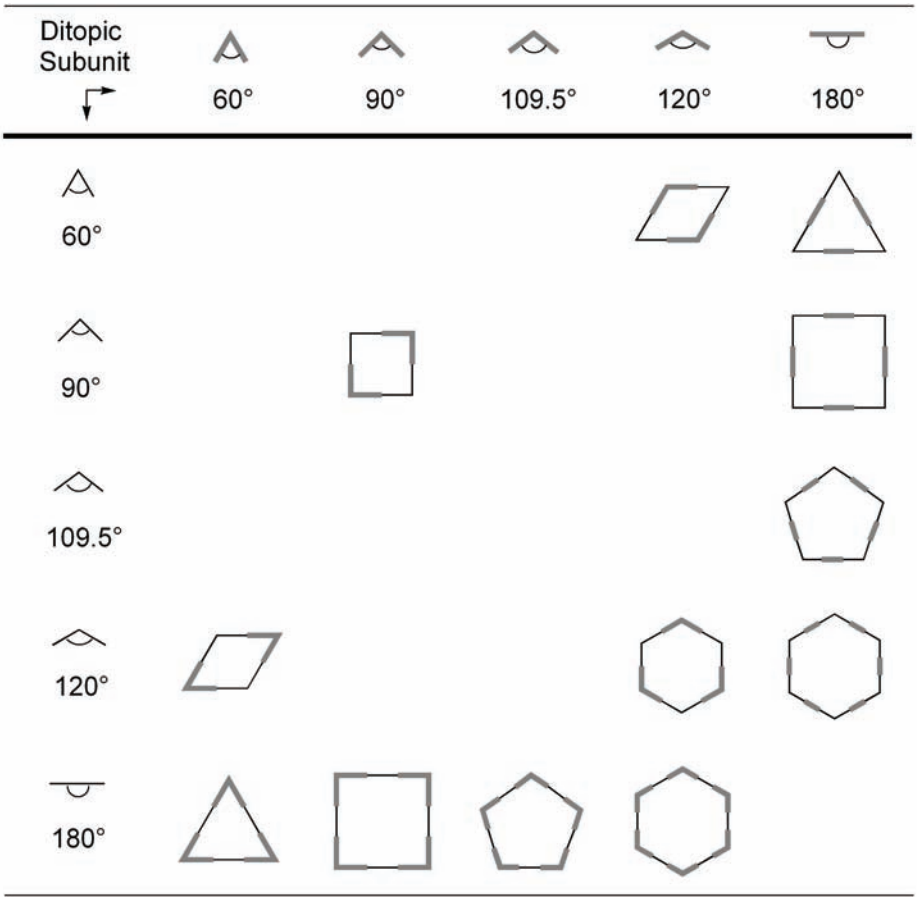

Figure I.5 Two-dimensional molecular topologies targeted by the directional bonding approach.[22, 23, 35]

Four different molecular squares, demonstrating both common and uncommon structural building blocks and features, are shown in Figure I.6. *Cis* protected Pt^{II} and Pd^{II} complexes acting as angular units and rigid ditopic bridging ligands acting as linear units are among the most common building blocks; a nice overview of employed building blocks has been compiled by Mirkin.[27]

Chelating phosphine ligands are most often used as directing ligands, but functionalisation with crown ethers, calixarenes[69] or for example ferrocene groups is possible, as shown by Stang for complex **E11**.[70] Ligands are in most cases very rigid and linear. Generally, this is achieved by fused or linked arenes. An interesting example is complex **E12**, in which porphyrines have been used as angular units linked by *trans*-$[Pd^{II}Cl_2]^{2+}$ metal centres acting as linear bridging units.[33] Complex **E10**[71] and **E9**[72] are exceptionally large. Complex **E9**, for example has a metal–metal diagonal length of 3.4 nm. This complex is also interesting, as the dipyridylperylene units retain their photophysical properties. Reversible electrochemistry of the ligand in the final Pt^{II} complex give raise to

potential applications as electro- or photochemical sensor for large guest molecules.[72, 73] The ligand has been further functionalised with ferrocene groups towards this aim.[74]

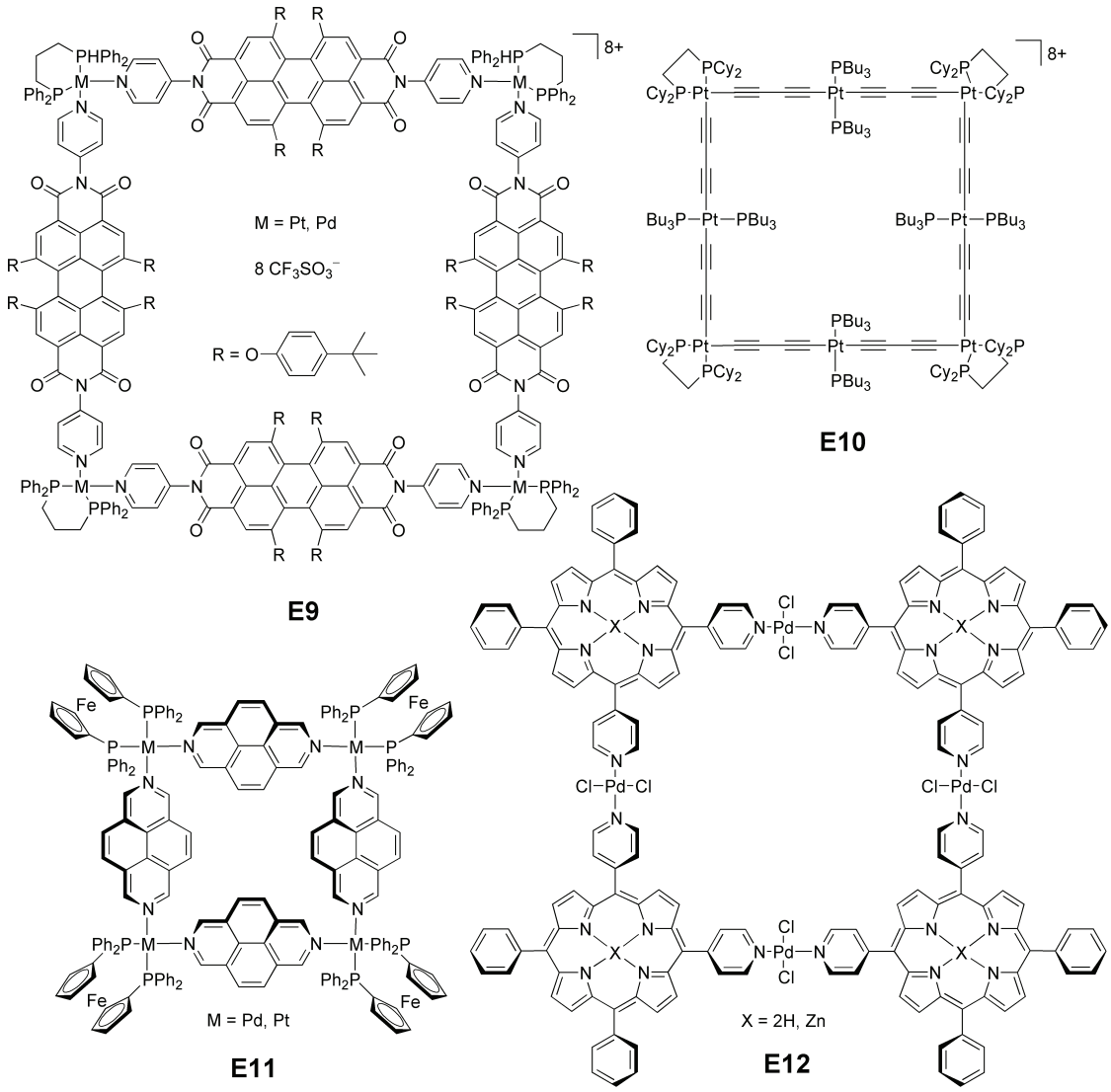

Figure I.6 Selected molecular squares obtained according to the directional bonding approach.

I.III.3.b Assembly of Polyhedra

Assembly of polyhedra can be either edge-directed or face-directed. In the first case, all building blocks lie on the edges. The shape of the polyhedra can be outlined by simply replacing the building blocks with strokes. If some or all faces of the target polyhedra are spanned by the building blocks, the approach is called face-directed. This approach is less intuitive, and it is sometimes quite difficult to 'recognize' the polyhedra. The self-

assembly of a molecular cube in edge-directed and face-directed fashion is shown in Scheme I.6 to illustrate both approaches.[20]

Eight tritopic corners with an 90° angle and twelve linear ditopic subunits are necessary to obtain a molecular cube according to the edge-directed approach. This strategy has been successful applied by several research groups.[75–78] Face directed self-assembly of a molecular cube has been demonstrated by Brisbois and coworkers using six tetratopic planar 90° faces and twelve ditopic 90° angles.[79]

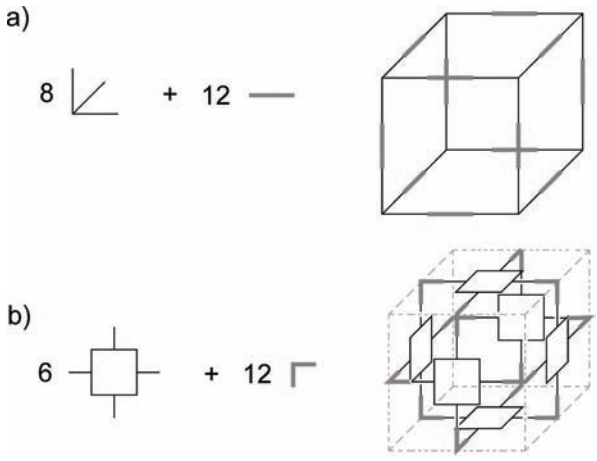

Scheme I.6 Edge-directed self-assembly (top) and face-directed self-assembly (bottom) illustrated at the example of a cubic cage.

All Platonic solids, as well of most of the Archimedean solids have been synthesised according to either one or both techniques. Polyhedra which can be obtained by combination of di- and tritopic building blocks following the edge-directed technique are presented in Figure I.7.

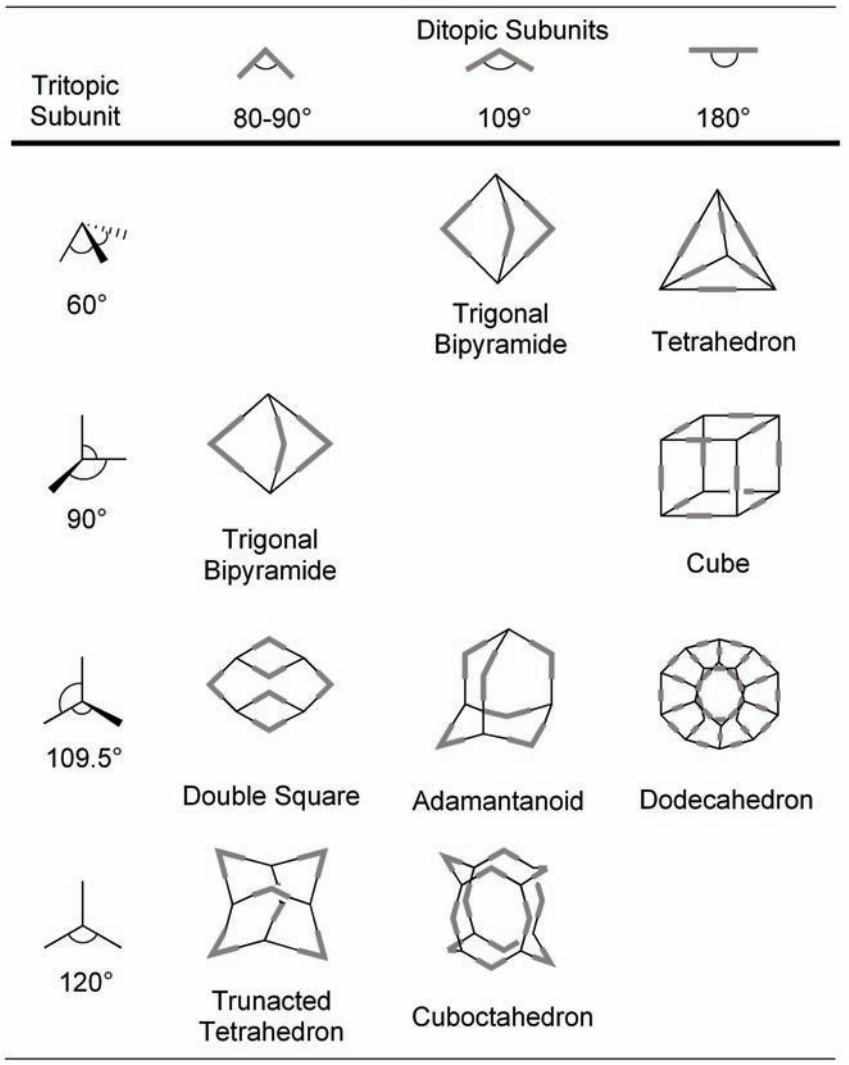

Figure I.7 Polyhedra obtained by combination of ditopic and tritopic building blocks.

Some of the most spectacular assemblies obtained so far are the octahedra **E13** and **E14** presented by Fujita[80, 81] and a cuboctahedron **E17** presented by Stang (Figure I.8).[82] Complex **E13** was obtained by self-assembly of the commonly used $[(en)Pd]^{2+}$ unit and 2,4,6-tris(4-pyridyl)-1,3,5-triazine acting as a tridentate triangular building block.[80] The metal centres occupy the corners of the octahedron, and four of the eight faces are occupied by triangular ligands. Alternatively, the hexahedral complex **E14** was obtained when using the hexadentate ligand 1,3,5-tris(3,5-pyrimidyl)benzene.[81] All six faces are occupied by the ligand and connected via 18 $[(en)Pd]^{2+}$ units, located this time on the edges of the octahedron instead at the corners. The cuboctahedral complex **E17** was obtained by self-assembly of the eight tridentate ligands **E15**, repre-

senting the triangular faces of the cuboctahedron, which were linked by twelve angular units **E16**.[82]

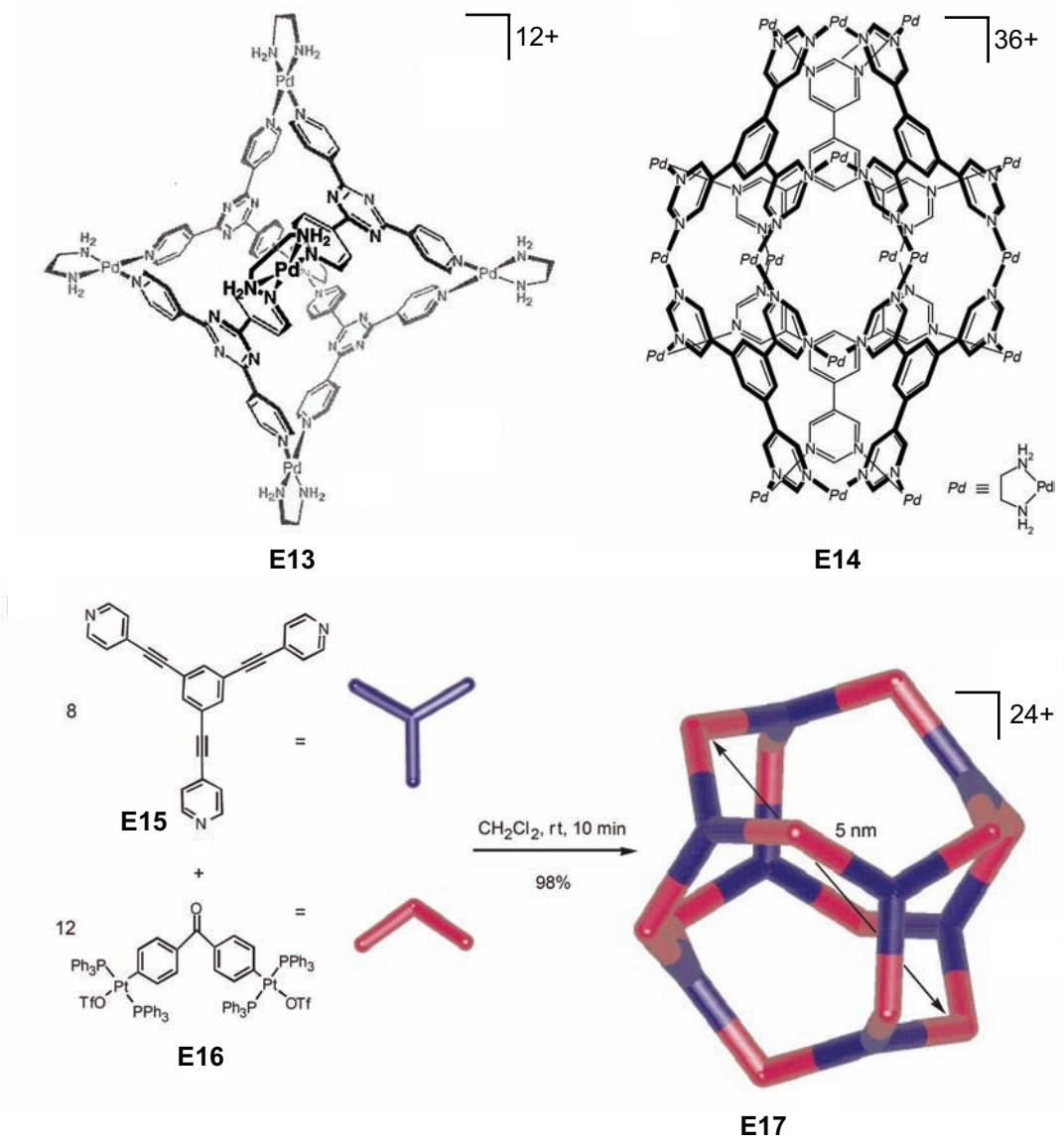

Figure I.8 Selected examples of molecular architecture obtained by employing the directional bonding approach.

Complex **E13** is outstanding as its simple preparation allows the synthesis on a commercial basis. The complex is well soluble in water and provides a large hydrophobic cavity with diagonal Pd–Pd distances of 2.2 nm. Most important, as only four of the eight faces are occupied by ligands, the cavity is accessible for large molecules. Applications using complex **E13** as reaction vessel are now starting to emerge.[83–91]

I.IV Halfsandwich Complexes in Metal-Directed Self-Assembly

Organometallic complexes of Ru^{II}, Rh^{III} and Ir^{III} have likewise been used as building blocks in transition metal based self-assembly. Dimeric halfsandwich complexes of the general formula $[(\pi\text{-ligand})MCl_2]_2$ are ideally suited starting materials, as they are either commercially available or easily accessible. They are soluble in organic solvents as well as in water. After abstraction of the chloro ligands, three facial coordination sites are available for neutral or anionic ligands. The metal centre displays a pseudo tetrahedral, piano stool like geometry. Organometallic halfsandwich complexes used for the assembly of molecular architecture as well as in this work are presented Figure I.9.

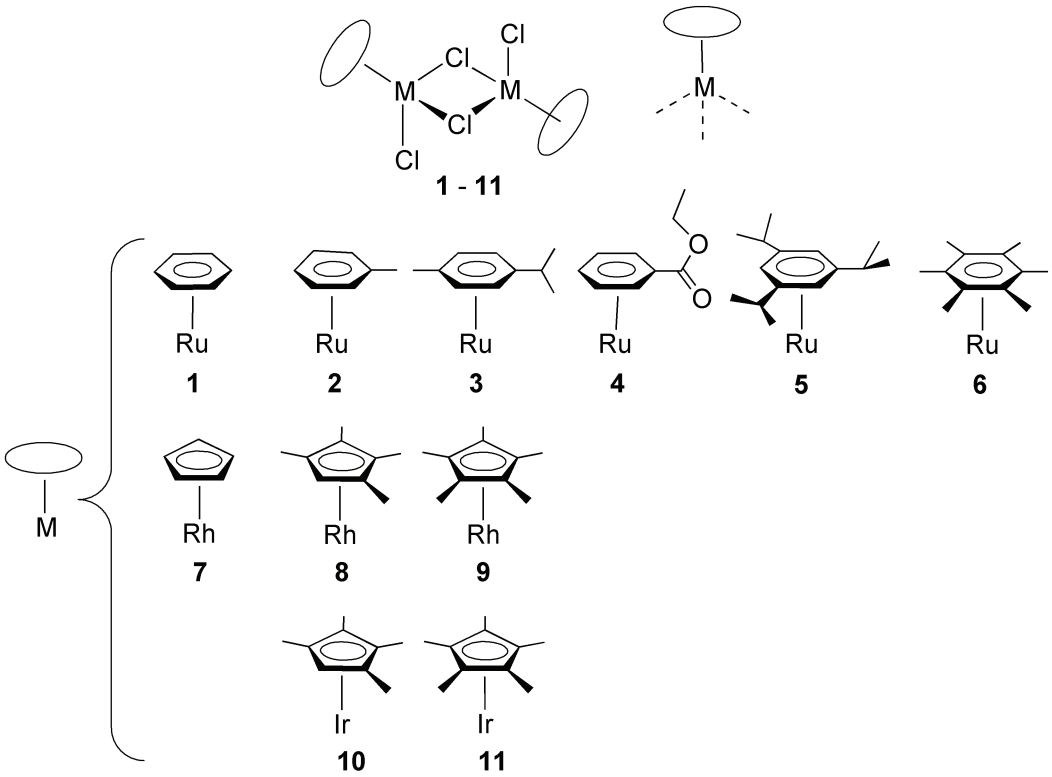

Figure I.9 Selected chloro-bridged organometallic halfsandwich complexes.

Two- and tridentate ligands have mainly been employed to obtain macrocyclic structures. Using bidentate ligands, such as cyanide,[75, 76, 78, 92–94] cyanamide,[95, 96] diisocyano compounds,[97–99] diamino compounds,[100] or 4,4'-bipyridine ligands[101, 102] molecular rectangles and cage like structures have been obtained.

Whereas tridentate planar ligands result in the formation of metallamacrocycles of different nuclearity, tridentate non-planar ligands give raise to three-dimensional topologies,

as recently demonstrated by Rauchfuss.[103] Reaction of $[Cp^*Rh(MeNO_2)_n]^{2+}$ and $[PhB(CN)_3]^-$ in nitromethane resulted in the formation of a hexagonal prism. The geometry of cyclic assemblies obtained from halfsandwich complexes and tridentate planar ligands depends on the relative arrangement of the donor atoms. The geometric shapes observed so far and their correlation to the relative orientation of the coordinate vectors are summarized in Figure I.10.

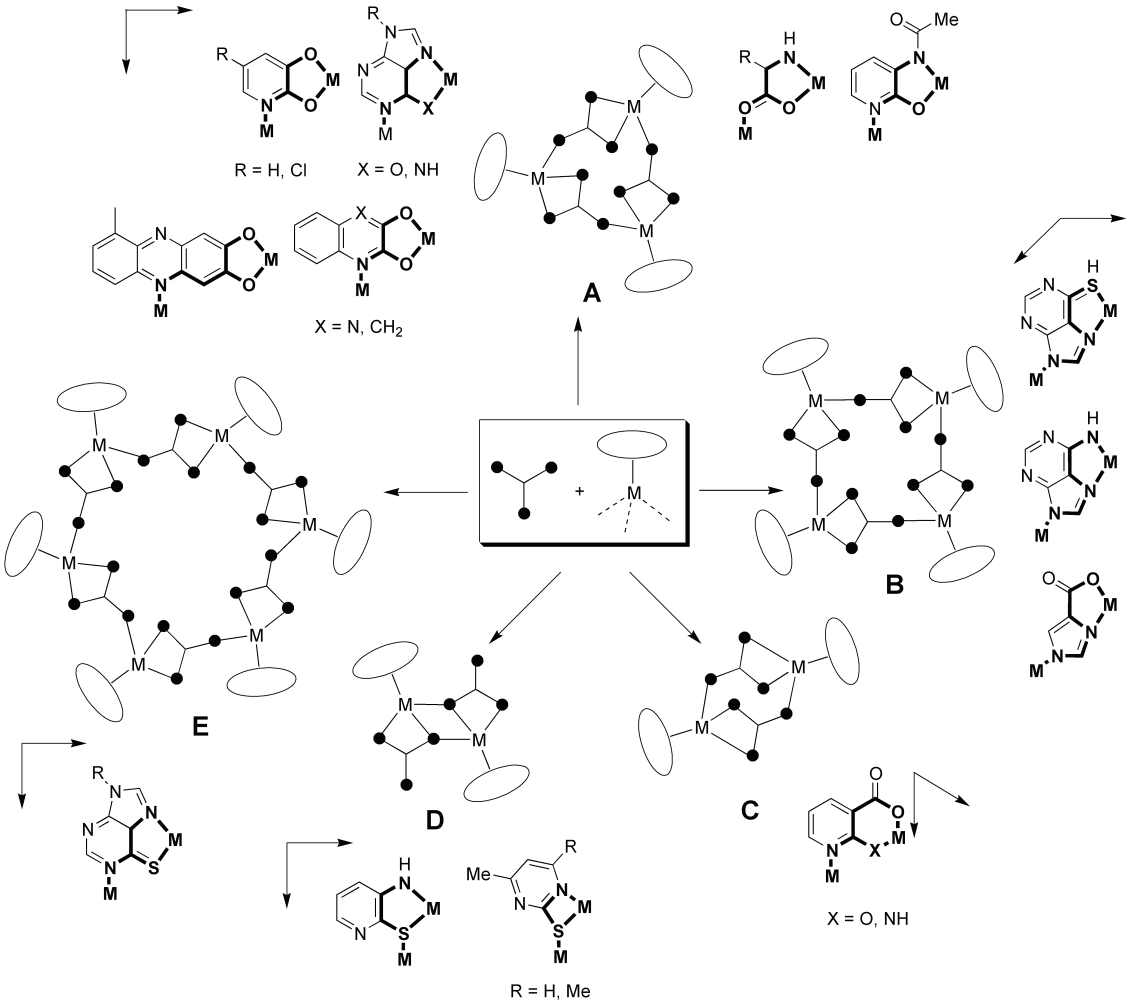

Figure I.10 Different metallamacrocyclic geometries obtained from reactions of halfsandwich complexes and tridentate ligands.

Most often, polycationic trinuclear species of type **A** have been reported. They were first described by Fish in 1992,[104] who studied the self-assembly of $[Cp^*RhCl_2]_2$ with adenine derivatives.[104–110] Structurally similar complexes using (arene)Ru^{II}, Cp^*Ir^{III}, Cp^*Rh^{III} were subsequently investigated by Sheldrick[111–113] and Yamanari.[114, 115] Recently, formation of trimeric assemblies from of the (9-ane-S_3)Ru^{II} moieties and 9-methyladenine have been reported.[116] Furthermore, trimeric metallamacrocycles were obtained using amino acids,[117–122] and 9-ethyl-hypoxanthine.[123] Using dianionic

bridging ligands, neutral species were obtained. Neutral trinuclear macrocycles have been especially developed by Severin and coworkers. They have been obtained with the following ligands: 3-acetamido-2-pyridone,[124] 2,3-dihydroxyquinoline,[125] 2,3-dihydroxyquinoxaline,[125] 6-methyl-2,3-dihydroxyphenazine,[125] and 3-hydroxy-2-pyridone[124, 126, 127] as well as its 5-chloro derivative.[128, 129] Although these ligands are very diverse, they have a common feature: the similar arrangement of the donor atoms results in the same orientation of the coordinate vectors.

For the free adenine ligand, a different coordination scheme was observed, resulting in tetranuclear assemblies of type **B**.[111, 113] Similar structures were obtained for 6-purinethione[130] and 4-imidazolecarboxylic acid,[125] both displaying the same arrangement of donor atoms as adenine. A hexanuclear macrocycle of type **E** has been obtained using 9-substituted 6-purinethione as ligand.[131] As shown, tridentate ligands can also adopt a coordination mode which leads to dinuclear species of type **D**[132] as well as of type **C**.[99, 125, 133]

I.V Metallacrown Complexes

Metallacrown complexes are among the earliest metallamacrocycles described and were first reported by Pecoraro in 1989.[134–136] Metallacrown complexes are inorganic analogues of crown ethers and obtained by replacing two carbon atoms of the latter with a metal and a heteroatom (such as nitrogen). In analogy to their organic counterparts, ring size and the number of oxygen donor atoms are indicated in their name, e.g. 12-metallacrown-4 has a total of twelve atoms defining the metallamacrocycle and four oxygen donor atoms pointing into the central cavity.[137, 138] A comparison of metallacrown complexes and crown ethers shown in Figure I.11 clearly demonstrate their analogy.[139]

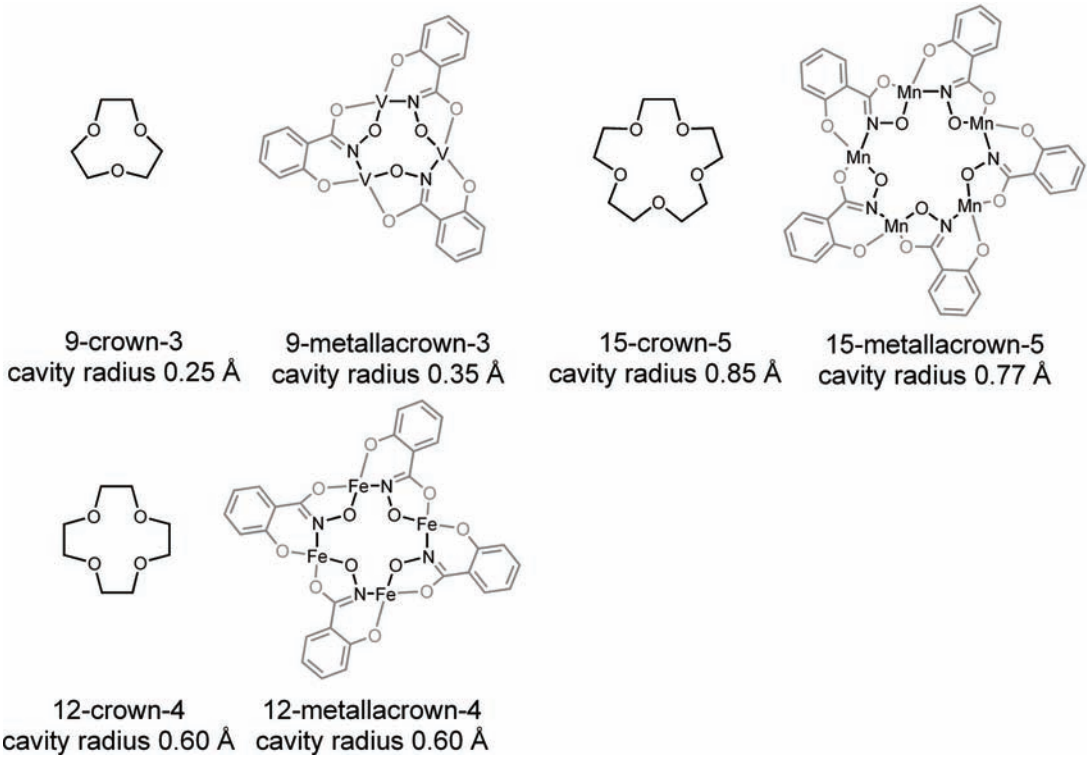

Figure I.11 Crown ethers and their analogous metallacrown complexes.

Despite the difference bond lengths of M–O or M–N bonds compared to C–C or C–O bonds, similar cavity sizes are found for metallacrown complexes and their organic counterparts. Thus, metallacrown complexes are also well suited to act as specific ion receptors. However, their binding affinity is in general increased compared to organic crown ethers due to the rigidity of their metallamacrocyclic framework and a higher polarization of the oxygen donor atoms.[134–136, 139–141]

To date, metallacrown complexes of various metals have been reported. The most commonly used bridging ligands are salicylhydroxamic acid and its derivatives with the same structural binding motif. Usually, metallacrown complexes are obtained in a single

step reaction in good yields.[142–150] Ring sizes from 9[134, 136] to 36 atoms[151] have been reported, as well as sandwich type metallacrown complexes[152, 153] and double crown complexes.[154–156] The metallacrown analogy has been expanded to metallacalixarenes[157] and metallacryptands.[158] Recently, inverse metallacrowns, i.e. the metal centres point into the cavity, so that these macrocycles function as anion receptors, have been presented.[159–163]

I.VI Neutral 12-Metallacrown-3 Complexes

Neutral trimeric macrocycles complexes using organometallic building blocks and tridentate rigid dianionic oxo-pyridonate ligands have been developed in the Severin group.[124, 126, 127, 164] The following chapter gives an introduction into the field, which is the basis of the presented work. 12-Metallacrown-3 complexes self-assemble easily from organometallic dimeric halfsandwich complexes $[(\pi\text{-ligand})MCl_2]_2$ and 3-hydroxypyridone ligands in the presence of a base such as Cs_2CO_3. The synthetic scheme (Scheme I.7) is very versatile, as not only the metal fragment, but also the ligand can be varied. Reactions perform generally in good yields (>> 60 %).

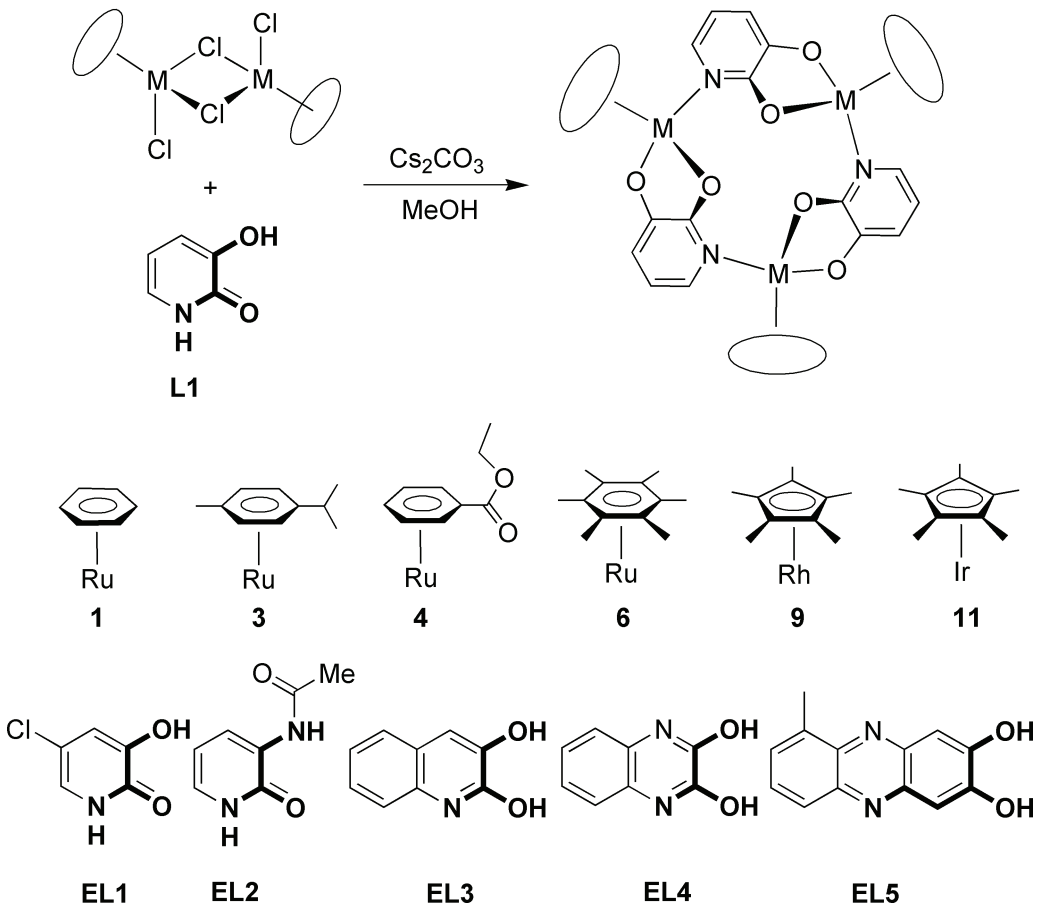

Scheme I.7 Synthesis of neutral 12-metallacrown-3 complexes. The relative arrangement of the donor atoms of the ligands is highlighted in bold.

Scheme I.7 shows the halfsandwich complexes and ligands used so far. Using 3-hydroxy-2-pyridone[a] **L1** as bridging ligand, complexes with various (arene)Ru[124, 126,

a. The use of 3-hydroxy-2-pyridone and 2,3-dihydroxypyridine is equivalent, as both compounds are in a tautomeric equilibrium with each other.

[164, 165] and Cp*M (M =Rh, Ir)[124, 165, 166] metal fragments have been obtained. Trinuclear species with different ligands were likewise obtained if the relative arrangement of the donor atoms was maintained. This is the case for 5-chloro-3-hydroxy-2-pyridone **EL1**,[128] 3-acetamido-2-pyridone **EL2**,[124] 2,3-dihydroxyquinoline **EL3** and 2,3-dihydroxyquinoxaline **EL4**.[125] Expanded trinuclear metallamacrocycles have been obtained for 6-methyl-2,3-dihydroxyphenazine **EL5** and $[(Me_3C_6H_3)RuCl_2]_2$.[125] The relative orientation of the coordinate vectors is maintained, but the donor atoms are further apart, leading to one of the largest metallamacrocycles based on organometallic halfsandwich complexes reported so far. However, investigations have mostly focused on assemblies derived from 3-hydroxy-2-pyridone as they present the most interesting host-guest chemistry. Although most of the following discussion is in general also valid for complexes obtained with alternative bridging ligands, only results from metallamacrocycles obtained from 3-hydroxy-2-pyridone will be presented.

I.VI.1 Structural Characterization

The self-assembly process is highly diastereoselective. Racemic mixtures of complexes with $M_RM_RM_R$ or $M_SM_SM_S$ configuration are obtained; their chiral resolution has been achieved by fractional crystallisation using the optical pure shift reagent [chinchonidinium][D-trisphat].[129] As shown by single crystal X-ray analysis, the structure of all complexes in the crystal is very similar. All assemblies show a pseudo C_3 symmetrical geometry with three tetrahedral (π-ligand)M corners connected by three dianionic 3-oxo-2-pyridonate ligands. The tridentate ligands are coordinated via two oxygen atoms to the metal, forming five-membered chelate rings; the nitrogen atoms of the pyridine rings are coordinated to the next metal atom. In total, twelve atoms form a metallamacrocylic framework similar to a crown, which contains three oxygen donor atoms. Thus, these type of metallamacrocycles can be seen as organometallic analogues of 12-crown-3 ethers (Figure I.14). PGSE studies have revealed an hydrodynamic radius r_H of 6.4 Å in CD_2Cl_2.[167] Both the catechol part and the pyridine part of the ligand are coordinated in a slightly bent fashion to the corresponding metal. Overall, the bond lengths and angles are very similar, and substitution of the metal fragment has only a very small influence on the overall structure. Nevertheless, the macrocycles show some flexibility, which is manifested in the differences of the M–M' distances, being between 5.32 and 5.46 Å apart. This is probably due to an increased repulsion between bulkier π-ligands. A similar lengthening of the M–M' distances is observed upon binding to sterically demanding guest molecules, such as NaI, but the changes upon coordination to metal salts of lithium and sodium remain small. The metallamacrocyclic framework is very rigid and undergoes only minor changes upon coordination of metal salts (see Table IX.10 on page 227 for a compilation of structural data for all 12-metallacrown-3 complexes and their metal salt adducts).

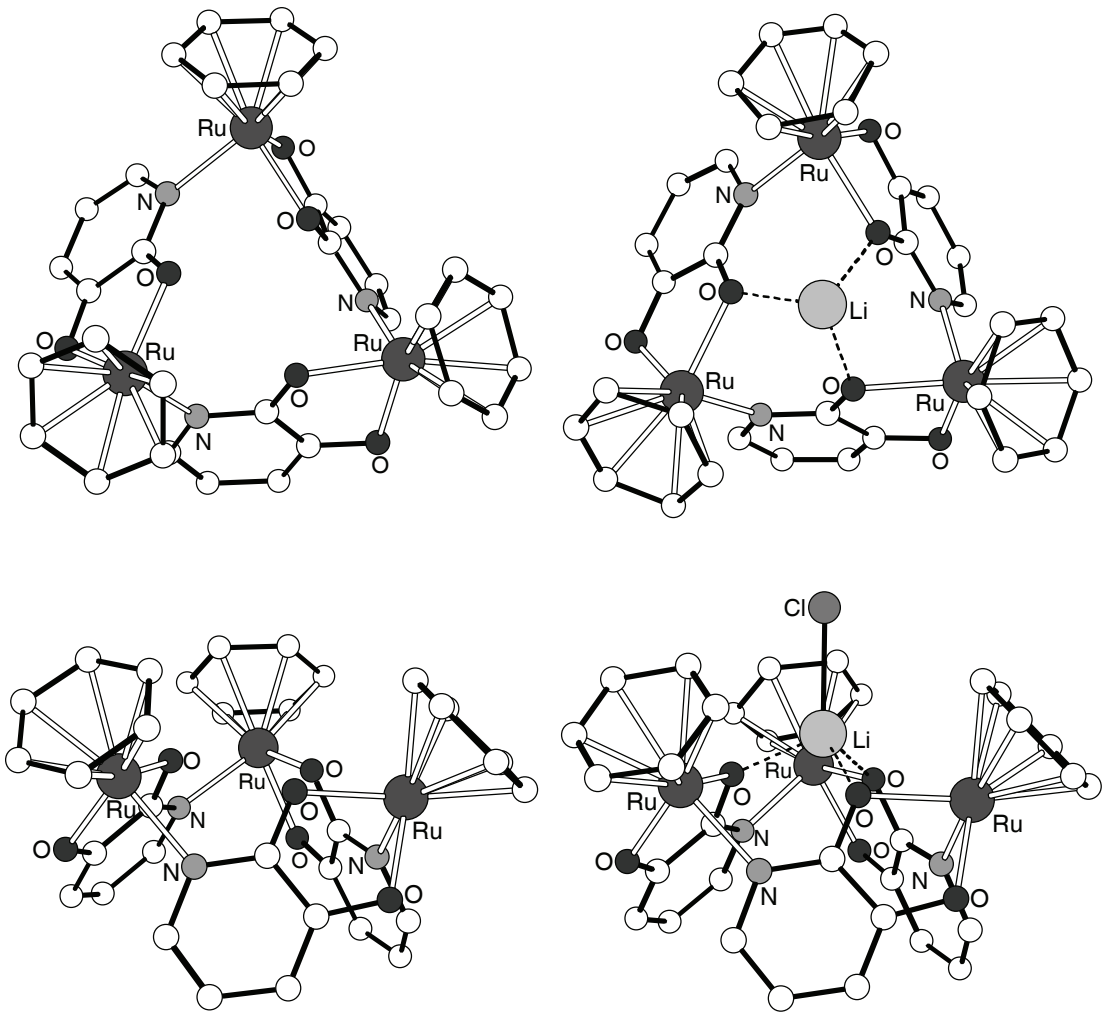

Figure I.12 Graphic representation of **[(benzene)Ru(L1–2 H$^+$)]$_3$** (left) and its LiCl adduct **[(benzene)Ru(L1–2 H$^+$)]$_3$ × LiCl** (right) in the crystal. Both pictures at the top show the structures along the pseudo C_3 axis; the pictures at the bottom visualize the crown structure. Hydrogen atoms and solvent molecules are omitted for reasons of clarity; the chloride anion sitting on top of the lithium cation is also omitted in the top right picture.

The complex **[(benzene)Ru(L1–2 H$^+$)]$_3$** and its LiCl adduct has been chosen as an representative example to illustrate the general structure of 12-metallacrown-3 complexes. Figure I.12 shows the graphic representation of **[(benzene)Ru(L1–2 H$^+$)]$_3$** and its LiCl adduct **[(benzene)Ru(L1–2 H$^+$)]$_3$ × LiCl** in the crystal. The two pictures at the top show the view along the pseudo C_3 axis and give an insight into the cavity formed by the three benzene ligands. At the bottom of this cavity three oxygen atoms of the pyridonate ligands come into close proximity to each other with an average O–O' distance of 3.04 Å forming the binding site for alkali metal ions. The bound Li^+ cation is located in the middle of the cavity, slightly above the plane defined by the three oxygen atoms. It displays a pseudo tetrahedral coordination, with the fourth coordination site occupied by the chlo-

ride anion (see right picture at the bottom of Figure I.12). The average O-Li distance is 1.96 Å and the chloride anion is 2.38 Å apart from the Li^+ cation. The images at the bottom visualise the crown like structure of the complex; upon binding only minor changes of the bond lengths are observed. The space filling representation in Figure I.13 shows nicely how the Li^+ ion is encapsulated by the π-ligands.

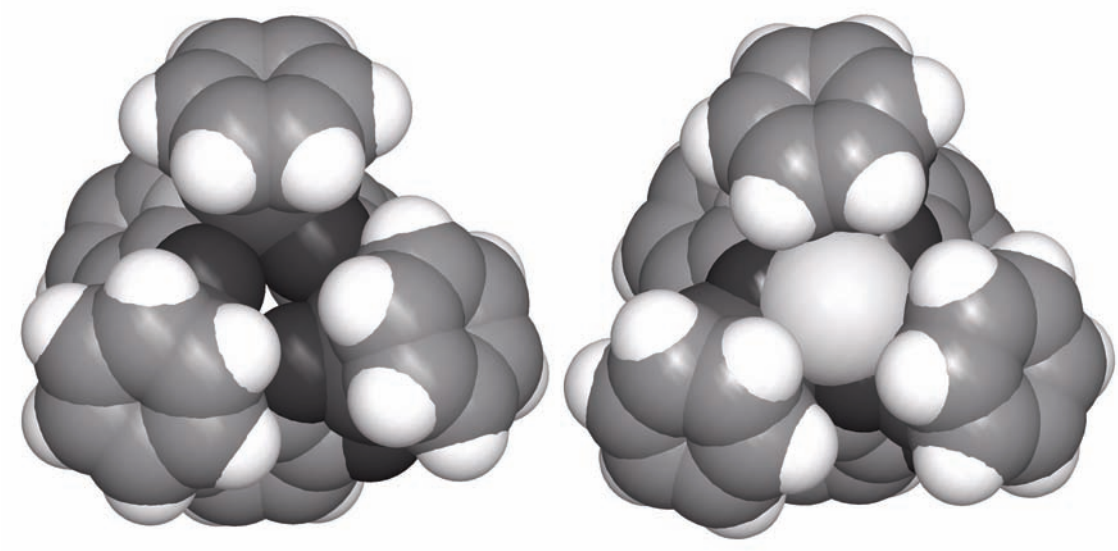

Figure I.13 Space filling representation of **[(benzene)Ru(L1–2 H^+)]$_3$** (left) and its LiCl adduct **[(benzene)Ru(L1–2 H^+)]$_3$ × LiCl** (right) in the crystal. Solvent molecules and the chloride anion sitting on top of the lithium cation are deleted for reasons of clarity.

I.VI.2 Host-Guest Chemistry

As illustrated above, the π-ligands of the complexes form a half sphere. At the bottom of this cavity, three oxygen donor atoms are in close proximity to each other, forming a binding site for small cations. Due to the steric demand of the π-ligands, only small alkaline ions such as Li^+ and Na^+ can access the binding site. Bigger alkaline ions such as K^+ and Cs^+ are effectively blocked. The metal ion is bound to the three adjacent oxygen atoms. The fourth coordination site is generally occupied by the counter anion (Figure I.12 and Figure I.14).

Adducts of lithium and sodium salts are easily obtained by mixing the metallamacrocycle with the corresponding metal salts in methanol. The coordination of guest molecules to the binding site can be detected using ^{1}H NMR spectroscopy. The signals of the bridging ligand and of the π-ligands undergo significant shifts downfield. If the lithium or sodium salt is added in substoichiometric amounts, two sets of signals can be detected,

indicating that the exchange is slow compared to the NMR time scale. Thus, stability constants can directly be obtained by integration of suited ^{1}H NMR signals.

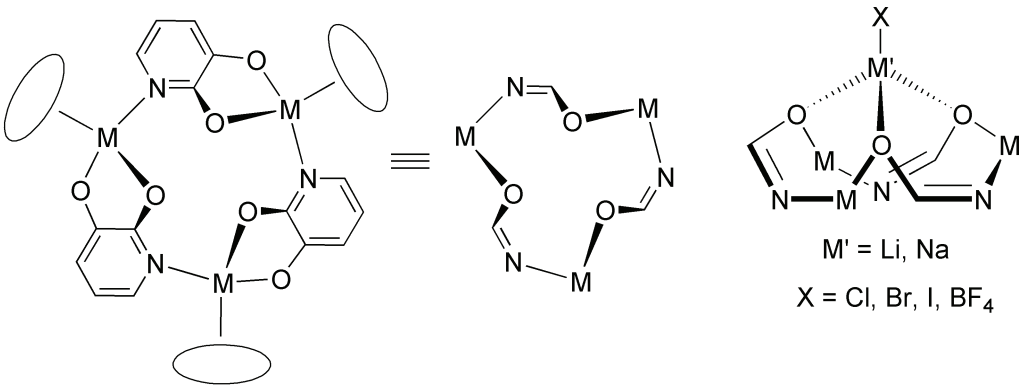

Figure I.14 The 12-metallacrown-3 framework and the coordination of lithium and sodium salts to the binding site.

I.VI.2.a Binding Affinity

The stability of the host-guest complexes is exceedingly high. The binding affinities in chloroform are not only significantly higher than those of crown ethers, but comparable to those of macrobicyclic ionophores such as the 2,2,1-cryptand for NaCl adducts and 2,1,1-cryptand for LiCl adducts. In methanol, lower values, as expected for more polar solvents, were found. Association constants for the corresponding NaCl adducts are between $K_a = (1.1 \pm 0.5) \times 10^2\ M^{-1}$ for $(C_6H_6)Ru$ complex and $K_a = (3.5 \pm 0.5) \times 10^3\ M^{-1}$ for the (cymene)Ru complex. Also, the binding affinity of sodium adducts has been found to depend on the anion employed: NaI adducts show lower K_a values than NaCl adducts.[124, 126] It has to be noted, however, that the binding constants are no longer in the range of cryptands, but similar to those of 15-crown-5.[140] This behaviour can be partly attributed to the fact that ion pairs are bound in chloroform in order to avoid energetically less favoured 'naked' halide anions. In methanol, this advantage seems to be less pronounced, decreasing the binding affinity over proportion. The Li^+ adducts are in general more stable than the corresponding Na^+ adducts and display, even in methanol, binding constants close or higher than $10^5\ M^{-1}$.[124, 126]

There are several factors adding up to the high stability of lithium and sodium salt adducts which also explain why metallamacrocycles, especially 12-metallacrown-3 complexes presented here, display intrinsically higher binding affinities than organic crown complexes.

1. The metallamacrocyclic framework is very *rigid*, and the binding site is ideally *preorganised* for the binding of small alkaline ions such as Li^+ or Na^+. Only

very small structural changes occur upon binding as verified by X-ray analysis.[124, 126]

2. There is a maximum of *one* solvent molecule which fits into the cavity formed by the π-ligands. The energetic costs for the *desolvation* of the binding site is therefore very low.

3. The metal salts are bound as ion pairs, an energetically very favourable feature in organic solvents such as chloroform.

4. The binding site of metallacrown complexes is highly polarized. Computational studies have shown that the three oxygen donor atoms display a significant higher partial negative charge than the oxygen atoms of normal crown ethers.[128] This is due to the higher electronegativity of the adjacent metal atoms compared to carbon atoms.

Classical organic crown ethers display none of these advantages.

The high affinity towards Li^+ and Na^+ allowed the stabilisation of molecular LiF and LiFHF inside the cavity of the receptor.[168] Likewise, Na_2SiF_6 could be encapsulated by two **[(cymene)Ru(L1–2 H$^+$)]$_3$** complexes.[169] Both are difficult to achieve, as the high lattice energy of the salts present a thermodynamic trap.

I.VI.2.b Binding Kinetics

A further difference between crown ether or cryptands and 12-metallacrown-3 complexes are their respective binding kinetics. The exchange kinetics decrease dramatically from crown ethers over cryptands to 12-metallacrown-3 complexes. The metal is slowly bound, once it is inside the binding cavity it is more or less trapped and only released extremely slow. The formation and dissociation rates of Li^+ by selected receptors given in Table I.1 support this statement.[b]

Table I.1: Formation rate k_f and dissociation rate k_d of the Li^+ complexation by complex **[Cp*Ir(L1–2 H$^+$)]$_3$**[a], 2,1,1-cryptand[a] and 18-crown-6[b].

Compound	k_f / M^{-1} s^{-1}	k_d / s^{-1}	K_a / M^{-1}
[Cp*Ir(L1–2 H$^+$)]$_3$[128]	1.6×10^{-3}	$< 10^{-8}$	$> 10^5$
2,1,1-Cryptand[171, 172]	4.8×10^5	4.4×10^{-3}	1.1×10^8
18-crown-6[173]	8×10^7	6×10^7	1.3

a. Solvent: methanol
b. Solvent: water

b. Binding constants and dynamics determined in different solvents should in principle not be compared. However, the release rate of crown ethers is generally several orders of magnitude higher than that of cryptands.[170]

I.VI.2.c Selectivity

The metallamacrocycles **[(π-ligand)M(L1–2 H^+)]$_3$** are not only very potent ionophores, they are also very selective. All complexes form lithium salt adducts, but only complexes containing the (C_6H_6)Ru, (cymene)Ru or ($C_6H_5CO_2Et$)Ru metal fragment are likewise able to coordinate sodium salts. None of the complexes is able to bind potassium ions. The pronounced selectivity can be partly explained with an size exclusion effect due to the size of the π-ligands. They effectively block the binding site for cations bigger than Na^+, such as K^+ or Cs^+. Furthermore, very bulky ligands such as $C_6H_3Et_3$, C_6Me_6 and Cp* narrow the entrance of the binding site further, so that binding of Na^+ is also not longer possible.

Although the exclusion of certain cations can be explained with the steric size of the π-ligands, the general preference of the receptors for Li^+, which are theoretically able to bind to both, Li^+ and Na^+, is less obvious. In this context it should be noted that the 'hole-size-relationship' of crown ethers is also ambiguous.[170] The binding affinity is often most pronounced if the size of the crown ether's interior cavity is about the same size as the cation,[140, 174] but there are also examples in which this is not the case. For a study of the binding behaviour of simple crown ethers (12-crown-4 to 24-crown-8) using methanol as solvent and metal chlorides as salts, it was found that K^+ was bound best for all crown ethers independent of their ring size. Furthermore, 18-crown-6 showed the highest binding affinity towards Na^+, K^+, Ca^{2+} and NH_4^+ of all investigated crown ethers.[175] Overall, in some cases the binding behaviour can be explained on the basis of the 'hole-size- relationship', but it is not a principle that should be applied universally. Other factors like the number of donor atoms as well as the hydration energy and preferred complexation geometry of the metal ions have to be considered too. A similar observation of enhanced affinity of 12-metallacrown-4 complexes for Li^+ over other cations was made by Pecorao.[137]

The high selectivity of 12-metallacrown-3 complexes for Li^+ ions can be illustrated at the example of complex **[($C_6H_5CO_2Et$)Ru(L1–2 H^+)]$_3$**. Even though the receptor is principally able to bind Li^+ and Na^+, a Li^+ specific extraction behaviour has been observed. If an aqueous solution of Li^+ containing a large excess of NaCl, KCl, CsCl, $MgCl_2$ and $CaCl_2$ was shaken with a chloroform solution of this receptor, only Li^+ was extracted.[165] This behaviour is interesting, as the extraction of LiCl from water is difficult to accomplish due to the high enthalpy of hydration of Li^+ and Cl^-.[176] In addition the enthalpy of the competing alkaline metal cations is much smaller.

I.VI.3 Sensing

Upon binding to metal ions, the redox potential of the metallamacrocycle changes substantially. This difference in the oxidation behaviour could be used to design a colori-

metric test for Li^+ in chloroform. After addition of DDQ (2,3-dichloro-5,6-dicyano-1,4-benzoquinone), solutions containing the free receptor turned immediately dark, whereas only slight colour changes were observed for the respective Li^+ or Na^+ complexes. The steric requirements of large π-ligands were used to design a fluoride specific chemosensor. Only the very small fluoride anion can access the Li^+ cation – which serve as binding site – bound in the cavity of the **[Cp*Rh(L1–2 H^+)]$_3$** complex. The binding event was detected by electrochemical means.[166]

I.VII Aims of the research project

The purpose of this work was to further investigate the supramolecular chemistry of 12-metallacrown-3 complexes with special emphasis on water as solvent.

1. The adaptive behaviour of dynamic combinatorial libraries (DCLs) was investigated theoretically, and the results were confirmed experimentally with small model DCLs generated through reversible metal fragment exchange between different 12-metallacrown-3 complexes.

2. Ligands which render 12-metallacrown-3 complexes soluble in water have been developed. Their coordination behaviour with halfsandwich complexes $[(\pi\text{-ligand})MCl_2]_2$ in water has been studied. The self-assembly process and their binding behaviour towards small alkaline ions such as Li^+ and Na^+ was investigated. Special attention was paid to methods, which allow to transduce the binding event into a readable signal in order to generate Li^+ specific sensors in water.

3. The size exclusion effect of bulky π-ligands upon binding to small alkaline ions has been investigated towards the ability of $^6Li/^7Li$ isotope separation.

4. Linking of two 3-hydroxy-2-pyridone units led to a new structural motif: expanded triple stranded helicates.

5. A prime concern was the development of new bridging ligands in order to modulate the features of 12-metallacrown-3 complexes.

Chapter II
Adaptive Behaviour of Dynamic Combinatorial Libraries

II.I Dynamic Combinatorial Chemistry

In classical organic synthesis bond formation is mostly achieved by kinetically controlled reactions resulting in strong and irreversible covalent bonds.[177] This strategy has been applied ever since by synthetic chemists and has led to some very efficient syntheses of both, natural and unnatural products. Although reversible reactions under thermodynamic control have been known since a very long time, their application in synthesis has been sparse compared to kinetically controlled reactions. Their main disadvantage is their reversibility associated with a mixture of products where one product is desired. Dynamic combinatorial chemistry (DCC) uses exactly this reversibility as a fundamentally new approach for the discovery of new species that take part in molecular recognition. Reversibility is no longer a disadvantage but the intrinsic strength of the system.

Thermodynamic vs. Kinetic Control Whereas in kinetically controlled reactions the relative magnitude of the transition states determines the product distribution, the relative thermodynamic stabilities of the products are responsible for the product ratio under thermodynamic control. The product distribution of kinetically controlled reactions can be influenced by the stabilisation of the transition state, implying a detailed knowledge of the reaction mechanism. Once the bond formation has taken place, the reaction should be quenched. The reversibility of thermodynamic controlled reactions requires a sufficiently long reaction time to shift the product distribution to the thermodynamically favoured product. This offers the possibility to influence the product ratio either by introducing certain features into the starting material which will increase the relative thermodynamic stability of the desired product or by applying the principle of Le Chatelier: Using a compound in excess or removal of a compound will force the equilibrium into one direction. A more subtle method of stabilisation is the addition of a template.[178]

II.I.1 Dynamic Covalent Chemistry

Dynamic covalent chemistry focuses on reversible covalent bond formation under thermodynamic control. A fundamental alteration of the perception of these reaction has occurred over the last decade. Whereas reversibility has been associated with vast product mixtures in the past, the term reversibility is now associated with the possibility of going back on the reaction path/coordinate, a feature which is best summarized with keywords like ‘error checking’ and ‘proof reading’. An extensive review by Rowan covers this field.[177] But the focus lies exclusively on reversible *covalent* reactions. Dynamic combinatorial chemistry includes both, reversible *covalent* and *non-covalent* bond formation. Non-covalent interactions such as hydrogen bonds, metal–ligand coordination, donor-acceptor and electrostatic interactions are naturally reversible and well known from supramolecular chemistry. The main difference between supramolecular chemistry

and dynamic covalent chemistry is the *velocity* of the equilibration process: non-covalent bonds exchange much faster, even though the equilibration of covalent bonds can be accelerated by using suited catalysts.

II.I.2 Dynamic Combinatorial Chemistry

A reversible reaction is dynamic, meaning that the equilibrium and thus the product ratio can be shifted by applying any kind of suited pressure on the system. Starting from a mixture of compounds, which are all interconnected to each other by dynamic equilibria, the external stimuli for re-equilibration could be the addition of a target molecule which can somehow interact with the compounds in the mixtures. Interaction of the target with a specific compound could lead to a thermodynamic stabilisation. The response of the system to the new thermodynamic situation would be a re-equilibration of the mixture resulting in the amplification of the stabilised complex. Such a mixture, in which the compounds are connected to each other by dynamic equilibria and which is able to adapt to the environment, is called a dynamic combinatorial library (DCL). DCC combines self-assembly and molecular recognition under thermodynamic control to pick out the best suited molecule out of a large potential collection.

This approach is illustrated in Figure II.1.[179] Several subunits assemble to form a small dynamic combinatorial library. The concentration of each member of the library depends on the corresponding relative thermodynamic stability, here represented by the number of small balls in the wells of the free energy landscape of the library. The added template interacts specifically with one member of the library. The host-guest complex will be thermodynamically stabilised leading to its amplification and the simultaneous extinction of the other members.[179–185] A comprehensive review about dynamic combinatorial chemistry has been appeared recently.[186]

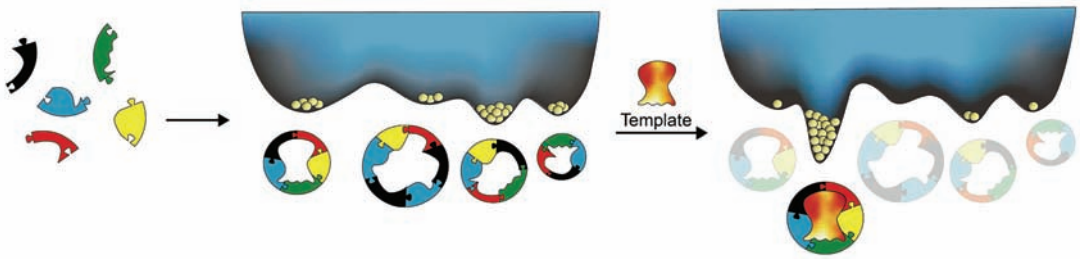

Figure II.1 A small dynamic combinatorial library and its free energy landscape showing the effect of adding a template that strongly and selectively binds to one of the equilibrating species. Reprinted with permission from Elsevier from ref. [179].

Amplification of the Fittest The paradigm of DCC states that the ratio of a library member in the mixture is correlated to the relative thermodynamic stability. Thus, the thermodynamically most stable member should be the species with the highest concentration in solution. Starting from a DCL without any thermodynamic preference – i.e. from a statistical distribution of the library members – the thermodynamically most stable member *after templating* should also show the highest amplification factor[c], leading to expressions such as 'amplification of the fittest' or 'molecular Darwinism'.[181, 187]

II.I.3 Dynamic Combinatorial Libraries

The term dynamic combinatorial library occurred for the first time in the mid 1990s, with some seminal publications from Sanders,[188–191] Lehn[192–194] and other research groups.[195–200] The group of Sanders presented the 'living' macrolactonisation of oligocholates and cinchonidine under thermodynamic control. Although, any kind of linear or cyclic compound could potentially be formed, only trimers were obtained in the case of cinchonidine,[188] and mixtures of dimers, trimers and tetramers in the case of oligocholates.[189] Lehn presented a metal-based system,[192–194] in which size and shape of the assemblies depended on the employed anion. A tris-bipyridine ligand was mixed with metal ions preferring octahedral coordination such as Fe^{II}. Thus, a DCL of circular helicates was generated, which could in principle differ in size from squares (four metal ions), to hexagons (six metal ions) and larger constructs. Using chloride anions as template, pentagonal helicates formed in quantitative yield; the use of larger anions resulted in the formation of hexagons.

A remarkable DCL has been presented recently by Sanders.[201] An acetylcholine target was shown to amplify a high affinity catenane receptor from a DCL of macrocycles with hydrazone linkages (Figure II.2). The library consists mostly of cyclic oligomers, and catenane species are not detectable in the absence of the target. Acetylcholine binds to a single catenane diastereomer in one specific conformation with an exceptional high binding constant. This example demonstrate nicely the power of DCC, as a catenane structure being the best binder was highly unexpected.[201]

Selection experiments with DCLs have been performed by using various target molecules such as alkali metal ions,[202–205] alkaline earth metal ions,[206] alkylammonium ions,[207–210] anions,[211] *N*-heterocycles,[212–214] crown ethers,[215] uracil derivatives,[216] halocarbons,[217–219] biphenyl,[220] nucleic acids,[221, 222] small peptides,[223, 224] proteins,[225, 226] protein crystals,[227] and transition state analogues.[228]

c. The amplification factor *f* is defined as the ratio of the stabilised and the non-stabilised library member.

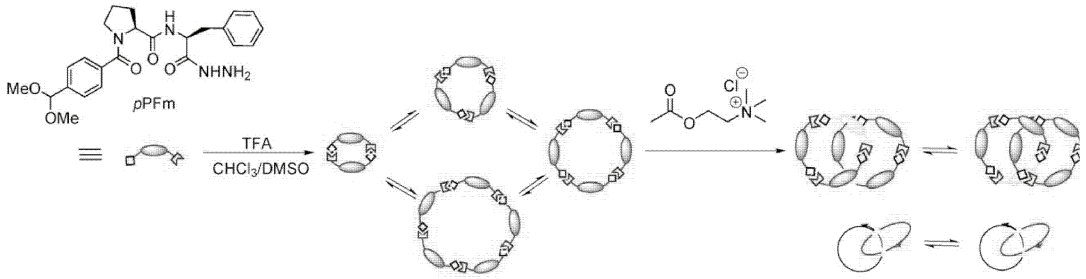

Figure II.2 Amplification of an interlocked structure as best binder from a DCL.[201]

Structural Diversity Structural diversity in DCLs can be obtained by covalent and non-covalent bond formation under thermodynamic control, as well as by reversible conformational or configurational changes and photochemical equilibria. In a DCL, several nearly isoenergetic assemblies[d] built up from the same reactive building blocks, define an ensemble of products. The number of products, which may potentially be formed, depends on the valency of the building blocks. Two fundamental systems can be distinguished. Whereas in an open system the number of products which may form is infinite, a predetermined number of products is characteristic for closed systems. Open systems are formed by building blocks with at least two valencies, and closed systems are formed by building blocks having only one valency. Therefore, a mixture of **m** amines and **n** aldehydes can not form more than $\mathbf{m} \times \mathbf{n}$ imines, but a mixture of **n** amino-aldehydes could form $\mathbf{n}^2$ different dimers, $\mathbf{n}^3$ trimers, $\mathbf{n}^4$ tetramers, and so on. More complex topologies can be accessed by mixing building blocks with different valencies. The diversity of an open system cannot be fully expressed and is for this reason termed virtual diversity.[181] In principle every kind of supramolecular or metal-directed self-assembly employing non-covalent bond formation could be seen as an open virtual system.

Virtual Combinatorial Libraries As pointed out by Lehn,[181] it can be distinguished between *dynamic* and *virtual* combinatorial libraries. The term dynamic is correct, but in most cases incomplete as it refers only to the ability of the library constituents to reversibly convert. However, if all *potential* combinations should be included in the description, whether they are present in the mixture or not, the term *virtual* seems better as it expresses both, reversibility and entireness of the system. In the following the term DCL will be used, and the term VCL only in cases where virtual member of the library are involved.

d. From now on, the notion 'assembly' will also include reversible covalent bond formation under thermodynamic control.

Casting & Molding The template, which will be added in order to shift the dynamic equilibrium, can be either a ligand or a receptor. The first case is called molding: the aim is to find a suited receptor for a certain ligand. The second case is called casting, as a receptor is employed to find the best suited ligand.[181] The concept of molding and casting is shown in Figure II.3.

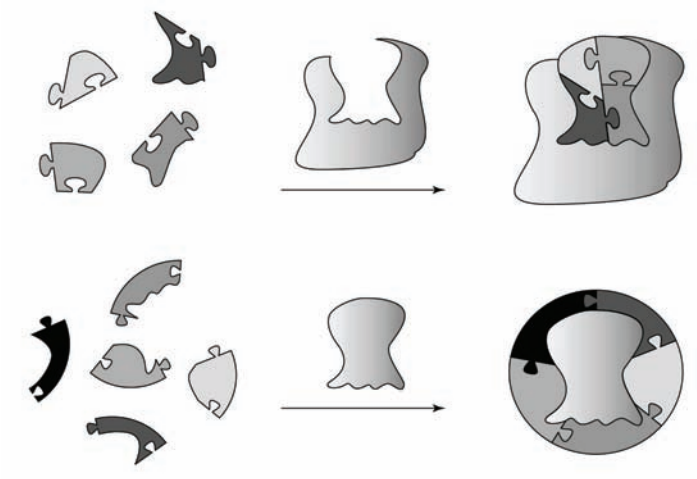

Figure II.3 DCLs can be templated by receptor molecules (top) or ligand molecules (bottom). Reprinted with permission from Elsevier from ref. [183].

Traditional vs. Dynamic Combinatorial Libraries Traditional combinatorial libraries (CLs) and DCLs are complementary in their characteristics as well as in their strengths and weaknesses. The strengths of one are the weaknesses of the other. Traditional CLs consist of a static and real set of molecular constituents which were synthesised in a systematic fashion in absence of any target. The different parts of the molecules are connected by covalent, non-reversible bonds. Generation and screening are two completely separated steps. DCLs on the other hand have a virtual and dynamic set of molecular or supramolecular constituents; their building blocks are connected to each other by reversible covalent or non-covalent bonds. There is no systematic synthesis of every single members, but recognition-directed self-assembly in the presence of the target will reveal certain members of the library as potential hits. There is no longer a distinct separation of generation and screening of the library. Traditional CLs are a collection of prefabricated discrete molecules, and DCLs only a collection of components. The library members are expressed as an adaptive response to the environment.[181]

Advantages There are three main advantages of DCLs over traditional CLs. As the building blocks are continuously interchanging between the different members of the DCL, a binding event leads to the *amplification* of the desired compound(s) at the *expense* of the other library members. This facilitates enormously the screening: a simple compar-

ison of the library distribution before and after templating is sufficient. In some cases amplification is even efficient enough to enable isolation of the hit directly from the library, in a preparative scale and in high yield. DCLs still follow the need of structural variety but with a large decrease in synthetic effort. Complex topologies are a lot easier to access, as only the building blocks have to be modified in a way to allow assembly of higher complexity. Ideally preparation, screening and isolation will be achieved in one step.[183]

Limitations Although the reversible linkage between the building blocks is the intrinsic advantage of DCLs, it constitutes also one of the major limitations, as there is only a very limited number of reversible reactions available. Also, many methods developed in traditional combinatorial chemistry are not compatible with DCC. Once formed, irreversible bonds remain fixed and unaffected by subsequent reactions, whereas reversible bonds do not necessarily. Maybe the most important point is solubility. Each library member of a DCL *must* be soluble enough. If the re-dissolving rate of a precipitate is very slow, the product, and all the building blocks it is comprised off, will be kinetically trapped. The sudden decrease of certain building blocks will have a significant influence on the overall composition of the library and the outcome of the DCL experiment in general.[183]

A summary of the comparison between traditional combinatorial libraries and DCLs is given in Table II.1.[183]

Table II.1: Comparison of traditional combinatorial libraries with DCLs.[183]

Traditional Combinatorial Libraries	Dynamic Combinatorial Libraries
Concentrations are unaffected by recognition events	Molecular recognition can induce amplification
Selected compounds need to be re-synthesised	Selected compounds can be isolated from the library
Complex topologies are difficult to access	Complex topologies are easily accessible
Many irreversible reactions available	Number of suitable reversible reactions is limited
Insolubility of library members of no consequence	All library members need to be soluble
Control over every individual reaction step	Limited control due to the reversibility

Employed Reversible Reactions Reactions which can be used in DCC should fulfil several requirements. The reaction has to be reversible and the exchange process should be fast. In addition, the reaction should be carried out under mild conditions, show tolerance towards other functional groups and no interference with the recognition event. For analytical reasons, the re-equilibration should be possible to switch off. The switch off of the exchange should neither affect the library composition nor the characteristics of the library members, such as binding properties etc. Finally, the isolated product should be stable under the conditions in which it will be used later.

These are severe limitations and the choice of possible reactions is narrowed down significantly. The remaining reactions can be classified into three different types: reversible covalent and non-covalent bond formation and reversible intramolecular processes. Examples of reversible covalent reactions are disulfide formation, Diels-Alder reactions, Michael reaction, olefin metathesis and reactions of the carbonyl group: imine and (hemi)acetal formation, transacylation and aldol formation. Non-covalent reversible reactions are hydrogen bonding, metal–ligand coordination, electrostatic and donor acceptor interactions. As reversible intramolecular processes can be cited configurational isomerisations (e.g. cis-trans isomerisations) and conformational changes such as internal rotations or ring inversions.[181, 229] Among the most commonly used reactions are hydrogen bonding, metal–ligand coordination, transimination of hydrazones and oximes, disulfide exchange and olefin metathesis.[183, 230]

II.II Results and Discussions

II.II.1 Classification of Dynamic Combinatorial Libraries

A DCL can assemble from one or several building blocks and the different members can have a fixed or variable stoichiometry.[e] In principle, it has also to be distinguished if the building blocks *or* the assemblies formed by them are the main species of the library (DCL vs. VCL). Furthermore, it makes a difference if each subunit can react with every other subunit and if each member of the library can be converted into every other member of the library (Type A vs. Type B & Type C). These different network topologies have a major influence on the adaptive behaviour of DCLs and have absolutely be considered when designing an amplification experiment. Three different main types of DCLs can be distinguished.[f]

Type A A DCL of Type A consists of only one building block. Structural diversity is generated by the number of building blocks which assemble (Scheme II.1). As only one subunit is employed, there are no restrictions regarding the reactivity of the building blocks towards each other; it also means that each member of the library can be converted into every other member. Experimental examples of libraries of Type A are by far the most common in the literature.[188, 192, 193, 204, 207, 208, 210, 215]

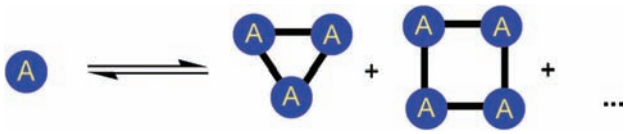

Scheme II.1 DCL of Type A: One building block assembles with variable stoichiometry.

Type B Libraries of Type B consist of different building blocks which assemble to oligomeric species with fixed aggregation number (Scheme II.2). It has to be distinguished between libraries in which each building block is able to associate with every other building block or not. Depending on the type of interaction which is used to link the subunits, this is not necessarily the case. Two characteristics are worthwhile to mention. First, the library can collapse into one single member, if this member reflects the overall composition of the library. Second, an amplification of a member comprised of one building block will always lead to the concomitant amplification of members comprised

e. The term 'stoichiometry' is used simply to indicate the number of subunits of a certain assembly. It is not meant to characterize the nature of the subunits.

f. In principle, all these types of DCL can be comprised of linear and/or cyclic assemblies – the graphical focus on cyclic assemblies was chosen for reasons of consistency with the later presented experimental data.

of the other building blocks leading therefore to the amplification of false positives. There are few experimental examples of libraries of Type B in the literature.[212, 231]

Scheme II.2 DCL of Type B: Different subunits assemble with fixed stoichiometry.

Type B* A variation of the latter class are DCLs of Type B*, which are obtained by assembly of different building blocks with uniform aggregation number but all members of the library have at least one common subunit, for example a common spacer or bridging ligand (Scheme II.3).

Scheme II.3 DCL of Type B*: Different building blocks assemble with fixed stoichiometry; the assemblies have at least one common building block.

Type C DCLs of Type C are a hybrid of Type A and Type B. Different building blocks assemble to form species with different aggregation numbers (Scheme II.4). As for Type B, false positives can be amplified and it has to be distinguished if each subunit can react with every other subunit. DCLs of Type C have been investigated experimentally.[209, 218, 228, 232]

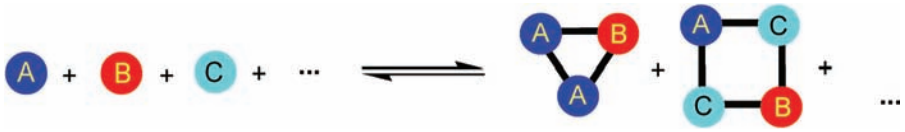

Scheme II.4 DCL of Type C: Different subunits assemble with different stoichiometries.

Compared to the wealth of experimental data there is a surprising lack of theoretical analyses concerning the adaptive behaviour of DCLs. Simple calculations of the steady-state concentrations of members of a DCLs as a function of their thermodynamic stabilisation to investigate the adaptive behaviour of DCLs have not been presented so far.

II.II.2 Theoretical Investigations

Numerical simulations have been performed to study the effect of thermodynamic differences on the steady-state concentration of members of a library of Type B. In libraries of Type B, several structurally diverse building blocks can form assemblies of fixed stoichiometry; cyclic trimeric assemblies X_3 were chosen.[g] In the following, it will be shown that DCLs of Type B and C can display an adaptive behaviour fundamentally different from that of libraries of Type A. It will be demonstrated, that there is no direct correlation between the relative amplification and the thermodynamic stability of the DCL members in such systems.

Assumptions The calculations are based on the assumption that all assemblies are in equilibrium with their corresponding building blocks. It is further assumed, that every building block is able to associate with every other building block. Equimolar amounts of three different building blocks A, B, and C assemble to form trimeric assemblies X_3. For the present discussion, the focus has been on DCLs, i.e. the equilibrium constants favour trimeric assemblies and were chosen so high that the concentration of the building blocks in the solution is neglectable. The association constants was therefore fixed to $K_{XXX} = 1 \times 10^5$ mM^{-2}. The relative steady-state concentration of the different library members were calculated using the program Gepasi, version 3.30.[233, 234]

Thermodynamic preferences were introduced by arbitrarily stabilizing certain members of the library. Conclusions about the characteristics of the adaptive behaviour of DCLs could be drawn by comparison of the steady-state concentrations of a library without thermodynamic preference with those having thermodynamic preferences. It has to be noted, that for the present discussion it is irrelevant whether the thermodynamic differentiation between the DCL members is caused by binding to a guest molecule, by binding to a receptor, or by arbitrarily introducing them. The underlying model is held purposely very simple and some extreme situations are presented to demonstrate the peculiar characteristics of these DCLs. The relative steady-state concentrations as a function of the relative stability of the respective library member are presented in Table II.2.

g. Cyclic trimeric assemblies were chosen for reasons of consistency with the experimental data presented later.

Table II.2: Calculated steady-state concentrations of a dynamic mixture of macrocycles with fixed stoichiometry X_3 obtained by assembly of three different building blocks ($[A]_{total} = [B]_{total} = [C]_{total}$).

Entry	Relative Stability Relative Concentration / %									
										
1	1 3.7	1 11.1	1 11.1	1 3.7	1 11.1	1 11.1	1 3.7	1 11.1	1 11.1	1 22.2
2	1000 28.1	1 0.5	1 3.4	1 7.2	1 21.5	1 21.5	1 7.2	1 0.5	1 3.4	1 6.8
3	1 0.0	1000 47.7	1 0.5	1 1.9	1 11.1	1 21.2	1 13.5	1 0.1	1 1.9	1 2.0
4	1 0.0	1 0.1	1 0.1	1 0.0	1 0.1	1 0.1	1 0.0	1 0.1	1 0.1	1000 99.6
5	1000 0.4	1 0.0	1 0.1	1 0.1	1 0.3	1 0.3	1 0.1	1 0.0	1 0.1	1000 98.6
6	900 0.1	600 2.1	300 22.8	1 0.5	1 1.6	1 1.6	1 0.5	600 2.1	300 22.8	300 47.7

The data for a statistical mixture without thermodynamic preferences is given in Entry 1. The following three entries describe the hypothetical[h] cases that only one member of the library is stabilised (e.g. by selective binding to a suited guest molecule). If the assembly AAA is stabilised by a factor of 1000, it is amplified relative to the original equilibrium concentration by a factor of $f_{AAA} = 7.6$ and subsequently represents the dominant species in solution (Entry 2). Upon selective stabilisation of AAB (Entry 3), a similar result is obtained: AAB is clearly the dominant species in solution (47.7%; $f_{AAB} = 4.3$). As typical for libraries of type B, in both cases species with a high content of B and C such as BBC and CCC are likewise amplified to a considerable extent (e.g. Entry 3: $f_{CCC} = 3.6$). A rather dramatic effect is observed upon selective stabilisation of ABC (Entry 4): the whole mixture collapses to give almost exclusively ABC. The steady state concentrations of a mixture in which both AAA and ABC are stabilised relative to the other members are given in Entry 5. Remarkably, only ABC is amplified and completely dominates the mixture (98.6%). The assembly AAA, on the other hand, goes nearly extinct (0.4%). A more equilibrated situation is described in Entry 6. The incorporation of the fragment A leads to an additive stabilisation by a factor of 300. In this mixture, three species of moderate stability are dominating having the same amplification factor: ABB, ACC and ABC ($f = 2.1$). The most stable assembly AAA, however, is the

h. The examples in Table II.2, entries 2–5 describe extreme situations in which only one or two species of the DCL are stabilised. They were chosen because their results demonstrate the peculiar characteristics of a DCL of Type B. A more balanced situation with a broader distribution of stability constants is more likely for 'real' systems.

species with the lowest concentration of all members (0.1 %). We thus observe the quasi-extinction of the thermodynamically most stable species in the mixture.

This theoretical analysis demonstrates that a DCL can adapt in a way, which is quite different from the paradigm 'amplification of the fittest'.[187] It is not necessarily the most stable member of the library, which is amplified the most. Quite contrary, it is possible that the most stable member goes extinct and that members of mediocre or low stability are amplified. Further analyses of related model systems show that a behaviour of this kind can also be found for DCLs of non-cyclic assemblies and for libraries of Type C as is presented in Table II.3 and Table II.4, respectively.

Table II.3: Calculated steady-state concentrations of a dynamic mixture of dimers obtained by assembly of different building blocks (K_{XX} >> 1; $[A]_{total} = [B]_{total} = [C]_{total}$).

	Relative Stability Relative Concentration / %					
Entry	A–A	A–B	B–B	A–C	B–C	C–C
1	1 11.1	1 22.2	1 11.1	1 22.2	1 22.2	1 11.1
2	1000 31.9	1 1.4	1 16.3	1 1.4	1 32.6	1 16.3
3	1 0.0	1000 64.6	1 0.0	1 2.0	1 2.0	1 31.3
4	1000 3.0	1000 60.1	1 0.3	1 0.6	1 6.0	1 30
5	10,000 6.5	1000 53.4	1 1.1	1 0.3	1 11.0	1 27.7
6	600 0.2	300 33.1	1 8.4	300 33.1	1 16.8	1 8.4

Table II.3 shows the data of a DCL of equimolar amounts of three different building blocks which can assemble into dimers. It should be noted, that this library can not collapse into one single member, as formation of dimers from three different building blocks will always leave at least one building 'unused' resulting in the concomitant amplification of dimers comprised of this building block. Absence of any thermodynamical preference results in a statistical distribution of all DCL members and is given in Entry 1. Stabilisation of dimer AA or AB results in their amplification by a factor of $f_{AA} = f_{AB} = 2.9$, respectively (Entry 2 and 3). Entry 4 shows a competition situation between the dimers AA and AB. Both are stabilised by a factor of 1000, but only AB is amplified and AA goes again almost extinct. A 10fold increase of its stabilisation compared to AB (Entry 5) does not lead to an amplification in its favour. Even when experiments to eliminate the false positives were carried out, the most stable member of the DCL would again be undetected. In a more equilibrated situation such as presented in Entry 6, the most stable mem-

ber AA goes also extinct and hetero-assemblies of mediocre stability are amplified the most. In all cases, the concomitant amplification of dimers comprised of the remaining building blocks is observed. This shows, that the behaviour of a DCL of linear assemblies is similar to the behaviour of a DCL comprised of cyclic assemblies.

An investigation of the behaviour of a DCL of Type C is shown in Table II.4. Equimolar amounts of three different building blocks A, B and C (100 mM each) can assemble into dimers and trimers. Whereas A and B can be linked to only one other building block, C can be linked to two other building blocks. Thus, a DCL of eight possible assemblies is generated: four linear dimers AA, AB, BB & CC, two linear trimers ACA & BCB and one cyclic trimer CCC.

Table II.4: Calculated steady-state concentrations of a dynamic mixture of dimers and trimers obtained by assembly of three different building blocks (K_1 = 1 x 10^8 M^{-1}, K_2 = 1 x 10^{13} M^{-2}; $[A]_{total} = [B]_{total} = [C]_{total}$ = 100 mM)

	Stability Constant Absolute Concentration / mM							
Entry					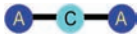	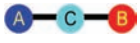		
1	K_1 12.5	K_1 25.0	K_1 12.5	K_1 10.0	K_2 12.5	K_2 25.0	K_2 12.5	K_2 10.0
2	$10^3 \times K_1$ 47.7	K_1 2.1	K_1 22.2	K_1 13.2	K_2 0.1	K_2 2.4	K_2 25.6	K_2 15.2
3	K_1 0.1	$10^3 \times K_1$ 99.6	K_1 0.1	K_1 16.9	K_2 0.1	K_2 0.1	K_2 0.1	K_2 22.0
4	K_1 0.1	K_1 2.5	K_1 0.3	K_1 0.4	$10^3 \times K_2$ 47.7	K_2 2.0	K_2 21.3	K_2 5.3
5	K_1 0.3	K_1 0.5	K_1 0.3	K_1 0.4	K_2 0.1	$10^3 \times K_2$ 98.9	K_2 0.1	K_2 0.1
6	K_1 0.0	K_1 0.1	K_1 11.1	K_1 3.1	$10^5 \times K_2$ 17.3	$10^3 \times K_2$ 65.3	K_2 6.2	K_2 1.7
7	K_1 2.8	K_1 5.7	K_1 2.8	K_1 0.0	K_2 0.0	$10^3 \times K_2$ 88.5	K_2 0.0	$10^5 \times K_2$ 3.8
8	$600 \times K_1$ 2.6	$300 \times K_1$ 32.3	K_1 2.6	K_1 8.0	$600 \times K_2$ 2.4	$300 \times K_2$ 57.8	K_2 2.4	K_2 7.2

The association constants K_1 and K_2 were chosen so as to result in a DCL without any thermodynamic preference in which the presence of each member reflects a statistical distribution (Entry 1). Stabilisation of a single member of the library by a factor of 1000 results in its amplification as well as in the concomitant amplification of members composed of 'unused' building blocks (Entry 2–4). Entry 5 shows a case, where the member which reflects the overall composition of the library, ACB, is stabilised by a factor of 1000. Similar to a DCL of Type B, the library collapses to give almost exclusively ACB.

Also in competition situations, the library behaves analogously. Stabilisation of ACB by a factor of 1000 and ACA or CCC by a factor of 100000 will still bias the library in favour of ACB (Entry 6 and 7). The reason for this behaviour can be seen in the fact that the amplification of a member of mediocre stability, which integrates all building blocks, will lead to a thermodynamically more stable *mixture* than the amplification of a member which integrates only parts of the subunits would do. This is even the case if this member is clearly the thermodynamically most stable one. The focus has to be on the thermodynamically most stable *mixture* and not on the thermodynamically most stable *member*.

Overall, the theoretical analyses predict that libraries of Type B and C behave in the same manner, whether the building blocks form linear, cyclic or both assemblies. In general, they display the following characteristics:

1. The selection of an assembly with a high content of one subunit will lead to the concomitant amplification of one or more assemblies comprised of the other subunit(s).
2. There is an intrinsic bias for the selection of hetero-assemblies, or more precisely, for assemblies, the composition of which reflects the overall composition of the library.[i]

For libraries of Type A, on the other hand, these ‘restrictions’ do not apply because the members compete for the same resource: the common building block. The same is true for DCLs which are based on reversible conformational changes.[198, 235]

II.II.3 Investigation of a synthetic DCL of Type B

To demonstrate that the above mentioned characteristics can indeed be found in synthetic DCLs, the equilibrium concentrations of dynamic mixtures of metallamacrocycles were investigated. 12-metallacrown-3 complexes were expected to be ideally suited starting materials for the generation of DCLs because their framework contains labile metal–ligand bonds. They consist of three subunits, which represent the building blocks of the library. In methanol, a fast equilibrium between the subunits and the trimeric assemblies exists, with the equilibrium far on the side of the assemblies. Mixing of different 12-metallacrown-3 complexes results in a library of Type B: different building blocks assemble into aggregates with a fixed stoichiometry of three subunits. The metallamacrocycles employed are shown in Scheme II.5.[124] In analogy to the presented theoretical data, they are named **aaa**, **bbb** and **ccc**, each letter representing a subunit of the trimeric structure $\mathbf{x_3}$.

i. A library of Type B composed of equal amounts of three different building blocks A, B and C, for example, will show a bias for the selection of the assembly ABC.

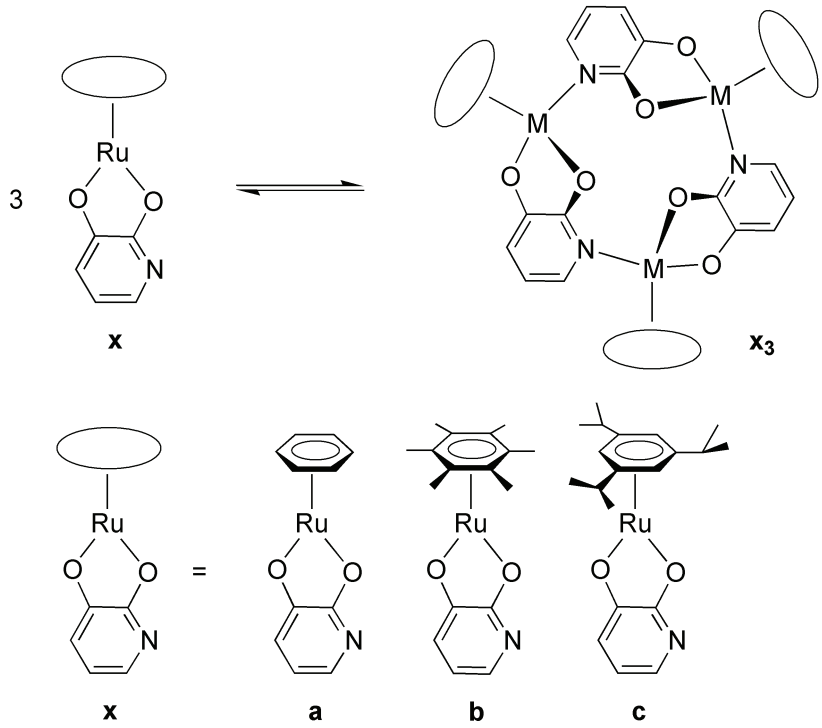

Scheme II.5 Trimeric 12-metallacrown-3 complexes employed for the generation of a DCL of Type B.

Instead of using a target molecule to induce the selection process, steric effects have been chosen to introduce thermodynamic differences among the DCL members. As already mentioned, for the present discussion it is irrelevant whether the thermodynamic differentiation between the DCL members is caused by binding to a guest molecule, by binding to a receptor, or by steric effects. For this purpose, the new metallamacrocycle **ccc** with sterically demanding π-ligands was synthesised. The structure of this complex in the crystal shows that the three triisopropylbenzene ligands are in very close proximity to each other and the space filling representation illustrates nicely the steric overload (Figure II.4).

As a result of this steric congestion, the Ru–Ru distance of 5.40 Å is increased when compared to the (benzene)Ru complex **aaa** (Ru–Ru = 5.32 Å) (see Table IX.10 on page 227 for more structural data). A similar expansion of the macrocycle was observed for the (hexamethylbenzene)Ru complex **bbb** (Ru–Ru = 5.46 Å).[124] These data indicate that the macrocycles **bbb** and **ccc** are less stable than **aaa** due to steric repulsion of the π-ligands.

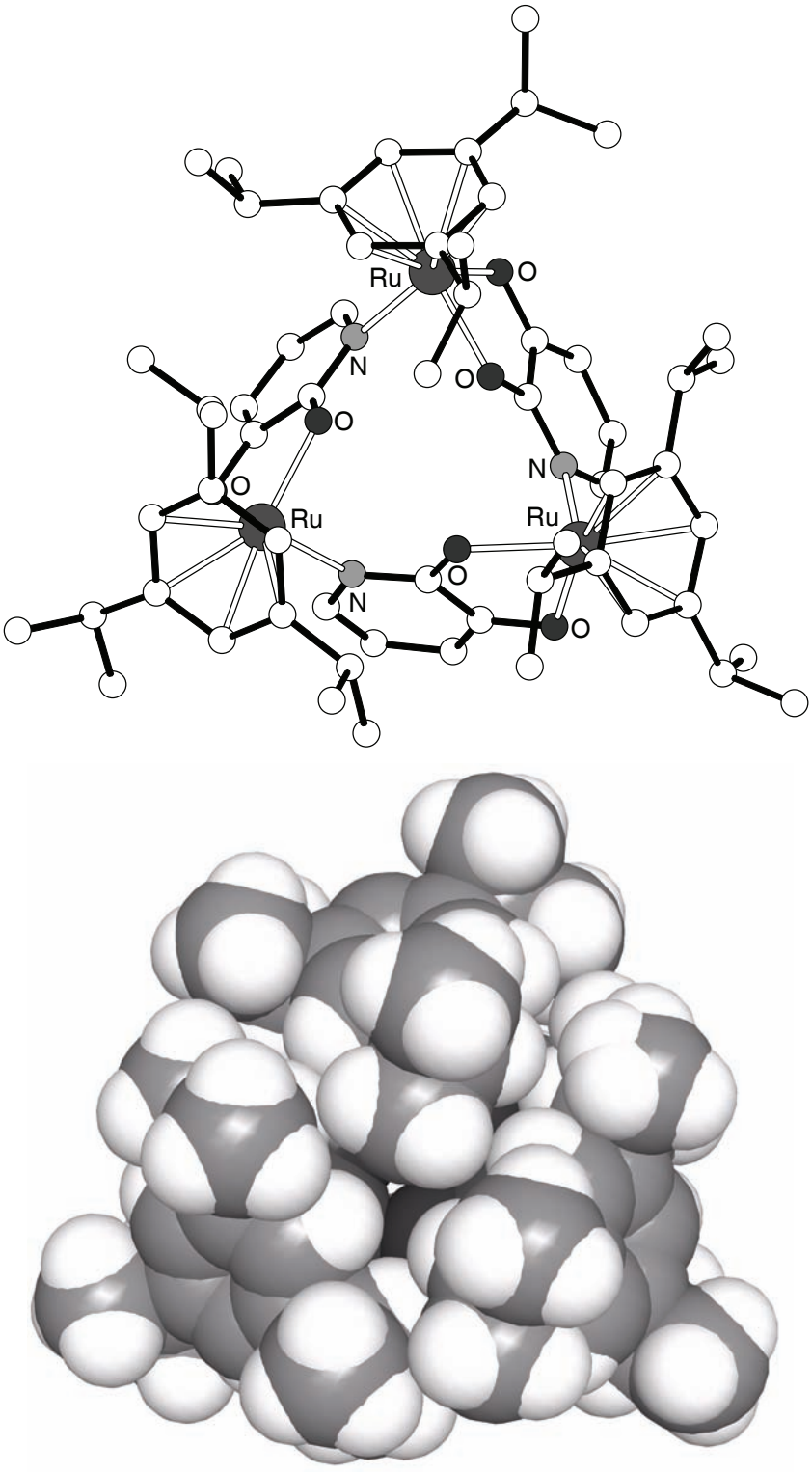

Figure II.4 Ball and stick (top) and space filling (bottom) representation of complex **[($C_6H_3{}^iPr_3$)Ru(L1−2 H^+)]$_3$** (**ccc**) in the crystal. Solvents molecules are omitted for clarity; hydrogen atoms are not depicted in the picture at the top.

Scrambling of the organometallic fragments occurs when a 1:1 mixture of the symmetrical complexes **aaa** and **ccc** in methanol is heated to 40 °C. The mixed complexes **aac** and **acc** can be observed within several minutes. The steady state concentrations are reached after twelve hours. The reaction can conveniently be followed by ^{1}H NMR spectroscopy if CD_3OD is employed (Figure II.5). Since the exchange of the fragments is slow on the NMR time scale, the relative concentration could be determined by integration of suited signals. The labelled signals correspond to the C_6H_6 (δ = 5.5–5.7 ppm) and to the $C_6H_3{}^iPr_3$ protons (δ = 5.0–5.2 ppm) of the π-ligands of **a** and **c**. The small signals between d = 5.5 and 6.8 ppm correspond to the protons of the bridging pyridonate ligands.

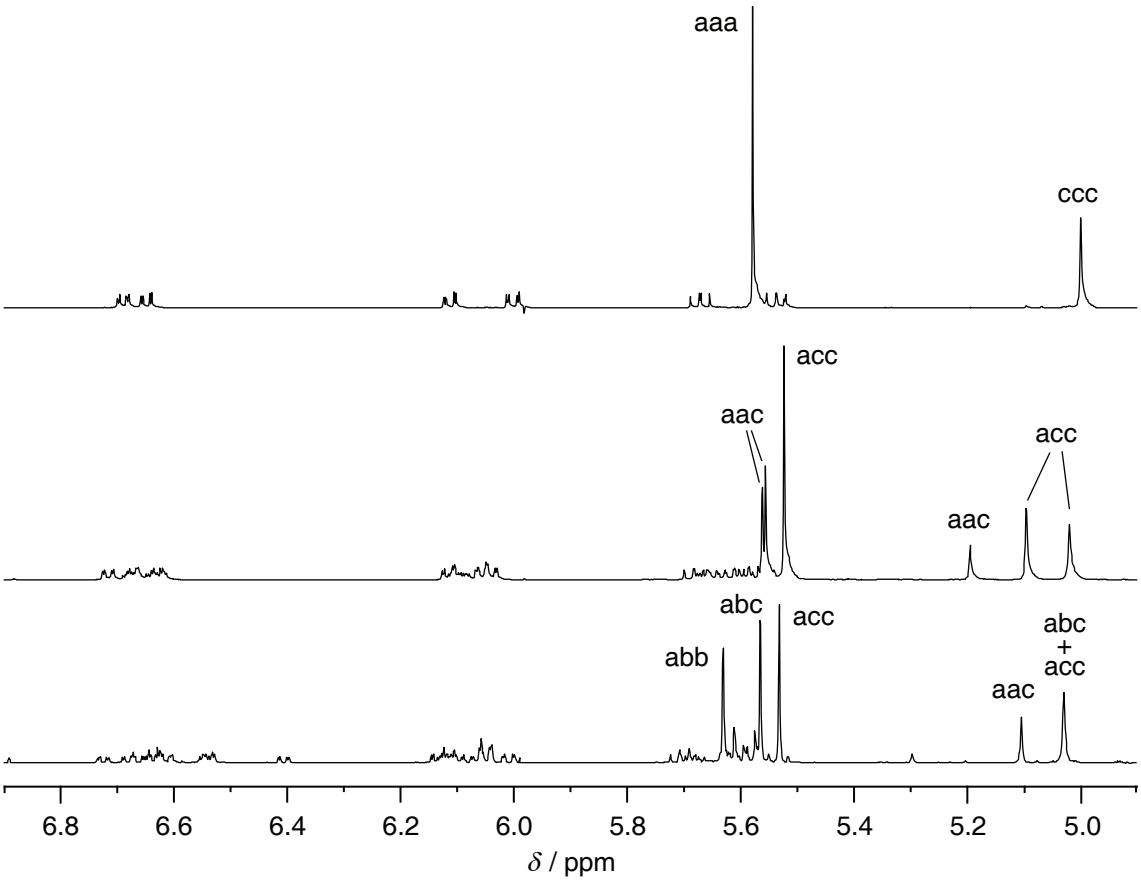

Figure II.5 Aromatic region of the ^{1}H NMR spectrum (CD_3OD) of an equimolar mixture of **aaa** and **ccc** before equilibration (top) and after equilibration (middle), and an equimolar mixture of **aaa**, **bbb** and **ccc** after equilibration (bottom).

The equilibrium concentrations of all possible binary mixtures of **aaa**, **bbb** and **ccc** are given in Table II.5. For a hypothetical mixture with equally stable members, a statistical distribution of 1:3:3:1 is expected. Concentrations approaching these theoretical values are found for a mixture of **bbb** and **ccc**: all four possible species can be detected in the mixture with slight preference for the mixed complex **bcc** (Entry 1). This result

points to the fact that the steric requirements of the large hexamethylbenzene and triisopropylbenzene π-ligands are comparable.

Table II.5: Equilibrium concentrations of the four metallamacrocycles obtained by scrambling of equimolar amounts of two homotrimeric complexes in CD_3OD.[a]

Entry	Starting mixture		Equilibrium mixture			
1			 14%	19%	49%	18%
2			 < 3%	45%	55%	< 3%
3			 < 3%	45%	55%	< 3%

a. The relative concentration was determined by integration of selected ^{1}H NMR signals. The error is estimated to be ± 3%.

As soon as thermodynamic differences are introduced, the relative distribution changes substantially (Entry 2 and 3). For mixtures with the small (benzene)Ru complex **aaa**, the hetero-assemblies are completely dominating after equilibration and only traces of the homotrimeric complexes can be detected (Figure II.5). Based on the size of the π-ligands, complexes should become more stable the more **a** fragments they contain. In accordance with the theoretical predictions, this leads to the selection of the mixed species **aab/abb** and **aac/acc**, respectively, and not of the most stable species **aaa**.

A DCL obtained by mixing all three complexes **aaa**, **bbb**, and **ccc** should display a behaviour which resembles the theoretical model described in Table II.2, Entry 6, since only the incorporation of the fragment **a** will lead to a stabilisation. Consequently, the complexes **abb**, **acc** and **abc** should be selected. And this is exactly what can be observed: the ^{1}H NMR spectrum of the equilibrium mixture showed that these three complexes are clearly dominating the mixture (Figure II.5). This result was confirmed by ^{13}C NMR spectroscopy. Again, it was not the most stable species **aaa**, **aab** and **aac** which were amplified. Quite contrary, the signals of complex **aaa** could not be detected. The competition situation in the described DCL has thus led to the extinction of the most stable assembly.

II.II.4 Amplification of the Fittest

There are possibilities to circumvent or reduce the 'problems', which may be encountered if DCLs of Type B and C are used for selection processes. First, one can conduct the experiment in a way that it is possible to separate the target and the bound DCL

members from the unbound members (e.g. using a target on a solid support or a reaction which destroys unbound members).[199, 221, 225] This will eliminate the false positives, which arise from the concomitant amplification of species, which do not bind to the target. However, this approach does not reduce the intrinsic bias for the selection of hetero-assemblies. Secondly, the DCL can be designed in a way that without target it has an equilibrium distribution in which the monomeric building blocks represent the dominating species and the various aggregates are present in only very small amounts. In this case, the selective stabilisation of one or several aggregates of this virtual combinatorial library[181] will give rise to amplification factors which are not only significantly higher, but which also correspond much closer to the relative thermodynamic stability. Furthermore, there will be no concomitant amplification of assemblies, which do not bind to the target. Some experiments, which confirm this prediction, have been described recently.[226, 236–238] A theoretical analysis of a VCL amplification experiment analogous to that of a DCL of Type B is shown in Table II.6.

Table II.6: Calculated steady-state concentrations of a virtual combinatorial library with fixed stoichiometry X_3 obtained by the assembly of three different building blocks (K_{XXX} = 0.1 M^{-1}; $[A]_{total} = [B]_{total} = [C]_{total}$ = 100 mM).

	Relative Stability Absolute Concentration / mM												
Entry	AAA	AAB	ABA	ABB	BBC	BCB	CCC	ACA	CAC	ABC	A	B	C
1	1 0.1	1 0.3	1 0.3	1 0.1	1 0.3	1 0.3	1 0.1	1 0.3	1 0.3	1 0.6	97.5	97.5	97.5
2	10^3 15.2	1 0.1	1 0.2	1 0.1	1 0.3	1 0.3	1 0.1	1 0.1	1 0.2	1 0.3	53.4	98.2	98.2
3	1 0.0	10^3 30.5	1 0.1	1 0.0	1 0.1	1 0.2	1 0.1	1 0.0	1 0.1	1 0.2	38.5	68.6	98.7
4	1 0.0	1 0.0	1 0.0	1 0.0	1 0.0	1 0.0	1 0.0	1 0.0	1 0.0	10^3 54.8	45	45	45
5	10^3 4.5	1 0.0	1 0.0	1 0.0	1 0.0	1 0.0	1 0.0	1 0.0	1 0.0	10^3 50.9	35.5	48.9	48.9
6	10^5 18.3	1 0.0	1 0.0	1 0.0	1 0.1	1 0.1	1 0.0	1 0.0	1 0.0	10^3 32.8	12.2	66.8	66.8
7	900 2.0	600 8.1	300 8.4	1 0.0	1 0.1	1 0.1	1 0.0	600 8.1	300 8.4	300 16.9	27.9	57.9	57.9

Three different building blocks A, B and C form trimeric cyclic assemblies; contrary to a DCL of Type B discussed before, the building blocks are now the main species present in the library. The assemblies are only virtually present as is shown for a statistical distribution of the assemblies in Entry 1. Stabilisation of AAA by a factor of 1000 will lead to an *152fold* amplification and is clearly the dominant *trimeric* species in solution (Entry 2). Entry 3 shows the stabilisation of the mixed assembly AAB by a factor of 1000

leading to a more than 100fold increase of its concentration. If ABC, the member which reflects the overall composition of the library, is stabilised, its concentration increases from 0.6 mM to 54.8 mM corresponding to an *169fold* amplification! In all three cases, no concomitant amplification of other members of the library occurs. If one member of the library is stabilised, the VCL will adapt in such a way that the stabilised member will be expressed. The thermodynamically most stable mixture is the mixture in which the thermodynamically most stable member is amplified the most.

Entry 5 describes the situation where AAA and ABC are both stabilised by a factor of 1000. Even though AAA is amplified by a factor of $f_{AAA} = 45$, ABC is amplified by a factor of $f_{ABC} = 85$, reflecting the bias for hetero-assemblies. In the case of Entry 6, where AAA is stabilised by a factor of 100000, thus 100fold more than ABC, the highest amplification factor *correlates* with the thermodynamic most stable member: AAA is amplified by a factor of $f_{AAA} = 183$ whereas ABC is only amplified by a factor of $f_{ABC} = 55$. However, in the potentially more realistic situation of Entry 7, in which each fragment of A leads to an additional stabilisation by a factor of 300, the bias for hetero-assemblies becomes again visible. The most stable member AAA is only increased by a factor $f_{AAA} = 20$, whereas members with mediocre and low stability will be amplified with a factor of $f_{AAA} = 27$. The highest amplification factors has again the member ABC ($f_{AAA} = 28$), the one reflecting the overall composition of the library to which the library is intrinsically biased.

In competition situations, the library composition still does not always reflect the thermodynamic stabilities of the respective library member. However, the most stable member goes no longer extinct but will also be amplified in solution. Even though the amplification factor does not always correlate with the thermodynamic stability of the members, all hits are present in detectable amounts and a further investigation of their properties will reveal the order of their thermodynamic stabilities.

II.III Conclusions

DCLs have been classified into different types and the adaptive behaviour of DCLs of Type B and Type C has been discussed. The presented theoretical and experimental data are in contradiction with a former paradigm of DCC, i.e. the expression of the thermodynamically most stable member. As the main conclusion it can be stated that it is not necessarily the strongest binder which will be amplified the most in a DCL experiment.

The herein presented data indicates that DCLs of Type B and C behave similarly, whether they are generated from cyclic or linear assemblies, but show a behaviour different from those of Type A. In competition situations, DCLs of Type B and C show an intrinsic bias for hetero-assemblies, especially for compounds which reflects the overall composition of the library. The selection of an assembly with a high content of one subunit involves the concomitant amplification of assemblies comprised of the others subunits. The amplification depends also strongly on whether the experiment is carried out in a virtual fashion or not. If the equilibrium is on the site of the building blocks and not on the site of the assemblies, the amplification factors correlate more closely with the relative thermodynamic stability of the members.

Further simulations have confirmed these results. A recent theoretical study of Severin investigated the adaptive behaviour of simple model DCLs of Type A, B, B* and C as a function of the binding affinity of the different members, the target and the building block concentration.[239] It has been found, that DCLs show generally an intrinsic bias for assemblies with small aggregation numbers and for hetero-assemblies. All examined DCLs show a region, in which the correlation between binding affinity and amplification factor breaks down. Noteworthy, at one specific point, no adaption at all occurs after templating, although the affinities of the DCL members to the target differ substantially. However, this behaviour seems reasonable, considering the urge of the DCL to maximize the binding interactions in the entire library. With a fixed amount of building blocks, the overall stabilisation of a mixture of many small moderate binders is simply higher than the overall stabilisation of a mixture of a few strong binders.

But theory provides also a hint how to design DCL experiments in which the correlation between binding affinity and amplification is acceptable. In general, the bias for small and hetero-assemblies is less pronounced for small binding constants. Most importantly, the thermodynamic gain in stability of a VCL experiment is far more pronounced for the formation of the thermodynamically most stable member. Now, the overall gain in energy is not any longer limited by the total number of building blocks, but by the interaction with the target. As it is not always possible to redesign a DCL into a VCL experiment, it is important to realise, that a similar situation to a VCL experiment is obtained if the common building blocks of DCLs of Type B* are used in substoichiometric quantities.

A different approach is the variation of the target concentration. Again, the thermodynamic gain of the DCL is not dictated by the number of the building blocks, but by the number of the target molecules. Thus, the energetic gain based on a fixed number of target molecules will be higher if thermodynamically more stable members will be expressed instead of members of mediocre stability. This behaviour has been confirmed experimentally by the groups of Severin and Sanders.[240, 241] The correlation between binding strength and amplification in large libraries (between 10 and 106 members) has been investigated theoretically by Sanders and coworkers.[242] In a systematic variation of the 'experimental conditions', they were able to map under which conditions the correlation is acceptable. They found that a disruption of the correlation can also occur in large libraries, but only under very specific conditions. In general, they advise to keep the template concentration at about one tenth of the building block concentration in order to have a high probability that the best binder is among the three most amplified members. For very low building block concentrations, only the template concentration determines the quality of the correlation between amplification and binding affinity.

In conclusion, even though the presented theoretical and experimental results challenged the DCC approach in its generality, it seems apparent that the usefulness of DCL techniques need not to be restricted. The presented work induced several theoretical[239, 242] and experimental[240, 241, 243] publications addressing the question whether the amplifications in DCL experiments reflect the binding affinities of the members and if DCL experiments can be designed in a fashion that they follow the paradigm of 'amplification of the fittest'. The importance of DCC and an enhanced comprehension of the adaptive behaviour of complex equilibrium systems has been highlighted recently.[244] However, success of DCC will finally depend on the creativity of researchers to design the right DCL for a given problem. An excerpt from Sjibren Otto, one of the pioneers of DCC, clearly states the point: "…, when using dynamic combinatorial chemistry, it is important to realise that – as with any combinatorial approach – it will only be successful if the right libraries are designed. Combinatorial chemistry is by no means an excuse to abandon rational design and ignore chemical intuition – it only reduces the level of structural detail required at the design stage."[230]

Chapter III
12-Metallacrown-3 Complexes with Different Metal Fragments

III.I Introduction

As described in the introduction, transition metal-based self-assembly processes have been used extensively to build macrocyclic compounds with diverse structures and functionalities.[27–29, 32, 35, 44, 245, 246] In the majority of these cases, metal complexes M with available coordination sites were combined with bridging ligands L to give symmetrical macrocycles of the type M_nL_n. These reactions are typically performed in a single step under thermodynamic control. Macrocycles containing two different metal fragments M and M', however, are generally constructed in a two-step procedure.[76, 247–261] For mixed-metal squares and rectangles, this is illustrated in Scheme III.1. In a first step, a ditopic ligand is coordinated to a metal M. The resulting complex ML_2 is then reacted with a metal M' to give the tetranuclear complex $M_2M'_2L_4$. Usually, the preformed metal complex ML_2 is kinetically inert under the reaction conditions employed in the second step (Scheme III.1a).[76, 247, 249–252, 254, 256–258, 260] This avoids scrambling reactions, which would lead to mixtures of assemblies with variable M–M' content and position. Alternatively, the formation of mixed-metal assemblies can be favoured by the utilization of ligands having two distinct donor sites, each of which with a pronounced selectivity for the respective metal fragment M or M', respectively (Scheme III.1b).[248, 253, 255, 259, 261] Additional specificity can be achieved by template effects. For the latter case, one-step syntheses of heterometallic macrocycles under thermodynamic control have been reported.[262, 263]

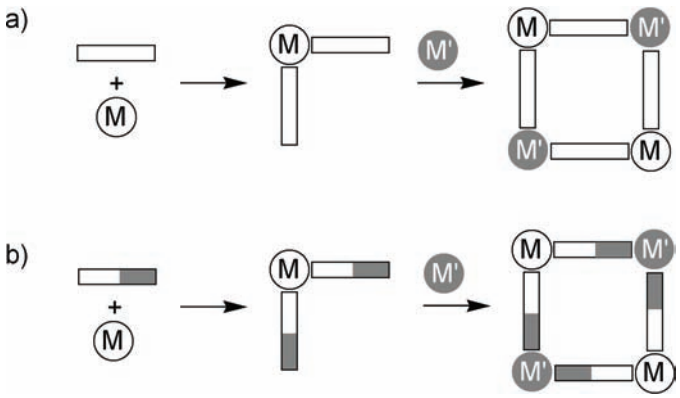

Scheme III.1 Stepwise synthesis of tetranuclear macrocycles containing two different metal fragments M and M'.

An alternative way to access complexes with different metal centres is the scrambling of assemblies with labile metal–ligand bonds. If such a dynamic mixture could be biased towards one product, mixed-metal complexes in synthetically interesting yields would be obtained.

III.II Kinetics of Metal Fragment Exchange

Mixed 12-metallacrown-3 complexes formed upon mixing of homotrimeric complexes via metal fragment exchange. The driving force of their formation is the intrinsic bias of dynamic mixtures towards hetero-assemblies as shown in the previous chapter. To obtain more information about the formation, the kinetics of the metal fragment exchange process were studied by ^{1}H NMR spectroscopy. First, the scrambling reaction of **[($C_6H_3{}^iPr_3$)Ru(L1−2 H^+)]$_3$** (**AAA**) and **[(cymene)Ru(L1−2 H^+)]$_3$** (**BBB**) has been investigated. The complexes were mixed in MeOH in a 1:1 ratio, with an initial concentration of 5.0 mM each. To accelerate the scrambling process, the solution was heated to 40 °C. The time course is depicted in Figure III.1.

The beginning of the reaction was marked by the fast decrease of **AAA**, and a rapid increase of **AAB.** The formation of **ABB** was almost negligible in the first 15 minutes. During this period, the decrease of **AAA** was almost twice as fast as the decrease **BBB**. After 40 minutes a turning point was reached. The concentration of **AAB** was at its maximum and represented 68 % of the total trimer concentration. Subsequently, a decrease of **AAB** and a concomitant increase of **ABB** was observed. Accordingly, the concentration-time profile of **ABB** showed a sigmoidal form. After six hours, the mixture was at equilibrium and only the two mixed complexes **AAB** and **ABB** were found in solution, both with an approximate concentration of 50 %.

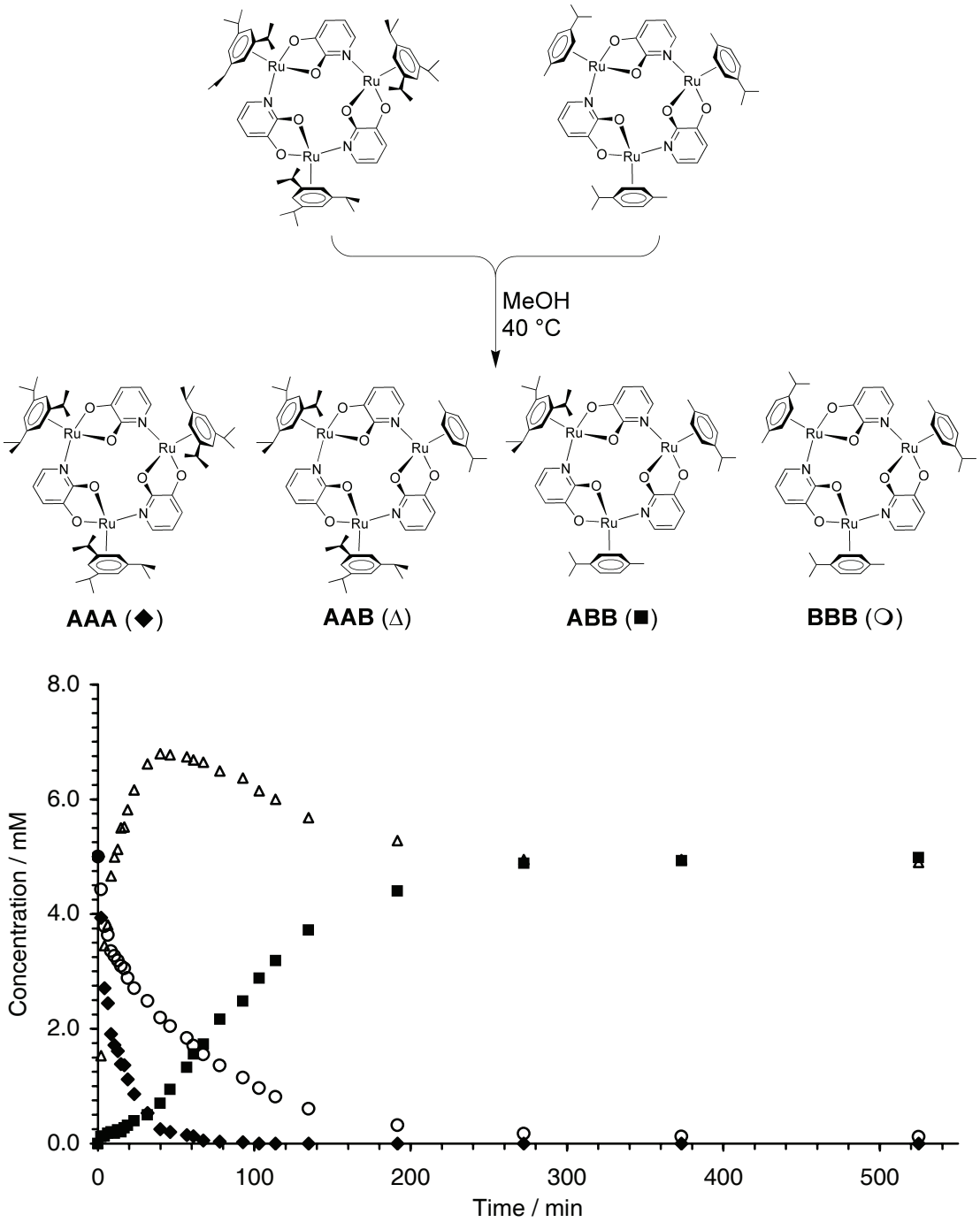

Figure III.1 Time course of the reaction between **AAA** (◆) and **BBB** (❍) to give the mixed-metal macrocycles **AAB** (Δ) and **ABB** (■) as determined by ^{1}H NMR spectroscopy. The reaction was performed in CD_3OD 40 °C with initial concentrations of $[\mathbf{AAA}]_0 = [\mathbf{BBB}]_0$.= 5.0 mM. The total trimer concentration was $[\text{trimer}]_{\text{total}}$ = 10 mM.

For equally stable macrocycles, a statistical mixture of **AAA**:**AAB**:**ABB**:**BBB** of 1:3:3:1 would be expected. At first glance, the complete dominance of **AAB** and **ABB** after equilibration might suggest a preferential stabilisation of the mixed complexes with respect to the homotrimers **AAA** and **BBB** (Situation a, Figure III.2). But there is another explanation for such a distribution: the B-rich species **ABB** and **BBB** are stabilized and the homotrimer **AAA** is significantly destabilised (Situation b, Figure III.2). For $\Delta\Delta G1 = \Delta\Delta G2 = ½\ \Delta\Delta G3$, the two situations result in the same equilibrium distribution with equal amounts of heterotrimers being the dominant species in solution.

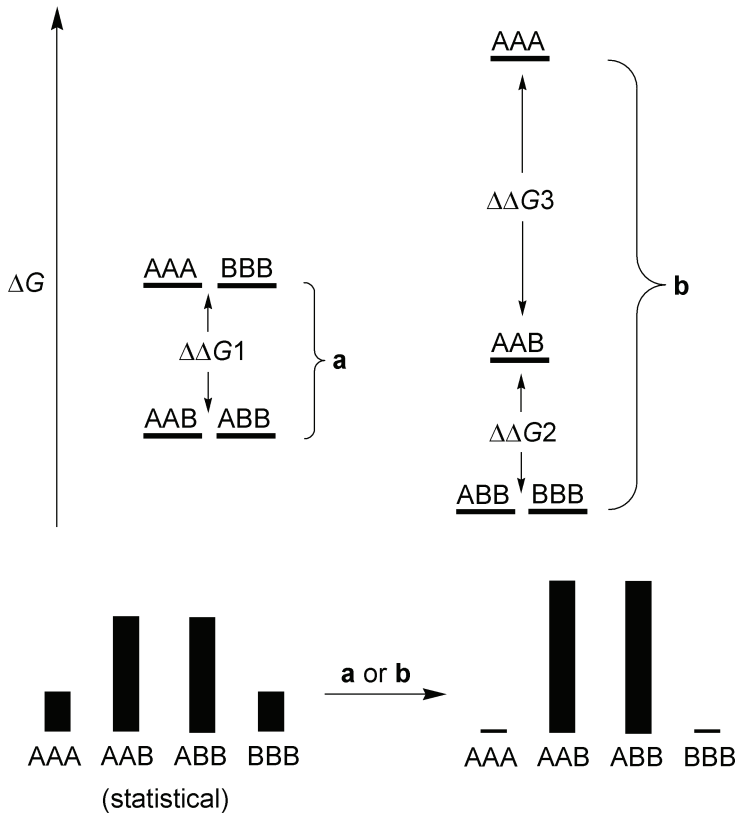

Figure III.2 For equally stable trimers **AAA**, **AAB**, **ABB** and **BBB**, a statistical 1:3:3:1 distribution is expected. The energetic situations shown in situation a and b both result in selective formation of the mixed trimers **AAB** and **ABB**.

An energy distribution similar to what is described in situation b of Figure III.2 is more likely to account for the dynamic mixture described above. Complex **AAA** has three sterically demanding triisopropylbenzene ligands. The π-ligands approach each other and destabilise the aggregate. For the mixed trimer **AAB**, only one unfavourable A–A interaction is found, whereas the aggregates **ABB** and **BBB** display no intramolecular A–A contacts at all. The kinetic data support this picture. The sterically encumbered trimer **AAA** rapidly reacts with the smaller cymene complex **BBB** to give **AAB**. This first reaction is

followed by a second, much slower reaction, in which **AAB** is converted into **ABB** (Scheme III.2).

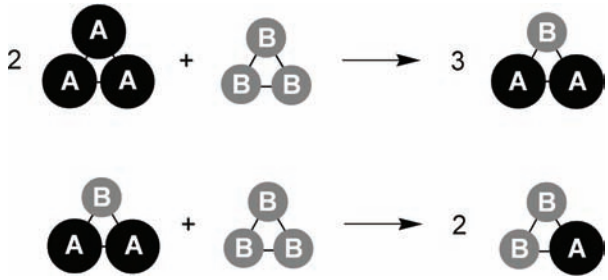

Scheme III.2 The equilibration of **[($C_6H_3{}^iPr_3$)Ru(L1–2 H^+)]$_3$** (**AAA**) and **[(cymene)Ru(L1–2 H^+)]$_3$** (**BBB**) proceeds in two steps. First, the sterically encumbered **AAA** is converted into **AAB**. This is followed by a second, much slower transformation, in which **ABB** is formed.

An interesting consequence from an asymmetric free energy distribution is the possibility to bias the equilibration process in favour of a certain species. For a dynamic mixture of equally stable trimers **AAA**, **AAB**, **ABB**, and **BBB**, the relative concentration of the mixed trimer **ABB** after equilibration can be increased from 37.5 % to a maximum theoretical value of 44.3 % by using two equivalents of **BBB** and only one equivalent of **AAA**. For a system such as the one described in situation b of Figure III.2, the maximum relative concentration of a mixed trimer after equilibration can be much higher.

To demonstrate this point, the scrambling reaction of **AAA** and **[(C_6H_6)Ru(L1–2 H^+)]$_3$** (**CCC**) has been investigated (Figure III.3). The small benzene complex **CCC** was chosen to further accentuate the difference between the π-ligands. This time, the complexes were mixed in a 1:2 ratio with initial concentrations of [**AAA**] = 2.0 mM and [**CCC**] = 4.1 mM. The time course of the reaction is shown in Figure III.3. The beginning of the equilibration process was again marked by the fast formation of the mixed complex **AAC** comprised of two large ($C_6H_3{}^iPr_3$)Ru moieties and the simultaneous rapid decrease of **AAA**. After 26 minutes, more than 95 % of the initial amount of complex **AAA** were converted and the concentration of **AAC** reached its maximum. Then, its concentration decreased in favour of **ACC**. The equilibrium was reached after ten hours. The heterotrimer **ACC** completely dominated the mixture (83 %) and only minor amounts of **AAC** (7 %) and **CCC** (10 %) were found in the solution.

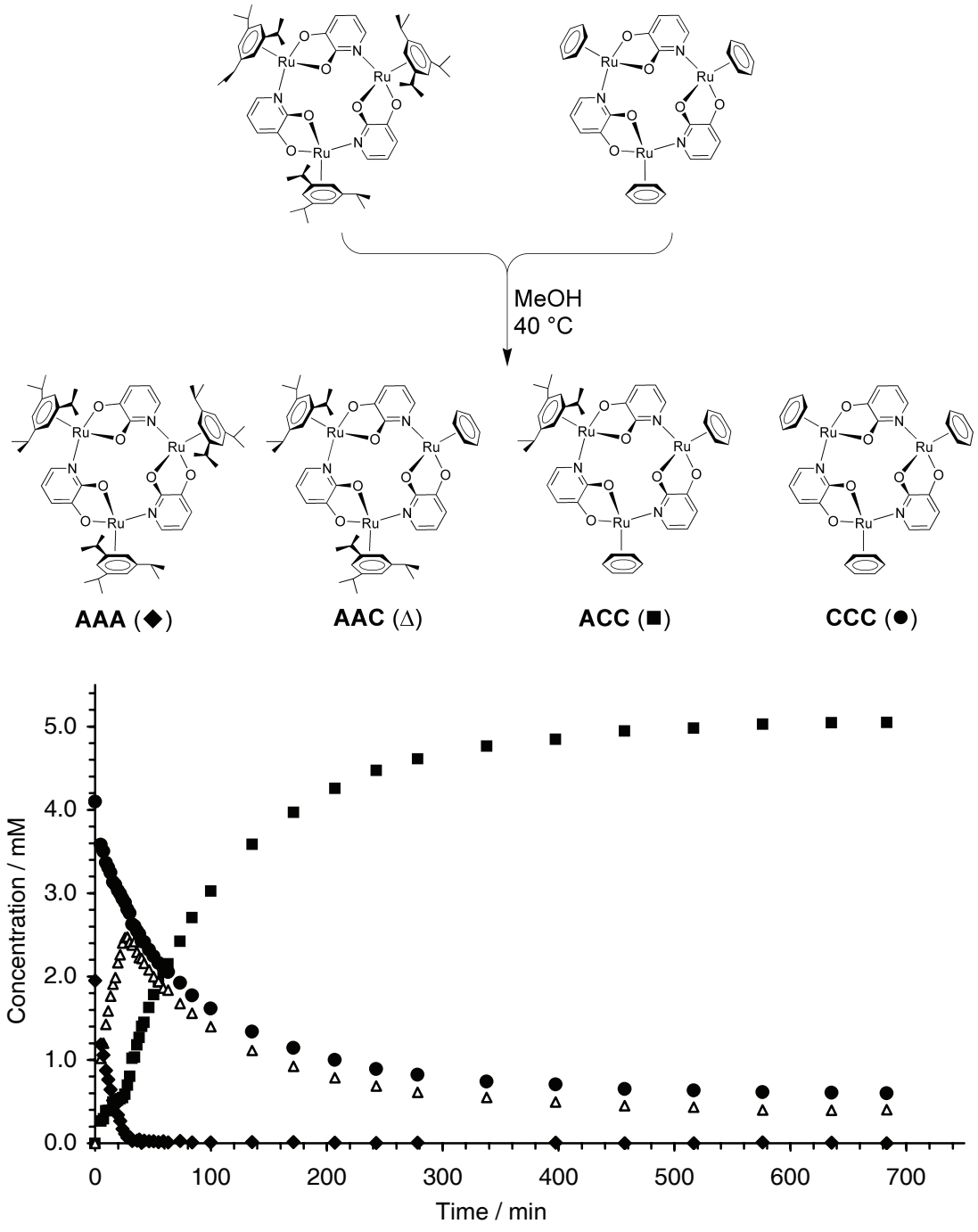

Figure III.3 Time course of the reaction between **AAA** (◆) and **CCC** (●, calculated) to give the mixed-metal macrocycles **AAC** (Δ) and **ACC** (■) as determined by ^{1}H NMR spectroscopy. The reaction was performed in CD_3OD 40 °C with initial concentrations of $[\mathbf{AAA}]_0$ = 1.95 mM and $[\mathbf{CCC_3}]_0$ = 4.13 mM. The total trimer concentration was $[\text{trimer}]_{\text{total}}$ = 6.08 mM.

Generally, mixtures comprised of two macrocycles, one owning large π-ligands, and the other one small π-ligands, show an unique kinetic behaviour, which can be described as follows:

1. Macrocycles with bulky π-ligands react significantly faster than macrocycles with small π-ligands.

2. Hetero-assemblies comprised of one small and two bulky π-ligands form very fast at the beginning of the exchange process, the concentration passes through a maximum and declines until the equilibrium is attained.

3. Hetero-assemblies comprised of two small and one bulky π-ligand form slowly at the beginning; once the bulky homotrimeric complexes have disappeared, their formation accelerates.

The main conclusion of the kinetic data is that steric congestion seems to be reduced stepwise by successive insertion of metal fragments with small π-ligands as shown in the cartoon of Figure III.2. Although the reaction mechanism can not be deduced from the data, one possibility can be excluded: a bimolecular mechanism, in which both starting complexes exchange one metal fragment. In this case, both hetero-assemblies would show equal concentrations at any moment of the reaction.

III.III Synthesis of Mixed-Metal Macrocycles

The results described above suggest that equilibration processes with 2:1 stoichiometries of complexes having significantly different π-ligands can be used for the controlled formation of mixed-metal macrocycles in preparative amounts. The following results show that this is indeed the case. Solutions comprised of two equivalents of the small benzene complex **[(C$_6$H$_6$)Ru(L1–2 H$^+$)]$_3$** (**CCC**) in combination with one equivalent of the trimers **[(C$_6$H$_3$*i*Pr$_3$)Ru(L1–2 H$^+$)]$_3$** (**AAA**), **[(C$_6$Me$_6$)Ru(L1–2 H$^+$)]$_3$** (**DDD**), or **[Cp*Rh(L1–2 H$^+$)]$_3$** (**EEE**), all of which have sterically demanding π-ligands, were tempered in methanol at 45 °C over night. Analysis by ^{1}H NMR spectroscopy revealed that the composition of the reaction mixtures was biased to over 80 % to the mixed-metal complex comprised of two (benzene)Ru fragments.

For practical reasons, the mixed-metal complexes were synthetised starting from two equivalents of the halfsandwich complex [(C$_6$H$_6$)RuCl$_2$]$_2$ (**1**), one equivalent of the halfsandwich complex [(C$_6$H$_3$*i*Pr$_3$)RuCl$_2$]$_2$ (**5**), [(C$_6$Me$_6$)RuCl$_2$]$_2$ (**6**) or [Cp*RhCl$_2$]$_2$ (**9**) and six equivalents of the bridging ligand **L1** in the presence of Cs$_2$CO$_3$. The reaction mixtures were equlibrated over night in methanol at 45 °C. After removal of the solvent under reduced pressure and extraction with dichloromethane, the products **ACC**, **DCC**, and **ECC** were isolated in 60 % yield and over 90 % purity.[j] It should be noted that exchange processes were found to be significantly slower in less polar solvents such as benzene and chloroform as compared to methanol. This allowed the characterization of the mixed trimers in pure form.

The ^{1}H NMR data of all three products were in agreement with the anticipated structure: three sets of signals were observed for aromatic protons of the bridging pyridonate ligands and two singlets were found for the chemically distinct benzene π-ligands. The complexes **DCC** and **ECC** were also characterized by a single crystal X-ray analysis (Figure III.4 and Figure III.5, respectively).

The bond lengths and angles found for the macrocyclic core of **DCC** and **ECC** are comparable to what has been observed for the corresponding homotrimeric complexes.[124, 126] Additional structural anisotropy due to the presence of different halfsandwich complexes was not observed. Indirect evidence for the reduced steric strain of the mixed-metal macrocycles **DCC** and **ECC** is the fact that their average metal–metal distances (**DCC**: 5.26 Å; **ECC**: 5.26 Å) are shorter than what has been observed for the homotrimers **DDD** (5.46 Å) and **EEE** (5.35 Å). A compilation of the most important structural data can be found in Table IX.10 on page 227. The importance of the size of the π-ligand for the stability of the trimeric aggregates is also evident from the space filling representations of **DCC** and **ECC** (Figure III.6).

j. In case of complex **ECC** a purity of 83 % was obtained.

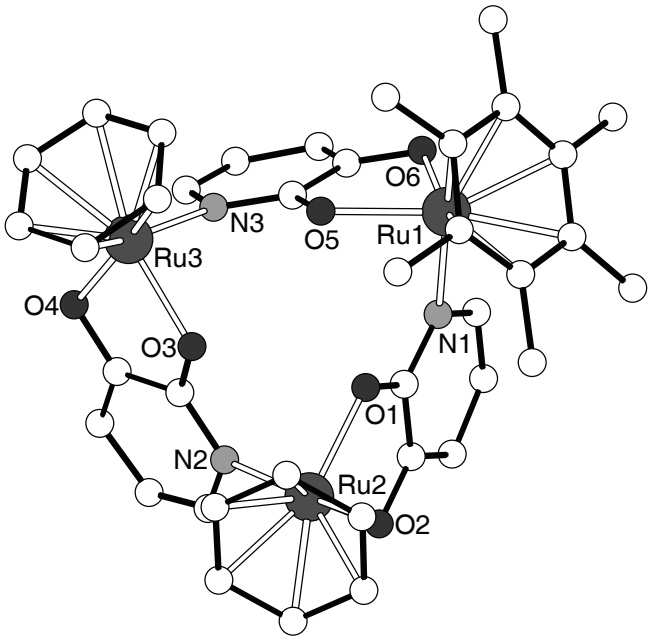

Figure III.4 Ball and stick representation of the molecular structure of **DCC** in the crystal. The hydrogen atoms and the solvent molecules are omitted for clarity. Selected bond lengths (Å): Ru1–N1 2.130(6), Ru1–O5 2.086(4), Ru1–O6 2.065(5), Ru2–O1 2.060(5), Ru2–O2 2.069(5), Ru2–N2 2.118(6), Ru3–O3 2.069(5), Ru3–O4 2.073(5), Ru3–N3 2.139(6).

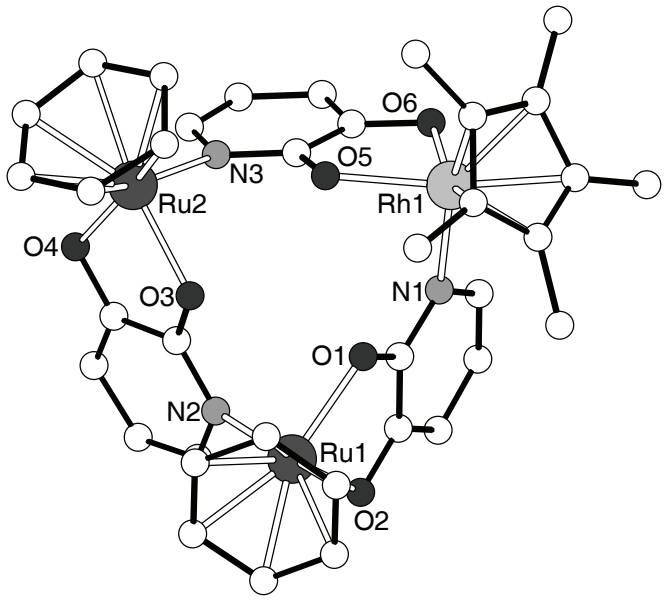

Figure III.5 Ball and stick representation of the molecular structure of **ECC** in the crystal. The hydrogen atoms and the solvent molecules are omitted for clarity. Selected bond lengths (Å): Rh1–O5 2.080(7), Rh1–O6 2.088(8), Rh1–N1 2.122(9), Ru1–O2 2.067(6), Ru1–O1 2.078(7), Ru1–N2 2.106(8), Ru2–O3 2.072(6), Ru2–O4 2.076(7), Ru2–N3 2.104(9).

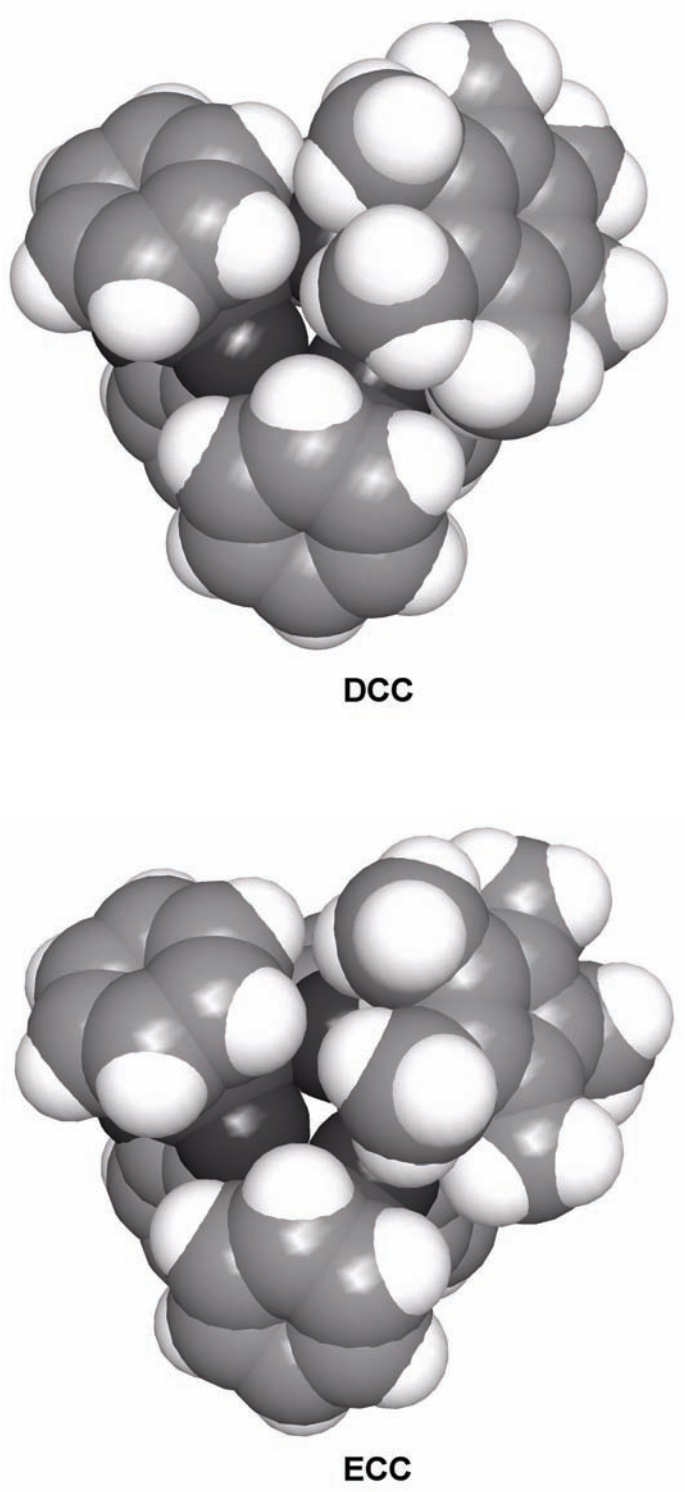

Figure III.6 Space filling representation of the molecular structure of **DCC** (top) and **ECC** (bottom) in the crystal. The solvent molecules have been omitted for clarity.

III.IV Conclusions

12-Metallacrown-3 complexes containing two different metal fragments have been presented and their formation by metal fragment exchange has been studied. It was found that the equilibration proceeds in two steps and that the final mixture is completely dominated by the mixed-metal macrocycles. The results are rationalized by assuming unfavourable steric interactions between adjacent bulky (π-ligand)M fragments (M = Ru, Rh). These steric interactions have been used to bias dynamic exchange processes in such a way that mixed-metal macrocycles are obtained in over 60 % yield under thermodynamic control. No additional anisotropy of the binding lengths or angles has been observed and the average metal–metal distances indicate that there is no steric repulsion between the π-ligands. The results are conceptually related to work on *mixed-ligand* metallamacrocycles and cages. Navarro and Romero have shown that scrambling of symmetrical (en)Pd^{II}-based macrocycles with bridging 4,7-phenantroline and 2-pyrimidinolate ligands can lead to the dominant formation of a single product given that appropriate stoichiometries are employed.[264] Fujita et al.[265, 266] and James at al.[267] have used steric interactions between ligands to achieve the quantitative formation of macrocycles and coordination cages containing two different heterocyclic ligands. It should be noted that rather small differences in free energy of the various aggregates can be sufficient to bias dynamic mixtures of metallamacrocycles (or cages) towards the formation of a defined product. For the system described in situation b of Figure III.2, for example, a difference of $\Delta\Delta G2 = ½\ \Delta\Delta G3 = 3.0$ kcal mol^{-1} results in an increase of the relative concentration of mixed product **ABB** from 44.3 % (statistical) to 91.6 % if the two complexes were mixed in a 2:1 ratio ($[\mathbf{AAA}]_{initial} = ½\ [\mathbf{BBB}]_{initial}$).[k] In view of the fact that asymmetric metallamacrocycles may display interesting functional differences (host-guest chemistry etc.) when compared to their symmetrical M_nL_n counterparts, the strategy discussed above should be regarded as an attractive alternative to step-wise synthetic procedures.

k. The equilibrium constants were calculated with the program Gepasi, version 3.30.[233, 234]

Chapter IV
Self-Assembled Organometallic Sensors for Li^+ Ions in Water

IV.I Introduction

"…progress in lithium research has been hampered by the unavailability of a sensitive and specific Li^+ spectroscopic tool." This statement can be found in the 'Concluding Remarks' of a recent review article about the pharmacological action of lithium salts.[268] In the following, water soluble Li^+-specific organometallic receptors and their binding properties will be presented. These receptors can be used to design a pH dependant Li^+ sensor and a 'naked eye' colorimetric test for Li^+ in water. Furthermore, it will be outlined, how simple structural modifications allow the development of a chemosensor for the selective detection of lithium ions in water using fluorescence spectroscopy.

IV.I.1 The Pharmacology of Lithium Ions

In 1949, John Cade reported that lithium salts have a calming effect on patients with acute mania.[269] The potential value in psychiatry was subsequently confirmed by many other studies and since the mid-1960s, lithium salts are among the most frequently used drugs for patients suffering from bipolar disorder.[270–272] Despite the development of alternative drugs, lithium 'remains the treatment of choice'[270] and the 'gold standard'[273] for acute episodes and the prevention of relapses. Recent studies suggest that lithium could also be used for the treatment of Alzheimer's disease[274, 275] and of schizophrenia and it was speculated whether lithium could become the 'aspirin of the brain'.[276] Apart from applications in the field of psychiatry and neurology, lithium salts have been employed to treat skin diseases, were shown to inhibit the replication of certain viruses and can affect the immune response.[271]

Unfortunately, the therapeutic range of lithium salts (0.5–1.2 mM) used in the treatment of bipolar disorder is very close to toxic levels (<2.0 mM).[277–279] Establishing the accurate dose is hence of crucial importance. Measurements are currently carried out using flame emission spectroscopy, a relative expensive method which give no immediate reply. But measurements should best taken at the office of the treating physician, i.e. in blood (buffer solution) in the presence of high concentrations of other small cations such as Na^+ and K^+. Tools to rapidly quantify lithium are therefore of prime importance.

Given the pharmacological relevance, it is not surprising that considerable efforts have been devoted towards the development of sensors for lithium ions.[277–279] From a chemical point of view, the synthesis of specific receptors is of special interest. So far, most investigations have focused on organic macrocycles, which are generally employed in a non aqueous environment.[277–294] The design of synthetic receptors, which can be used directly in water, represents a special challenge. First of all, the host needs to be soluble in water. This severely limits the type of building blocks, which can be employed to construct the receptor. Secondly, the hydration enthalpy of Li^+ is very high ($-519\ kJ\,mol^{-}$

^{1}).[176] As a consequence, the binding constants of artificial hosts are significantly lower in water when compared to organic solvents. The Li^+ specific ionophore 12-crown-4, for example, displays a binding constant of $\log K = 4.25$ in acetonitrile whereas in water, no interaction with Li^+ could be detected at all ($\log K \sim 0$).[295] Apart from an innovative alternative approach using gold nanoparticles,[296] aza-macrobicyclic cage molecules play a dominant role among the few receptors, which are able to bind Li^+ in water with high affinity.[297–303] One of the highest stability constants was found for the 2,1,1-cryptand ($\log K = 5.5$).[297] This receptor also displays a good selectivity for Li^+ over Na^+ (200:1). For potential applications, however, aza-macrobicyclic receptors show several severe disadvantages: the synthesis of these compounds generally requires several steps and proceeds with modest overall yields.[297–303] Additionally, commercially available cryptands are in general very expensive, and their purity may be modest, e.g. only 90 % in the case of the Li^+ specific 2,1,1-cryptand.

An ideal sensor should be able to detect Li^+ at the millimolar level in the presence of other alkaline and earth-alkaline cations by colorimetric or fluorescent means. The synthesis of such a sensor should be simple and using easily available starting materials.

IV.I.2 12-Metallacrown-3: Ionophores in Organic Solvents

As presented in chapter I.VI, metallamacrocyclic ionophores for the small alkaline ions Li^+ and Na^+ in organic solvents have been developed recently in the Severin group.[124, 126, 127] These macrocyclic hosts self-assemble from halfsandwich complexes [(π-ligand)MCl_2]$_2$ and 3-hydroxy-2-pyridone in the presence of Cs_2CO_3 (Scheme IV.1). The metal fragment adopts a piano stool like pseudo tetrahedral geometry and the deprotonated 3-hydroxy-2-pyridone acts as tridentate bridging ligand.

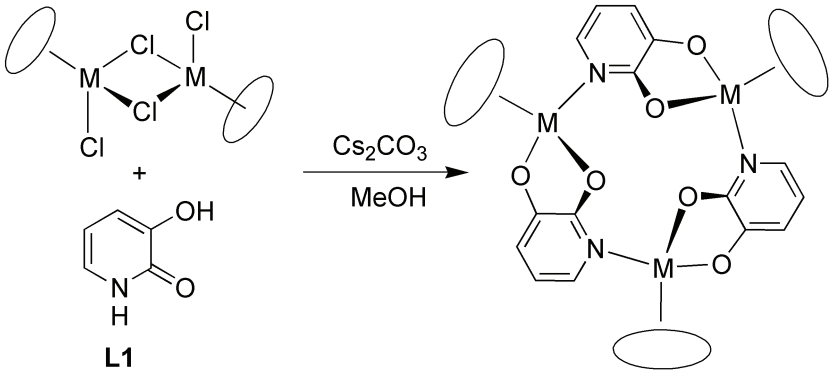

Scheme IV.1 Self-assembly of metallamacrocyclic ionophores from [(π-ligand)MCl_2]$_2$ and 3-hydroxy-2-pyridone.

IV.II pH Triggered Self-Assembly of Organometallic Receptor for Li^+ Ions in Water

IV.II.1 Employed Ligands and Halfsandwich Complexes

The ligands **L2–L5** (Figure IV.1) were chosen for the synthesis of water soluble receptors because

1. They contain the 3-hydroxy-2-pyridone structural motif, which favours the formation of trinuclear metallamacrocycles.[124–126, 128, 165, 166, 168, 169]
2. They contain a tertiary amino group, which is able to enhance the solubility of the resulting complexes (formation of ammonium groups) without interfering with the self-assembly process.

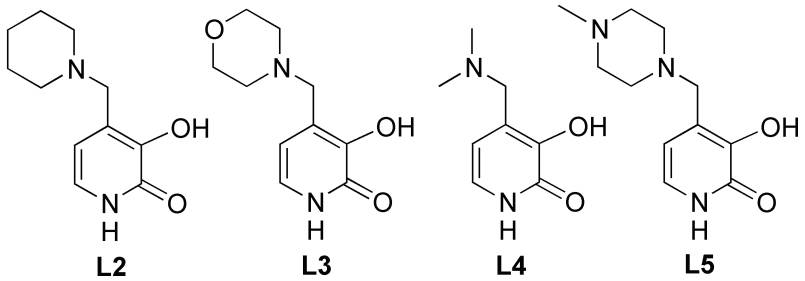

Figure IV.1 Ligands **L2–L5** used for the self-assembly of water soluble metallamacrocycles.

All ligands were easily prepared in a Mannich reaction of 3-hydroxy-2-pyridone, formaldehyde and the corresponding secondary amine (Scheme IV.2).[304–307] Attack occurred first at the more reactive C4-position, and if more than one equivalent was used, reaction occurred also at the C6-position. However, investigation of the self-assembly of halfsandwich complexes and bridging ligands bearing two methyleneamino groups did not result in trinuclear metallamacrocyclic structures.

As the reaction partner, organometallic halfsandwich complexes of ruthenium (**1–6**), rhodium (**7–9**) and iridium (**10** and **11**) have been employed. Although some of these complexes are commercially available (**1**, **3**, **9** and **11**), all halfsandwich complexes have been synthesised in the laboratory. Their structures are presented in Figure IV.2.

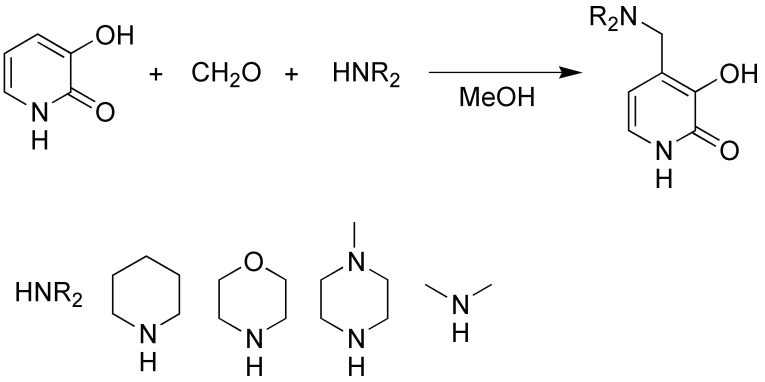

Scheme IV.2 Mannich reaction of 3-hydroxy-2-pyridone, formaldehyde and a secondary amine to obtain ligands **L2**–**L5**.

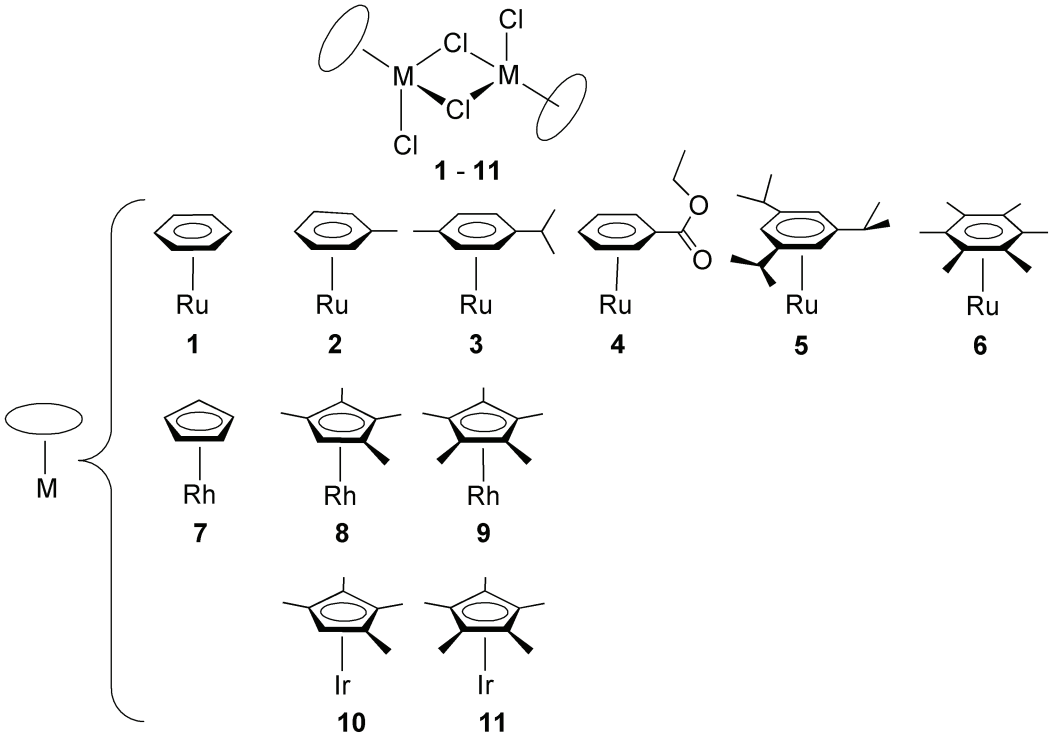

Figure IV.2 Dimeric halfsandwich complexes $[(\pi\text{-ligand})MCl_2]_2$ employed for the self-assembly of water soluble metallamacrocycles.

IV.II.2 Formation of Monomeric Complexes in Water

First, the reaction of the complexes **1**–**11** with the ligands **L2**–**L5** in plain water was investigated. When the chloro-bridged halfsandwich complexes were stirred with 2 equiv. of the respective ligand, clear yellow to orange solutions were obtained after

several minutes. ^{1}H NMR spectroscopic investigation of the resulting mixtures showed the presence of a single complex. Given the known tendency of hydroxy-pyridone ligands to form O,O'-chelates with halfsandwich complexes,[124, 308, 309] it appeared likely that mononuclear complexes of type A had formed (Scheme IV.3). This was confirmed for several examples by single crystal X-ray analysis (see chapter IV.II.4).

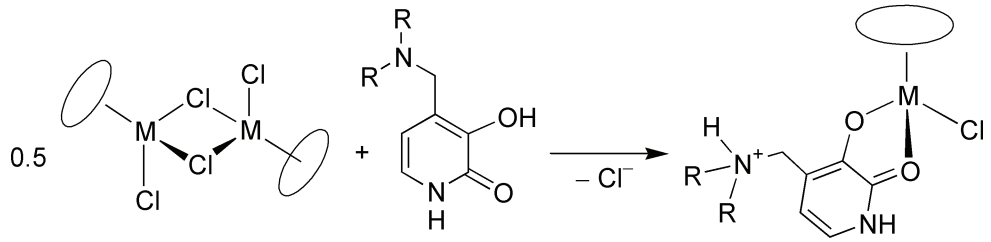

1–**11** **L2**–**L5** **A**

Scheme IV.3 Formation of mononuclear complexes of type A.

The chloro ligands of complexes of type A are expected to be labile because upon abstraction of the ligand, a cationic complex is formed, which can be described by two mesomeric forms: one in which the positive charge is located at the metal and another in which the positive charge is localized on the nitrogen atom of the pyridine ring (Scheme IV.4).

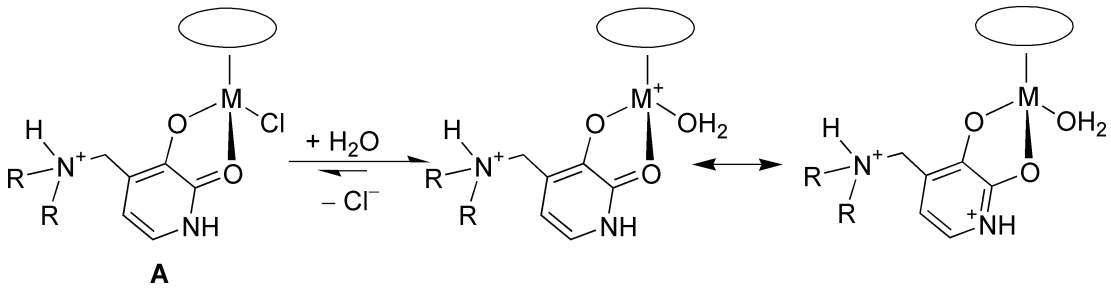

A

Scheme IV.4 Chloro vs. aqua complexes.

In a good donor solvent such as water, it is thus expected that the chloro-ligands are substituted by water. The following experiments suggest that this is indeed the case. An aqueous solution (D_2O) containing the monomeric complex formed from **3** and **L2** was treated with 10 equiv. of $AgNO_3$. A white precipitate of AgCl formed immediately, which was separated by filtration. The ^{1}H NMR spectrum of the resulting complex was identical to that of the starting material indicating that the nature of the anion (NO_3^- vs. Cl^-) has a minor effect on the ruthenium complex. Similar results were obtained with the rhodium and iridium complexes obtained from **L2** and **9** or **11**, respectively.

Table IV.1: Selected ^1H NMR signals (ppm) of monomeric halfsandwich complexes obtained by reaction of the complexes **1**–**11** with the ligands **L2**–**L5** in D_2O.

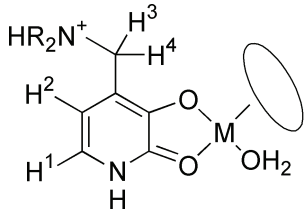

Entry	Complex	Ligand	H^{1a}	H^{2a}	$H^{3/4}$
1	—	**L2**	6.69	6.28	4.05
2	—	**L3**	7.02	6.38	3.73
3	—	**L4**	6.62	6.20	3.98
4	—	**L5**	6.90	6.33	3.70
5	**1**	**L2**	6.91	6.53	4.22
6	**1**	**L5**	6.91	6.55	3.68
7	**2**	**L2**	6.92	6.53	4.23
8	**2**	**L5**	6.89	6.54	3.71
9	**3**	**L2**	6.88	6.49	4.21
10	**3**	**L3**	6.90	6.53	4.33
11	**3**	**L4**	6.70	6.50	4.25
12	**3**	**L5**	6.88	6.53	3.70
13	**4**	**L2**	6.92	6.70	4.23
14	**4**	**L5**	6.91	6.55	3.75
15	**5**	**L2**	6.86	6.49	4.21
16	**5**	**L5**	6.84	6.51	3.70
17	**6**	**L2**	6.82	6.46	4.21
18	**6**	**L3**	6.81	6.46	4.27
19	**6**	**L4**	6.82	6.46	4.27
20	**6**	**L5**	6.81	6.49	3.69
21	**7**	**L2**	6.92	6.53	4.19
22	**7**	**L5**	6.92	6.57	3.70
23	**8**	**L2**	6.74	6.38	4.09
24	**8**	**L5**	6.84	6.51	3.74
25	**9**	**L2**	6.81	6.45	4.18
26	**9**	**L5**	6.82	6.49	3.72
27	**10**	**L2**	6.89	6.50	4.21
28	**10**	**L5**	6.89	6.52	3.78
29	**11**	**L2**	6.89	6.49	4.23
30	**11**	**L5**	6.86	6.50	3.77

a. The signals appear as doublets with a coupling constant of $^3J = 7$ Hz.

The coordination of the metal to the oxygen atoms of the ligand results in a translocation of a proton from the hydroxy to the amine group. This is reflected by the chemical shift of the signals for the methylene group next to the nitrogen atom ($H^{3/4}$, Table IV.1). While for the free ligands, the signals of these protons appear between $\delta = 3.70$ and 4.05 ppm (Table IV.1, entries 1–4), the corresponding signals for the metal complexes with **L2**, **L3** and **L4** appear between $\delta = 4.09$ and 4.33 ppm in agreement with the presence of a protonated amine group. For complexes with the ligand **L5**, on the other hand, the signals of the methylene protons are only slightly shifted. This indicates that it is predominantly the terminal nitrogen atom of the piperazine group, which is protonated (Figure IV.3).

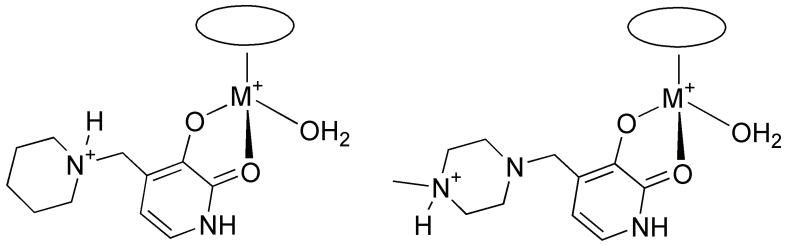

Figure IV.3 Proton translocation of monomeric halfsandwich complexes containing the ligands **L2** (left) and **L5** (right).

The fact that the $MeNR_2$ nitrogen of ligand **L5** is more basic was confirmed in ^1H NMR titration experiments with DCl. Upon addition of incremental amounts of DCl (0.0–2.0 equiv.) to a solution of ligand **L5**, it was first the signals of the NMe (peak 2) protons, which were shifted. Significant differences in chemical shift for the $H^{3/4}$ protons (peak 1) were only observed upon addition of more than 1.0 equiv. of DCl as shown in Figure IV.4.

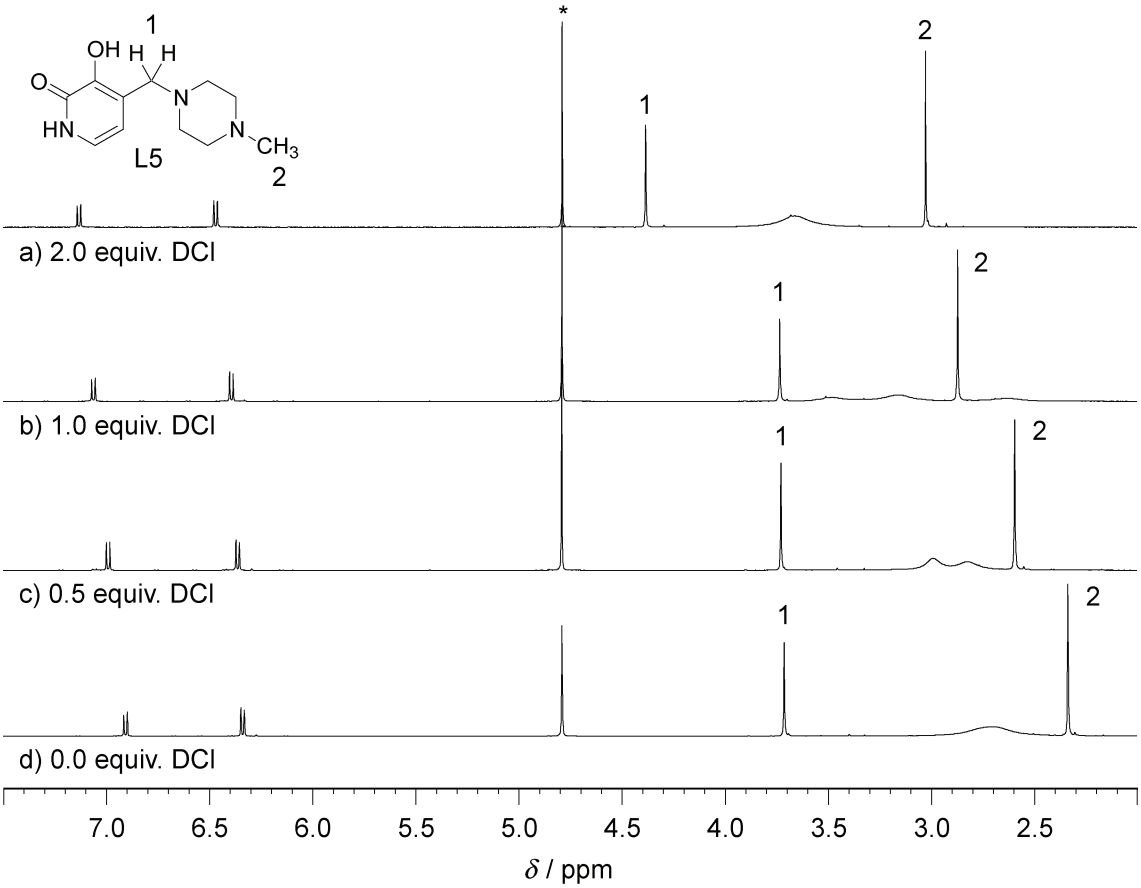

Figure IV.4 ^1H NMR spectrum of **L5** in D_2O (spectrum d) and after addition of increasing amounts of DCl. First, the NMe group is protonated (spectra b & c), then the NCH_2 group (spectrum a). The solvent peak is denoted by an asterisk.

IV.II.3 pH Triggered Assembly of 12-Metallacrown-3 Complexes

Next, the influence of the pH was investigated using potentiometric titrations. Increasing amounts of CsOH (0.0–1.0 equiv.) were added to solutions of monomeric complexes of type A (15.0 mM). In all cases, a pH profile characteristic of a weak acid was obtained. The data obtained for the ruthenium complexes **1**–**4** and the ligand **L2** are depicted in Figure IV.5;[1] the corresponding data for the rhodium and iridium complexes **7**–**11** are shown in Figure IV.6.

1. The (triisopropylbenzene)Ru complex **5** and the (hexamethylbenzene)Ru complex **6** were not included in this study because of the low solubility of the resulting complexes in water. However, the corresponding trimers could be synthesised in MeOH in the presence of Cs_2CO_3.

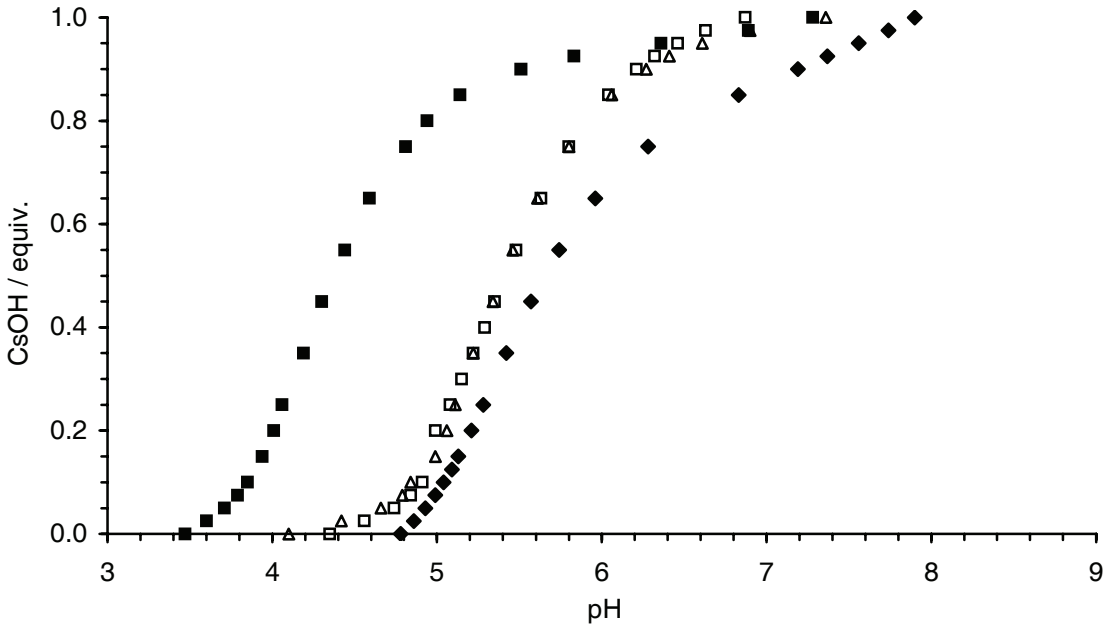

Figure IV.5 The pH of solutions containing the ligand **L2** (15.0 mM) and the complexes **1** (◆), **2** (□), **3** (Δ) and **4** (■) ([Ru] = 15.0 mM) after addition of increasing amounts of CsOH (0.0–1.0 equiv.).

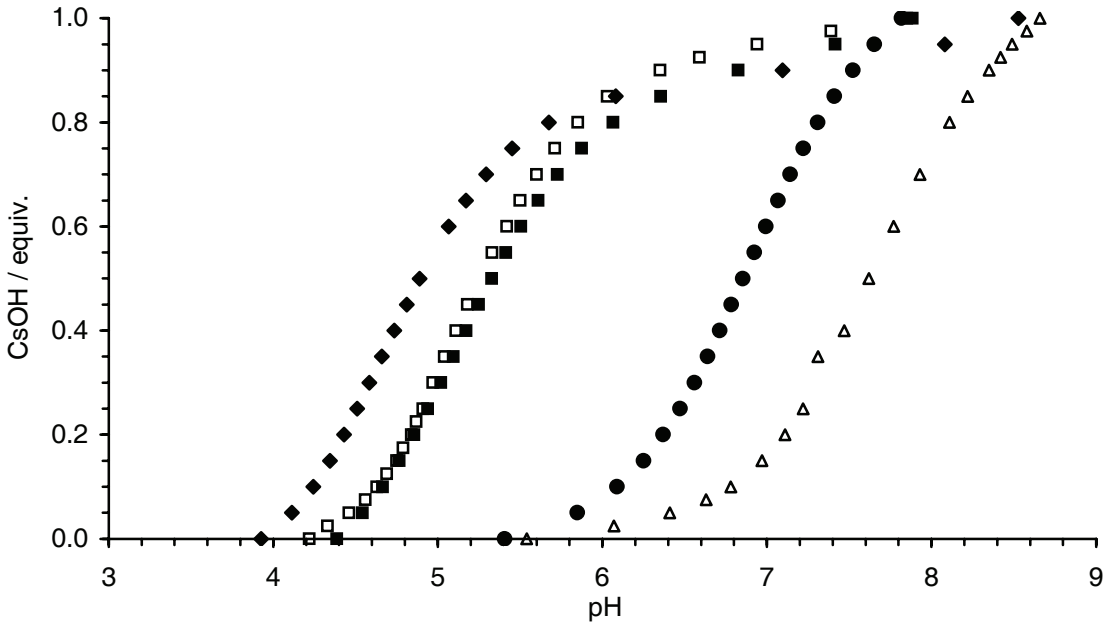

Figure IV.6 The pH of solutions containing the ligand **L2** (15.0 mM) and the complexes **7** (■), **8** (●), **9** (Δ), **10** (◆) and **11** (□) ([Rh] = [Ir] = 15.0 mM) after addition of increasing amounts of CsOH (0.0–1.0 equiv.).

The ruthenium complexes **1**–**3** all behave very similar with an inflection point at pH ~ 5.5. The $(C_6H_5CO_2Et)$Ru complex **4** having an electron withdrawing ester side chain, on the other hand, is slightly more acidic with an inflection point at pH = 4.3. The acidity of the complexes is not only affected by the nature of the π-ligand but also by the metal ion. This is evidenced by comparing the data of the rhodium complexes **8** and **9** with that of the iridium complexes **10** and **11** (Figure IV.6). Clearly, the iridium complexes are more acidic than the rhodium complexes having the same type of π-ligands (**8** vs. **10** and **9** vs. **11**).

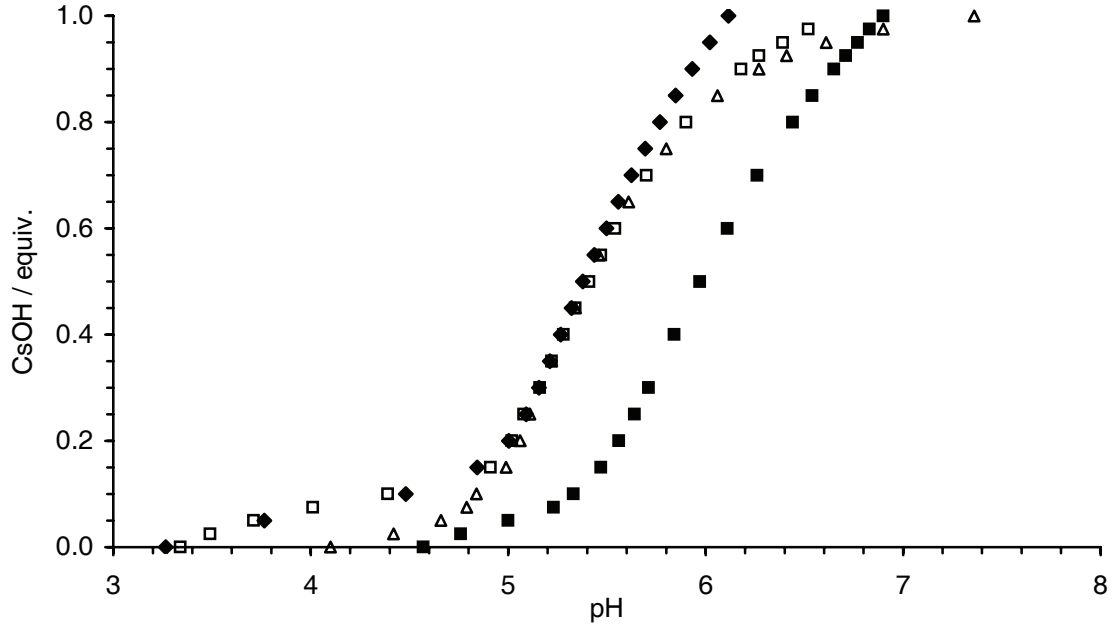

Table IV.2: The pH of solutions containing the complex **3** ([Ru] = 15.0 mM) and the ligands **L2** (△), **L3** (◆), **L4**(□) and **L5** (■) (15.0 mM) after addition of increasing amounts of CsOH (0.0–1.0 equiv.).

When combined with the (cymene)Ru complex **3**, the pyridone ligands **L2**, **L3** and **L4** gave rise to very similar pH profiles with $pK_a = 5.4$. For the piperazine ligand **L5**, on the other hand, the inflection point was found at slightly higher pH ($pK_a = 6.9$). Tables compiling the inflection points are given in the Appendix (Table IX.6 and Table IX.7 on page 216).

For some metal–ligand combinations, precipitation occurred after addition of 1.5–2.0 equiv. of CsOH (pH ~ 9.0–10.5, [metal] = 15 mM). This indicates that the fully deprotonated complexes display a lower solubility in water. There are various metal–ligand mixtures, however, for which no precipitation was observed after addition of 2 equiv. of CsOH. In particular, complexes with (C_6H_6)Ru (**1**), (C_6H_5Me)Ru (**2**), CpRh (**7**) and (C_5HMe_4)Ru (**8**) metal fragments show a relatively high solubility (> 5 mM),

even in the fully deprotonated form. The solubility was not only influenced by the metal fragment, but also by the ligand. In general, the solubility increased in the following order: **L2** < **L3** ~ **L4** < **L5**. The equivalents of CsOH after which precipitation of 12-metallacrown-3 complexes occured are compiled in Table IX.4 on page 215.

In order to obtain more information about the complexes which are formed at different pH, ^{1}H NMR titration experiments for selected metal–ligand combinations have been performed. Part of the ^{1}H NMR spectra obtained for a mixture of the (cymene)Ru complex **3** and the ligand **L2** upon addition of CsOH (0.0–1.0 equiv.) is shown in Figure IV.7. For the monomeric complex obtained in plain D_2O (spectrum e), one can observe a singlet for the NCH_2 group at 4.21 ppm, two doublets between 5.5 and 6.0 ppm for the aromatic CH protons of the cymene π-ligand and two doublets between 6.5 and 7.0 ppm for pyridone CH protons. Upon addition of CsOH, the signals of a second complex can be detected. The latter is completely dominating the solution after addition of one equivalent of CsOH.

The signals of the new complex can be assigned to a trimeric macrocycle of type B (Scheme IV.5). An important difference between the spectra of the monomeric and the trimeric complex is the multiplicity of the aromatic CH protons of the cymene π-ligand and of the NCH_2 protons. Although the metals represent stereogenic centres in both complexes, only the rigid metallamacrocycle is conformationally stable on the NMR time scale. As a consequence, we can observe two doublets for the diastereotopic NCH_2 protons at ~ 4 ppm and four doublets for the cymene CH protons between 5.2 and 6.2 ppm (spectrum ‘a’ of Figure IV.7).

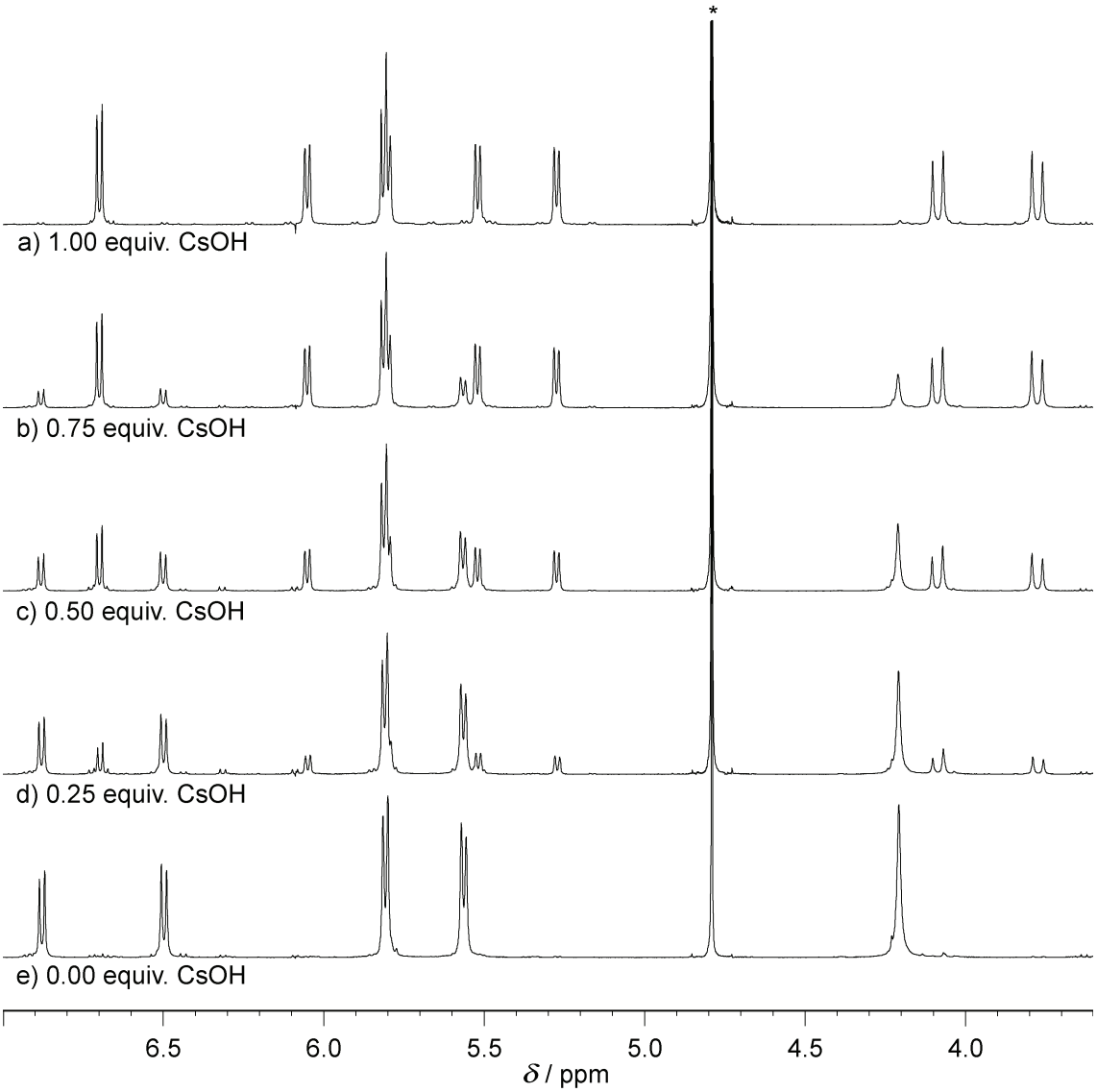

Figure IV.7 Part of the ^{1}H NMR spectrum (D_2O) of a solution containing $[(cymene)RuCl_2]_2$ (**3**) (7.5 mM) and the ligand **L2** (15.0 mM) after addition of different amounts of CsOH: a) 1.00 equiv. b) 0.75 equiv. c) 0.50 equiv. d) 0.25 equiv. e) 0.00 equiv.. The spectrum 'a' corresponds to the trimer B and the spectrum 'e' corresponds to the monomer A. The solvent peak is denoted by an asterisk.

NMR titration experiments using the iridium complex **10** and the ligand **L2** gave similar results: upon addition of CsOH, one could observe the signals of a second complex (Figure IV.8). With one equivalent of CsOH, this complex is the dominant species in solution (> 95 %). The two doublets for the NCH_2 protons confirm the presence of a chiral complex, which is conformationally stable on the NMR time scale.

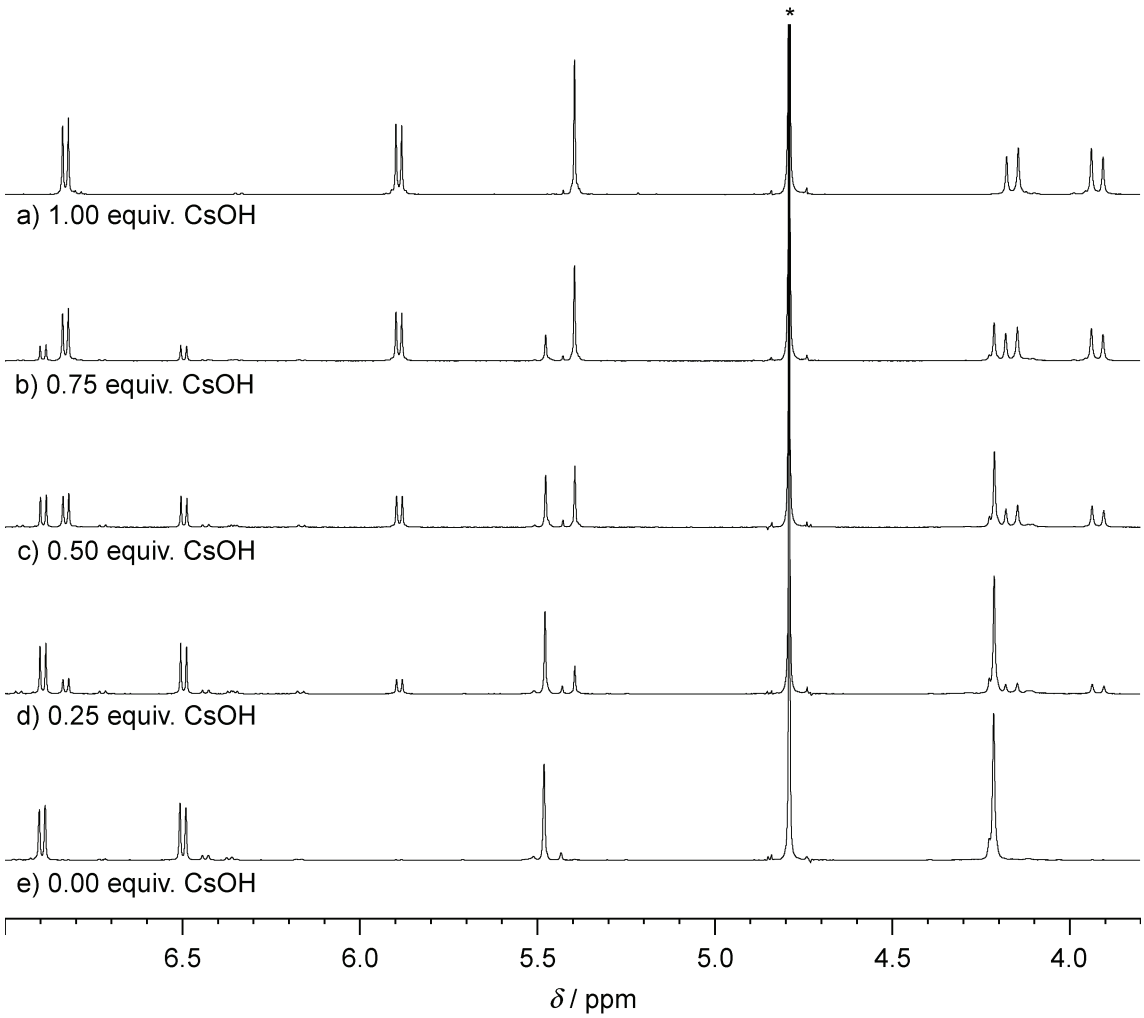

Figure IV.8 Part of the ^{1}H NMR spectrum (D_2O) of a solution containing $[(C_5Me_4H)IrCl_2]_2$ (**10**) (7.5 mM) and the ligand **L2** (15.0 mM) after addition of different amounts of CsOH: a) 1.00 equiv. b) 0.75 equiv. c) 0.50 equiv. d) 0.25 equiv. e) 0.00 equiv.. The spectrum 'a' corresponds to the trimer B and the spectrum 'e' corresponds to the monomer A. The solvent peak is denoted by an asterix.

The ^{1}H NMR data described above are in agreement with a pH dependant self-assembly process as shown in Scheme IV.5. After deprotonation of the pyridone, the ring nitrogen is able to coordinate to a metal, thereby replacing a weakly bound water ligand. The pH at which 50 % of the monomer A is converted to the trimer B varies substantially (Figure IV.5 and Figure IV.6). It is plausible that steric effects influence the aggregation but electronic effects also seem to be of importance as evidenced by the unusual behaviour of the ester substituted ruthenium complex **4**.

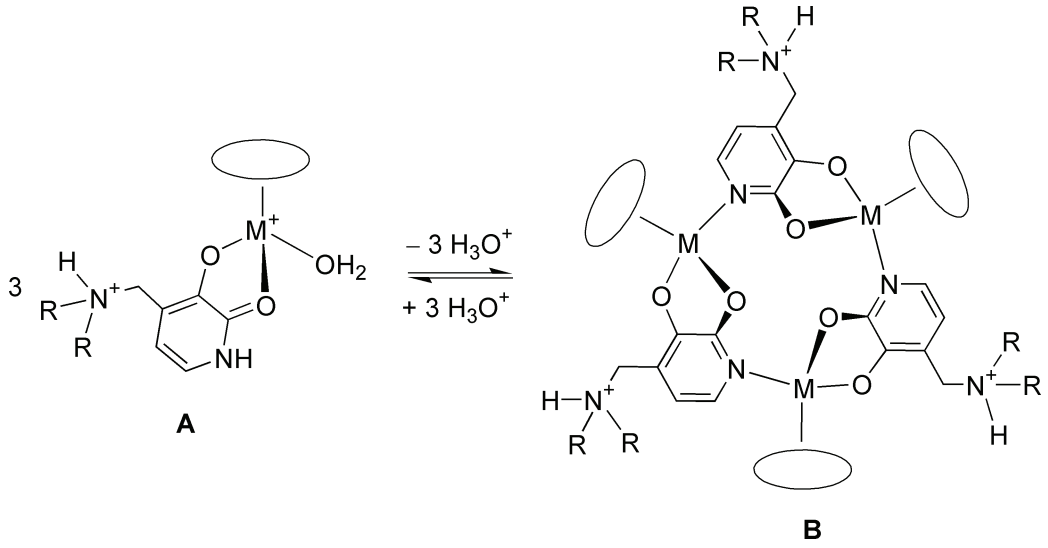

Scheme IV.5 pH dependant self-assembly of trinuclear metallamacrocycles of type B.

Additional evidence for the presence of trimeric macrocycles was obtained by ESI mass spectroscopy; spectra of solutions containing ligand **L2** and metal complexes **3** or **11** in phosphate buffer solution (PBS) at pH 8 showed isotopically resolved peaks for the monoprotonated trimers.

NMR titration experiments with mixtures, which display a $pK_a > 6$, gave slightly different results since more than one equivalent of CsOH with respect to the ligand was needed to complete the assembly process. The amount of CsOH that was required to generate the metallamacrocycle was found to depend on the nature of the metal complex and the ligand. Whereas for a combination of the ligand **L5** with the (cymene)Ru complex **3**, the addition of 1.25 equiv. of CsOH was sufficient to obtain over 95 % of the respective trimer, for the $(C_5Me_4H)Rh$ complex **8** almost 2 equiv. were needed (Figure IV.9). For some other mixtures such as the Cp*Rh complex **9** and the ligand **L5**, precipitation was observed before completion of macrocyclisation.[m]

m. The pH dependant assembly of Cp*Rh complexes using nucleobase ligands has been investigated extensively by the Fish's group.[108, 110]

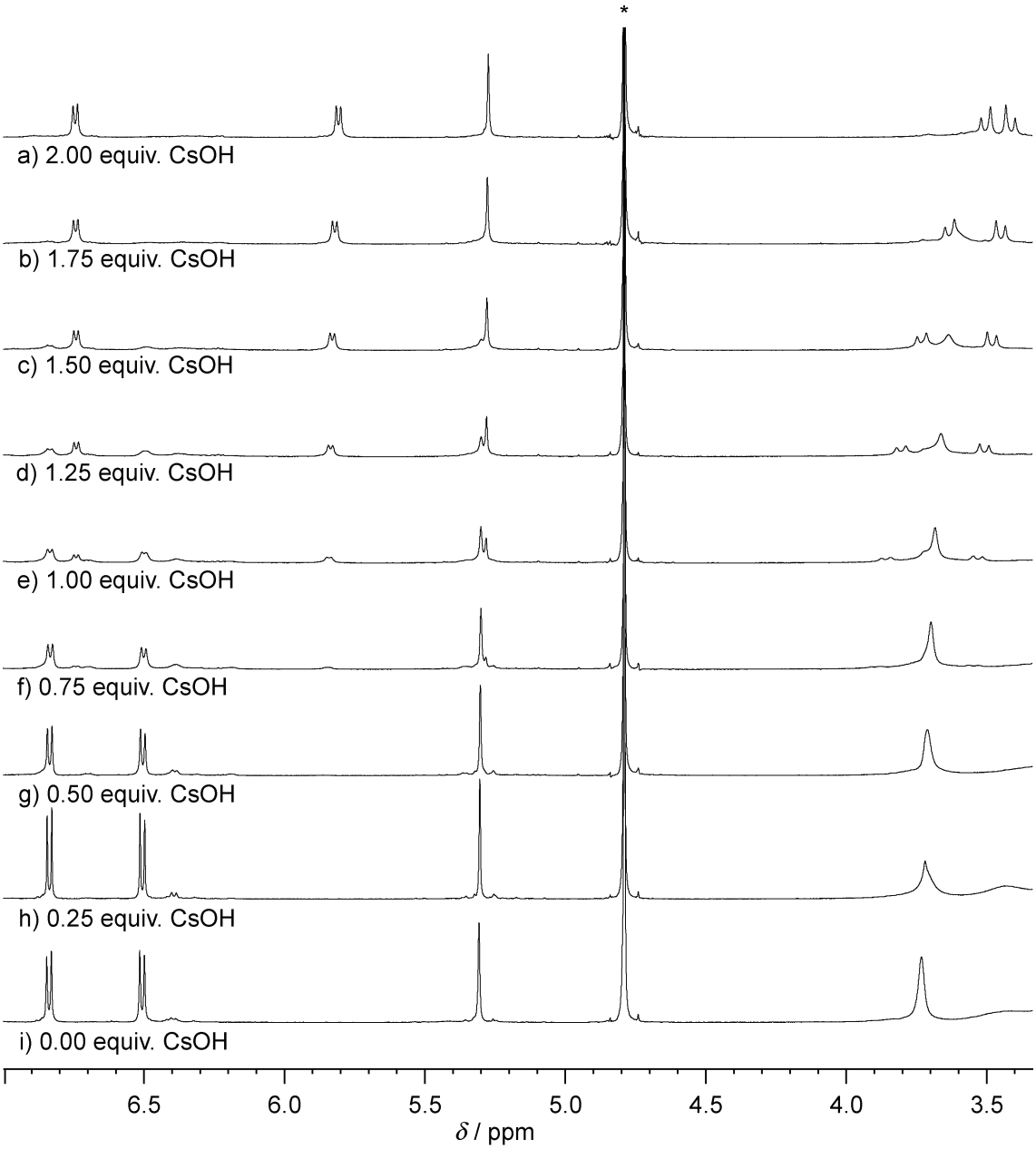

Figure IV.9 Part of the ^1H NMR spectrum (D_2O) of a solution containing $[(C_5Me_4H)RhCl_2]_2$ (7.5 mM) and the ligand **L5** (15.0 mM) after addition of different amounts of CsOH: a) 2.00 equiv. b) 1.75 equiv. c) 1.50 equiv. d) 1.25 equiv. e) 1.00 equiv. f) 0.75 equiv. g) 0.50 equiv. h) 0.25 equiv. i) 0.00 equiv.. The spectrum 'a' corresponds to the trimer B and the spectrum 'i' corresponds to the monomer A. The solvent peak is denoted by an asterisk.

For the above mentioned cases, the pyridone proton has a comparable acidity as the ammonium side-chain. Accordingly, we observe the partial deprotonation of the side-chain before the deprotonation of the pyridone. Since macrocyclisation necessitates the deprotonation of the pyridone NH proton, more than one equivalent of CsOH is needed.

For the extreme case of complex $[(C_5HMe_4)RhCl_2]_2$ **8** and ligand **L5**, this situation is illustrated in Scheme IV.6. When the chloro-bridged complex **8** is dissolved with two equivalents of the ligand **L5**, the monomeric complex **$[(C_5HMe_4)Rh(L5)(H_2O)]^{2+}$** is formed. Addition of base initially leads to a deprotonation of the side chain. The assembly process to generate the macrocycle **$[(C_5HMe_4)Rh(L5–2\ H^+)]_3$** therefore requires 2 equiv. of base (with respect to the ligand).

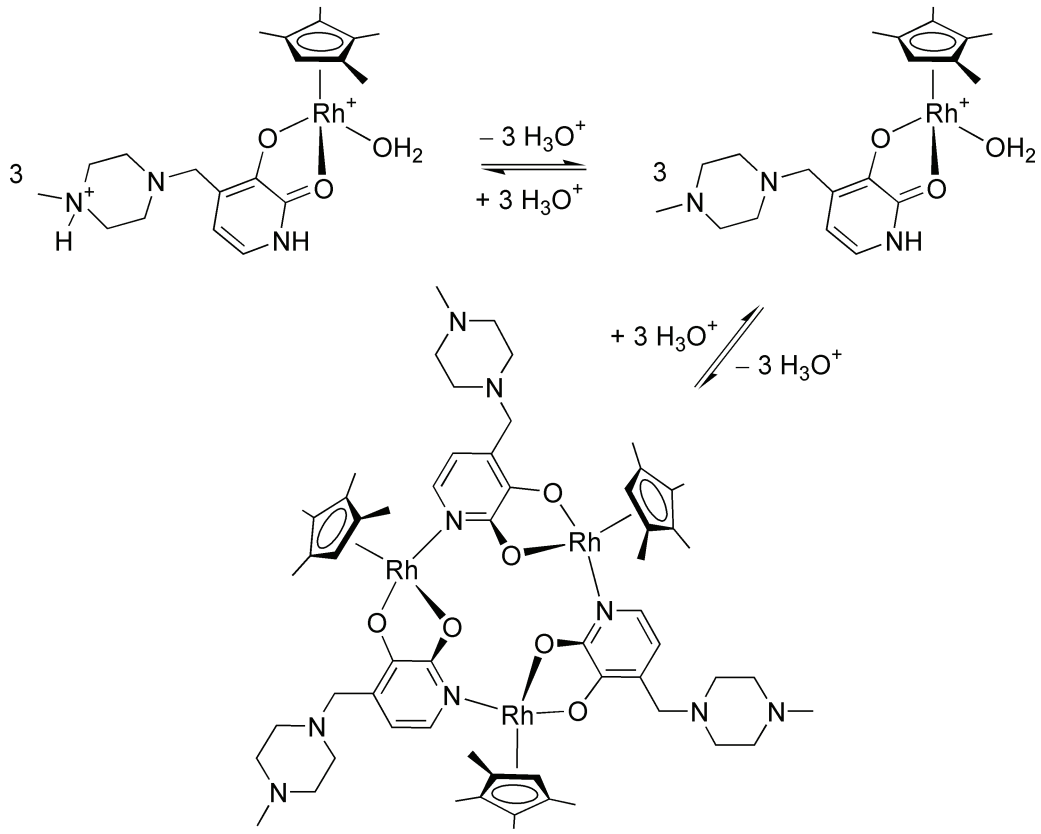

Scheme IV.6 pH dependant self-assembly of trinuclear metallamacrocycles of type B requiring more than 1.0 equiv. of CsOH.

Self-assembly occured not only after addition of base, but also in buffer solution.[310] When a mixture of $[(\pi\text{-ligand})MCl_2]_2$ and 2 equiv. of ligand **L2** was stirred in a phosphate buffer solution in D_2O (100 mM) at pH 7.0, clear orange solutions were obtained. As presented above, the self-assembly process is pH dependant. Thus, pronounced differences were observed for the various metal complexes. Whereas ^1H NMR spectroscopy indicated the formation of a trimeric structure for $[(C_6H_6)RuCl_2]_2$, $[(C_6H_5Me)RuCl_2]_2$, $[(cymene)RuCl_2]_2$, $[(C_6H_5CO_2Et)MCl_2]_2$ and $[Cp^*IrCl_2]_2$, a monomeric structure was observed for $[Cp^*RhCl_2]_2$ (Figure IV.10). This is in agreement with the more basic inflection point of rhodium complexes compared to iridium complexes. It should be noted, that the observed differences are caused only by the electronical differences of rhodium and iridium. If the pH was raised, the partial formation of a macrocyclic complex

was likewise observed. The spectra of trinuclear complexes in phosphate buffer solution were identical to those obtained after addition of CsOH.

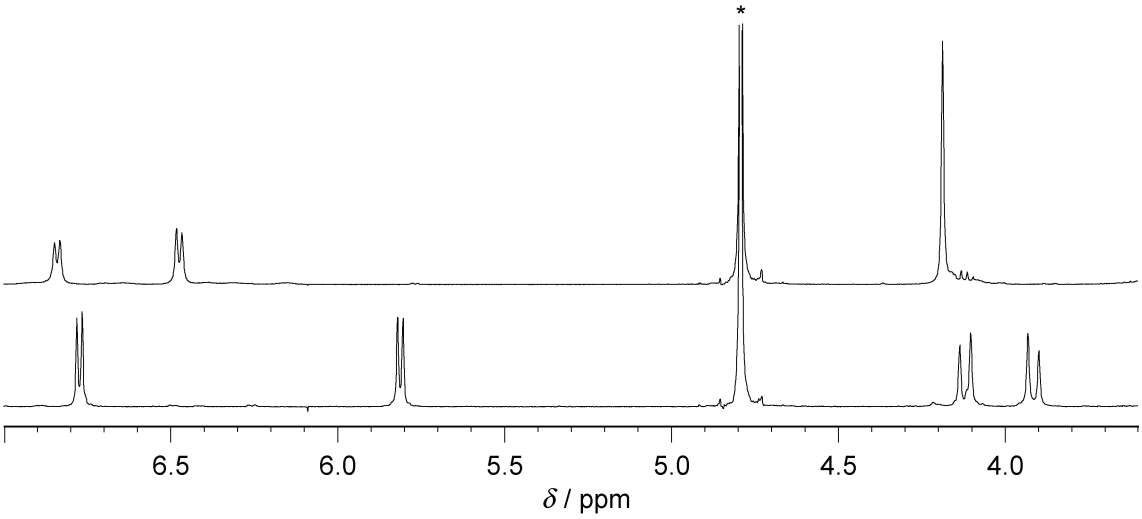

Figure IV.10 Part of the ^{1}H NMR spectra in phosphate buffer solution (D_2O) at pH 7.0 of the products obtained in reactions of ligand **L2** with $[Cp^*RhCl_2]_2$ (bottom) and $[Cp^*IrCl_2]_2$ (top). Two doublets for diastereotopic NCH2 protons at $\delta \sim 4$ ppm are observed only for $[Cp^*IrCl_2]_2$. The solvent peak is denoted by an asterisk.

IV.II.4 Structural Investigations.

In order to obtain structural information about monomeric complexes of type A, the reaction products of various metal–ligand combinations without the addition of base have been crystallised. Suited single crystals were obtained for reactions of the hexamethylbenzene ruthenium complex $[(C_6Me_6)RuCl_2]_2$ (**6**) with the ligands **L2**, **L3**, and **L4**. The molecular structures of one enantiomer of the resulting complexes in the crystal are depicted in Figure IV.11.

Overall, the molecular structures are very similar. The ligands are coordinated to the Ru atoms via the two pyridone O-atoms forming five-membered chelate rings. As suggested by NMR data, the ligands are in a zwitterionic form with a deprotonated 3-hydroxy group and an ammonium side-chain. In case of the ruthenium complexes, the NH proton of the ammonium group displays a hydrogen bond to the chloride counter ion. A second hydrogen bond can be observed between the chloride counter ion and the pyridone NH proton of an adjacent, symmetry-related complex. As a result, we observe the dimerization of the two enantiomeric ruthenium complexes present in the crystal via hydrogen bonding to two chloride anions (Figure IV.12). This arrangement seems to be energetically quite stable because it is observed for all three complexes. Since the crystals were obtained from organic solvents, the second chloride is coordinated to the metal and not

replaced by an aqua ligand. A summary of selected bond length and angles for the three complexes is given in Table IV.3.

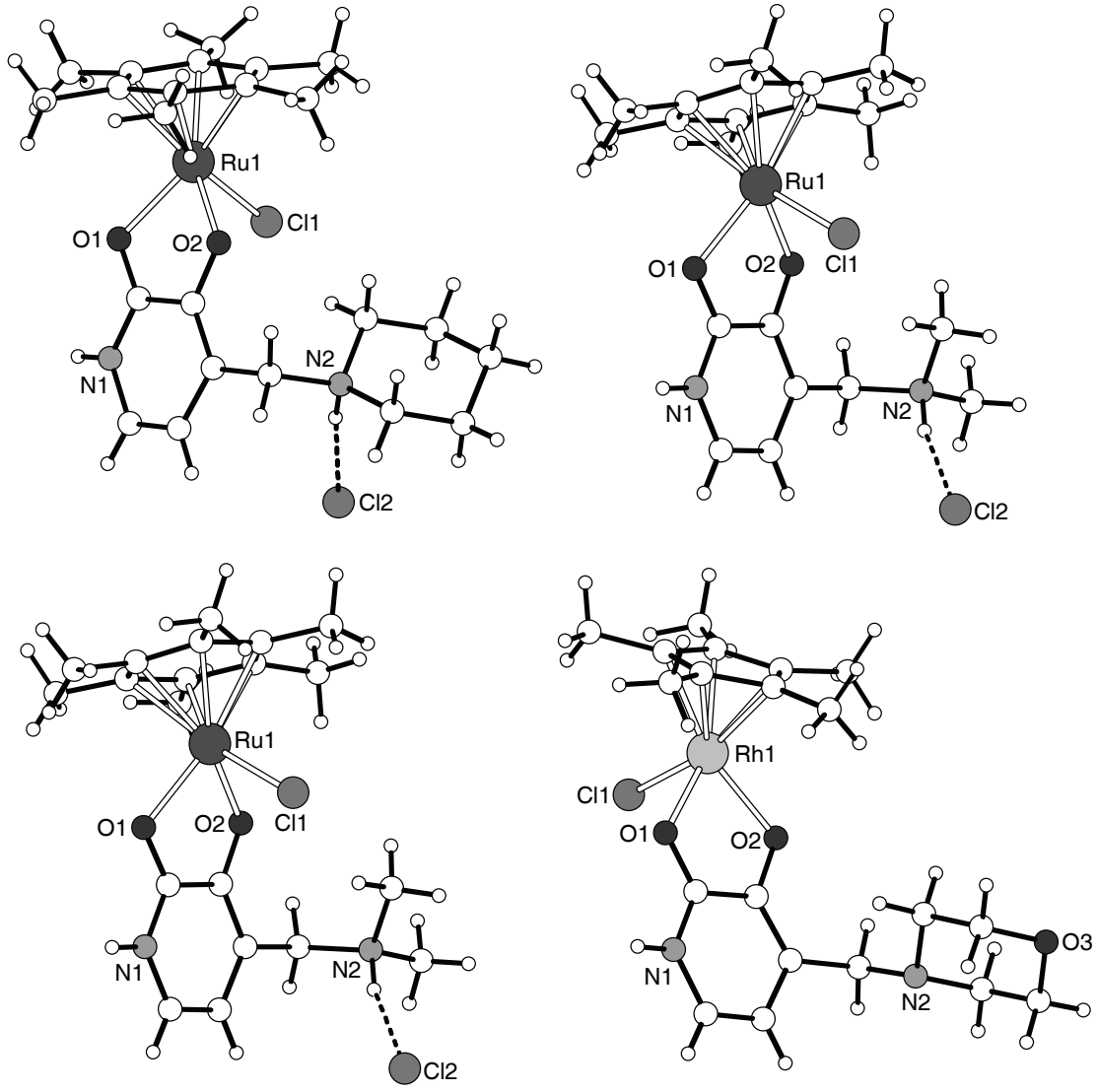

Figure IV.11 Graphic representations of the molecular structures of the monomeric complexes **[(C_6Me_6)Ru(L2)Cl]Cl** (top left), **[(C_6Me_6)Ru(L3)Cl]Cl** (top right), **[(C_6Me_6)Ru(L4)Cl]Cl** (bottom left) and **[Cp*Rh(L3–1 H^+)Cl]** (bottom right) in the crystal. The complexes were obtained in reactions of the complex **6** or **9** with two equivalents of the ligands **L2**, **L3** or **L4**, respectively. Solvent molecules are not shown for clarity.

Crystals were also obtained for the intermediate between monomeric form A and trimeric form B. As shown in Figure IV.11 (bottom right), the complex **[Cp*Rh(L3–H^+)Cl]** show a similar structure to the monomeric complexes presented above, but the

side chain is deprotonated and the counterion is missing. Selected bond length and angles are given together with the monomeric complexes of type A in Table IV.3.

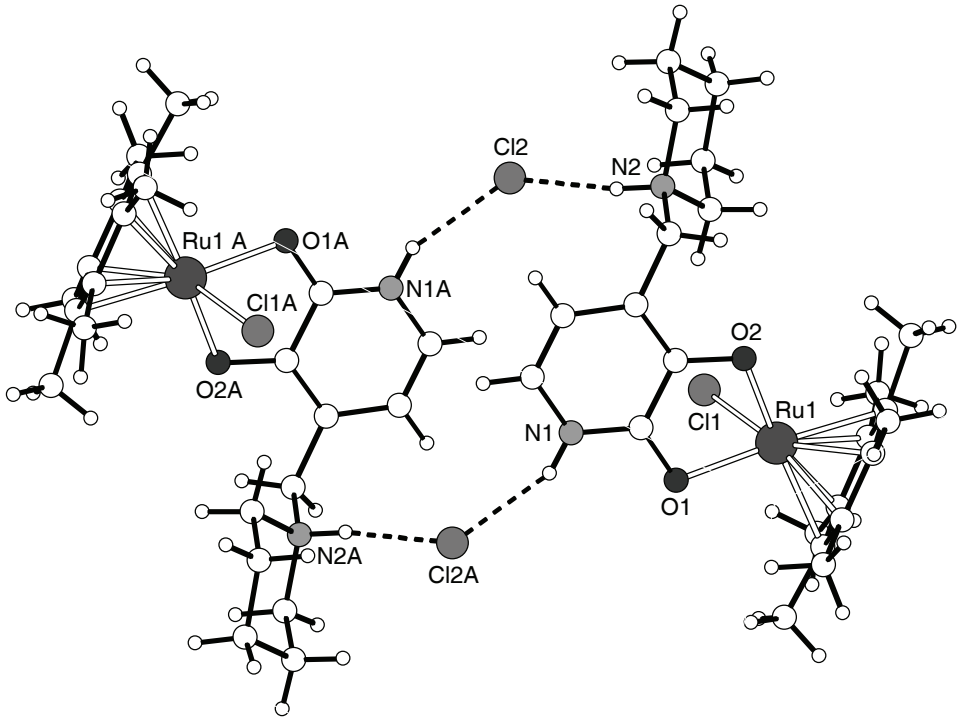

Figure IV.12 In the crystal, two cationic complexes **[(C_6Me_6)Ru(L2)Cl]$^+$** are connected via hydrogen bonding to the chloride counter ions. A similar arrangement is found for the complexes **(C_6Me_6)Ru(L3)Cl]Cl** and **[(C_6Me_6)Ru(L4)Cl]Cl**.

Table IV.3: Selected bond lengths (Å) and angles (°) of the monomeric complexes **[(C_6Me_6)Ru(L2)Cl]Cl**, **[(C_6Me_6)Ru(L3)Cl]Cl**, **[(C_6Me_6)Ru(L4)Cl]Cl** and **[Cp*Rh(L3–H^+)Cl]**.

Complex	M–Cl	M–O1	M–O2	O1–M–O2	O1–M–Cl1	M–O1–C1–C2	N2–Cl2	N1–Cl2
[(C_6Me_6)Ru(L2)Cl]Cl	2.42	2.15	2.09	78.6	83.3	14.23	3.08	3.14
[(C_6Me_6)Ru(L3)Cl]Cl	2.43	2.17	2.07	78.4	84.5	11.24	3.07	3.17
[(C_6Me_6)Ru(L4)Cl]Cl	2.43	2.14	2.08	78.3	85.2	13.79	3.02	3.14
[Cp*Rh(L2–H^+]Cl	2.42	2.14	2.13	78.3	86.9	7.52	—	—

Cationic complexes of type B were found to be difficult to crystallise, presumably due to the presence of three chloride counter ions. We thus focused on the neutral, completely deprotonated complexes. They were obtained by reaction of the respective chloro-bridged complexes with two equivalents of the pyridone ligands and an excess of base (Cs_2CO_3) in methanol (Scheme IV.7). After evaporation of the solvent, the products were separated from the salts by extraction with CH_2Cl_2 or hexane. A table with all synthesised

complexes can be found in the Appendix (Table IX.3 on page 214). Suited single crystals for X-ray analysis were obtained for the complexes **[(cymene)Ru(L2–2 H$^+$)]$_3$**, **[(cymene)Ru(L3–2 H$^+$)]$_3$**, **[(cymene)Ru(L5–2 H$^+$)]$_3$**, **[(C$_5$HMe$_4$)Rh(L5–2 H$^+$)]$_3$**, **[Cp*Rh(L5–2 H$^+$)]$_3$** and **[Cp*Ir(L3–2 H$^+$)]$_3$**. Graphic representations of the molecular structures in the crystal are depicted in Figure IV.14 and Figure IV.13.

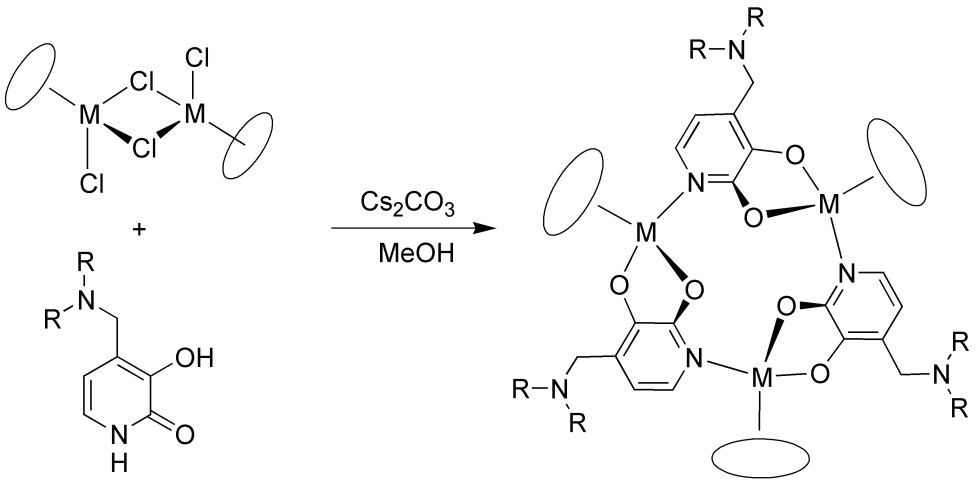

Scheme IV.7 Synthesis of deprotonated trinuclear metallamacrocycles in MeOH in the presence of CsOH.

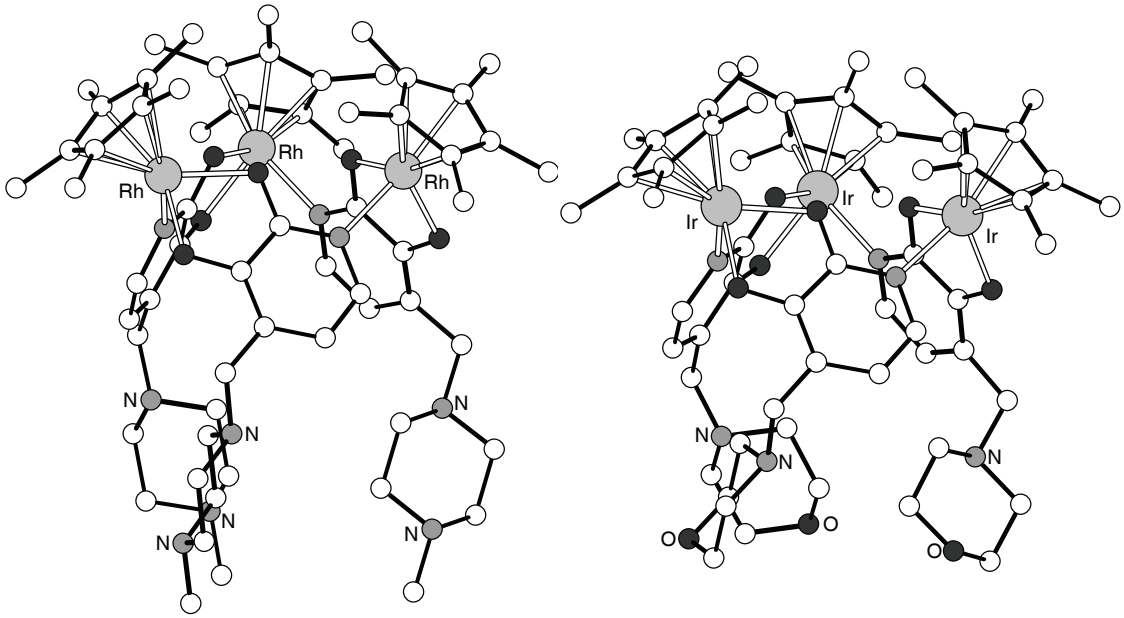

Figure IV.13 Graphic representations of the molecular structures of the trimeric complexes **[Cp*Rh(L5–2 H$^+$)]$_3$** (left) and **[Cp*Ir(L3–2 H$^+$)]$_3$** (right), in the crystal. Hydrogen atoms and solvent molecules are omitted for clarity.

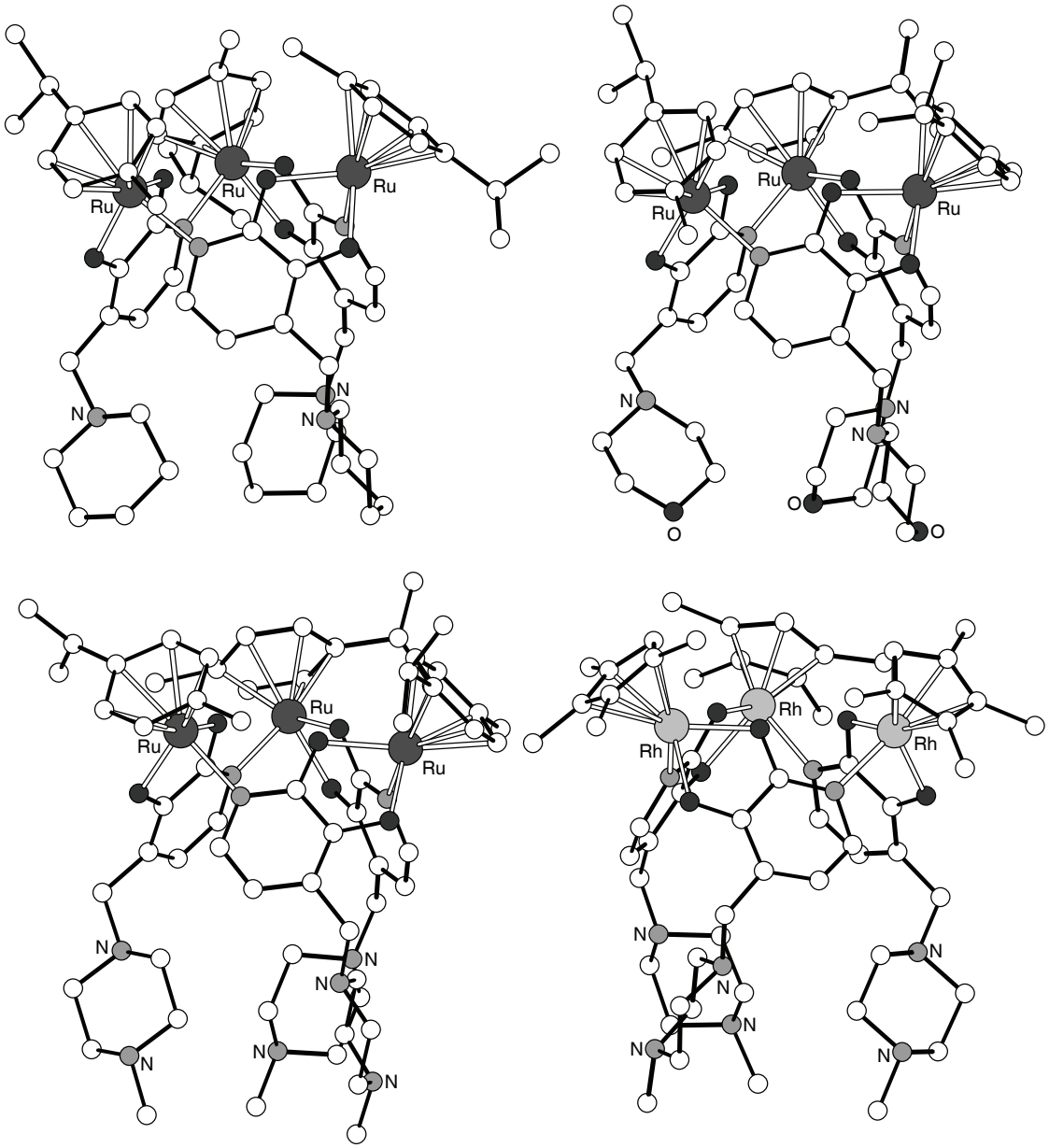

Figure IV.14 Graphic representations of the molecular structures of the trimeric complexes **[(cymene)Ru(L2–2 H^+)]$_3$** (top left), **[(cymene)Ru(L3–2 H^+)]$_3$** (top right), **[(cymene)Ru(L5–2 H^+)]$_3$** (bottom left) and **[(C_5HMe_4)Rh(L5–2 H^+)]$_3$** (bottom right) in the crystal. Hydrogen atoms and solvent molecules are omitted for clarity.

All six complexes show the expected trinuclear metallamacrocyclic structure with the metal centres being bridged by the two adjacent O-atoms and the N-atom of the pyridonate ligand. A comparison of important structural parameter shows that the substitution of the (cymene)Ru fragment with a Cp*Rh or a Cp*Ir fragment has only a small influence on the macrocyclic framework (Table IV.4).

Table IV.4: Selected bond lengths (Å) and angles (°) for 12-metallacrown-3 complexes of 3-hydroxy-2-pyridone ligands with diverse metal fragments.

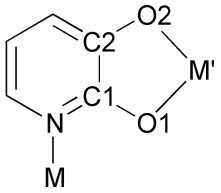

Complex	M–N	M–O1	M–O2	O1–M–O2	M–O–C1–C2	M–N–C1–C2	O–O'	M–M'
[(cymene)Ru(L2–2 H^+)]$_3$[a]	2.14	2.08	2.07	79.6	11.7	7.0	3.10	5.43
[(cymene)Ru(L3–2 H^+)]$_3$[a]	2.14	2.09	2.06	79.1	13.4	9.7	3.13	5.37
[(cymene)Ru(L5–2 H^+)]$_3$[a]	2.14	2.08	2.05	79.5	12.8	8.7	3.10	5.34
[(C_5HMe_4)Rh(L5–2 H^+)]$_3$	2.12	2.08	2.09	78.0	9.9	16.2	3.15	5.32
[Cp*Rh(L5–2 H^+)]$_3$	2.13	2.09	2.05	80.1	12.4	7.4	3.11	5.35
[Cp*Ir(L3–2 H^+)]$_3$	2.13	2.12	2.09	78.6	8.8	5.8	3.04	5.37

a. Averaged values are given.

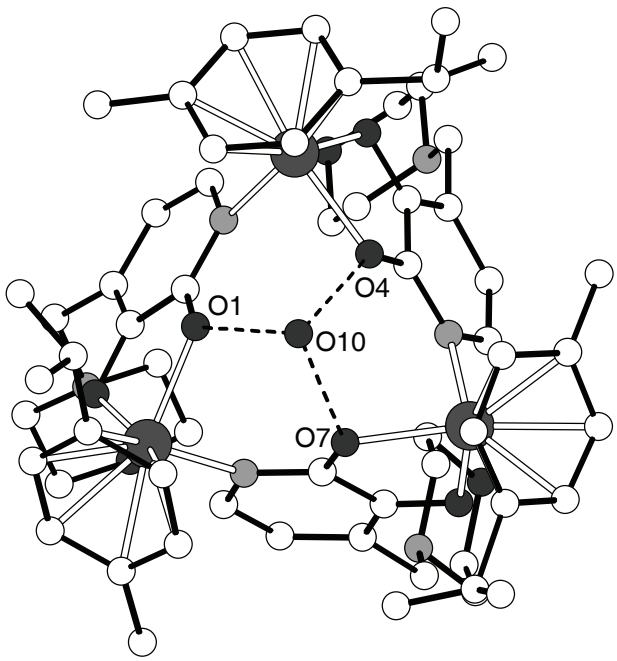

Figure IV.15 View along the pseudo C3 symmetry axis of the (cymene)Ru complex **[(cymene)Ru(L3–2 H^+)]$_3$** highlighting the hydrogen bonded water molecules within the cavity of the macrocycle. Distances (Å): O1–O10 = 2.942(5); O4–O10 = 2.895(5); O7–O10 = 2.980(5).

A difference between the crystal structures of the Cp*M complexes on one side and the (cymene)Ru and (C_5HMe_4)Rh complexes on the other side, is that the for the latter, a

water molecule can be found in the macrocyclic cavity.[n] These water molecules are within hydrogen bond distance to the bridging O-atoms (Figure IV.15). This is of special interest, since the O-atoms represent the binding site for alkali metal ions (see chapter IV.II.5).

IV.II.5 Host-Guest Chemistry.

Macrocyclic complexes of type B (Scheme IV.5) can be regarded as organometallic analogues of 12-crown-3.[137, 138] Similar to their organic counterparts,[311, 312] they are able to bind lithium ions although with a much higher affinity and selectivity (Scheme IV.8).

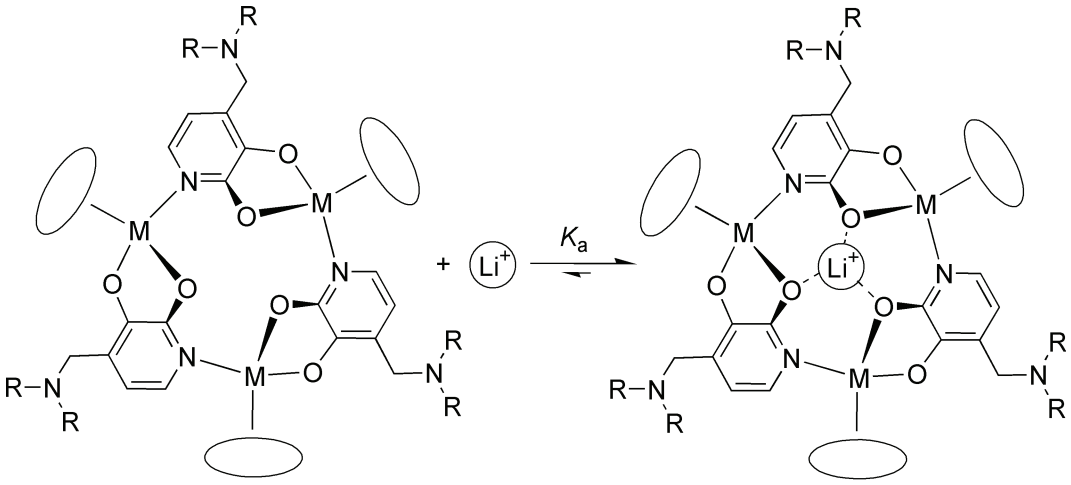

Scheme IV.8 Binding of Li^+ to trinuclear metallamacrocyclic receptors.

A central point of the present study was to investigate, how the affinity of these self-assembled receptors is influenced by structural modifications of the ligand and/or the metal fragment. The Li^+ binding constants for several complexes of type B using the metal/ligand combinations specified in Table IV.5 have been therefore determined. The assembly process was induced in situ using CsOH. For all complexes, the binding constant was determined by ^1H NMR spectroscopy. The complexation of Li^+ results in pronounced differences in chemical shifts and the exchange of Li^+ is slow compared to the NMR time scale (for a representative example see Figure IV.16). This allows calculating K_a directly by integration of suited signals.

First, the influence of the different metal fragments was investigated using the ligand **L2** (entry 1–3, 7, 8, & 10–13). For the ruthenium complexes **1–4**, the data suggest a cor-

n. The hydrogen atoms could not be localised, presumably due to a rotational disorder along the pseudo C_3 symmetry axis.

relation between the electronic properties of the arene π-ligand and the association constant K_a. The lowest value of $K_a = (28 \pm 6)\ M^{-1}$ is found for the $(C_6H_5CO_2Et)Ru$ complex **4** having an electron-withdrawing ester substituent (entry 7). For the (arene)Ru complexes **1**–**3**, the binding constants increase with number of the electron donating alkyl groups from $K_a = (7.5 \pm 0.6) \times 10^2\ M^{-1}$ to $K_a = (2.1 \pm 0.6) \times 10^3\ M^{-1}$ (entry 1–3). Similarly, the $(C_5HMe_4)Rh$ complex **8** displays a higher affinity for Li^+ ($K_a = (1.3 \pm 0.2) \times 10^4\ M^{-1}$) than the CpRh complex **7** ($K_a = (2.9 \pm 0.5) \times 10^3\ M^{-1}$, entry 9 and entry 10). For the Cp*Rh complex **9**, on the other hand, a relatively low binding constant of $K_a = (1.3 \pm 0.4) \times 10^1\ M^{-1}$ was observed (entry 11). Here, the negative effect of the sterically demanding Cp* π-ligands, which block the binding site, dominates over the positive electronic effect of the five methyl groups on the cyclopentadienyl ligand.

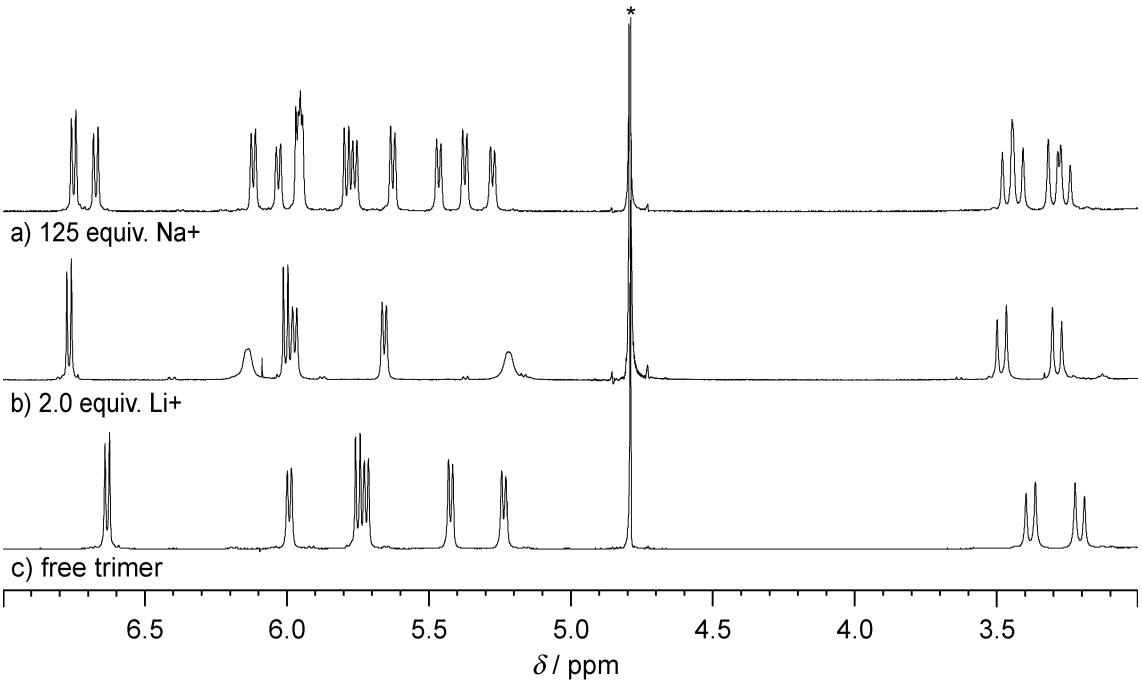

Figure IV.16 Part of the ^1H NMR spectrum (D_2O) of a solution containing the receptor **[(cymene)Ru(L5–2 H^+)]$_3$** (5.0 mM) and a) Na_2SO_4 (125 mM), b) LiCl (10.0 mM) and c) no alkali metal salt. The addition of LiCl results in quantitative adduct formation whereas for Na_2SO_4, a mixture between the free and the complexed receptor can be observed. The solvent peak is denoted by an asterisk.

The nature of the metal ion is a second important factor influencing the binding constants. Rhodium complexes were found to display higher binding constants than their analogous iridium complexes (entry 10 vs. 12; entry 11 vs. 13). It is known that the polarity of the metal-oxygen bond is a crucial factor for the binding affinity of metallacrown

complexes[128] and the observed difference between rhodium and iridium can possibly be attributed to a less polar binding site (oxygen atoms) in the case of iridium receptors.

Table IV.5: Binding constants K_a for the complexation of Li^+ and Na^+ of selected trinuclear metallamacrocycles.[a]

Entry	Complex	Ligand	equiv. of CsOH[b]	equiv. of MX[c]	K_a / M^{-1}
1	**1**	**L2**	1.0	2.0 LiCl	$7.5 \pm 0.6 \times 10^2$
2	**2**	**L2**	1.0	2.0 (4.0) LiCl[d]	$1.2 \pm 0.6 \times 10^3$
3	**3**	**L2**	1.0	2.0 LiCl	$2.1 \pm 0.6 \times 10^3$
4	**3**	**L2**	1.0	1.0 Li_2SO_4	$2.2 \pm 0.6 \times 10^3$
4	**3**	**L2**	1.0	2.0 $LiNO_3$	$2.3 \pm 0.6 \times 10^3$
6	**3**	**L2**	1.0	50 LiOAc	$2.2 \pm 0.6 \times 10^3$
7	**4**	**L2**	1.0	2.0 (6.0) LiCl	$2.8 \pm 0.6 \times 10^1$
8	**7**	**L2**	1.0	2.0 (4.0) LiCl	$2.9 \pm 0.5 \times 10^2$
9	**7**	**L2**	1.5	2.0 LiCl	$1.6 \pm 0.5 \times 10^3$
10	**8**	**L2**	1.5	2.0 LiCl	$1.3 \pm 0.2 \times 10^4$
11	**9**	**L2**	1.3	50 Li_2SO_4	$1.3 \pm 0.4 \times 10^1$
12	**10**	**L2**	1.0	2.0 (4.0) LiCl	$2.6 \pm 0.5 \times 10^2$
13	**11**	**L2**	1.0	50 Li_2SO_4	$9.0 \pm 2.0 \times 10^{-2}$
14	**3**	**L3**	1.0	2.0 LiCl	$2.3 \pm 0.6 \times 10^3$
15	**3**	**L4**	1.0	2.0 LiCl	$2.4 \pm 0.6 \times 10^3$
16	**1**	**L5**	1.0	2.0 LiCl	$4.0 \pm 0.6 \times 10^3$
17	**2**	**L5**	1.0	2.0 LiCl	$5.4 \pm 0.5 \times 10^3$
18	**2**	**L5**	1.5	2.0 LiCl	$1.3 \pm 0.5 \times 10^4$
19	**2**	**L5**	2.0	2.0 LiCl	$3.0 \pm 0.6 \times 10^4$
20	**3**	**L5**	2.0	2.0 LiCl	$5.8 \pm 1.0 \times 10^4$
21	**7**	**L5**	2.0	2.0 LiCl	$2.7 \pm 0.6 \times 10^3$
22	**8**	**L5**	2.0	2.0 LiCl	$5.6 \pm 2.1 \times 10^4$
23	**10**	**L5**	1.0	2.0 LiCl	$1.2 \pm 0.6 \times 10^3$
24	**3**	**L2**	1.0	50 Na_2SO_4	$5.0 \pm 1.0 \times 10^{-1}$
25	**8**	**L2**	1.5	50 Na_2SO_4	1.3 ± 0.3
26	**3**	**L3**	1.0	50 Na_2SO_4	$6.0 \pm 1.0 \times 10^{-1}$
27	**3**	**L4**	1.0	50 Na_2SO_4	$6.0 \pm 1.0 \times 10^{-1}$
28	**3**	**L5**	2.0	15 (25) Na_2SO_4	5.0 ± 1.0
29	**8**	**L5**	2.0	15 (25) Na_2SO_4	7.0 ± 1.0

a. Binding constants were determined by ^1H NMR spectroscopy at receptor concentrations of 1.0 or 5.0 mM for Li^+ and Na^+, respectively.
b. Equivalents with respect to the amount of ligand.
c. Equivalents with respect to the amount of formed receptor.
d. Two different MX concentrations were employed to determine K_a.

Macrocycles containing the ligands **L2**, **L3** and **L4** showed very similar affinities for Li^+ (entry 3, 14 and 15). Receptors based on ligand **L5**, on the other hand, displayed higher binding constants (entry 1 vs. 16; entry 2 vs. 17; entry 12 vs. 23). As described above, a unique feature of ligand **L5** is that the protons are located on the terminal methylamino groups and not on the amino group adjacent to the pyridone. This means that the protons – and thus the positive charges – are located further away from the Li^+ binding site, which increases the affinity.

The importance of the charges raised the question which influence the change of the pH would have on the binding constants. The addition of more than one equivalent of CsOH with respect to the ligand was expected to lead to a deprotonation of the amino side chains and therefore to a higher affinity for Li^+. This was indeed the case: if one equivalent of CsOH was added to a mixture of the (C_6H_5Me)Ru complex **2** and ligand **L5**, a binding constant of $K_a = (5.4 \pm 0.5) \times 10^3\ M^{-1}$ was determined[o]. This value increased to $K_a = (1.3 \pm 0.5) \times 10^4\ M^{-1}$ and finally to $K_a = (3.0 \pm 0.6) \times 10^4\ M^{-1}$ upon addition of 1.5 or 2.0 equiv. of CsOH, respectively (entry 17–19). A similar trend was observed for the CpRh complex **7** in combination with **L2** (entry 8 and 9). These studies were restricted to metal–ligand combinations for which complete deprotonation did not result in precipitation.

Overall, the best Li^+ receptors were the macrocycles obtained from a combination of the ligand **L5** with the (cymene)Ru complex **3** ($K_a = (5.8 \pm 1.0) \times 10^4\ M^{-1}$) or the (C_5Me_4H)Rh complex **8** ($K_a = (5.6 \pm 2.1) \times 10^4\ M^{-1}$) with two equivalents of CsOH (entry 20 and 22). It should be noted that these values are amongst the highest ever reported for Li^+ complexation in water.[277–279] For potential applications, the (cymene)Ru complex is particularly appealing because the starting material **3** is commercially available. The corresponding receptor **[(cymene)Ru(L5–2 H^+)]$_3$** can either be prepared in situ by base induced self-assembly or be synthesised prior to binding studies as outlined in Scheme IV.7. The Li^+ binding constant was found to be identical.

In organic solvents, 12-metallacrown-3 complexes were found to bind lithium and sodium salts as ion pairs.[127] Consequently, the binding constants depend on the nature of the anion. For the water soluble receptors presented above, a dependence of this kind was not observed: the binding constants for the complexation of LiCl, Li_2SO_4, $LiNO_3$ and LiOAc were – within the limits of accuracy – all the same (entry 3–6).

A remarkable feature of the new receptors is their extremely high selectivity for Li^+ over Na^+. For most metal–ligand combinations, it was not possible to observe a complexation of Na^+ under the conditions employed ([receptor] = 5.0 mM, [Na^+] = 500 mM). Only for the high affinity receptors formed from **3** and **8** it was possible to observe Na^+

o. With only 1.0 equiv. of CsOH, the macrocyclisation was not quantitative, and 10 % of a monomeric complex of type A was observed. For the calculation of the binding constant, the concentrations were adjusted accordingly.

adducts by ^{1}H NMR spectroscopy and thus to calculate the binding constants. As listed in Table IV.5, the values for the complexation of Na^+ are approximately *four orders of magnitude lower* than the values determined for Li^+ (entry 24–29).

In order to obtain more information about the differences of the high affinity host **[(cymene)Ru(L5–2 H$^+$)]$_3$** and the cationic host obtained from **3**, **L2** and 1.0 equiv. of CsOH (entry 3), we have investigated the kinetics of the Li^+ complexation. A stock solution of LiCl ($[Li^+]_{final}$ = 9.8 mM) was added to a solution of the respective receptor in D_2O (4.9 mM). The time course of adduct formation was then determined by ^{1}H NMR spectroscopy. The results are depicted in Figure IV.17. Fitting of the experimental data to a simple bimolecular reaction model with the help of the program Gepasi[233, 234] (version 3.30, using a preinstalled Levenberg-Marquart algorithm) showed that the complexation rates k_{on} for both receptors are very similar: for the combination of **3** and **L2** a value of $(2.72 \pm 0.02) \times 10^{-4}$ mM^{-1} s^{-1} was determined whereas for **[(cymene)Ru(L5–2 H$^+$)]$_3$**, a value of $(2.94 \pm 0.03) \times 10^{-4}$ mM^{-1} s^{-1} was found. The difference in affinity can therefore be attributed to a difference in the decomplexation rates k_{off} of the two hosts. For **3**/**L2**/1.0 equiv. CsOH, a value of $k_{off} = (1.17 \pm 0.05) \times 10^{-4}$ s^{-1} was determined. The resulting calculated binding constant of $K_a = k_{on}/k_{off} = 2.3 \times 10^{-3}$ M^{-1} corresponds well to what was determined by ^{1}H NMR spectroscopy under equilibrium conditions (Table IV.5, entry 3). For the high affinity receptor **[(cymene)Ru(L5–2 H$^+$)]$_3$**, a meaningful decomplexation rate could not be deduced from the kinetic data, because the quantitative formation of the Li^+ adduct was observed by ^{1}H NMR under the employed conditions. Using the value for the binding constant determined at a lower receptor concentration of 1.0 mM (Table IV.5, entry 20), however, a decomplexation rate $k_{off} = 5 \times 10^{-6}$ s^{-1} can be estimated.

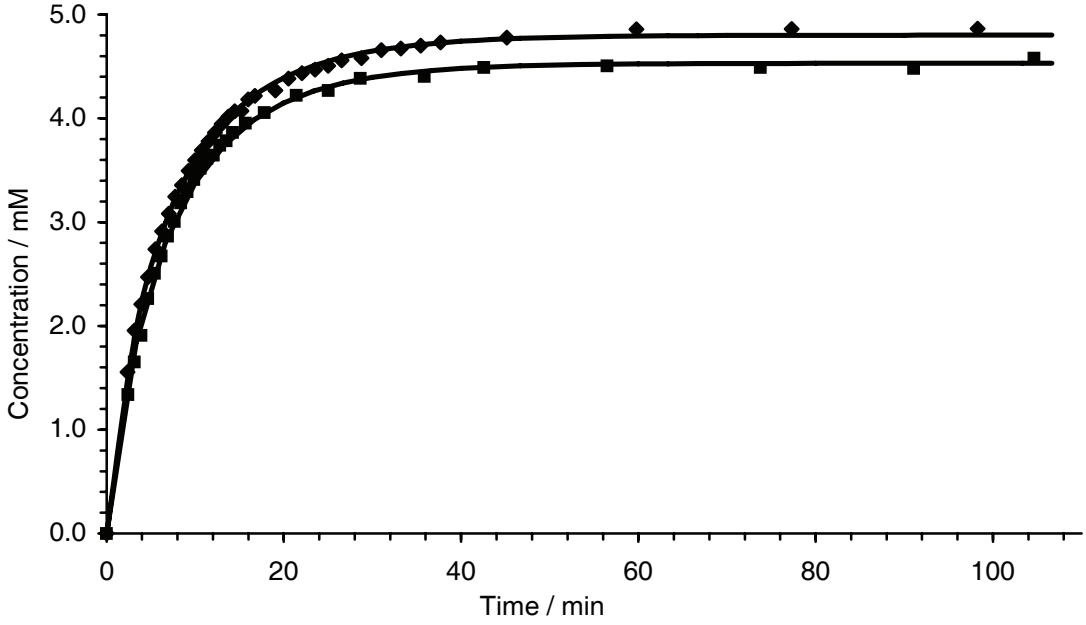

Figure IV.17 Time course of Li^+ adduct formation of the receptor obtained from **3**, **L2** and 1.0 equiv. of CsOH (■) and of receptor **[(cymene)Ru(L5–2 H^+)]$_3$** (◆) as determined by ^{1}H NMR spectroscopy (D_2O; [Li^+] = 9.8 mM; [receptor] = 4.9 mM).

IV.III From Receptors to Sensors

IV.III.1 A pH Sensor for Li^+ Ions

The base induced macrocyclisation of **3** and **L5** to give receptor **[(cymene)Ru(L5–2 H^+)]$_3$** was found to be a reversible process: when 6 equiv. of DCl were added to solution of **[(cymene)Ru(L5–2 H^+)]$_3$** in D_2O, the spectrum of the monomeric complex **[(cymene)Ru(L5)(H_2O)]$^+$** was observed by ^1H NMR spectroscopy (Scheme IV.9). Accordingly, a potentiometric titration of **[(cymene)Ru(L5–2 H^+)]$_3$** with HCl gave a curve, which was nearly identical with what was found for **3**, **L5** and CsOH (Figure IV.18).[p]

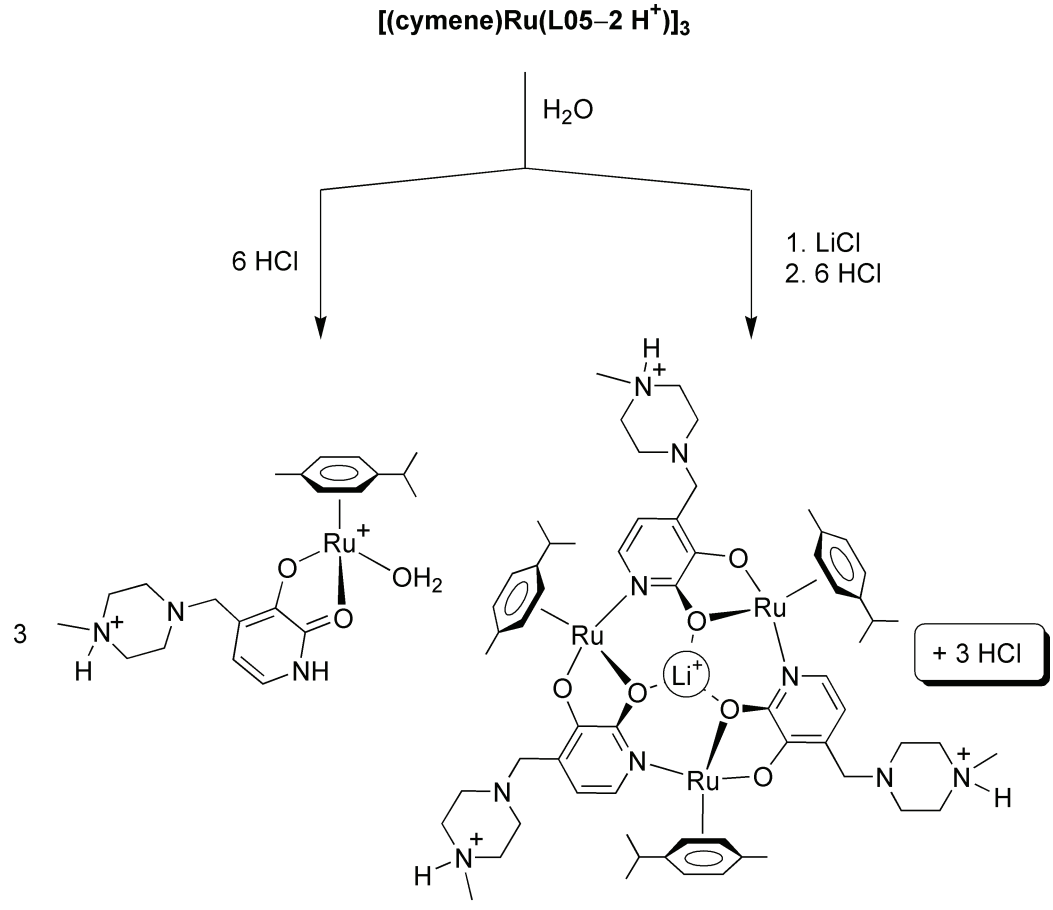

Scheme IV.9 Design of a pH dependant sensor for Li^+ ions in water.

p. Small deviations with respect to the reverse titration curve with CsOH were observed in the final part of the curve (5–6 equiv. of HCl). They could be reduced if the titrations were performed very slowly.

In the presence of LiCl, however, a different behaviour was observed. Addition of HCl to a solution of **[(cymene)Ru(L5–2 H^+)]$_3$** containing lithium ions resulted in the immediate protonation of the amine side chains but not in the cleavage of the macrocycle (Scheme IV.9). This is reflected by the titration curves with HCl: the first part is identical for titrations with and without Li^+ but after addition of three equivalents of HCl, a sharp drop in pH was observed for solutions containing Li^+ because the acid is not consumed to form monomeric complexes (Figure IV.18).

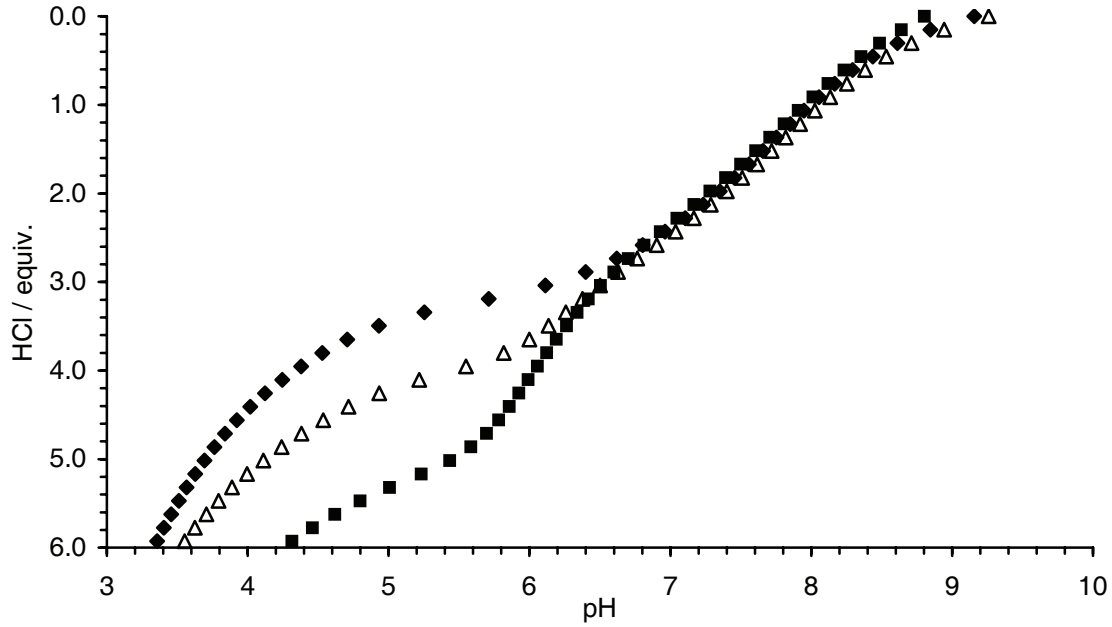

Figure IV.18 pH of solutions containing receptor **[(cymene)Ru(L5–2 H^+)]$_3$** (5.0 mM) after addition of increasing amounts of HCl (equivalents with respect to the trimeric receptor). The titrations were performed in the presence of 1.0 equiv. LiCl (◆), 0.5 equiv. LiCl (Δ) and without LiCl (■).

The different behaviour of receptor **[(cymene)Ru(L5–2 H^+)]$_3$** in the presence and absence of lithium ions offers the possibility to detect Li^+ in water by a simple pH measurement. Various amounts of Li^+ (0.0–1.5 equiv. with respect to the receptor) were added to a solution of receptor **[(cymene)Ru(L5–2 H^+)]$_3$** (5.0 mM). After equilibration, 4.5 equiv. of HCl (with respect to the receptor) were added and the pH was determined (Figure IV.19). Between 0.0 and 1.0 equiv. of Li^+, the resulting pH differs by more than two units. This difference is sufficient to allow a semiquantitative determination of Li^+ in the low millimolar concentration range using commercially available pH strips (accuracy: 0.5 pH units).

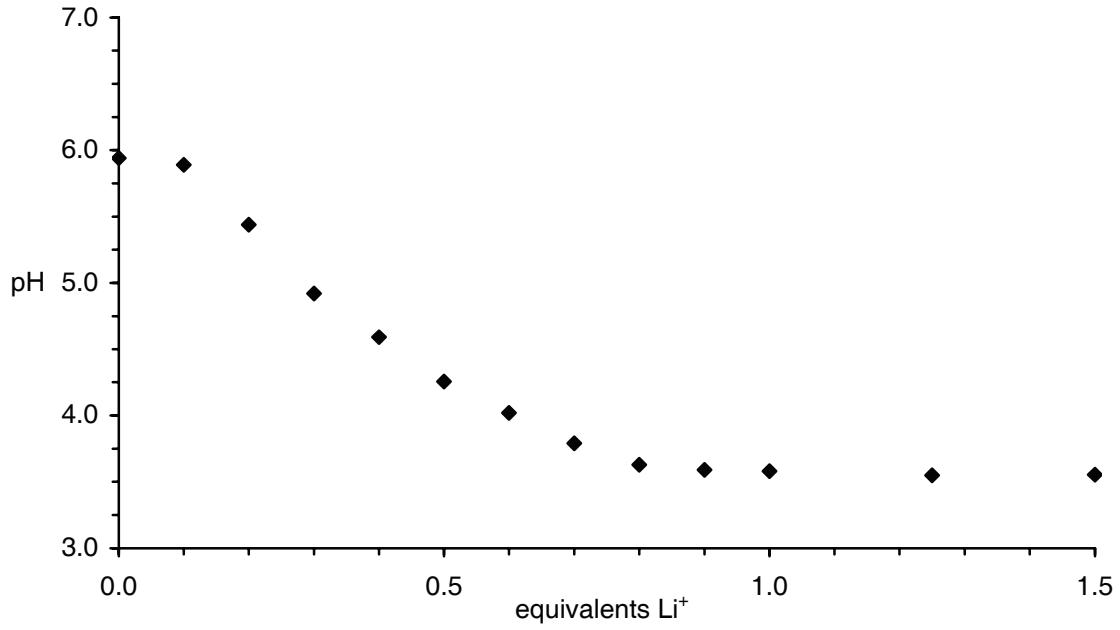

Figure IV.19 pH of solutions containing the receptor **[(cymene)Ru(L5–2 H^+)]$_3$** (5.0 mM) in the presence of various amounts of LiCl (0.0–1.5 equiv.) after addition of HCl (4.5 equiv. with respect to the receptor).

IV.III.2 A Colorimetric Test for Li^+ Ions in Water

From the reactions with HCl it was apparent that the kinetic and thermodynamic stability of receptor **[(cymene)Ru(L5–2 H^+)]$_3$** was enhanced in the presence of lithium ions. This raised the question whether a difference between the free receptor **[(cymene)Ru(L5–2 H^+)]$_3$** and the host-guest complex **[(cymene)Ru(L5–2 H^+)]$_3$ × Li^+** can also be observed for other chemical reactions. Screening of a number of different reagents revealed that simple Fe(III) salts are ideally suited: when an excess of $FeCl_3$ was added to an aqueous solution of **[(cymene)Ru(L5–2 H^+)]$_3$**, the receptor immediately decomposed to give a dark brown solution from which a brown powder slowly precipitated.[q] In the presence of lithium ions, this reaction was kinetically inhibited and addition of $FeCl_3$ lead to no immediate colour change.[r] This difference in reactivity can be used for the 'naked eye' detection of Li^+ in water in the pharmacologically relevant concentration range of 0.5–1.2 mM.[277–279] An example is shown in Figure IV.20. Nine solutions with three different receptor concentrations (0.5, 1.0 and 1.6 mM) and three different Li^+ concentrations (0.1, 1.0 and 1.6 mM) were prepared. Upon addition of an excess of $FeCl_3$ (~ 3 equiv.

q. Attempts to identify the product of the reaction were not successful.

r. After 15 min., a dark precipitate was also observed in the presence of lithium ions.

with respect to **[(cymene)Ru(L5–2 H^+)]$_3$**), a colour change was only observed for solutions in which the receptor was not saturated with Li^+. A 3 × 3 assay of this kind can thus be used to determine whether the Li^+ concentration is in the range 0.0–0.5 mM, 0.5–1.0 mM, 1.0–1.5 mM or above 1.5 mM. It remains to be seen whether a colorimetric test of this kind can be used to determine Li^+ in more complicated matrixes, such as body fluids. From previous studies, it is known that peptides may show a high affinity to half-sandwich complexes of Rh^{II} and Rh^{III}.[313–315] It therefore seems likely that peptides would have to be removed from samples prior to testing.

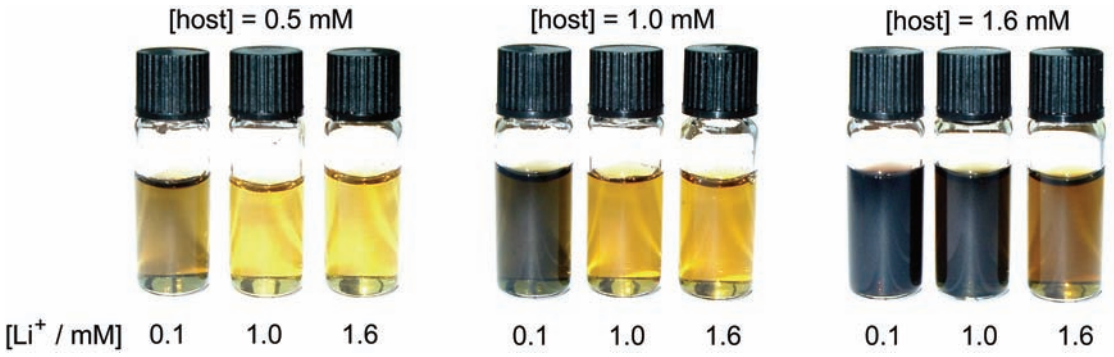

Figure IV.20 Photos of aqueous solutions containing different concentrations of host **[(cymene)Ru(L5–2 H^+)]$_3$** (0.5, 1.0 and 1.6 mM) and different concentrations of Li^+ (0.1, 1.0 and 1.6 mM) after addition of an excess of $FeCl_3$ (3 equiv. with respect to the receptor). A brown colour is observed for solutions in which the receptor **[(cymene)Ru(L5–2 H^+)]$_3$** is not saturated with Li^+. The photos were recorded one minute after addition of $FeCl_3$.

IV.III.3 Functionalisation of the Bridging Ligand

Two building blocks were used to generate 12-metallacrown-3 receptors: the 3-hydroxy-2-pyridone ligands and the dimeric halfsandwich complexes $[(\pi\text{-ligand})MCl_2]_2$. For the development of Li^+ specific sensors on the basis of these metallamacrocyclic receptors, further modifications are necessary. As these modifications should not interfere with the self-assembly process or with the binding properties of the receptor, it seemed best to concentrate on further modifications at the C4-position of the hydroxy-pyridone ligand. Although the Mannich reaction proofed to be quite useful for the modification of the bridging ligands, it is limited to the use of secondary amines. A tailored functionalisation such as attaching a fluorophore is thus not possible. Given the importance of further modifications of the bridging ligand, a convenient way to access structural diversity had to be found.

Ligand **L6** was prepared from 3-hydroxy-2-pyridone, formaldehyde and dibenzylamine in 28 % yield. It should be noted that 2 equiv. of dibenzylamine had to be employed in order to obtain a pure product. The use of only 1 equiv. resulted in the for-

mation of a mixture of the ligands **L1** and **L6** in a ratio 1:1. Purification in this case was achieved by extraction of **L1** with water from a solution of the product mixture in chloroform.

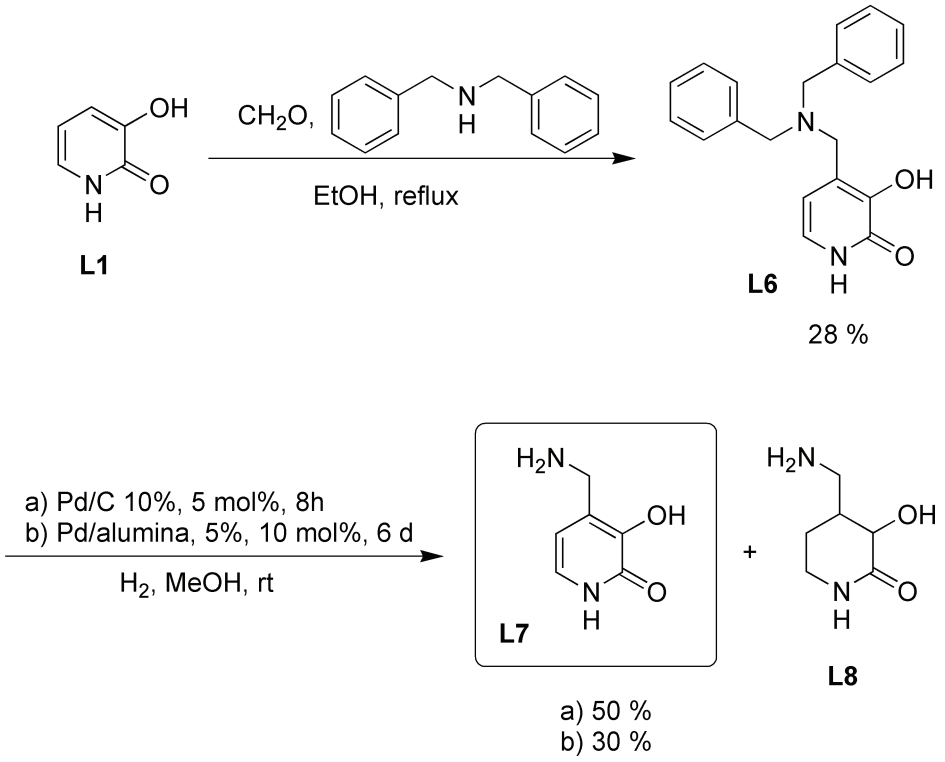

Figure IV.21 Synthesis of precursor 4-aminomethylene-3-hydroxy-2-pyridone **L7**.

Subsequent cleaving of the benzyl groups by hydrogenation in the presence of Pd/C as catalyst led to ligand **L7**. Unfortunately, Pd/C is not only able to cleave the benzyl groups, but also to reduce the aromatic ring in considerable amounts, leading to compound **L8** as side product. Optimization of the reaction conditions by stringent control of the reaction time, the substrate and the catalyst concentration allowed to increase the yield of the hydrogenation step to 50 %. An alternative approach to circumvent the problem of side product formation is a slight decrease of the catalyst activity. Thus, no side product was observed if Pd/Al_2O_3 was employed. However, the decrease of the catalyst activity resulted in a multifold increase of the reaction time.

Overall, ligand **L7** can be obtained in high purity from commercially available and cheap starting materials in two steps. Attaching an primary amino group to the pyridone ligand resulted in a versatile precursor giving access to a variety of functionalised 3-hydroxy-2-pyridones. Examples for its versatility are the synthesis of ligands to which a fluorescent unit is attached (see chapter IV.III.4) and the synthesis of bridged 3-hydroxy-2-pyridone units such as **EL6** and **EL7** (Figure IV.22), the latter one carried out by a postdoctoral coworker. These molecules are in so far interesting, as they give poten-

tial access to hexanuclear complexes with a helical like structure similar to those presented later on (see chapter VI). Three 3-hydroxy-2-pyridone units attached together, such as molecule **EL8** could give access to structurally very complex cage compounds.

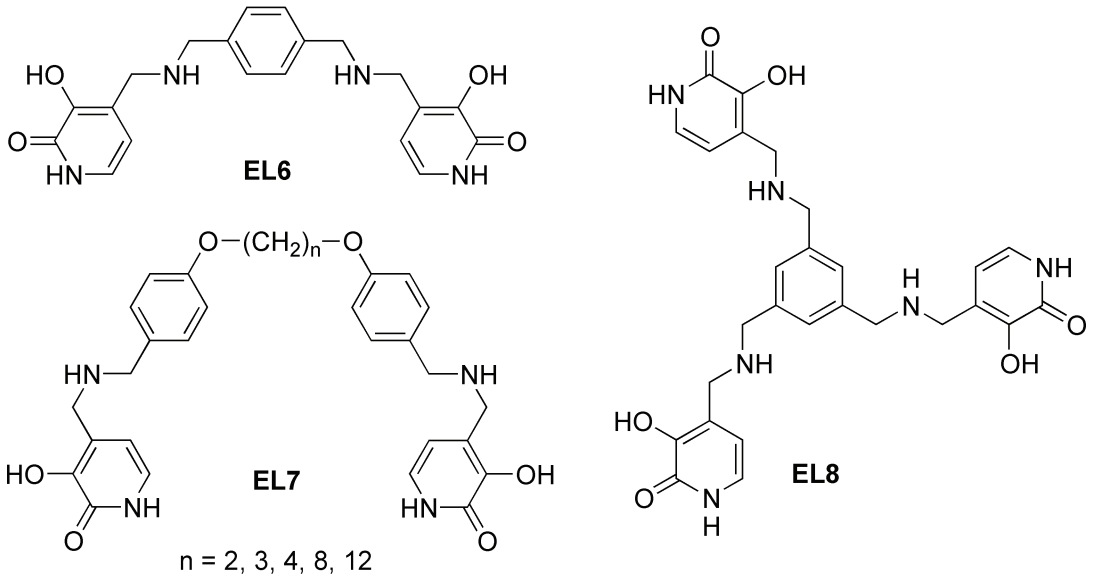

Figure IV.22 Bridged 3-hydroxy-2-pyridone ligands.

IV.III.4 A Fluorescence Sensor for Li^+ Ions in Water

Due to its sensitivity, fluorescence spectroscopy is one of the most important analytical tools in chemistry. Generally, a chemosensors displays a fluorescent unit attached either with or without spacer to a binding unit. Upon binding of the analyte, the fluorescent behaviour changes. Two different design principles of fluorescent chemosensors can be distinguished: photoinduced electron transfer (PET) and photoinduced charge transfer (PCT).[316]

In the case of a fluorescent PET cation sensor, the fluorescence is quenched until a binding event occurs. Thus, fluorescence turns ‘on’ in the present of analyte. The principle is depicted in Figure IV.23 (bottom). The fluorophore acts as an acceptor, whereas the receptor has to be a potential electron donor. If the fluorescent unit is excited, an electron is promoted from the highest occupied molecular orbital HOMO to the lowest unoccupied molecular orbital LUMO. The HOMO of the free receptor unit is energetically higher than the HOMO of the fluorescent unit and photoinduced electron transfer (PET) occurs, causing constant fluorescence quenching. Upon binding, the redox potential of the receptor increases, leading to a decrease in energy of the HOMO of the donor group of the receptor. Hence, PET is not longer possible and fluorescence quenching is suppressed.

Most often the receptor units contains amines which act as donor groups, but the use of transition metals to quench the fluorescence is also known.[317, 318] Generally, very simple fluorescent units such as naphthalene or anthracene have been employed and fluorescent PET chemosensors for cations based on crown units, cryptands, podands, calixarene and chelating units have been realised.[316] The first fluorescent PET chemosensor for Li^+ ions in organic solvents has been presented by Gunnlaugson in 2004[290, 294] but no Li^+-specific fluorescent chemosensors, which are operational in *water* are known so far.

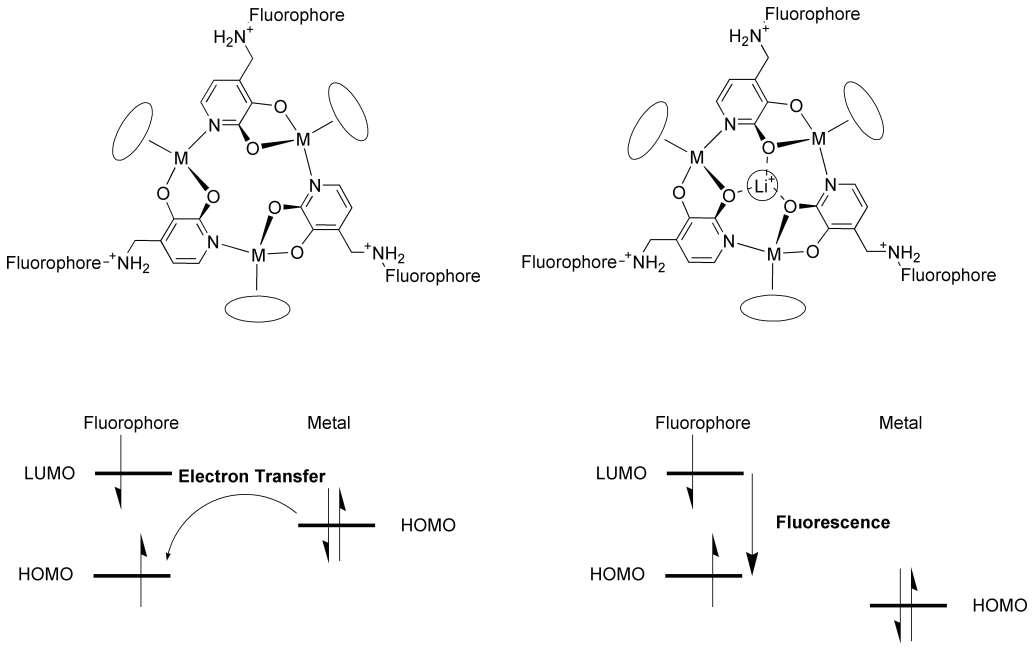

Figure IV.23 Basic principle of a fluorescent photoinduced electron transfer (PET) cation sensor. In the absence of analyte, PET occurs from the HOMO of the metal centre to the HOMO of the fluorophore causing quenching of the fluorescence (left). In the presence of Li^+, the redox potential is increased and the energetic level of the HOMO of the metal centre decreased. PET is not any longer possible, and the fluorescence turns on.

The design of a potential Li^+ fluorescent sensor in water is presented in Figure IV.23. A fluorescent unit is attached via an amine group to the 12-metallacrown-3 complex. Water solubility is achieved via protonation of the three amine groups and electron transfer from the transition metal to the fluorophore will partially quench fluorescence. In the presence of lithium ions, the metal ions are more difficult to oxidize and quenching is reduced. The difference of the redox potential is expected to be around 300 mV.[124] However, one intrinsic problems has to be mentioned: any change in the pH of the solution leads automatically to a change in the protonation degree of the amine groups which will cause a fluorescence change. Thus, in order to keep the pH constant, meausurements have to be carried out in buffer solution. For potential applications of Li^+ sensing in blood this is an intrinsic advantage, because blood itself is buffered.

Pyrene and anthracene units have been chosen to act as fluorescent units. Coupling to the 3-hydroxy-2-pyridone structural motif was achieved by reaction of ligand **L7** with 1-pyrenecarboxaldehyde or 9-anthraldehyde. The Schiff base was subsequently reduced with $NaBH_4$ to give ligand **L10** and **L12**, respectively (Scheme IV.10).

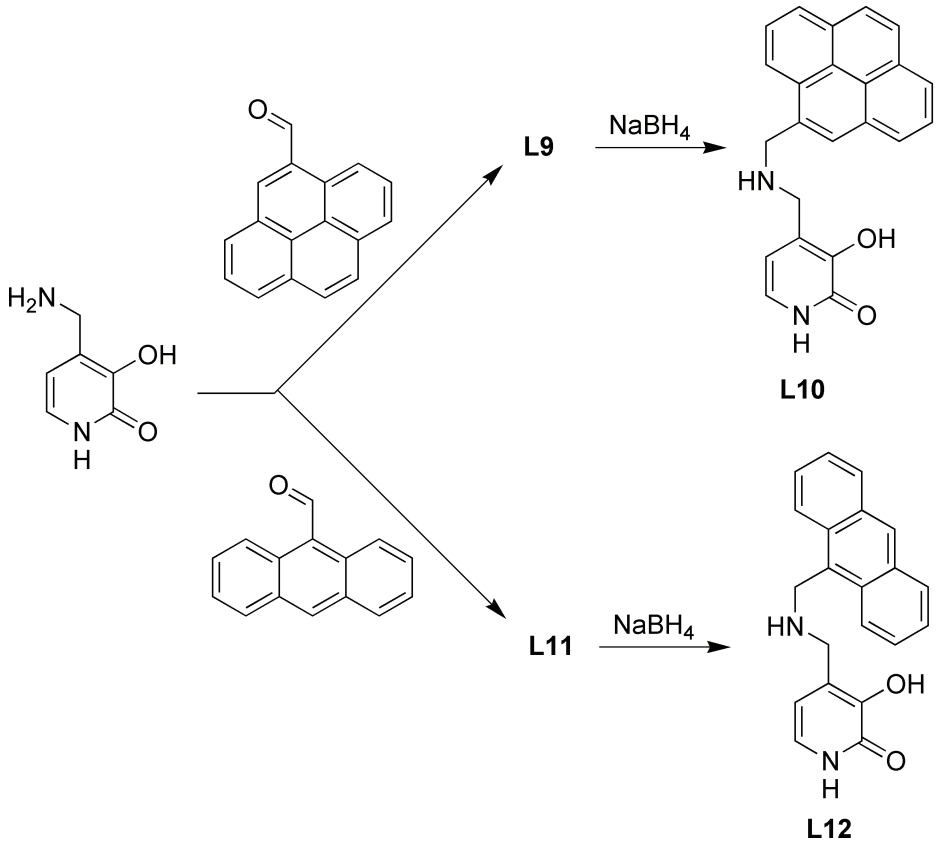

Scheme IV.10 Synthesis of 3-hydroxy-2-pyridones functionalised with a fluorescent unit.

Preliminary measurements indicate indeed an increase of the fluorescence in the presence of lithium ions, but the results have still to be confirmed.

IV.IV Conclusions

The utilization of assembly processes to build artificial receptors[319–322] or chemosensors[323–325] is conceptually very appealing, given that the building blocks are easily accessible. Potent receptors for the pharmacologically interesting lithium ion have been obtained by base-induced assembly of halfsandwich complexes with simple 3-hydroxy-2-pyridone derivatives. Due to the inherent flexibility of this approach, it was possible to investigate the host-guest chemistry of a large variety of receptors in relatively short time. Of all receptors tested, the ruthenium complex **[(cymene)Ru(L5–2 H$^+$)]$_3$** displayed the most interesting characteristics. In water, it shows a Li^+ binding constant of $K_a = (5.8 \pm 1.0) \times 10^4\ M^{-1}$. This value is among the highest ever reported for Li^+ complexation in water[277–279] and it is sufficient for the quantitative complexation of Li^+ in the pharmacologically relevant concentration range of ~ 1 mM. The selectivity of **[(cymene)Ru(L5–2 H$^+$)]$_3$** is extremely high: the complexation of K^+ or Cs^+ could not be detected at all and its affinity for Na^+ is four orders of magnitude lower than for Li^+. In order to use receptor **[(cymene)Ru(L5–2 H$^+$)]$_3$** for sensing, three methods to transduce the binding event into a signal output were developed. The first is based on the Li^+ induced stabilisation of **[(cymene)Ru(L5–2 H$^+$)]$_3$** against de-aggregation by acid and allows to detect low millimolar concentrations of Li^+ by a change of pH. The second is based on the different reactivity of **[(cymene)Ru(L5–2 H$^+$)]$_3$** and its lithium adduct towards $FeCl_3$. Since this reaction is accompanied by strong a change of colour, it is possible to detect Li^+ at concentrations of ~ 1 mM by the ‘naked eye’. For potential applications it is of importance that the receptor can be synthesised in situ by self-assembly, using the commercially available complex $[(cymene)RuCl_2]_2$ and the pyridone ligand **L5**, which is accessible in a one-step procedure. The third method uses an increase of fluorescence to indicate the presence of lithium.

Chapter V
$^{6}Li/^{7}Li$ Isotope Separation

V.I Introduction

Lithium does not occur free in nature, but in form of over 150 different minerals. Two stable isotopes are known: ^{6}Li and ^{7}Li. Their natural abundance is 92.41 % and 7.59 %, respectively, but these values underlie fluctuations of up to several percent depending on the geological location. A large interest in the isotopic separation is given due to the fact that ^{6}Li is used in form of ^{6}LiD or $^{6}Li_2DT$ in the hydrogen bombe, and that ^{6}Li is a precursor for ^{3}H for future fusion reactors.

The ionic radii of the ^{7}Li isotope and the ^{6}Li isotopes are slightly different. The tabulated value of the crystal radius of hexacoordinated Li^+ is 0.90 Å[326] and the difference between the two isotopes was crystallographically determined to be 0.04 pm (0.0004 Å)[327] with $^{7}Li^+$ being the smaller isotope.[s] This value correlates well with the theoretical value of 0.05 pm calculated by Knyazev.[328] Note, that the separation of the Li^+ ion from the Na^+ ion – whose ionic radii differ by 40 pm (0.4 Å)[t] – is already a difficult task.

Generally, isotopic separation is achieved by using a biphasic system in which one isotope is enriched in one of the two phases, either by kinetic or thermodynamic means. The degree of separation is expressed by the isotopic separation factor α, which is defined by the equilibrium constant of both isotopes between two phases P1 and P2 (Figure V.1).

$$^{7}Li_{P1} + {}^{6}Li_{P2} \rightleftharpoons {}^{7}Li_{P2} + {}^{6}Li_{P1}$$

Figure V.1 Equilibrium of ^{6}Li and ^{7}Li between two phases

The equilibrium constant K for this system is shown in Equation V.1. Usually, the isotopic separation factor α is given as shown in Equation V.2. The elementary isotopic fractionation effect δ is defined as α–1 (Equation V.3). A separation factor greater than 1 means that ^{7}Li was enriched in phase P2, wheras a separation factor less than 1 means thas ^{7}Li has been enriched in phase P1.

$$K = \frac{[^{7}Li]_{P2} \cdot [^{6}Li]_{P1}}{[^{7}Li]_{P1} \cdot [^{6}Li]_{P2}} \qquad \text{Eq. V.1}$$

s. The radius depends on various parameters such as coordination number, counter ion, etc. and values differ from reference to reference, as well as from the method of determination.

t. Considered was the crystal radius of tetracoordinated metal ions based on $r(^{VI}F^-) = 1.19$Å (0.73 pm and 1.13 pm for Li^+ and Na^+, respectively).[326]

$$\alpha \equiv K = \frac{\left(\frac{[^{7}Li]_{P2}}{[^{6}Li]_{P2}}\right)}{\left(\frac{[^{7}Li]_{P1}}{[^{6}Li]_{P1}}\right)} = \frac{\left(\frac{[^{7}Li]}{[^{6}Li]}\right)_{P2}}{\left(\frac{[^{7}Li]}{[^{6}Li]}\right)_{P1}} \qquad \text{Eq. V.2}$$

$$\delta = \alpha - 1 \qquad \text{Eq. V.3}$$

All crown ethers and cryptands show some degree of isotopic recognition, although small in most cases.[329] Since they exhibit typically fast exchange kinetics,[140, 174] only the intrinsic difference of the free energy between the two complexes has to be considered. In the case of 12-crown-4, for example, an enthalpic difference of −0.78 kJ/mol and an entropic difference of −2.4 J/mol K is responsible for a separation factors of 1.057.[330] Meanwhile, separation has been achieved by using inorganic ion exchanger,[331–333] resins to which crown ethers have been attached[334–337] and liquid-liquid amalgan based equilibration systems.[338] Interestingly, it seems that inorganic ion exchanger and polyethers prefer to take up the larger ^{6}Li isotope.[330, 333]

V.II Structural Investigations

12-Metallacrown-3 complexes are potent ionophores for small alkaline cations such as Li^+ or Na^+. Selectivity is achieved via a size exclusion effect. The binding site is shielded by three π-ligands, which effectively block bigger cations such as K^+ or Cs^+. If bulky π-ligands are employed, even the access of Na^+ to the binding site is prevented. Noteworthy, not the binding cavity itself is too small to accomodate the Na^+ ion, but only the entrance is too narrow to pass through. This blocking effect was anticipated to distinguish even very small differences in size as the ones of the two lithium isotopes. The access to the binding site should be easier for the smaller ^7Li isotope. Compared to crown ethers and cryptands, the lithium complexation and dissociation by 12-metallacrown-3 complexes is slow. Once the lithium is bound, the dissociation kinetics are to slow to allow equilibration on a reasonable time scale in favour for the thermodynamically more stable lithium adduct. Any initial isotopic separation should be preserved through the experiment. Thus, any isotopic enrichment should be due to a kinetic isotope effect.

Four 12-metallacrown-3 complexes have been investigated in order to demonstrate the ability of ^6Li and ^7Li isotope separation (Figure V.2). The C_6H_5Me ligands of the **$[(C_6H_5Me)Ru(L1–2\ H^+)]_3$** complex are the smallest ligands employed and the complex displays thus the largest entrance to the binding site. There is no special hindrance to access the binding site and no separation effect is expected. The other three ligands $C_6H_3{}^iPr_3$, C_6Me_6 and Cp* are much bulkier and the smaller ^7Li isotope should be preferentially complexed by the corresponding receptors.

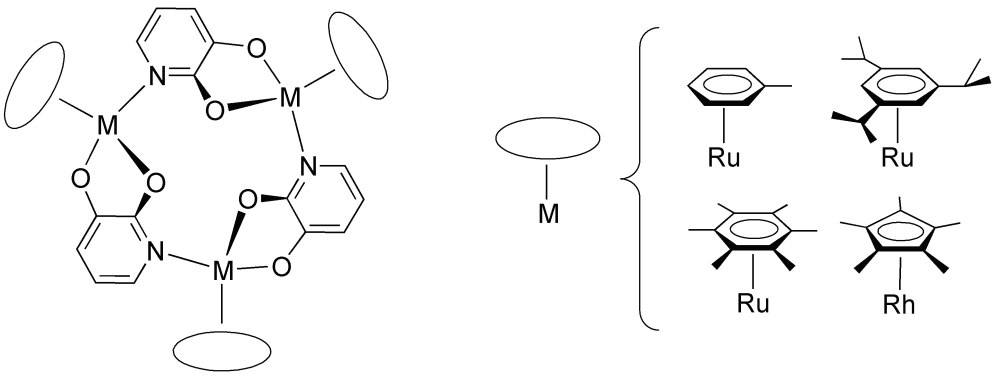

Figure V.2 12-Metallacrown-3 complexes investigated concerning their ability of ^6Li and ^7Li isotope separation.

As described in chapter I.VI, the complexes self-assemble from $[(\pi\text{-ligand})MCl_2]_2$ and 3-hydroxy-2-pyridone in MeOH in the presence of Cs_2CO_3. The structure in the crystal of

the new complexes **[(C$_6$H$_5$Me)Ru(L1–2 H$^+$)]$_3$** and **[(C$_6$H$_3$*i*Pr$_3$)Ru(L1–2 H$^+$)]$_3$**[u] and their LiCl adducts are shown in Figure V.3 and Figure V.4. As expected, trinuclear assemblies had formed. The oxygen atoms of the bridging ligands are coordinated to one metal centre and the ring nitrogen atom to the next metal centre, thus connecting the metal fragments. The ligands are bound in a slightly bent fashion. A comparison of the most relevant structural data (Table V.1) reveals similar M–O and M–N bond lengths for all complexes. The M–M' distances can be considered as a measure of the steric congestion of the π-ligands in the complex. Clearly, the complex **[(C$_6$H$_5$Me)Ru(L1–2 H$^+$)]$_3$** displays the smallest M–M' distance. The steric congestion increases from the Cp* ligand to the C$_6$H$_3$*i*Pr$_3$ ligand and is most pronounced for the C$_6$Me$_6$ ligand. A space filling representation along the pseudo C_3 axis showing the size of the opening of all four complexes is depicted in Figure V.5. The M–M' and O–O' distances are assumed to represent the size of the entrance to the binding site. Therefore, an isotopic enrichment should be most pronounced for the **[(C$_6$Me$_6$)Ru(L1–2 H$^+$)]$_3$** complex. Upon binding of LiCl, the overall structure undergoes only minor changes. Most notably, the M–M' distances increase, probably due to the additional steric repulsion between the π-ligand and the chloride anion, coordinated on top of the Li$^+$ ion and in between the π-ligands.

Table V.1: Selected bond lengths (Å) and angles (°) for 12-metallacrown-3 complexes of 3-hydroxy-2-pyridone ligands with diverse metal fragments.

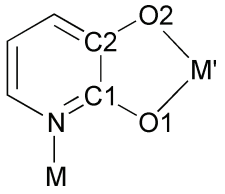

12-Metallacrown-3	M–N	M–O1	M–O2	O1–M–O2	M–O–C1–C2	M–N–C1–C2	O–O'	M–M'
[(C$_6$H$_5$Me)Ru(L1–2 H$^+$)]$_3$	2.14	2.09	2.08	79.5	4.5	7.4	3.04	5.37
[(C$_6$H$_5$Me)Ru(L1–2 H$^+$)]$_3$ × LiCl	2.14	2.12	2.08	79.5	8.7	5.8	2.96	5.40
[(C$_6$H$_3$*i*Pr$_3$)Ru(L1–2 H$^+$)]$_3$	2.14	2.09	2.06	79.5	13.5	8.7	3.15	5.39
[(C$_6$H$_3$*i*Pr$_3$)Ru(L1–2 H$^+$)]$_3$ × LiCl	2.14	212	2.03	79.5	11.7	11.8	3.07	5.48
[(C$_6$Me$_6$)Ru(L1–2 H$^+$)]$_3$[124]	2.14	2.12	2.05	78.6	15.1	9.8	3.21	5.46
[Cp*Rh(L1–2 H$^+$)]$_3$[124]	2.13	2.09	2.06	80.1	11.2	5.8	3.10	5.35
[Cp*Rh(L1–2 H$^+$)]$_3$ × LiCl[124]	2.12	2.14	2.06	79.2	10.8	9.1	3.07	5.47

u. Complex **[(C$_6$H$_3$*i*Pr$_3$)Ru(L1–2 H$^+$)]$_3$** has already been discussed in chapter II.II.3.

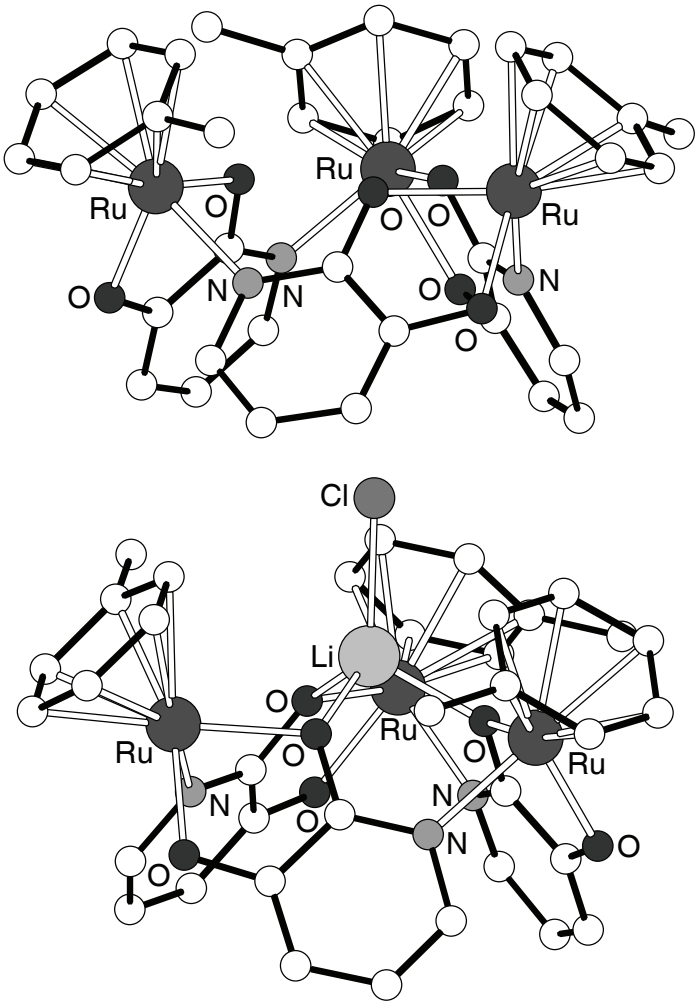

Figure V.3 Graphic representation of the structure of the complex **$[(C_6H_5Me)Ru(L1{-}2\,H^+)]_3$** (left) and its LiCl adduct **$[(C_6H_5Me)Ru(L1{-}2\,H^+)]_3 \times LiCl$** (right) in the crystal. Solvent molecules and hydrogen atoms were omitted for clarity.

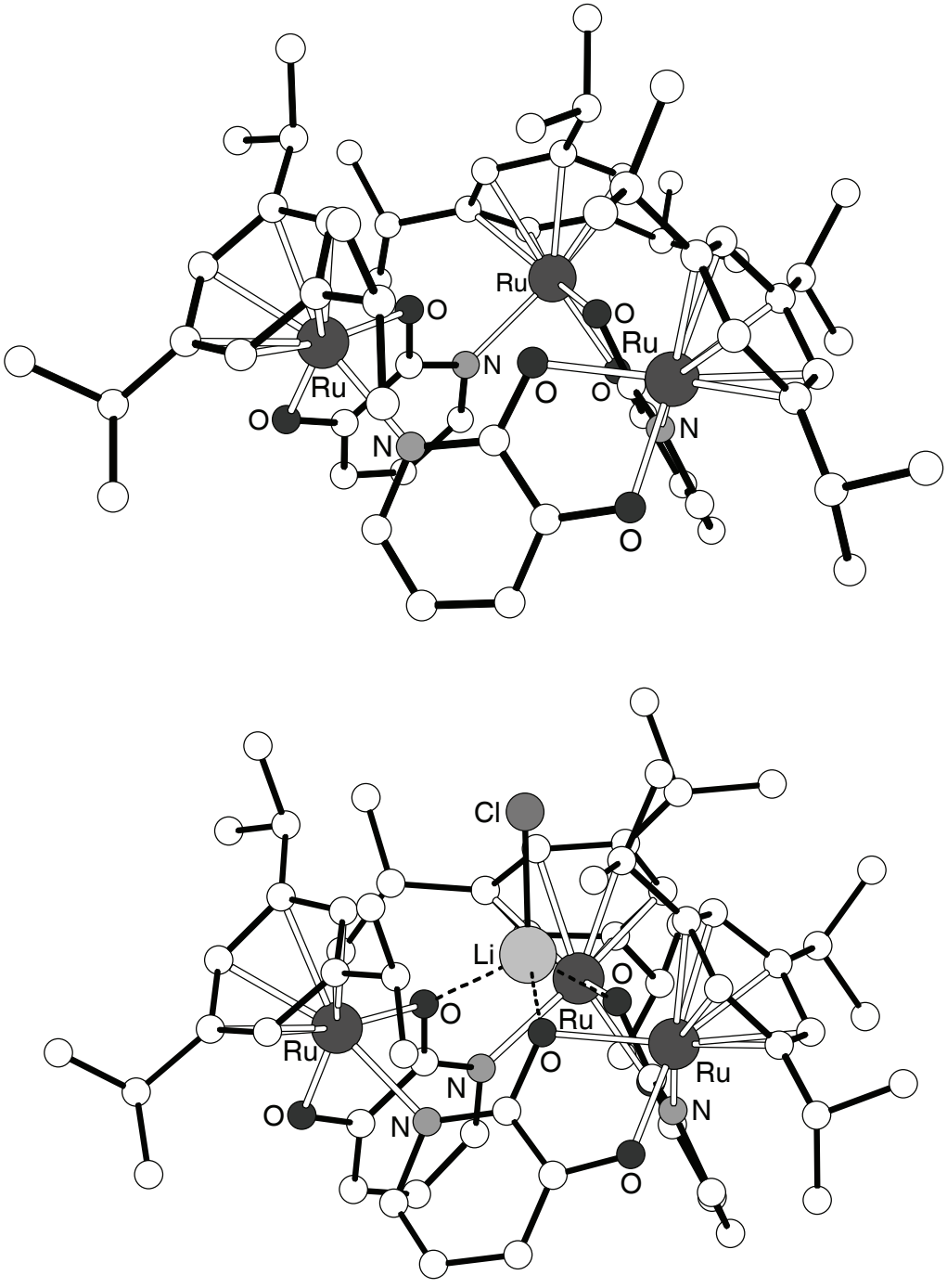

Figure V.4 Graphic representation of the structure of the complex **[(C$_6$H$_3$^{i}Pr$_3$)Ru(L1–2 H$^+$)]$_3$** (top) and its LiCl adduct **[(C$_6$H$_3$^{i}Pr$_3$)Ru(L1–2 H$^+$)]$_3$ × LiCl** (bottom) in the crystal. Solvent molecules and hydrogen atoms were omitted for clarity.

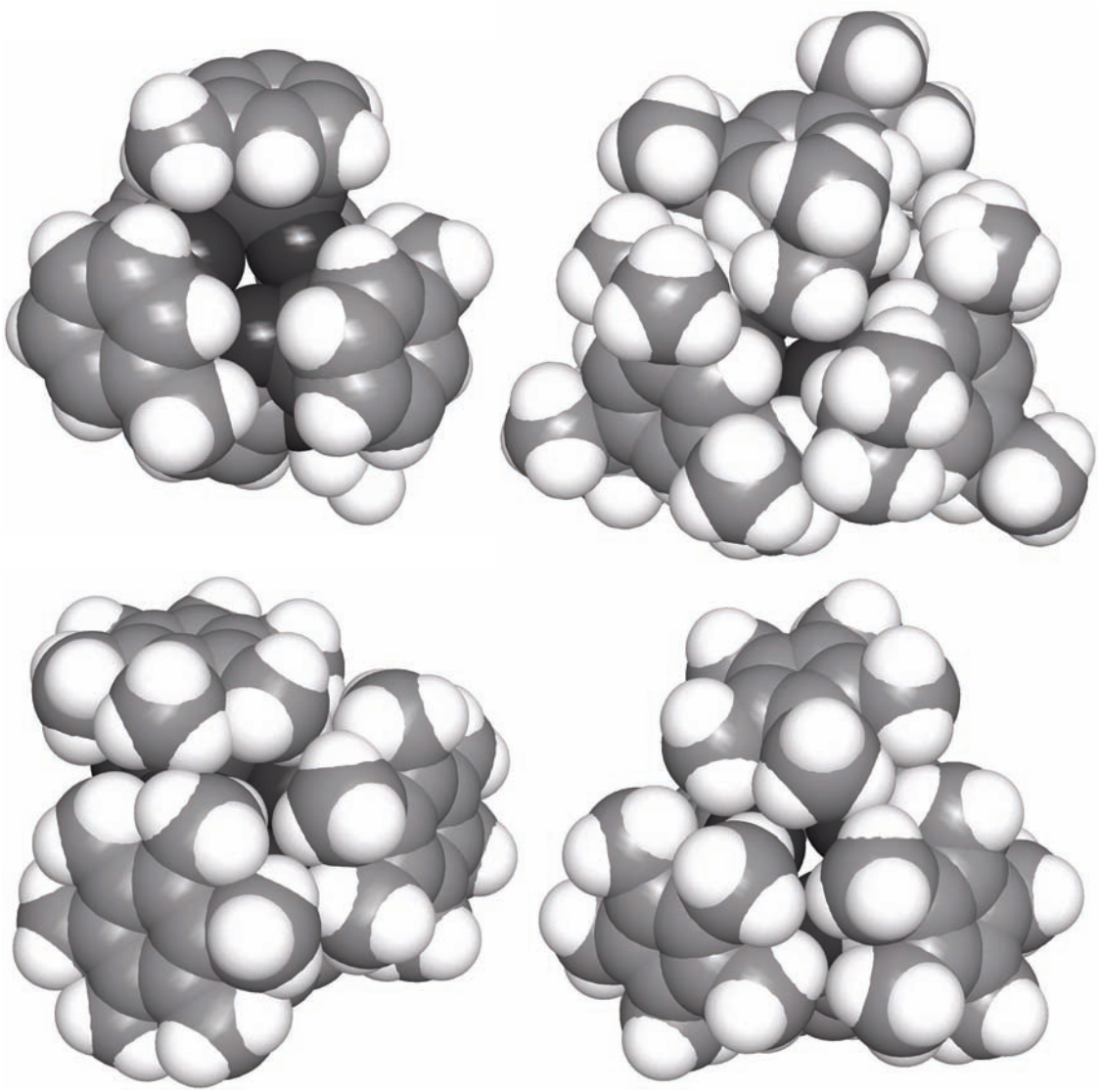

Figure V.5 Comparison of the entrance to the binding cavity of the complexes **$[(C_6H_5Me)Ru(L1–2\ H^+)]_3$** (top left), **$[(C_6H_3{}^iPr_3)Ru(L1–2\ H^+)]_3$** (top right) **$[(C_6Me_6)Ru(L1–2\ H^+)]_3$** (bottom left) and **$[(Cp^*)Rh(L1–2\ H^+)]_3$** (bottom right). Solvent molecules and hydrogen atoms were omitted for clarity.

V.III Extraction Experiments

The isotopic separation behaviour has been investigated by complexation of LiCl in MeOH. The different 12-metallacrown-3 complexes were solubilized in MeOH containing 100 equiv. of LiCl. The solution was stirred for one hour, the solvent removed and the macrocycle separated from the salt by extraction with $CHCl_3$. ^{1}H NMR spectroscopy of the isolated product revealed the presence of a single product: the receptor complexed with LiCl. The separation factor α was defined as the quotient of the $^{7}Li/^{6}Li$ ratio in phase P2 and phase P1 (Equation V.2) Phase P2 is represented by the 12-metallacrown-3 complex, whereas MeOH is representing phase P1. Thus, the separation factor α is equivalent to the $^{7}Li/^{6}Li$ ratio in the receptor divided by the ratio of the lithium ions remaining in solution (Equation V.4). A factor greater than 1 means that ^{7}Li has been enriched in the macrocycle, whereas a value less than 1 indicates an enrichment of ^{6}Li. As 100 equiv. of LiCl with respect to the receptor were used, the $^{7}Li/^{6}Li$ ratio in solution can be set as constant and equal to the isotopic ratio of the LiCl salt employed (Equation V.5). Therefore, the isotopic ratio of the Li^{+} complexed in the macrocycle has been compared to the isotopic ratio of the used LiCl salt (Equation V.6). The enrichment of ^{7}Li in the macrocycle is expressed as $\delta(^{7}Li)$ in % (Equation V.7) A positive value indicates the enrichment of ^{7}Li and a negative value the enrichment of ^{6}Li.

$$\alpha(^{7}Li) = \frac{(I_{^{7}Li}/I_{^{6}Li})_{12\text{-Metallacrown-3}}}{(I_{^{7}Li}/I_{^{6}Li})_{LiCl}} \qquad \text{Eq. V.4}$$

$$(I_{^{7}Li}/I_{^{6}Li})_{LiCl\ solution} = (I_{^{7}Li}/I_{^{6}Li})_{LiCl} = \text{constant} \qquad \text{Eq. V.5}$$

$$\alpha(^{7}Li) = \frac{(I_{^{7}Li}/I_{^{6}Li})_{12\text{-Metallacrown-3}}}{(I_{^{7}Li}/I_{^{6}Li})_{LiCl}} \qquad \text{Eq. V.6}$$

$$\delta(^{7}Li) = \left[\frac{(I_{^{7}Li}/I_{^{6}Li})_{12\text{-Metallacrown-3}}}{(I_{^{7}Li}/I_{^{6}Li})_{LiCl}} - 1\right] \cdot 100\ \% = (\alpha - 1) \cdot 100\ \% \qquad \text{Eq. V.7}$$

Measurements of the initial $^{7}Li/^{6}Li$ isotopic ratio of the employed LiCl salt by laser atomic absorption spectroscopy revealed a value of 17.08 ± 0.46. This corresponds to 94.47 % ^{7}Li and 5.57 % ^{6}Li. The ^{7}Li percentage is significantly higher than the natural abundance given in the literature. However, such a strong deviation in favour for ^{7}Li in chemical reagents has been reported before.[339] The average ^{7}Li enhancement was found to be 5.4 % for the complex **$[(C_6Me_6)Ru(L1–2\ H^{+})]_3$**. The value of the enhancement differs depending on how the experimental data were treated. A value of (4.4 ± 1.0) % was obtained when the peak height of the signals or the surface between 30 % of the peak height and the maximum peak height were evaluated. A slightly higher value of (5.8 ± 1.0) % was obtained when the surface between 10 % of the peak height and the

maximum peak height was considered. Integration of the total surface beneath the signals led to a value of ^{7}Li enrichment of (7.0 ± 2.8) %. In the latter case the standard deviation was increased due to a more pronounced uncertainty when placing the base line. As expected, no effect was observed for the complex **[(C$_6$H$_5$Me)Ru(L1–2 H$^+$)]$_3$**, but neither complex **[(C$_6$H$_3$*i*Pr$_3$)Ru(L1–2 H$^+$)]$_3$** nor complex **[(Cp*)Rh(L1–2 H$^+$)]$_3$** showed any enhancement either (Table V.2). This is surprising, because the M–M' distances indicate in both cases a pronounced sterical congestion (Table V.1). Given that the separation effect is expected to be of kinetic nature, the complexation kinetics have been investigated by ^{1}H NMR spectroscopy. The slower, both complexation as well as dissociation rate, the more distinct should be a kinetic isotopic effect.

The dissociation rate itself could not be determined directly because the binding constants in MeOH were too high. The focus has thus been directed on the complexation rates. The time $t_{1/2}$, after which half of the receptor had bound Li^+ was determined. By far the slowest Li^+ complexation was observed for complex **[(C$_6$Me$_6$)Ru(L1–2 H$^+$)]$_3$**. After 35 hours, not even half of the macrocycle in solution had bound Li^+. Although complex **[(C$_6$H$_3$*i*Pr$_3$)Ru(L1–2 H$^+$)]$_3$** showed likewise a relatively slow complexation ($t_{1/2}$ =9.5 h) of Li^+, no separation effect were observed. The macrocycle **[(C$_6$H$_5$Me)Ru(L1–2 H$^+$)]$_3$** was fully complexed in less than five minutes. The fast complexation of Li^+ is in aggreement with a sterically not hindered binding site. Interestingly, receptor **[(Cp*)Rh(L1–2 H$^+$)]$_3$** also displayed a relatively fast complexation kinetic with a half-time of complexation of 45 minutes. Apparently, the complexation rate depends not only on the size of the π-ligands, but also on the nature of the metal centre.

The reason why no isotopic separation is observed in the case of complex **[(C$_6$H$_3$*i*Pr$_3$)Ru(L1–2 H$^+$)]$_3$** and complex **[(Cp*)Rh(L1–2 H$^+$)]$_3$** can only be guessed. In the latter case the complexation rate might be too fast. Another explanation might be that the steric congestion is simply not pronounced enough. In case of all receptors, however, it is estimated that the dissociation rates are too slow to allow the establishment of a thermodynamic equilibrium.

Table V.2: ^{7}Li isotope enrichement and half-time of Li^{+} complexation of 12-metallacrown-3 complexes.[a]

		$\delta(^{7}Li)$			
Complex	$t_{1/2}$	peak height	10 % p. h.[b]	30 % p. h.[b]	total surface
$[(C_6H_5Me)Ru(L1–2\ H^+)]_3$	<< 5 min	(–0.1 ± 2.2) %	(–1.9 ± 2.9) %	n.d.	(–1.2 ± 3.0) %
$[(C_6H_3{}^{i}Pr_3)Ru(L1–2\ H^+)]_3$	9.5 h	(1.3 ± 0.7) %	(–0.1 ± 1.0) %	n.d.	(–2.9 ± 3.3) %
$[(C_6Me_6)Ru(L1–2\ H^+)]_3$[c]	>> 35 h	(4.4 ± 1.0) %	(5.8 ± 1.0) %	(4.4 ± 0.9) %	(7.0 ± 2.8) %
$[(Cp^*)Rh(L1–2\ H^+)]_3$	45 min	(0.2 ± 1.3) %	(0.1 ± 4.7) %	n.d.	(–0.3 ± 2.9) %

a. n.d.: not determined
b. Enrichment obtained when evaluating the signal surface at the specified percentage of the peak height (p. h.).
c. The standard deviation of the mean is given as error.

The kinetic investigation of the half-time of complexation revealed another interesting point: the LiCl complexation was carried out by stirring the corresponding macrocycle in a LiCl solution in MeOH for *one hour*. After this time, only a very small part of receptor is actually complexed. However, only the complexed receptor has been detected by ^{1}H NMR spectroscopy after extraction. This means that the major part of the complexation happened during the 15 minute period, in which the solvent was removed under reduced pressure. The solubility of LiCl in MeOH is rather high (10 M[340]), so that its concentration can increase up to 20fold during the removal of the solvant. This probably forces the Li^{+} ion into the cavity of the receptor. Better separation factors can thus be expected with increased complexation time. Removal of the solvent by lyophilisation may have also an effect, in any case it should allow a time resolved study of the isotope separation.

V.IV Conclusions

Four 12-metallacrown-3 complexes have been investigated regarding their ability to separate the $^{7}Li/^{6}Li$ isotopes. The average enrichment of ^{7}Li has been found to be 5.4 % for complex **$[(C_6Me_6)Ru(L1–2\ H^+)]_3$**. No isotopic separation effect has been detected for the complexes **$[(C_6Me_6)Ru(L1–2\ H^+)]_3$**, **$[(C_6H_3{}^{i}Pr_3)Ru(L1–2\ H^+)]_3$** and **$[(Cp^*)Rh(L1–2\ H^+)]_3$**.

Chapter VI
Expanded Triple-Stranded Helicates

VI.I Bridged Dihydroxypyridine Ligands for the Synthesis of Expanded Helicates

Ligands, in which two catechol groups are connected by a spacer, have been used extensively as building blocks in supramolecular chemistry. Various architectures have been realized including metallamacrocycles,[341–345] heterometallic clusters,[346–349] tetrahedral coordination cages,[24, 26, 30] and most notably triple-stranded helicates.[24, 59, 61, 350] In the following, it will be demonstrated, that the exchange of the catechol group with a dihydroxypyridine group allows the access to a new structural motif, which can be described as an expanded triple-stranded helicate. In these complexes, the two chiral ML_3 units are replaced by likewise chiral M_3L_3 units (Scheme VI.1). Structural evidence is presented that expanded helicates with a length of 2.8 nm can be obtained.

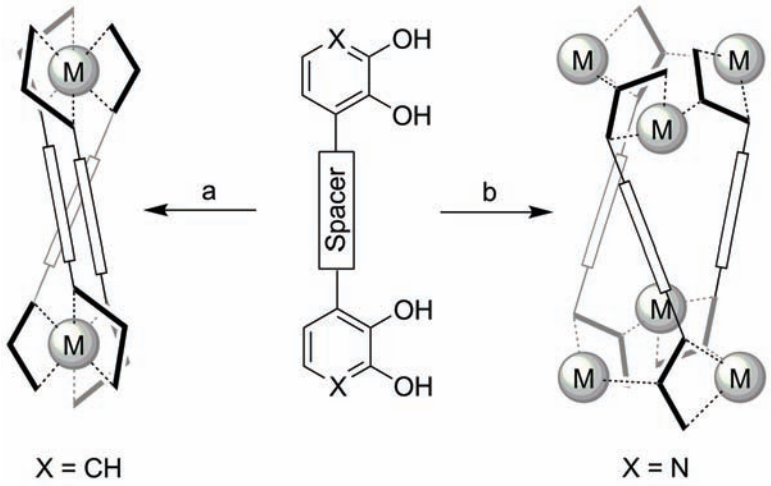

Scheme VI.1 The metal-based self-assembly of bridged catechol or dihydroxypyridine ligands can lead to the formation of a) helicates or b) expanded helicates.

As presented in chapter IV.II.1, the Mannich reaction of 3-hydroxy-2-pyridone[v] with formaldehyde and secondary amines is known to give 4-aminomethyl-substituted products.[304–307] In a similar fashion, diamines have been used to obtain a new type of multifunctional ligands: bridged dihydroxypyridines. Mannich reaction of 3-hydroxy-2-pyridone, formaldehyde and the commercially available diamines piperazine, N,N'-dimethylethylenediamine, and 1,3-di(4-piperidyl)propane gave the corresponding ligands **L13**, **L14** and **L15** (Scheme VI.2).

v. The use of 3-hydroxy-2-pyridone and 2,3-dihydroxypyridine is equivalent, as both compounds are in a tautomeric equilibrium with each other

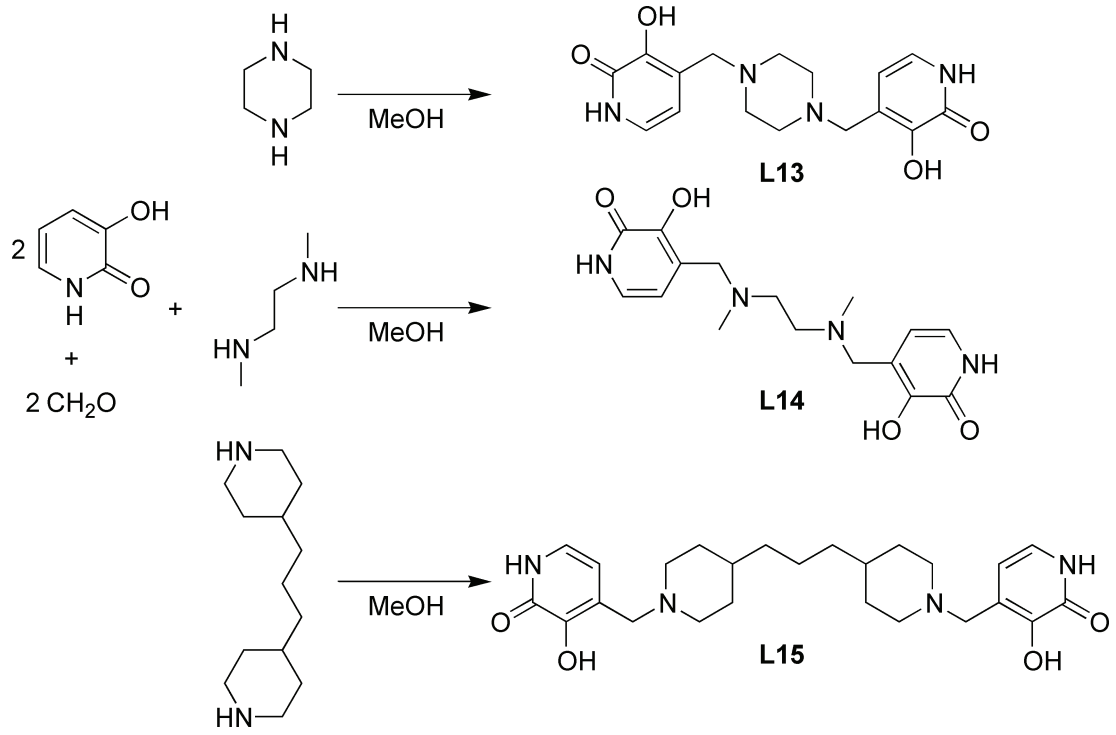

Scheme VI.2 Synthesis of the ligands **L13**, **L14** and **L15** by Mannich reaction of 3-hydroxy-2-pyridone, formaldehyde and the commercially available diamines piperidine, N,N'-dimethylethylenediamine, or 1,3-di(4-piperidyl)propane.

Subsequently, the reaction of these three ligands with the dimeric half sandwich complexes $[(\pi\text{-ligand})MCl_2]_2$ have been examined. When an aqueous solution of complex $[(C_6H_6)RuCl_2]_2$ (**1**) or $[(C_6H_5Me)RuCl_2]_2$ (**2**) and equivalent amounts of ligand **L13** or **L14** was carefully layered with NEt_3, the complexes **$[\{(C_6H_6)Ru\}_2(L13–4\ H^+)]_3$** (**12**), **$[\{(C_6H_5Me)Ru\}_2(L13–4\ H^+)]_3$** (**13**) and **$[\{(C_6H_5Me)Ru\}_2(L14–4\ H^+)]_3$** (**14**) were obtained in the form of orange crystals in 58 %, 60 % and 41 % yield, respectively. A similar reaction with ligand **L15** did not provide a crystalline material.[w] However, using the dimer $[(C_5HMe_4)RhCl_2]_2$, complex **$[\{(C_5HMe_4)Rh\}_2(L15–4\ H^+)]_3$** (**15**) was isolated in 37 % yield. The complexes were characterized by NMR spectroscopy and single crystal X-ray analysis.

w. Since NMR spectroscopy is not suited to distinguish between trinuclear and hexanuclear complexes, only complexes which have been obtained in crystalline form have been focused.

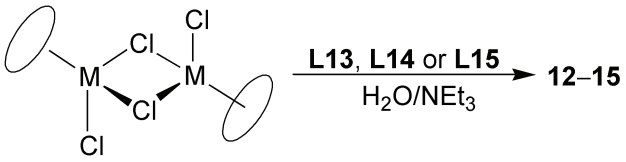

	(π-ligand)M	ligand
12	$(C_6H_6)Ru$	**L13**
13	$(C_6H_5Me)Ru$	**L13**
14	$(C_6H_5Me)Ru$	**L14**
15	$(C_5Me_4H)Rh$	**L15**

Figure VI.1 Synthesis of hexanuclear extended triple-stranded helicates.

The ^1H NMR spectra of the Ru complexes **13** and **14** in $CDCl_3$ showed a single set of signals for the toluene and the hydroxypyridine ligand, which was indicative of a highly symmetrical structure (Figure VI.2, spectra a and b). Five distinct signals were observed for the aromatic protons of the π-ligand and two doublets were found for the methylene protons adjacent to the pyridine ring. This was a clear sign for the presence of stereogenic centres. The ^1H NMR spectrum of the rhodium complex **15** showed likewise a single set of signals (Figure VI.2, spectrum c). Four singlets were observed for the CH_3 groups of the tetramethylcyclopentadienyl ligand and well resolved diastereotopic methylene protons were found for the NCH_2 group next to the heterocycle. The only signal indicating stereogenic centres in the case of complex **12** are the two doublets of the NCH_2 groups. Due to some flexibility, the CH_2 signals of the diamines are very broad.

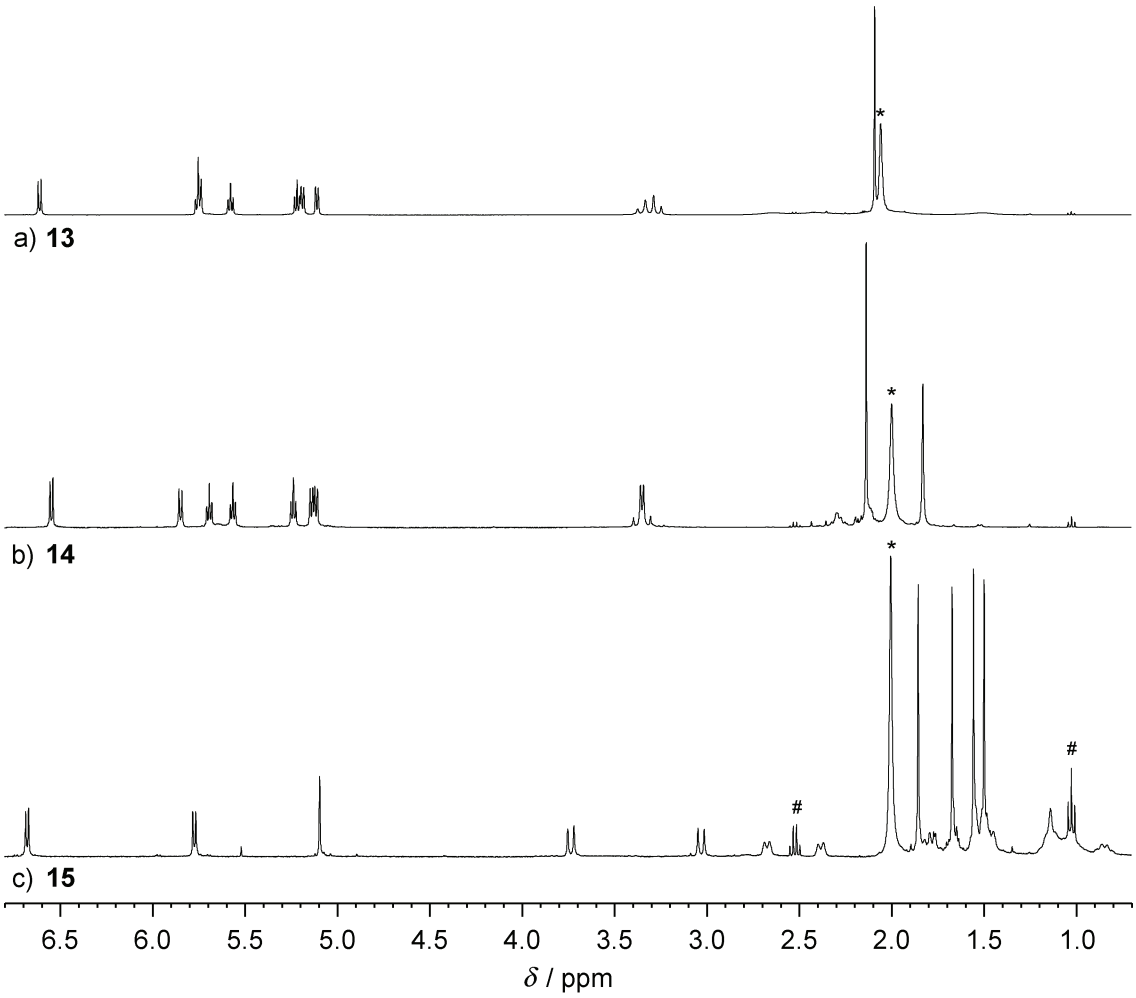

Figure VI.2 1H NMR spectra of the expanded helicates **13** (a), **14** (b) and **15** (c) in $CDCl_3$. The presence of five distinct aromatic signals or four singlets for the CH_3 groups of the C_5HMe_4 ligands, as well as two doublets for the NCH_2 protons indicate the presence of stereogenic centres. Water is denoted by an asterisk and NEt_3 by a rhomb.

The NMR data for the complexes in solution were in agreement with the structures observed in the solid state (Figure VI.3 and Figure VI.4). All four complexes are comprised of six (π-ligand)M fragments, which are connected by three deprotonated ligands. Two pairs of 12-membered metallamacrocycles are observed for each complex, with the metals coordinated to the two O atoms and the N atom of the dihydroxypyridine group. The diamine linker connects the two macrocycles to form a cylindrical structure. The lengths of these cylinders (maximum H-to-H distance) are 2.0 nm for complex **12**, 2.1 nm for complex **13**, 1.9 nm for complex **14** and 2.8 nm for complex **15**.

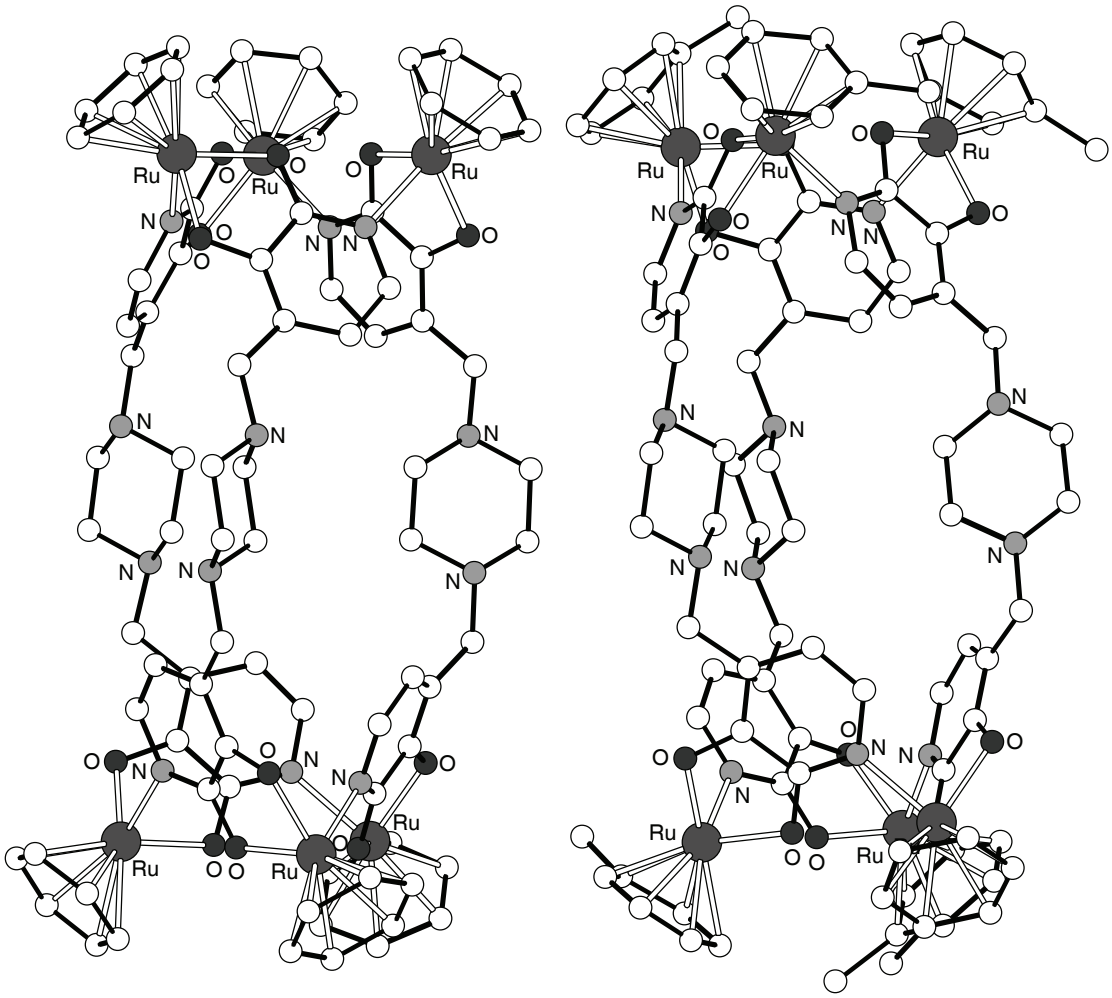

Figure VI.3 Graphic representation of the molecular structures of the complexes **12** and **13** in the crystal. The lengths of the cylinders are 2.0 and 2.1 nm, respectively. Hydrogen atoms and the co-crystallised solvent molecules are not shown for clarity.

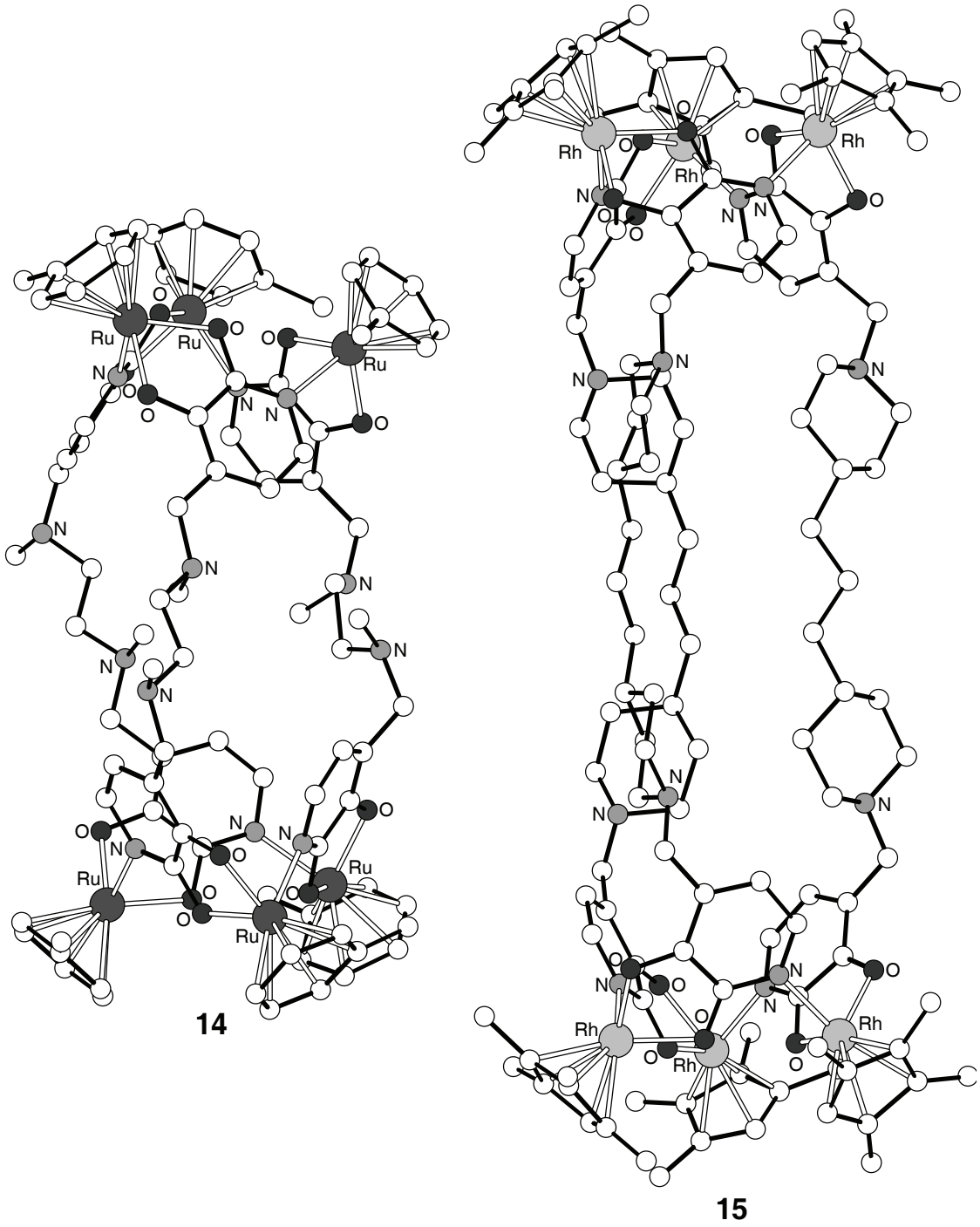

Figure VI.4 Graphic representation of the molecular structures of the complexes **14** and **15** in the crystal. The lengths of the cylinders are 1.9 and 2.8 nm, respectively. Hydrogen atoms and the co-crystallised solvent molecules are not shown for clarity.

Complex **15** is not only remarkable because of its length of nearly 3 nm. The macrocycles formed between two opposite metals have a ring size of 44 atoms containing a total

of 18 CH_2 groups, only eight of which are part of the semi-rigid piperidine units. Complex **15** is thus a rare example of a discrete, multinuclear complex, which was obtained by metal-based self-assembly with a highly flexible ligand.[351–358]

The Ru complexes **12**, **13** and **14** display pseudo D_3 symmetry, with all six metal centres having the same configuration. The Rh complex **15**, on the other hand, has a crystallographic C_3 axis and an idealized overall C_{3h} symmetry. The metal centres at one end of the molecule have thus the opposite configuration to the metal centres at the other end. Interestingly, this parallels what has been observed for catecholate-based triple-stranded helicates: ligands with an even number of methylene groups in the spacer were found to form chiral helicates, whereas ligands with an odd number of methylene groups in the spacer gave rise to achiral meso-helicates, in which the metal centres have the opposite configuration.[59, 61, 350, 359–361]

Preliminary attempts to study the self-assembly process in situ by ^{1}H NMR spectroscopy have been carried out. Mixing of equimolar amounts of halfsandwich complexes [(π-ligand)MCl_2]$_2$ and ligands **L13**, **L14** and **L15** in D_2O resulted in clear orange solutions. In each case, ^{1}H NMR data indicated the formation of a monomeric complex, in which two (π-ligand)M fragments were bridged via the bis(dihydroxypyridone) ligand leading to dinuclear complexes of type C. Addition of incremental amounts of CsOH induced the self-assembly process into hexanuclear complexes of type D (Scheme VI.3).

Coordination of the ligand to the metal fragments results most probably in the translocation of a proton from the hydroxy to the amine group. Due to the low solubility of the ligands, a study of the chemical shifts of the NCH_2 protons upon coordination was not possible. Theoretically, 2.0 equiv. of base[x] are necessary to induce trimerisation into protonated, hexanuclear complexes of type D, in which two trimers are bridged together. Solubility in water is facilitated by the protonation of the six amino groups. These complexes represent the protonated forms of the corresponding expanded triple-stranded helicates and further addition of base leads to the generation of the latter one.

x. Equivalents with respect to the amount of ligand.

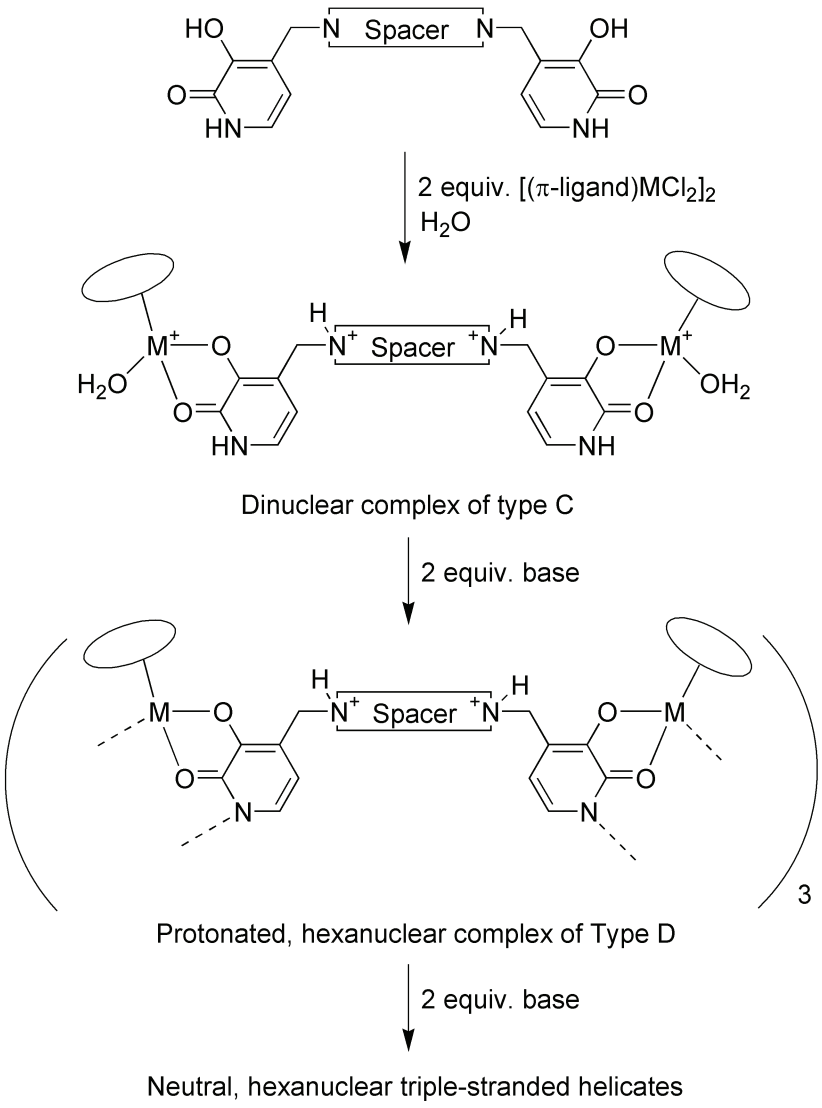

Scheme VI.3 Base-induced formation of hexanuclear expanded triple-stranded helicates.

However, the illustration of the base induced self-assembly is simplified. In the case of the short ligands **L13** and **L14** the six positive charges are in very close proximity to each other. Thus, it is not clear to which degree the amine groups are protonated. This is supported by the observation that precipitation often occurred before the self-assembly process was completed as for example the base induced self-assembly of $[(C_6H_5Me)RuCl_2]_2$ and the TFA salt of **L14**. For the study of the self-assembly process in water, the TFA salts of ligands purified by HPLC have been used. Therefore, two additional equivalents of CsOH were necessary to neutralise the acid and to generate the free ligand. Part of the ^1H NMR spectra of solutions containing $[(C_5HMe_4)RhCl_2]_2$ & the TFA salt of **L15** or $[(C_6H_5Me)RuCl_2]_2$ & the TFA salt of **L13** are shown in Figure VI.5 and Figure VI.6, respectively.

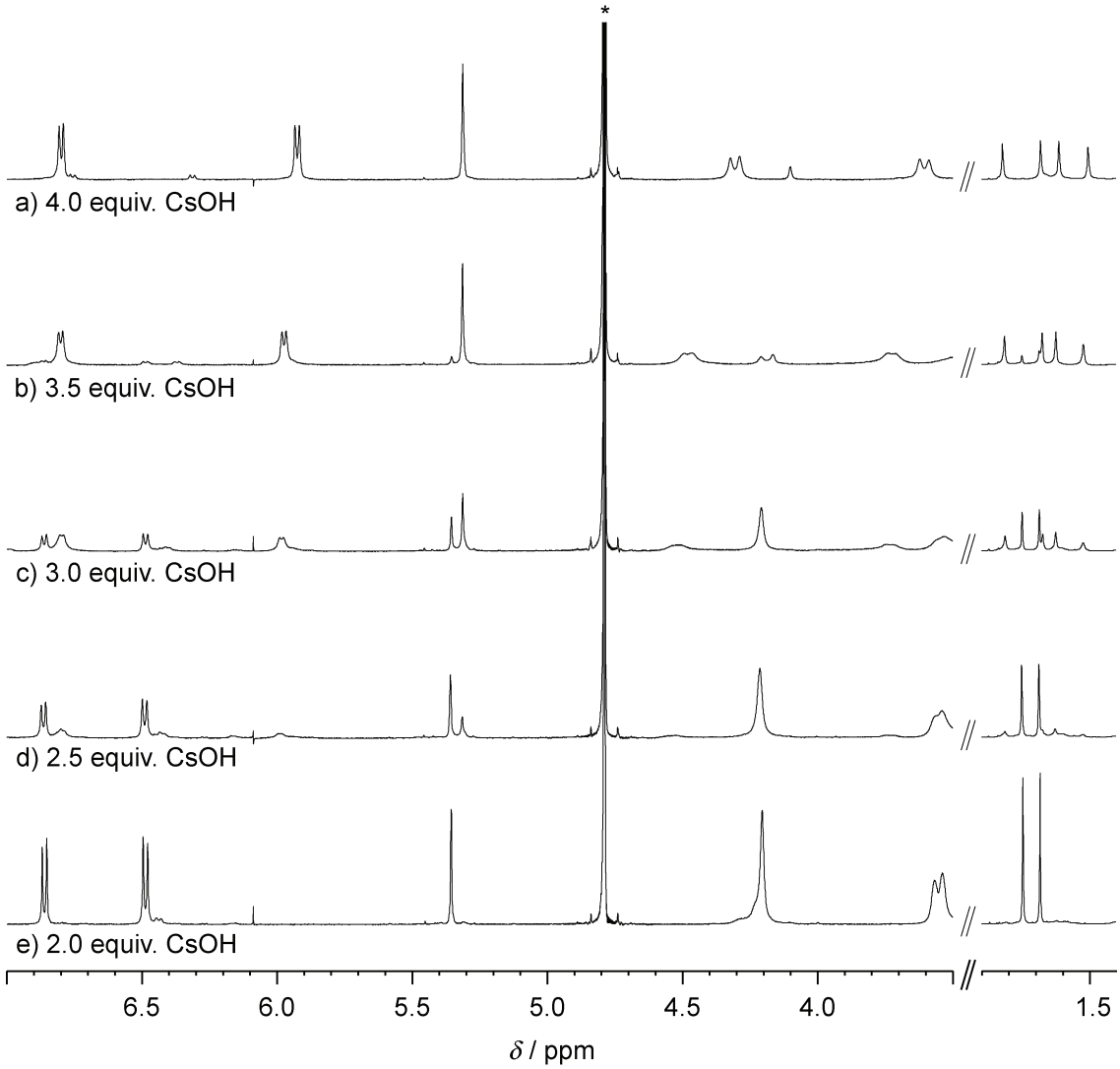

Figure VI.5 Part of the ^{1}H NMR spectrum (D_2O) of solutions containing $[(C_5HMe_4)RhCl_2]_2$ (5.4 mM) and the TFA salt of ligand **L15** (5.4 mM) after addition of different amounts of CsOH: a) 4.0, b) 3.5, c) 3.0, d) 2.5 and e) 2.0 equiv.. Spectrum 'a' corresponds to the protonated form of the hexanuclear complex **15** and spectrum 'e' represents the dinuclear complex **$[\{(C_5HMe_4)Rh\}_2(L15)(H_2O)_2]^{2+}$**; note that two equiv. of CsOH are necessary to neutralise the trifluoric acid. The solvent peak is denoted by an asterisk.

After addition of 2.0 equiv. of CsOH (0.0–2.0 equiv.) to a solution containing $[(C_5HMe_4)RhCl_2]_2$ and the TFA salt of **L15**, a single set of signals was observed. The appearance of the NCH_2 protons as singlet, as well as the observation of only two singlets for the CH_3 groups of the $(C_5HMe_4)Rh$ fragments are in agreement with the formation of a dinuclear complex of type C. Upon addition of more CsOH (2.0–4.0 equiv.), the generation of a second species was observed. The second species completely dominated the

solution after addition of 4.0 equiv. of base. The appearance of two doublets for the NCH_2 protons and four singlets for the CH_3 protons of the C_5HMe_4 ligands, as well as the typical high field shift of one of the pyridone signals, supported strongly the formation of hexanuclear complexes of type D.

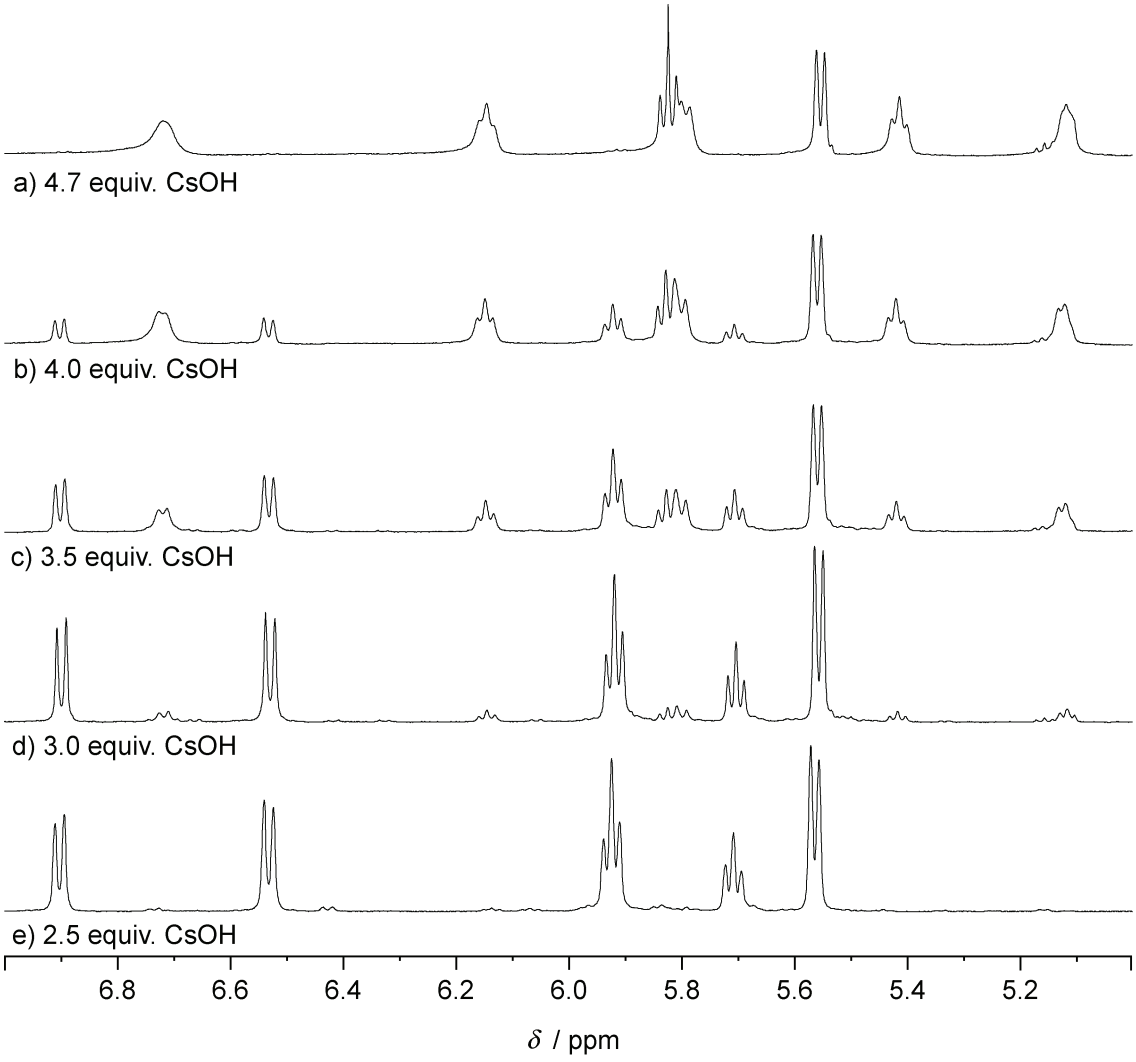

Figure VI.6 Part of the ^1H NMR spectrum (D_2O) of solutions containing $[(C_6H_5Me)RuCl_2]_2$ (7.5 mM) and the TFA salt of ligand **L13** (7.5 mM) after addition of different amounts of CsOH: a) 4.7, b) 4.0, c) 3.5, d) 3.0 and e) 2.5 equiv.. Spectrum 'a' corresponds to the protonated form of the hexanuclear complex **13** and spectrum 'e' represents the dinuclear complex $\mathbf{[\{(C_6H_5Me)Ru\}_2(L13)(H_2O)_2]^{2+}}$; note that at least two equiv. of CsOH are necessary to neutralise the trifluoric acid. The solvent peak is denoted by an asterisk.

A similar situation was found for a mixture of $[(C_6H_5Me)RuCl_2]_2$ and the TFA salt of **L13**. Upon addition of 2.5 equiv. of CsOH, the ^1H NMR data indicated the formation of a dinuclear complex, and further addition of CsOH resulted in the appearance of a second species. This second complex totally dominated the solution after addition of 4.7 equiv. of

base. In contrast to the above presented self-assembly process, more than stoichiometrical amounts of base were necessary to completely generate the dinuclear as well as the hexanuclear complex. The reason for this behaviour was probably a contamination of ligand **L13** with trifluoric acid. A similar behaviour was not observed for the ligands **L14** and **L15**.

Overall, the spectra of expanded helicates and their corresponding protonated forms are very similar (spectrum 'a' of Figure VI.5 vs. spectrum 'c' of Figure VI.2 and spectrum 'a' of Figure VI.6 vs. spectrum 'a' of Figure VI.2). However, in the case of the investigated complexes, ^{1}H NMR spectroscopy is not suited to distinguish whether the *meso* or the chiral form was obtained. In the case of complexes with an even number of methylene groups in the spacer, such as **15**, the *meso* and the chiral form can in principle be distinguished by ^{1}H NMR spectroscopy because the multiplicity of the central CH_2 groups of the linker is different. Unfortunately, these signals were not well resolved. Also, it is presently not clear whether the respective isomer had formed under thermodynamic or kinetic control. Prolonged heating of the complexes, either in $CDCl_3$ or D_2O, led unfortunately to partial decomposition of the complexes.

As shown in chapter IV.II, trinuclear organometallic macrocycles based on 3-hydroxy-2-pyridones are configurationally stable on the NMR time scale, even in polar solvents such as water. Epimerisation processes at the metal centres of the hexanuclear complexes **12–15** were likewise expected to be slow. The NMR data of the self-assembly processes therefore suggested that the same diastereomer is obtained in solution as was found in the solid state. This led to the conclusion that the ligands – despite their flexibility – are able to control the stereochemistry of all six metal centres.

VI.II Conclusions

In summary, the syntheses and the structures of four hexanuclear complexes have been described. They were obtained by base-induced assembly of organometallic halfsandwich complexes with bis(dihydroxypyridine) ligands. The complexes display a unique structural motif: two chiral $[(\pi\text{-ligand})M]_3L_3$ fragments were connected by three flexible linkers. They can thus be described as expanded triple-stranded helicates. The synthetic concept appears to be quite flexible because the bridging ligand as well as the metal fragment can be varied. Complexes of this kind are expected to display an interesting host-guest chemistry because they contain 12-metallacrown-3 sites, which should be suited for the complexation of small metal ions (see chapter IV.II.5),[127, 165, 310, 362] as well as a flexible cavity decorated by amine groups.

Chapter VII
General Conclusions

VII.I General Conclusions

12-Metallacrown-3 complexes are macrocycles composed of three metal fragment subunits. They self-assemble from halfsandwich complexes $[(\pi\text{-ligand})MCl_2]_2$ (M = Ru, Rh, Ir) and 3-hydroxy-2-pyridone ligands in the presence of base. When macrocycles with different metal fragments were mixed, reversible metal fragment exchange occurred. This allowed the generation of small dynamic combinatorial libraries (DCLs). DCLs were classified into different types and their adaptive behaviour was investigated theoretically. Two main characteristics were predicted: i) the selection of an assembly with a high content of one subunit will lead to the concomitant amplification of one or more assemblies comprised of the other subunit(s) and ii) there is an intrinsic bias for the selection of hetero-assemblies, especially for the member whose composition reflects the overall composition of the library. For example, a library composed of equal amounts of three different building blocks A, B and C will show a strong bias for the selection of the assembly ABC. These predictions were confirmed experimentally by introducing thermodynamic differences among the library members of DCLs obtained from 12-metallacrown-3 complexes.[363] This means that it is not necessarily the most stable member of the library which will be amplified the most. The presented theoretical and experimental results are in contradiction with a former paradigm of dynamic combinatorial chemistry, i.e. the amplification of the thermodynamically most stable member. In the meantime, these results were confirmed and have been generally accepted.[186, 239, 240, 242, 244] A possibility to obtain a better correlation between thermodynamic stability and amplification of the library members is to conduct the experiment in a virtual fashion.[239, 363]

The kinetics of the metal fragment exchange of 12-metallacrown-3 complexes were investigated. The equilibration proceeds in two steps with successive decrease of steric constraint. It was found that the composition of the dynamic mixture can be further biased towards one hetero-assembly if the starting materials were mixed in a 2:1 ratio. Thus, mixed-metal complexes comprised of two small (benzene)Ru fragments and one large (C_6Me_6)Ru, $(C_6H_3{}^iPr_3)$Ru or Cp*Rh fragment could be synthesised in over 60 % yield.[364]

12-Metallacrown-3 complexes are potent and selective ionophores for Li^+ ions. The use of modified 3-hydroxy-2-pyridone bridging ligands rendered these complexes soluble in water. Monomeric O,O'-chelate complexes were formed upon mixing of $[(\pi\text{-ligand})MCl_2]_2$ and 3-hydroxy-2-pyridone ligands substituted with amino groups. Addition of base induced the self-assembly process into trimeric assemblies. The investigation of the host-guest chemistry of a large variety of different water soluble 12-metallacrown-3 complexes revealed two receptors with outstanding high affinity and selectivity for Li^+ ions in water: the complexes **[(cymene)Ru(L5–2 H^+)]$_3$** and **[(C_5HMe_4)Rh(L5–2 H^+)]$_3$**. Their binding constants are as high as $K_a = 6 \times 10^4\ M^{-1}$ and their Li^+ over Na^+ selectivity is 10000:1. These values are among the highest ever reported for Li^+ com-

plexation in water.[277–279] Thus, the quantitative complexation of Li+ in the pharmacologically relevant concentration range of ~ 1 mM is possible. The complexation of Li^+ has been visualised by colorimetric, fluorescent and potentiometric means.[362]

The size exclusion effect of 12-metallacrown-3 complexes with sterically very demanding π-ligands was used to separate the two stable lithium isotopes ^6Li and ^7Li. In extraction experiments with complex **$[(C_6Me_6)Ru(L1–2\ H^+)]_3$**, an enrichment of ^7Li of 5.4 % was observed. The separation effect is of kinetic nature, as the dissociation rate is assumed to be too slow to allow the establishment of a thermodynamic equilibrium.

Two 3-hydroxy-2-pyridone units were connected by Mannich reaction of the latter with diamines and formaldehyde. Base-induced self-assembly of these bis(dihydroxypyridine) ligands with halfsandwich complexes in water gave hexanuclear complexes. Two chiral trimeric macrocycles $[(\pi\text{-ligand})M]_3L_3$ fragments were connected by three flexible linkers. The complexes can be regarded as expanded triple stranded helicates and display a length up to 2.8 nm. The metal centres at one end of the molecule can have either the same or the opposite configuration to the metal centres at the other end. In the first case, the complex is chiral and enantiomers are formed, whereas in the second case an achiral meso compound is obtained. If a ligand with an even number of chain links was used, chiral helicates were obtained. The use of a ligand with an odd number of chain links resulted in the formation of achiral meso-helicates.[365]

In summary, the supramolecular chemistry of 12-metallacrown-3 complexes in both, organic and aqueous media has been investigated. Special emphasis has been paid on the reversible metal fragment exchange, the pH dependant self-assembly process and the host-guest chemistry as well as the synthesis and characterisation of new complexes.

Chapter VIII
Experimental Part

VIII.I General & Instrumentation

VIII.I.1 General

All reactions were carried out under an atmosphere of dry dinitrogen using standard Schlenk techniques unless specified otherwise. It should be noted, however, that most of the organometallic complexes are not very air sensitive; aqueous solutions could be handled in air for a few hours without significant decomposition.

Solvents (analytical grade purity) were degassed and stored under a dinitrogen atmosphere. They were used without further purification. Benzene, hexane, chloroform, dichloromethane and diethyl ether were dried and degassed by chromatography if not specified otherwise.

The weight of the compounds given in the detailed synthesis procedures is impurity corrected.

VIII.I.2 Instrumentation

NMR Spectroscopy The ^{1}H, ^{13}C and ^{7}Li NMR spectra were recorded on a Bruker Advance DPX 400 MHz spectrometer. The residual solvent signals were used as internal reference. Routine ^{1}H NMR spectra in D_2O were referenced to the residual HDO signal, but ^{13}C NMR spectra in D_2O, as well as ^{1}H and ^{13}C NMR spectra in 0.1 M DCl in D_2O were calibrated using dioxane (3.75 ppm). LiCl in D_2O was used as external reference for ^{7}Li NMR spectra. All spectra were recorded at room temperature (22 °C).

Mass Spectroscopy ESI mass spectra were measured with a MicroMass Q-Tof Ultima spectrometer.

UV/VIS UV/VIS spectra were measured on a Perkin-Elmer Lambda 40 or Perkin-Elmer Lambda 35 spectrometer.

HPLC Purifications by reversed phase HPLC were carried out using a Waters system consisting of a Waters 600 controler unit, a Water Delta 600 pump and a Waters 2487 dual wavelength absorbance detector. A Sunfire preparative C_{18} coloumn (5 µm, 10×250 mm) was used as stationary phase, and millipore water and acetonitrile (HPLC grade purity) with 0.1 % (v/v) trifluoroacetic acid as mobile phase.

Titrations Potentiometric titrations and pH measurements were performed using a Metrohm Titrino 716 DMS instrument. A combined LL pH glass electrode (Metrohm Ecotrode) was used; and in cases of very small volumes, a combined LL micro pH glass electrode (Metrohm Biotrode).

Elemental Analysis Elemental Analysis was performed on a EA 1110 CHN or a EA 1108 CHNS-O Carlo Erba instrument.

ICP Measurements Inductively coupled plasma (ICP) measurements were perfomed on a Perkin-Elmer ICP-OES 2000 DV instrument.

Crystallographic Investigations Diffraction data were collected using MoKa radiation on different equipments and at different temperatures: a 4-circle kappa goniometer equipped with an Oxford Diffraction KM4 Sapphire CCD, a mar345 IPDS or a Bruker APEX II CCD. Cell refinement and data reduction was performed with CrysAlis RED 1.7.1. All structures were refined using the full-matrix least-squares on F^2 with all non-H atoms anisotropically defined. The hydrogen atoms were placed in calculated positions using the 'riding model'. Structure refinement and geometrical calculations were carried out with SHELXL-97.[366, 367] All graphic representations were generated with Diamond 3.1a from the corresponding cif files.

VIII.I.3 Purchase of Compounds

Cs_2CO_3 (99.9 %), 1,2,3,4-tetramethyl-1,3-cyclopentadiene (technical, 85 %), 1,3-di(4-piperidyl)propane (97 %) and $NaBH_4$ (98 %) were purchased at Sigma-Aldrich. 3-hydroxy-2-pyridone (practical, 97 %), paraformaldehyde (95 %), piperidine (98 %), N,N'-dimethylethylenediamine (>98 %), sodium (metallic), 1,3,5-triisopropylbenzene (97 %), 1,2,3,4,5-pentamethylcyclopentadiene (95 %), DCl (38 % in D_2O), LiCl (anhydrous, >98 %), K_2HPO_4 (>99.5 %, TraceSelect) and 9-anthracenecarboxaldehyde (>97 %,) were purchased at Fluka. Formaldehyde (37 % in water, stabilized with 10–15 % MeOH), α-terpinene (technical, 85 %), 1,4-cyclohexadiene 97 %), dicyclopentadiene (95 %), piperazine (anhydrous, 99 %), morpholine (99+ %), dimethylamine (40 % in H_2O), N-methylpiperazine (99+ %), $CsOH \cdot H_2O$ (99.5 %) and Pd/C (unreduced, 10 %) were purchased at Acros. Pd on alumina (5 %), dibenzylamine (98 %), 1-methyl-1,3-cyclohexadiene (technical, 90 %), and 1-pyrenecarboxaldehyde (99 %) were purchased at Alfa Aesar. The hydrated salts $RuCl_3 \cdot x\ H_2O$, $RhCl_3 \cdot 3\ H_2O$ and $IrCl_3 \cdot 3\ H_2O$ were purchased from Precious Metals Online. Trifluoroacetic acid (99.9 %) for HPLC was purchased from SDS.

VIII.II Synthesis

VIII.II.1 π-Ligands

The complexes $[(C_6H_6)RuCl_2]_2$ (**1**),[368, 369] $[(C_6H_5Me)RuCl_2]_2$ (**2**),[369] $[(cymene)RuCl_2]_2$ (**3**),[369, 370] $[(C_6H_5CO_2Et)RuCl_2]_2$ (**4**),[371] $[(C_6Me_6)RuCl_2]_2$ (**6**),[370] $[(C_6H_3{}^iPr_3)RuCl_2]_2$ (**5**),[372] $[(C_5H_5)RhCl_2]_2$ (**7**),[373] $[(C_5Me_4H)RhCl_2]_2$ (**8**),[374] $[Cp^*RhCl_2]_2$ (**9**)[375] and $[Cp^*IrCl_2]_2$ (**11**)[375] were synthesised according to literature procedures. In general, the synthesis of the dimeric halfsandwich complexes was well described. However, modifications and a typical procedure will be given.

All complexes were soluble in water and in PBS. Whereas in water generally two sets of signals were observed, one species formed in most cases in PBS, probably a phosphato complex. The solubility in PBS was enhanced compared to water. In general, Rh^{III} complexes showed the highest solubility, whereas the Ir^{III} complexes showed a very low solubility. The solubility of the ruthenium(II) complexes depend on the type of the π-ligand: complexes bearing very unpolar π-ligands such as hexamethylbenzene and triisopropylbenzene were much less soluble than complexes bearing more polar π-ligands.

VIII.II.1.1 $[(C_6H_6)RuCl_2]_2$[368, 369]

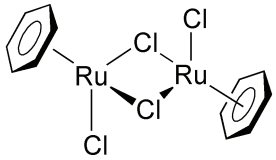

Yields close to the literature (>90 %) were obtained by using only 4.0 equiv. of 1,4-cyclohexadiene instead of 14 equiv.. Representative synthetic procedure: $RuCl_3 \cdot x\ H_2O$ (39 % Ru, 3.1 g, 12.0 mmol) and 1.4-cyclohexadiene (4.6 mL, 47.3 mmol, 3.9 equiv.) were heated in EtOH (150 mL) to reflux for 4 h. An orange-brown precipitate was filtered off, washed with cold EtOH (2×5 mL) and dried in vacuo. The product was obtained in 92 % yield (2.76 g, 5.52 mmol). MeOH can be used alternatively to EtOH. The ^1H NMR spectrum showed always a small impurity of about 5 % at 6.52 ppm.

^1H NMR (400 MHz, DMSO): δ (ppm) = 5.97 (s, 12 H, C_6H_6).

VIII.II.1.2 $[(C_6H_5Me)RuCl_2]_2$[369]

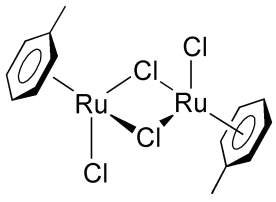

Although the complex was mentioned in the literature, neither a detailed synthesis procedure nor a yield was given. Representative synthetic procedureRepresentative synthetic procedure: $RuCl_3 \cdot x\ H_2O$ (39 % Ru, 3.0 g, 11.6 mmol) and 1-methyl-1,4-cyclohexadiene (6.0 mL, 53.1 mmol, 4.6 equiv.) were heated in EtOH (150 mL) to reflux for 16 h.

The reaction was left to cool down to room temperature and then placed in the freezer over night to ensure complete crystallisation. Dark red microcrystals were filtered off, washed with cold EtOH (2×5 mL) and dried in vacuo. The product was obtained in 93 % yield (2.84 g, 5.37 mmol). It happened that the product was contaminated with small traces of metallic ruthenium. In this case, the crystals were solubilized in $CHCl_3$ and the ruthenium was filtered off (air sensitive!). The solution was concentrated and the product crystallised upon addition of hexane.

^{1}H NMR (400 MHz, $CDCl_3$): δ (ppm) = 2.22 (s, 6 H, Me), 5.35 (d, ^3J = 6 Hz, 4 H, C_6H_5), 5.57 (t, ^3J = 6 Hz, 2 H, C_6H_5), 5.66 (t, ^3J = 6 Hz, 4 H, C_6H_5).

VIII.II.1.3 [(Cymene)$RuCl_2$]$_2$[369, 370]

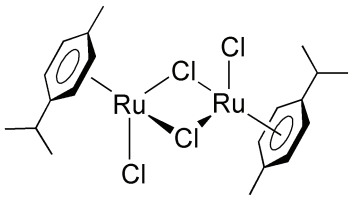

α-Terpinene was used instead of α-phellandrene. Again, the use of 6.0 equiv. of α-terpinene were completely sufficient to ensure yields between 80 and 90 %. The reaction could be scaled up to 5 g of starting material, using 200 mL of solvent (either EtOH or MeOH). Best yields were obtained by placing the reaction mixture in the freezer over night to crystallise. The product crystallised in large dark red crystals; a microcrystalline, orange precipitate was obtained after addition of Et_2O to the reaction mixturer. Representative synthetic procedure: $RuCl_3$ ·x H_2O (39 % Ru, 5.0 g, 19.3 mmol) and α-terpinene (21 mL, 116 mmol, 6.0 equiv.) were heated in EtOH (150 mL) to reflux for 4 h. The reaction was left to cool down to room temperature and placed in the freezer over night for complete crystallisation. Dark red crystals were filtered off, washed with cold EtOH (2×5 mL) and dried in vacuo. The complex was obtained in 92 % yield (5.43 g, 8.86 mmol). MeOH can be used instead of EtOH.

^{1}H NMR (400 MHz, $CDCl_3$): δ (ppm) = 1.28 (d, ^3J = 7 Hz, 12 H, CH_3CH), 2.16 (s, 6 H, CH_3CH(CH_3)$_2$), 2.92 (sept, ^3J = 7 Hz, 2 H, CH(CH_3)$_2$), 5.34 (d, ^3J = 6 Hz, 4 H, Me$C_6H_4{}^i$Pr), 5.47 (d, ^3J = 6 Hz, 4 H, Me$C_6H_4{}^i$Pr).

VIII.II.1.4 [($C_6H_5CO_2Et$)$RuCl_2$]$_2$[371]

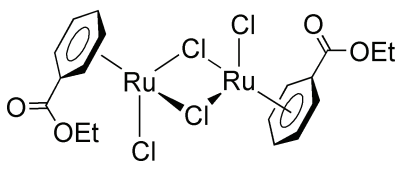

Representative synthetic procedure: $RuCl_3$ ·x H_2O (39% Ru, 3.5 g, 13.5 mmol) and ethyl-1,4-cyclohexadiene-3-carboxylate (8.2 g, 54.0 mmol, 4.0 equiv., crude product from Birch reduction of benzyl acetate) were heated in EtOH (100 mL) to reflux for 5 h. The reaction was left to cool down to room temperature and placed in the freezer over night for complete crystallisation. The orange-brown precipitate was filtered off, washed with cold EtOH (2×5 mL) and dried in vacuo. The crude product was

obtained in 91 % yield (3.96 g, 6.15 mmol). Purification was achieved by Soxhlet extraction with ethanol; a brown residue remained on the fritte.

^{1}H NMR (400 MHz, $CDCl_3$): δ (ppm) = 1.42 (t, ^3J = 7 Hz, 6 H, CH_3CH_2), 4.47 (q, ^3J = 7 Hz, 4 H, CH_3CH_2), 5.78 (t, ^3J = 6 Hz, 4 H, C_6H_5), 5.98 (t, ^3J = 6 Hz, 2 H, C_6H_5), 6.47 (d, ^3J = 6 Hz, 4 H, C_6H_5).

VIII.II.1.5 $[(C_6H_3{}^iPr_3)RuCl_2]_2$[372]

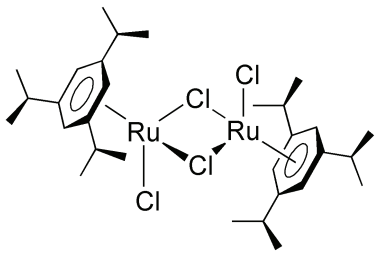

Contrary to the literature procedure, $[(cymene)RuCl_2]_2$ has to be heated about 4 hours in triisopropylbenzene to guarantee complete exchange of the arene. Triisopropylbenzene was generally reused, either without purification when stored under a dinitrogen atmosphere or after distillation. Representative synthetic procedure: $[(cymene)RuCl_2]_2$ (**3**) (1.5 g, 2.45 mmol) was heated in triisopropylbenzene (50 mL, excess) to 200 °C for 4 h under vigourous stirring. The $[(cymene)RuCl_2]_2$ complex was completely solubilized. The reaction mixture was allowed to cool down to room temperature and placed in the fridge over night. Dark red crystals were filtered off and the crude product washed with CH_2Cl_2 through a fritte (air sensitive!) in order to remove traces of metallic ruthenium. The complex precipitated after concentration of the solution under reduced pressure and addition of hexane. A red microcrystalline product was obtained in 63 % yield (1.16 g, 1.54 mmol).

^{1}H NMR (400 MHz, $CDCl_3$): δ (ppm) = 1.27 (d, ^3J = 7 Hz, 36 H, $(CH_3)_2CH$), 3.05 (sept, ^3J = 7 Hz, 6 H, $(CH_3)_2CH$), 5.13 (s, ^{6} H, C_6H_3).

VIII.II.1.6 $[(C_6Me_6)RuCl_2]_2$[370]

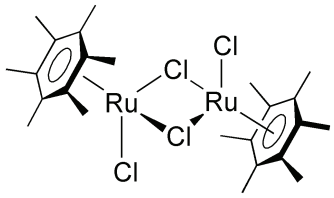

The reaction was best carried out in an 500 mL round bottom flask equipped with an air cooled condenser. An inert dinitrogen atmosphere is not necessary and not advisable, as the sublimating hexamethylbenzene has to be scraped periodically from the walls of the flask. To avoid a very hard solidified melt, hexane was added when the melt was still hot and liquid (careful!). In case of difficulties to remove the hexamethylbenzene, purification was best achieved by sublimation under reduced pressure. Representative synthetic procedure: $[(cymene)RuCl_2]_2$ (**3**) (2.0 g, 3.27 mmol) and hexamethylbenzene (15 g, excess) were heated to 200 °C for 4 h under stirring of the melt. The flask was taken out of the oil bath and hexane (300 mL) was added. The orange precipitate was filtered off and washed with hexane until the hexamethylbenzene was completely removed. The complex was obtained as an orange powder in 77 % yield (1.68 g, 2.52 mmol).

^{1}H NMR (400 MHz, $CDCl_3$): δ (ppm) = 2.02 (s, 36 H, C_6Me_6).

VIII.II.1.7 $[(C_5H_5)RhCl_2]_2$[373]

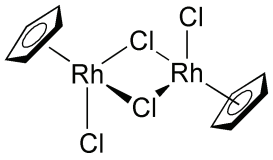

General procedure: $RhCl_3 \cdot 3\ H_2O$ (3.0 g, 11.4 mmol) and freshly distilled cyclopentadiene (3.8 mL, 45.6 mmol, 4.0 equiv.) were heated in MeOH (100 mL) to reflux for 48 h. The reaction mixture was cooled down to room temperature and placed in the freezer over night. The precipitate was filtered off, washed with MeOH (2×5 mL) and dried in vacuo. An orange powder was obtained in 41 % yield (1.12 g, 2.34 mmol).

^{1}H NMR (400 MHz, D_2O): δ (ppm) = 6.09 (s, 10 H, Cp).

VIII.II.1.8 $[(C_5HMe_4)RhCl_2]_2$[374]

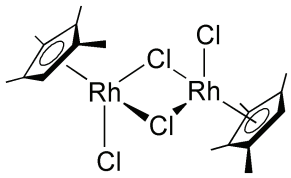

Neither a detailed reaction procedure, yield or spectroscopic data were given in the literature. Although the reaction was carried out as refered to, considerable amounts of an insoluble byproduct have been formed. General sample procedure: $RhCl_3 \cdot 3\ H_2O$ (3.0 g, 11.4 mmol) and 1,2,3,4-tetramethyl-1,3-cyclopentadiene (4.0 mL, 22.8 mmol, 2.0 equiv.) were heated in MeOH (100 mL) to reflux for 48 h. The reaction mixture was cooled down to room temperature and placed in the freezer over night. An orange precipitate was filtered off, washed with Et_2O (2×10 mL) and was then washed through a fritte with CH_2Cl_2 (N_2). The solvent was removed under reduced pressure and the product dried in vacuo. A brown-orange powder (electrostatic) was obtained in 37 % yield (1.25 g, 2.12 mmol).

^{1}H NMR (400 MHz, $CDCl_3$): δ (ppm) = 1.64 (s, 12 H, CH_3), 1.70 (s, 12 H, CH_3), 5.01 (s, 2 H, C_5HMe_4).

VIII.II.1.9 $[Cp^*RhCl_2]_2$[375]

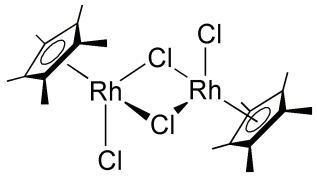

Representative synthetic procedure: $RhCl_3 \cdot 3\ H_2O$ (3.0 g, 11.4 mmol) and pentamethylcyclopentadiene (2.0 mL, 12.5 mmol, 1.1 equiv.) were heated in MeOH (100 mL) to reflux for 48 h. The reaction mixture was cooled down to room temperature and placed in the freezer over night. Dark red microcrystals were filtered off, washed with cold MeOH (2×5 mL) and dried in vacuo. The complex was obtained in 82 % yield (2.89 g, 4.67 mmol).

^{1}H NMR (400 MHz, $CDCl_3$): δ (ppm) = 1.62 (s, 30 H, Cp*).

VIII.II.1.10 $[(C_5HMe_4)IrCl_2]_2$

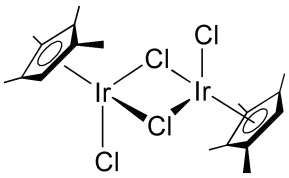

Contrary to what was reported by Werner,[376] the complex could be obtained by reaction of $IrCl_3 \cdot 3\ H_2O$ and 1,2,3,4-tetramethyl-1,3-cyclopentadiene. General sample procedure: $IrCl_3 \cdot 3\ H_2O$ (1.0 g, 2.83 mmol) and 1,2,3,4-tetramethyl-1,3-cyclopentadiene (1.0 mL, 5.66 mmol, 2.0 equiv.) were heated in MeOH (100 mL) to reflux for 48 h. The reaction mixture was cooled down to room temperature and placed in the freezer over night. Orange crystals were filtered off, and washed with Et_2O (2×10 mL) and dried in vacuo. The product was obtained in 41 % yield (447 mg, 1.16 mmol).

^{1}H NMR (400 MHz, $CDCl_3$): δ (ppm) = 1.63 (s, 12 H, CH_3), 1.68 (s, 12 H, CH_3), 5.26 (s, 2 H, C_5HMe_4).

VIII.II.1.11 $[Cp^*IrCl_2]_2$[375]

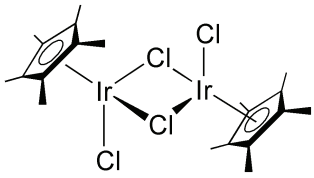

The yields obtained routinely in the laboratory were considerably lower than those given in the literature. The complex was used without recrystallisation from chloroform/hexane. General procedure: $IrCl_3 \cdot 3\ H_2O$ (1.0 g, 2.84 mmol) and pentamethylcyclopentadiene (0.5 mL, 3.12 mmol, 1.1 equiv.) were heated in MeOH (50 mL) to reflux for 48 h. The reaction mixture was cooled down to room temperature and placed in the freezer over night. An orange precipitate was filtered off, washed with MeOH (2×5 mL) and dried in vacuo. The complex was obtained in 54 % yield (0.613 g, 0.77 mmol).

^{1}H NMR (400 MHz, $CDCl_3$): δ (ppm) = 1.59 (s, 30 H, Cp*).

VIII.II.2 Bridging Ligands

The Ligands **L2**, **L3** and **L4** were synthesised by a Mannich reaction of 3-hydroxy-2-pyridone, formaldehyde and the corresponding secondary amine according to modified literature procedures.[304–306] The ligands **L5**, **L6**, **L13**, **L14** and **L15** were synthesised in a similar manner. Ligands **L2**, **L4** and **L5** were obtained in high purity and were used without further purification. Generally, impurities could be removed by recrystallisation from $CHCl_3$ and acetone. 3-Hydroxy-2-pyridone present in ligand **L6** was also removed by extraction with water from a solution of the ligand in $CHCl_3$. Ligands **L13**, **L14** and

L15 showed extrem low solubilities in water and organic solvents. Purification was achieved by reversed phase HPLC from TFA solutions.

VIII.II.2.1 L2[304–306]

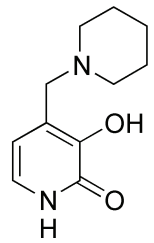

3-Hydroxy-2-pyridone (2.00 , 17.5 mmol, 1.0 equiv.), formaldehyde (1.31 mL, 37 wt% in H_2O, 17.5 mmol, 1.0 equiv.) and piperidine (1.72 mL, 17.5 mmol, 1.0 equiv.) were heated in MeOH (75 mL) to reflux for 7 h and then stirred at room temperature for 5 h. The cream colored precipitate was filtered off and washed with acetone. The filtrate was concentrated to less than 10 mL and acetone was added. A second crop of ligand was filtered off. Both fractions were dried in vacuo. The product was obtained in 73 % yield (2.65 g, 12.7 mmol).

^{1}H NMR (400 MHz, D_2O): δ (ppm) = 1.62 (m, br, 2 H, CH_2), 1.78 (m, br, 4 H, CH_2), 3.14 (m, br, 4 H, NCH_2), 4.05 (s, 2 H, NCH_2), 6.28 (d, ^3J = 6 Hz, 1 H, pyridone), 6.69 (d, ^3J = 7 Hz, 1 H, pyridone).

^{1}H NMR (400 MHz, $CDCl_3$): δ (ppm) = 1.49 (m, br, 2 H, CH_2), 1.65 (m, 4 H, CH_2), 2.53 (m, br, 4 H, NCH_2), 3.55 (s, 2 H, NCH_2), 5.92 (d, ^3J = 7 Hz, 1 H, pyridone), 6.87 (d, J = 7 Hz, 1 H, pyridone), 13.03 (s, br, 1 H, NH).

VIII.II.2.2 L3[304–306]

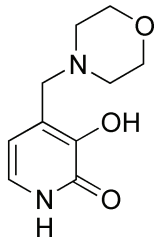

3-Hydroxy-2-pyridone (2.00 , 17.5 mmol, 1.0 equiv.), formaldehyde (1.31 mL, 37 wt% in H_2O, 17.5 mmol, 1.0 equiv.) and morpholine (1.53 mL, 17.5 mmol, 1.0 equiv.) were heated in MeOH (75 mL) to reflux for 5 h and then stirred at room temperature for 5 h. The cream colored precipitate was filtered off, washed with acetone and dried in vacuo. The product was obtained in 45 % yield (1.65 g, 7.84 mmol). About 7 % 3-hydroxy-2-pyridone remained as an impurity, which could not be removed by recrystallisation from $CHCl_3$ and acetone.

^{1}H NMR (400 MHz, D_2O): δ (ppm) = 2.72 (m, br, 4 H, NCH_2), 3.73 (s, 2 H, NCH_2), 3.80 (m, 4 H, OCH_2), 6.38 (d, ^3J = 7 Hz, 1 H, pyridone), 7.02 (d, ^3J = 7 Hz, 1 H, pyridone).

^{1}H NMR (400 MHz, $CDCl_3$): δ (ppm) = 2.59 (m, br, 4 H, NCH_2), 3.59 (s, 2 H, NCH_2), 3.76 (m, 4 H, OCH_2), 6.05 (d, ^3J = 7 Hz, 1 H, pyridone), 6.90 (d, ^3J = 7 Hz, 1 H, pyridone) 10.18 (s, br, 1 H, OH), 12.56 (s, br, 1 H, NH).

VIII.II.2.3 L4[304–306]

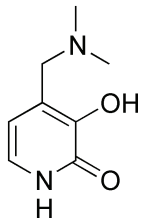

Formaldehyde (1.31 mL, 37 wt% in H_2O, 17.5 mmol, 1.0 equiv.) and dimethylamine (40 % in H_2O, 2.12 mL, 17.5 mmol, 1.0 equiv.) were stirred in 10 mL MeOH for 0.5 h, and then added to 3-hydroxy-2-pyridone (2.00 , 17.5 mmol, 1.0 equiv.) in MeOH (75 mL). The reaction mixtures was refluxed for 2 h and then stirred at room temperature over night. The cream colored precipitate was filtered off, washed with acetone and dried in vacuo. The product was obtained in 41 % yield (1.21 g, 7.17 mmol).

^{1}H NMR (400 MHz, D_2O): δ (ppm) = 2.79 (s, 6 H, NMe_2), 4.07 (s, 2 H, NCH_2), 6.29 (d, ^3J = 7 Hz, 1 H, pyridone), 6.71 (d, ^3J = 7 Hz, 1 H, pyridone).

^{1}H NMR (400 MHz, $CDCl_3$): δ (ppm) = 2.35 (s, 6 H, NMe_2), 3.52 (s, 2 H, NCH_2), 5.97 (d, ^3J = 7 Hz, 1 H, pyridone), 6.90 (d, ^3J = 7 Hz, 1 H, pyridone), 13.38 (s, br, 1 H, NH).

VIII.II.2.4 L5

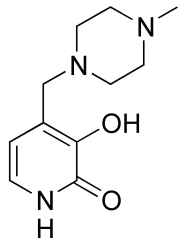

3-Hydroxy-2-pyridone (2.00 , 17.5 mmol, 1.0 equiv.), formaldehyde (1.31 mL, 37 wt% in H_2O, 17.5 mmol, 1.0 equiv.) and 1-methylpiperazine (1.95 g, 17.5 mmol, 1.0 equiv.) were heated in MeOH (75 mL) to reflux for 7 h and then stirred for 5 h. The slightly brown solution was concentrated to less than 25 mL and acetone was added. The cream colored precipitate was filtered off, washed with acetone and was dried in vacuo. The product was obtained in 45 % yield (1.76 g, 7.88 mmol).

^{1}H NMR (400 MHz, D_2O, 1.5 mM Dioxane): δ (ppm) = 2.36 (s, 3 H, NMe), 2.73 (m, br, 8 H, NCH_2, piperazine), 3.73 (s, 2 H, NCH_2), 6.36 (d, ^3J = 7 Hz, 1 H, pyridone), 6.93 (d, ^3J = 7 Hz, 1 H, pyridone).

^{13}C NMR (101 MHz, D_2O, 1.5 mM Dioxane): δ (ppm) = 44.56, 51.66, 53.50, 57.08 (NMe, NCH_2), 111.45, 122.18, 126.76, 149.37, 160.51 (pyridone).

^{1}H NMR (400 MHz, $CDCl_3$): δ (ppm) = 2.30 (s, 3 H, NMe), 2.35–2.80 (m, br, 8 H, NCH_2, piperazine), 3.59 (s, 2 H, NCH_2), 5.99 (d, ^3J = 6 Hz, 1 H, pyridone), 6.91 (d, ^3J = 7 Hz, 1 H, pyridone), 12.93 (s, br, 1 H, NH).

^{13}C NMR (101 MHz, $CDCl_3$): δ (ppm) = 46.02, 52.88, 54.96, 59.58 (NMe, NCH_2), 107.68, 123.81, 125.39, 146.78, 159.75 (pyridone).

VIII.II.2.5 L6

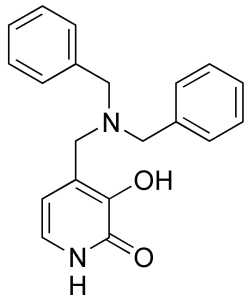

3-Hydroxy-2-pyridone (5.00 g, 43.6 mmol, 1.0 equiv.), formaldehyde (3.54 mL, 37 wt% in H_2O, 43.65 mmol, 2.0 equiv.) and dibenzylamine (16.7 mL; 87.2 mmol, 2.0 equiv.) were heated to reflux for three days in EtOH (400 mL). After a couple of hours, a precipitate formed in the reaction mixture. The reaction was complete when this precipitate had completely disappeared. It has also to be noted, that dibenzylamine has to be used in excess; the use of less than 2 equiv. resulted in the formation of a 1:1 mixture of ligand **L6** and 3-hydroxy-2-pyridone. The slightly brown solution was filtered and the filtrate concentrated under reduced pressure to 75 mL. The cream coloured precipitate was filtered off and dried in vacuo. The crude product was dissolved in $CHCl_3$ (200 mL), filtered over celite and the solution concentrated to 75 mL. After addition of acetone a white product precipitated which was filtered off and dried in vacuo. The product was obtained in 28 % (3.92 g, 12.2 mmol) yield.

^{1}H NMR (400 MHz, $CDCl_3$): δ (ppm) = 3.60 (s, 2 H, NCH_2), 3.62 (s, 4 H, NCH_2), 6.14 (d, ^3J = 7 Hz, 2 H, pyridone), 6.92 (d, ^3J = 7 Hz, 2 H, pyridone), 7.24–7.36 (m, 10 H, phenyl), 10.07 (s, br, 1 H, OH), 13.13 (s, br, 1 H, NH).

^{13}C NMR (101 MHz, 0.1 M DCl in D_2O, 1.5 mM Dioxane): δ (ppm) = 54.06, 58.38 (NCH_2), 108.06, 123.73, 127.00, 127.78, 128.76, 129.54, 137.20, 146.08, 159.56 (pyridone & phenyl).

Elemental analysis (%) calcd (found) for $C_{20}H_{20}N_2O_2$: C 74.68 (74.98); H 6.24 (6.29); N 8.92 (8.74).

VIII.II.2.6 L7

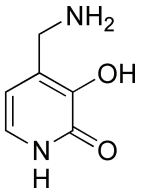

The ligand can be synthesised either by using Pd/C or Pd/Al_2O_3 as catalyst. In the first case, partial hydrogenation of the pyridine ring is observed; the best reaction time was found to be 8 h. If the reaction was scaled up, or less solvent was used, a decrease of yield and purity was observed.

L6 (1.00 g, 3.12 mmol) was solubilized in MeOH (200 mL) in a 500 mL round bottom schlenk and the solution was degassed. Pd/Al_2O_3 (0.664 g, 0.312 mmol, 10 mol%) was added under a gentle flux of N_2. The nitrogen atmosphere was replaced by an hydrogen atmosphere and the reaction mixture was stirred for 6 days. The progress of the reaction was monitored observing the disappearance of the **L6** TLC spot (Eluent: $CHCl_3$:EtOH 8.5:1.5,). The reaction mixture was filtered over celite and the solvent was removed under reduced pressure. A small amount of MeOH (about 10 mL) was added to the residue, the resulting crystalline solid was filtered off and dried in vacuo. The product was obtained in 30 % yield (131 mmol, 0.94 mmol). Remark: The crude product showed

only small amounts of starting material and use without further purification should be possible. MeOH was found in the ^{1}H NMR spectra, even after prolonged drying of the product in vacuo.

^{1}H NMR (400 MHz, D_2O): δ (ppm) = 4.00 (s, 2 H, NH_2), 6.33 (d, ^3J = 7 Hz, 2 H, pyridone), 6.71 (d, ^3J = 7 Hz, 2 H, pyridone).

^{13}C NMR (101 MHz, D_2O): δ (ppm) = 40.55 (NCH_2), 111.35, 117.931, 123.44, 155.82, 163.19 (pyridone).

VIII.II.2.7 L9

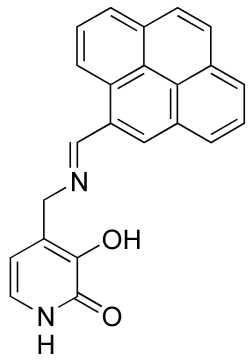

L7 (200 mg, 1.43 mmol) and 1-pyrenecarboxaldehyde (329 mg, 1.43 mmol) were stirred in dry MeOH (75 mL) for 2 h. The resulting faint ocher precipitate was filtered off, washed with MeOH (2 × 5 mL) and dried in vacuo. The product was obtained in 74 % yield (372 mg, 1.06 mmol).

^{1}H NMR (400 MHz, DMSO): δ (ppm) = 4.89 (s, 2 H, NCH_2), 6.30 (d, ^3J = 7 Hz, 1 H, pyridone), 6.90 (d, ^3J = 7 Hz, 1 H, pyridone), 8.13 (t, ^3J = 8 Hz, 1 H, pyrene), 8.23 (d, ^3J = 9 Hz, 1 H, pyrene), 8.29 (d, ^3J = 9 Hz, 1 H, pyrene), 8.31–8.41 (m, 4 H, pyrene), 8.59 (d, ^3J = 8 Hz, 1 H, pyrene), 9.13 (d, ^3J = 10 Hz, 1 H, pyrene), 9.55 (s, 1 H, CHN).

^{13}C NMR (101 MHz, DMSO): δ (ppm) = 58.19 (NCH_2), 106.57, 123.01, 123.20, 123.80, 124.08, 125.11, 125.91, 126.21, 126.49, 126.66, 127.30, 127.48, 128.43, 128.75, 128.84, 129.42, 130.17, 130.85, 132.46, 143.56 (pyrene, pyridone, CHN), 157.96, 161.99 (pyridone).

VIII.II.2.8 L10

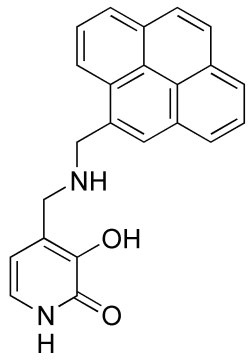

A suspension of **L9** (250 mg, 0.71 mmol) and $NaBH_4$ (96 mg, 2.48 mmol, 3.5 equiv.) was stirred in dry MeOH (50 mL) for 2 h. The color of the precipitate changed from orange to white. The solid was filtered off, washed with MeOH (2 × 5 mL) and dried in vacuo. A white microcrystaline product in 64 % yield (161 mg, 0.45 mmol) was obtained.

^{1}H NMR (400 MHz, DMSO): δ (ppm) = 3.76 (s, 2 H, NCH_2), 4.40 (s, 2 H, NCH_2), 6.30 (d, ^3J = 7 Hz, 1 H, pyridone), 6.86 (d, ^3J = 7 Hz, 1 H, pyridone), 8.07 (t, ^3J = 8 Hz, 1 H, pyrene), 8.10 (d, ^3J = 8 Hz, 1 H, pyrene), 8.15 (m, 2 H, pyrene), 8.21 (d, ^3J = 9 Hz, 1 H, pyrene), 8.26 (d, ^3J = 8 Hz, 1 H, pyrene), 8.28 (d, ^3J = 8 Hz, 1 H, pyrene), 8.29 (d, ^3J = 8 Hz, 1 H, pyrene), 8.44 (d, ^3J = 9 Hz, 1 H, pyrene), 11.57 (s, br, 1 H, NH).

^{13}C NMR (101 MHz, DMSO): δ (ppm) = 46.44, 50.18 (NCH_2), 106.37, 122.96, 123.70, 124.00, 124.10, 124.66, 125.01, 125.08, 126.18, 126.87, 127.21, 127.44, 127.87, 128.62, 129.97, 130.37, 130.81, 134.21, 144.25, 157.86 (pyrene, pyridone).

VIII.II.2.9 L11

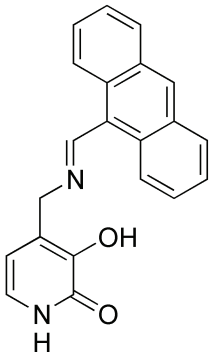

L7 (200 mg, 1.43 mmol) and 9-anthraldehyde (303 mg, 1.43 mmol) were stirred in dry MeOH (60 mL) for 2 h. The resulting yellow precipitate was filtered off, washed with MeOH (2 × 5 mL) and dried in vacuo. The product was obtained in 71 % yield (334 mg, 1.02 mmol) as a yellow powder.

^{1}H NMR (400 MHz, DMSO): δ (ppm) = 4.94 (s, 2H, NCH_2), 6.29 (d, ^{3}J = 7 Hz, 1 H, pyridone), 6.90 (d, ^{3}J = 6 Hz, 1 H, pyridone), 7.59 (m, 4 H, anthracene), 8.14 (d, ^{3}J = 9 Hz, 2 H, anthracene), 8.61 (d, ^{3}J = 8 Hz, 2 H, anthracene), 8.72 (s, 1 H, anthracene), 9.13 (s, br, 1 H, OH), 9.63 (s, 1 H, CHN), 11.67 (s, br, 1 H, NH).

^{13}C NMR (101 MHz, DMSO): δ (ppm) = 58.99 (NCH_2), 106.80, 123.24, 124.94, 125.50, 126.64, 126.89, 127.99, 128.79, 129.27, 129.43, 130.81 (anthracene & pyridone, CHN), 144.08, 158.12, 162.13 (pyridone).

VIII.II.2.10 L12

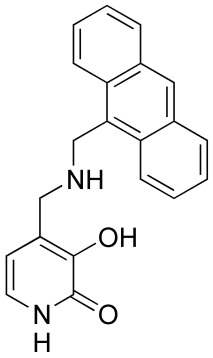

A suspension of **L11** (200 mg, 0.61 mmol) and $NaBH_4$ (82 mg, 2.14 mmol, 3.5 equiv.) was stirred in dry EtOH (50 mL) for 2 h. The color of the precipitate changed from yellow to faint yellow. The reaction mixture was placed in the fridge over night, the solid filtered off and washed with MeOH (2 × 5 mL). The faint yellow solid was dried in vacuo. The product was obtained in 60 % yield (101 mg, 0.31 mmol). All peaks except those of the pyridone ring of the ^{1}H NMR spectra recorded in 0.1 M DCl in D_2O were very susceptible to minor changes of the concentration. A ^{13}C NMR spectrum could not be recorded because of crystallisation of the compound. Deuterated DMSO was not suited as solvent because the peaks were broad.

^{1}H NMR (400 MHz, 0.1 M DCl in D_2O): δ (ppm) = 4.14 (s, 2H, NCH_2), 4.14 (s, 2H, NCH_2), 5.92 (d, ^{3}J = 7 Hz, 1 H, pyridone), 6.83 (d, ^{3}J = 6 Hz, 1 H, pyridone), 7.48 (m, 4 H, anthracene), 7.76 (d, ^{3}J = 9 Hz, 1 H, anthracene), 7.92 (d, ^{3}J = 8 Hz, 1 H, anthracene), 8.33 (s, 1 H, anthracene).

VIII.II.2.11 L13

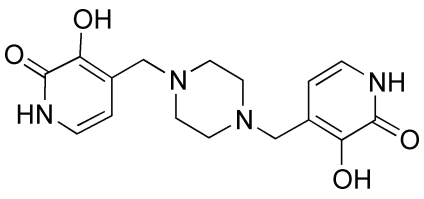

Piperazine (0.50 g, 5.75 mmol, 1.0 equiv.), 3-hydroxy-2-pyridone, (1.61 g, 13.8 mmol, 2.4 equiv.) and formaldehyde (1.0 mL, 37 wt% in H_2O, 13.8 mmol, 2.4 equiv.) were heated for 24 h in EtOH (130 mL). A cream colored precipitate formed, which was isolated and dried in vacuo. The crude product was obtained in 85 % purity and 90 % yield (1.72 g, 5.17 mmol). The product was purified by reversed phase HPLC (H_2O/CH_3CN + 0.1 % TFA, gradient: 98:2 to 96:4 in 9 min, λ_{max} = 305 nm, sample: 2 mL, 10 mM in 0.2 % TFA, R_f = 6.0 min).

^{1}H NMR (400 MHz, 0.1 M DCl in D_2O): δ (ppm) = 3.76 (s, br, 8 H, NCH_2, piperazine), 4.47 (s, 4 H, NCH_2), 6.47 (d, ^3J = 7 Hz, 2 H, pyridone), 7.13 (d, ^3J = 7 Hz, 2 H, pyridone).

^{13}C NMR (101 MHz, 0.1 M DCl in D_2O, 1.5 mM Dioxane): δ (ppm) = 49.00 (NCH_2, piperazine), 54.36 (NCH_2), 110.62, 119.28, 125.40, 147.58, 159.25 (pyridone).

VIII.II.2.12 L14

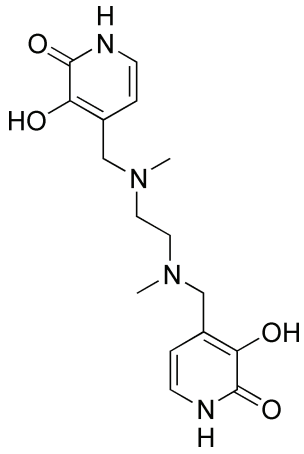

N,N'-Dimethylethylenediamine (0.55 mL, 5.00 mmol, 1.0 equiv.), 3-hydroxy-2-pyridone, (1.40 g; 12.0 mmol, 2.40 equiv.) and formaldehyde (1.0 mL, 37 wt% in H_2O, 12.0 mmol, 2.4 equiv.) were heated for 24 h in ethylene glycol dimethyl ether (130 mL). A cream colored precipitate formed, which was isolated and dried in vacuo. The crude product was obtained in about 90 % purity and 71 % yield (1.19 g, 3.56 mmol). The product was purified by reversed phase HPLC (H_2O/CH_3CN + 0.1 % TFA, gradient: 98:2 to 97.3:2.7 in 9 min, λ_{max} = 305 nm, sample: 2 mL, 40 mM in 0.8 % TFA, R_f = 5.4 min).

^{1}H NMR (400 MHz, 0.1 M DCl in D_2O): δ (ppm) = 2.98 (s, 6 H, NCH_3), 3.79 (s, 4 H, NCH_2, ethylenediamine), 4.41 (s, 4 H, NCH_2), 6.46 (d, ^3J = 7 Hz, 2 H, pyridone), 7.13 (d, ^3J = 7 Hz, 2 H, pyridone).

^{13}C NMR (101 MHz, 0.1 M DCl in D_2O, 1.5 mM Dioxane): δ (ppm) = 41.72 (NCH_3), 50.11, 55.11 (NCH_2) 110.45 (pyridone), 116.82 (q, ^1J(C,F) = 292 Hz, TFA), 120.27, 125.58, 147.19, 159.15 (pyridone), 163.39 (q, ^1J(C,F) = 36 Hz, TFA).

VIII.II.2.13 L15

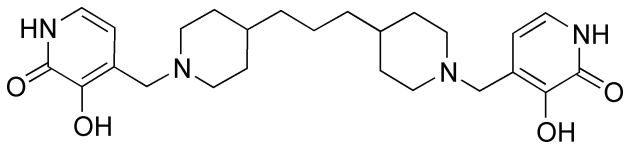

1,3-Di(4-piperidyl)propane (1.17 g, 5.00 mmol, 1.0 equiv.), 3-hydroxy-2-pyridone (1.15 g; 10.0 mmol, 2.0 equiv.) and formaldehyde (0.75 mL, 37 wt% in H_2O, 10.0 mmol, 2.0 equiv.) were heated for 24 h in EtOH (130 mL). A cream colored precipitate formed, which was filtered off and dried in vacuum. The crude product was obtained in about 85 % purity and 80 % yield (1.18 g, 3.55 mmol). The product was purified by reversed phase HPLC (H_2O/CH_3CN + 0.1 % TFA, gradient: 98:2 to 92:8 in 14 min, λ_{max} = 305 nm, sample: 1 mL, 20 mM in 1.0 % TFA, R_f = 22.6 min).

^{1}H NMR (400 MHz, 0.1 M DCl in D_2O): δ (ppm) = 1.20–1.40 (m, 10 H, CH_2), 1.55 (m, br, 2 H, CH), 1.97 (m, 4 H, CH_2), 3.05 (m, 4 H, NCH_2), 3.55 (m, 4 H, NCH_2), 4.23 (s, 4 H, NCH_2), 6.45 (d, ^3J = 7 Hz, 2 H, pyridone), 7.11 (d, ^3J = 7 Hz, 2 H, pyridone).

^{13}C NMR (101 MHz, 0.1 M DCl in D_2O, 1.5 mM Dioxane): δ (ppm) = 23.09, 29.74, 33.24, 35.40 (CH & CH_2), 53.95, 54.71 (NCH_2) 111.02 (pyridone), 116.96 (q, ^1J(C,F) = 293 Hz, TFA), 121.00, 125.10, 147.04, 159.28 (pyridone) 163.56 (q, ^1J(C,F) = 36 Hz, TFA).

VIII.II.3 Monomeric Complexes in Water

Monomeric complexes of composed of half-sandwich complexes [(π-ligand)$MCl_2]_2$ and ligands **L2**, **L3**, **L4** and **L5** are described. Monomeric complexes were characterized by ^{1}H NMR spectroscopy, except for cases in which single crystals suited for X-ray crystallography were obtained. The ^{1}H NMR spectra were calibrated to the internal HDO signal. The methylpiperazine CH_2 signals are often very broad, especially when the monomer was formed in situ; however, the signals could be much more distinct when crystals were solubilized in deuterated water.

General procedure for the formation of monomeric complexes in water: A mixture of halfsandwich complex [(π-ligand)$MCl_2]_2$ (37.5 µmol) and ligand (75.0 µmol) were stirred in water (5.00 mL) until a clear solution (15 mM) was obtained.

General procedure for the formation of monomeric complexes in $CHCl_3$: A mixture of halfsandwich complex [(π-ligand)$MCl_2]_2$ (37.5 µmol) and ligand (75.0 µmol) were stirred in $CHCl_3$ (5.00 mL) until a clear solution (15 mM) was obtained. The solvent was removed under reduced pressure and the product obtained in quanitative yield.

General procedure for the synthesis of monomeric complexes by crystallisation: A mixture of [(π-ligand)$MCl_2]_2$ (75.0 µmol) and ligand **L2**, **L3** or **L4** (150 µmol) was stirred

in chloroform or dichloromethane (20 mL) until a clear solution was obtained (about 15 minutes). The solution was divided into five test tubes and crystals were obtained by layering carefully Et_2O or pentane over the monomer solution. It was not possible to obtain any crystals for complexes containing ligand **L5**.

VIII.II.3.1 [(C$_6$H$_6$)Ru(L2)Cl]Cl

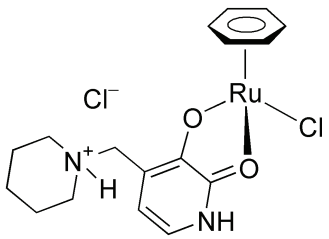

^{1}H NMR (400 MHz, D_2O): δ (ppm) = 1.40–2.05 (m, 6 H, CH_2, piperidine), 3.00 (m_c, 2 H, CH_2, piperidine), 3.48 (m_c, 2 H, CH_2, piperidine), 4.22 (s, 2 H, NCH_2), 5.59 (s, 6 H, C_6H_6), 6.53 (d, ^3J = 7 Hz, 1 H, pyridone), 6.91 (d, ^3J = 7 Hz, 1 H, pyridone).

VIII.II.3.2 [(C$_6$H$_6$)Ru(L5)Cl]Cl

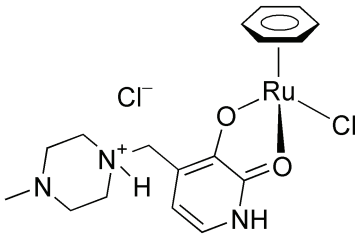

^{1}H NMR (400 MHz, D_2O): δ (ppm) = 2.60 (m, br, 2 H, CH_2, piperazine), 2.85 (s, 3 H, NCH_3), 3.09 (m, br, 4 H, CH_2, piperazine), 3.46 (m, br, 2 H, CH_2, piperazine), 3.68 (s, 2 H, NCH_2), 5.87 (s, 6 H, C_6H_6), 6.55 (d, ^3J = 7 Hz, 1 H, pyridone), 6.91 (d, ^3J = 6 Hz, 1 H, pyridone).

VIII.II.3.3 [(C$_6$H$_5$Me)Ru(L2)Cl]Cl

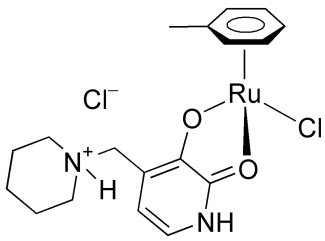

^{1}H NMR (400 MHz, D_2O): δ (ppm) = 1.35–2.05 (m, 6 H, CH_2, piperidine), 2.26 (s, 3 H, $CH_3C_6H_5$), 3.03 (m_c, 2 H, CH_2, piperidine), 3.51 (m_c, 2 H, CH_2, piperidine), 4.23 (s, 2 H, NCH_2), 5.59 (d, ^3J = 6 Hz, 2 H, C_6H_5Me), 5.74 (t, ^3J = 6 Hz, 1 H, C_6H_5Me), 5.95 (t, ^3J = 6 Hz, 2 H, C_6H_5Me), 6.53 (d, ^3J = 7 Hz, 1 H, pyridone), 6.92 (d, ^3J = 6 Hz, 1 H, pyridone).

VIII.II.3.4 [(C$_6$H$_5$Me)Ru(L5)Cl]Cl

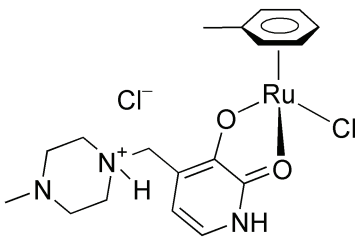

^{1}H NMR (400 MHz, D_2O): δ (ppm) = 2.22 (s, 3 H, $CH_3C_6H_5$), 2.45–3.65 (m, 8 H, CH_2, piperazine), 2.85 (s, 3 H, NCH_3), 3.71 (s, 2 H, NCH_2), 5.54 (d, ^3J = 6 Hz, 2 H, C_6H_5Me), 5.69 (t, ^3J = 6 Hz, 1 H, C_6H_5Me), 5.91 (t, ^3J = 6 Hz, 2 H, C_6H_5Me), 6.54 (d, ^3J = 7 Hz, 1 H, pyridone), 6.89 (d, ^3J = 7 Hz, 1 H, pyridone).

VIII.II.3.5 [(cymene)Ru(L2)Cl]Cl

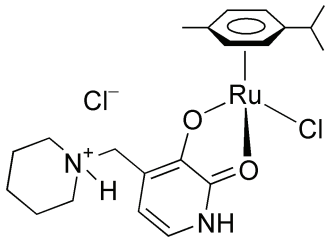

Crystals[y] were obtained by slow diffusion of Et_2O into a mixture of **3** and **L2** (ratio 1:2) in $CHCl_3$.

^1H NMR (400 MHz, D_2O): δ (ppm) =1.28 (d, ^3J = 7 Hz, 6 H, $CH(CH_3)_2$), 1.35–2.05 (m, 6 H, CH_2, piperidine), 2.23 (s, 2 H, $CH_3C_6H_4{}^iPr$), 2.82 (sept, ^3J = 7 Hz, 1 H, $CH(CH_3)_2$), 2.00 (m_c, 2 H, CH_2, piperidine), 3.48 (m_c, 2 H, CH_2, piperidine), 4.21 (s, 2 H, NCH_2), 5.56 (d, ^3J = 6 Hz, 2 H, $MeC_6H_4{}^iPr$), 5.81 (d, ^3J = 6 Hz, 2 H, $MeC_6H_4{}^iPr$), 6.50 (d, ^3J = 7 Hz, 1 H, pyridone), 6.88 (d, ^3J = 7 Hz, 1 H, pyridone).

Elemental analysis (%) calcd (found) for $C_{21}H_{30}Cl_2N_2O_2Ru \times 2\,CHCl_3$: C 36.68 (37.64), H 4.28 (5.03), N 3.72 (3.94).

VIII.II.3.6 [(cymene)Ru(L3)Cl]Cl

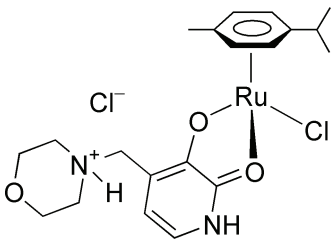

Crystals[y] were obtained by slow diffusion of n-pentane into a mixture of **3** and **L3** (ratio 1:2) in $CHCl_3$.

^1H NMR (400 MHz, D_2O): δ (ppm) = 1.30 (d, ^3J = 7 Hz, 6 H, $CH(CH_3)_2$), 2.25 (s, 2 H, $CH_3C_6H_4{}^iPr$), 2.84 (sept, ^3J = 7 Hz, 1 H, $CH(CH_3)_2$), 3.29 (m, br, 2 H, CH_2, morpholine), 3.47 (m, br, 2 H, CH_2, morpholine), 3.80 (m, br, 2 H, CH_2, morpholine), 4.12 (m, br, 2 H, CH_2, morpholine), 4.33 (s, 2 H, NCH_2), 5.59 (d, ^3J = 6 Hz, 2 H, $MeC_6H_4{}^iPr$), 5.83 (d, ^3J = 6 Hz, 2 H, $MeC_6H_4{}^iPr$), 6.53 (d, ^3J = 7 Hz, 1 H, pyridone), 6.90 (d, ^3J = 6 Hz, 1 H, pyridone).

Elemental analysis (%) calcd (found) for $C_{20}H_{28}Cl_2N_2O_3Ru \times 1/6\,CHCl_3$: C 45.16 (45.34), H 5.29 (5.24), N 5.22 (5.15).

VIII.II.3.7 [(cymene)Ru(L4)Cl]Cl

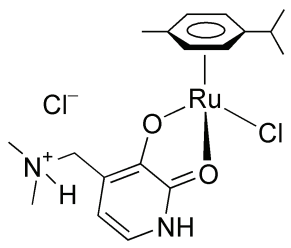

Crystals[y] were obtained by slow diffusion of Et_2O into a mixture of **3** and **L4** (ratio 1:2) in $CHCl_3$.

^1H NMR (400 MHz, D_2O): δ (ppm) = 1.26 (d, ^3J = 7 Hz, 6 H, $CH(CH_3)_2$), 2.22 (s, 2 H, $CH_3C_6H_4{}^iPr$), 2.83 (sept, ^3J = 7 Hz, 1 H, $CH(CH_3)_2$), 2.89 (s, 6 H, NCH_3), 4.25 (s, 2 H, NCH_2), 5.56 (d, ^3J = 5 Hz, 2 H, $MeC_6H_4{}^iPr$), 5.81 (d, ^3J = 6 Hz, 2 H,

y. Although crystals were obtained, these were not suited for single crystal X-ray analysis.

$MeC_6H_4{}^iPr$), 6.50 (d, ^3J = 6 Hz, 1 H, pyridone), 6.88 (d, ^3J = 6 Hz, 1 H, pyridone).

Elemental analysis (%) calcd (found) for $C_{18}H_{26}Cl_2N_2O_2Ru \times 0.5\ CHCl_3$: C 41.60 (41.76), H 5.00 (5.28), N 5.25 (4.57).

VIII.II.3.8 [(cymene)Ru(L5)Cl]Cl

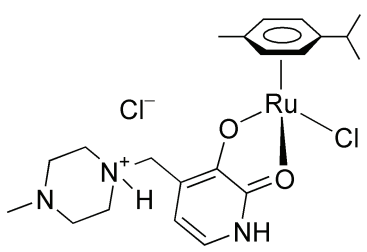

^{1}H NMR (400 MHz, D_2O): δ (ppm) = 1.25 (d, ^3J = 7 Hz, 6 H, $CH(CH_3)_2$), 2.23 (s, 2 H, $CH_3C_6H_4{}^iPr$), 2.65 (m, br, 2 H, CH_2, piperazine), 2.80 (sept, ^3J = 7 Hz, 1 H, $CH(CH_3)_2$), 2.84 (s, 3 H, NCH_3), 3.10 (m, br, 4 H, CH_2, piperazine), 3.45 (m, br, 2 H, CH_2, piperazine), 3.70 (s, 2 H, NCH_2), 5.56 (d, ^3J = 6 Hz, 2 H, $MeC_6H_4{}^iPr$), 5.79 (d, ^3J = 6 Hz, 2 H, $MeC_6H_4{}^iPr$), 6.53 (d, ^3J = 7 Hz, 1 H, pyridone), 6.88 (d, ^3J = 7 Hz, 1 H, pyridone).

VIII.II.3.9 [($C_6H_5CO_2Et$)Ru(L2)Cl]Cl

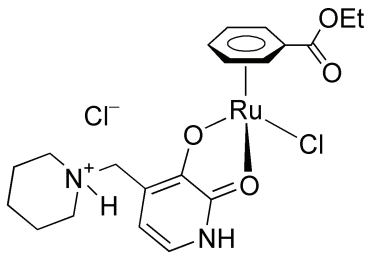

The complex trimerised already in significant amounts in absence of any base. The ^{1}H NMR data indicated, also the presence of free ligand and a π-ligand-aqua species in addition to the monomeric and trimeric complexes. The peaks were broad, but became well defined with increased trimerisation.

^{1}H NMR (400 MHz, D_2O): δ (ppm) = 1.25 (t, ^3J = 7 Hz, 3 H, $CO_2CH_2CH_3$), 1.30–2.05 (m, 6 H, CH_2, piperidine), 2.99 (m_c, 2 H, CH_2, piperidine), 3.46 (m, br, 2 H, CH_2, piperidine), 4.23 (s, 2 H, NCH_2), 4.39 (q, ^3J = 7 Hz, 2 H, $CO_2CH_2CH_3$), 5.99 (m, br, 2 H, $C_6H_5CO_2Et$), 6.37 (m, br, 1 H, $C_6H_5CO_2Et$), 6.54 (m, br, 1 H, pyridone), 6.70 (d, ^3J = 5 Hz, 2 H, $C_6H_5CO_2Et$), 6.92 (m, br, 1 H, pyridone).

VIII.II.3.10 [($C_6H_5CO_2Et$)Ru(L5)Cl]Cl

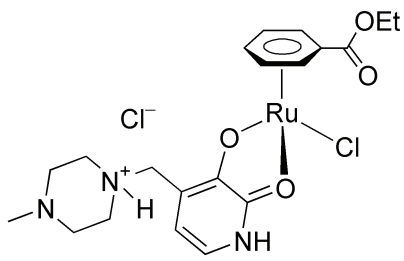

^{1}H NMR (400 MHz, D_2O): δ (ppm) = 1.21 (t, ^3J = 7 Hz, 3 H, $CO_2CH_2CH_3$), 2.45–3.65 (m, br, 8 H, CH_2, piperazine), 2.88 (s, 3 H, NCH_3), 3.75 (s, 2 H, NCH_2), 4.36 (q, ^3J = 7 Hz, 2 H, $CO_2CH_2CH_3$), 5.98 (m, br, 2 H, $C_6H_5CO_2Et$), 6.25 (m, br, 1 H, $C_6H_5CO_2Et$), 6.55 (d, ^3J = 6 Hz, 1 H, pyridone), 6.68 (d, ^3J = 6 Hz, 2 H, $C_6H_5CO_2Et$), 6.91 (d, ^3J = 6 Hz, 1 H, pyridone).

VIII.II.3.11 [($C_6H_3{}^iPr_3$)Ru(L2)Cl]Cl

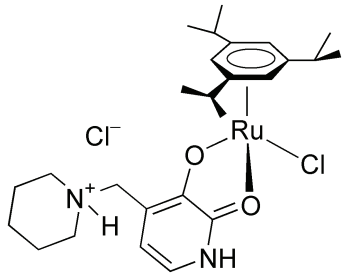

The monomeric complex was difficult to obtain by direct mixing of **5** and **L2** in water. However, crystals[y] were obtained by slow diffusion of Et_2O into a mixture of **5** and **L2** (ratio 1:2) in $CHCl_3$. The crystals were soluble in water and chloroform. Alternatively, extended stirring of a less concentrated mixture (3 mM) also gave the monomeric complex.

^{1}H NMR (400 MHz, D_2O): δ (ppm) = 1.32 (d, ^3J = 7 Hz, 18 H, $CH(CH_3)_2$), 1.45–2.05 (m, br, 6 H, CH_2, piperidine), 2.86 (sept, ^3J = 7 Hz, 1 H, $CH(CH_3)_2$), 3.00 (m, br, 2 H, CH_2, piperidine), 3.46 (m, br, 2 H, CH_2, piperidine), 4.21 (s, 2 H, NCH_2), 5.61 (s, 3 H, $C_6H_3{}^iPr_3$), 6.49 (d, ^3J = 6 Hz, 1 H, pyridone), 6.86 (d, ^3J = 7 Hz, 1 H, pyridone).

VIII.II.3.12 [($C_6H_3{}^iPr_3$)Ru(L5)Cl]Cl

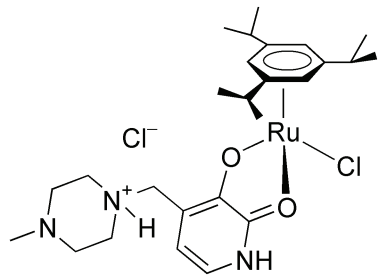

Extended stirring of a less concentrated mixture (3 mM) gave access to the monomeric complex.

^{1}H NMR (400 MHz, D_2O): δ (ppm) = 1.31 (d, ^3J = 7 Hz, 18 H, $CH(CH_3)_2$), 2.83 (s, 3 H, NCH_3), 2.65 (m, br, 2 H, CH_2, piperazine), 2.87 (sept, ^3J = 7 Hz, 1 H, $CH(CH_3)_2$), 3.10 (m, br, br, 4 H, CH_2, piperazine), 3.45 (m, br, 2 H, CH_2, piperazine), 3.70 (s, 2 H, NCH_2), 5.56 (s, 3 H, $C_6H_3{}^iPr_3$), 6.51 (d, ^3J = 7 Hz, 1 H, pyridone), 6.84 (d, ^3J = 6 Hz, 1 H, pyridone).

VIII.II.3.13 [(C_6Me_6)Ru(L2)Cl]Cl

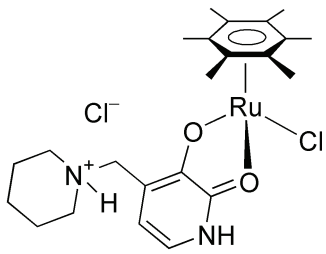

Crystals suited for singe crystal X-ray analysis were obtained by slow diffusion of Et_2O into a mixture of **6** and **L2** (ratio 1:2) in dichloromethane.

^{1}H NMR (400 MHz, D_2O): δ (ppm) = 1.30–2.30 (m, br, 6 H, CH_2, piperidine), 2.14 (s, 18 H, C_6Me_6), 3.04 (m, br, 2 H, NCH_2, piperidine), 3.50 (m, br, 2 H, NCH_2, piperidine), 4.21 (s, 2 H, NCH_2), 6.46 (d, ^3J = 7 Hz, 1 H, pyridone), 6.82 (d, ^3J = 7 Hz, 1 H, pyridone).

^{13}C NMR (101 MHz, D_2O): δ (ppm) = 17.86 (CH_3, C_6Me_6), 23.92, 25.80, (CH_2, piperidine), 56.15, 57.42 (NCH_2), 91.79 (C_6Me_6), 117.02, 121.56, 123.48, 161.41, 167.58 (pyridone).

Elemental analysis (%) calcd (found) for $C_{23}H_{34}Cl_2N_2O_2Ru \times 0.5\ CH_2Cl_2$: C 48.25 (48.88), H 6.03 (6.09), N 4.79 (4.42).

VIII.II.3.14 [(C_6Me_6)Ru(L3)Cl]Cl

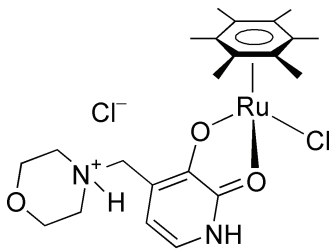

Crystals suited for singe crystal X-ray analysis were obtained by slow diffusion of pentane into a mixture of **6** and **L3** (ratio 1:2) in chloroform.

^{1}H NMR (400 MHz, D_2O): δ (ppm) = 2.13 (s, 18 H, C_6Me_6), 3.34 (m, br, 4 H, NCH_2, morpholine), 3.93 (m, br, 4 H, OCH_2, morpholine), 4.27 (s, 2 H, NCH_2), 6.46 (d, ^3J = 7 Hz, 1 H, pyridone), 6.81 (d, ^3J = 7 Hz, 1 H, pyridone).

^{13}C NMR (101 MHz, D_2O): δ (ppm) = 17.87 (CH_3, C_6Me_6), 54.54, 57.50, 66.77 (NCH_2, OCH_2), 91.81 (C_6Me_6), 116.99, 121.39, 128.55, 161.73, 167.68 (pyridone).

Elemental analysis (%) calcd (found) for $C_{22}H_{32}Cl_2N_2O_6Ru \times 0.5\ CHCl_3$: C 44.73 (44.43), H 5.42 (5.29), N 4.64 (4.44).

VIII.II.3.15 [(C_6Me_6)Ru(L4)Cl]Cl

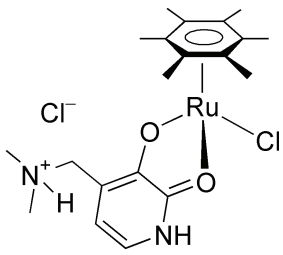

Crystals suited for singe crystal X-ray analysis were obtained by slow diffusion of pentane into a mixture of **6** and **L4** (ratio 1:2) in chloroform.

^{1}H NMR (400 MHz, D_2O): δ (ppm) = 2.14 (s, 18 H, C_6Me_6), 2.90 (s, 6 H, NMe_2), 4.27 (s, 2 H, NCH_2), 6.46 (d, ^3J = 7 Hz, 1 H, pyridone), 6.82 (d, ^3J = 7 Hz, 1 H, pyridone).

^{13}C NMR (101 MHz, D_2O): δ (ppm) = 17.84 (CH_3, C_6Me_6), 45.49, 58.54 (NMe_2, NCH_2), 91.83 (C_6Me_6), 116.44, 121.46, 123.59, 161.45, 167.61 (pyridone).

Elemental analysis (%) calcd (found) for $C_{20}H_{29}Cl_2N_2O_2Ru \times 0.5\ CHCl_3$: C 43.96 (44.43), H 5.13 (5.73), N 5.00 (5.22).

VIII.II.3.16 [(C_6Me_6)Ru(L5)Cl]Cl

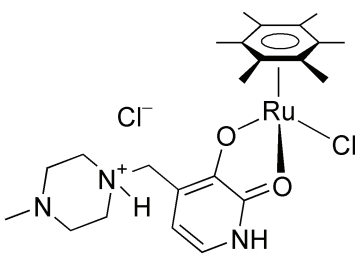

Extended stirring of a less concentrated mixture gave access to the monomeric complex (3 mM). The quality of the obtained spectrum was inferior compared to other spectra of monomeric complexes.

^{1}H NMR (400 MHz, D_2O): δ (ppm) = 2.12 (s, 18 H, C_6Me_6), 2.60 (m, br, 2 H, CH_2, piperazine), 2.86 (s, 3 H,

NCH_3), 3.15 (m, br, 4 H, CH_2, piperazine), 3.47 (m, br, 2 H, CH_2, piperazine), 3.69 (s, 2 H, NCH_2), 6.49 (d, ^3J = 7 Hz, 1 H, pyridone), 6.81 (d, ^3J = 7 Hz, 1 H, pyridone).

VIII.II.3.17 [CpRh(L2)Cl]Cl

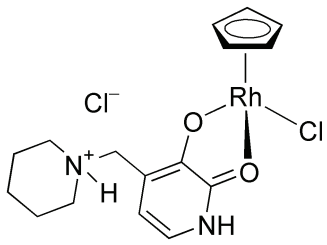

^{1}H NMR (400 MHz, D_2O): δ (ppm) = 1.30–2.05 (m, 6 H, CH_2, piperidine), 2.98 (m_c, 2 H, CH_2, piperidine), 3.47 (m_c, 2 H, CH_2, piperidine), 4.19 (s, 2 H, NCH_2), 5.90 (s, 5 H, Cp), 6.53 (d, ^3J = 6 Hz, 1 H, pyridone), 6.92 (d, ^3J = 7 Hz, 1 H, pyridone).

VIII.II.3.18 [CpRh(L5)Cl]Cl

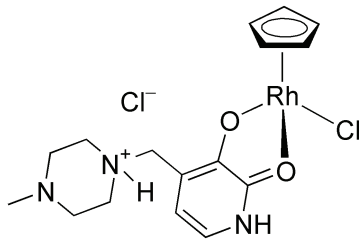

^{1}H NMR (400 MHz, D_2O): δ (ppm) = 2.45–3.65 (m, 8 H, CH_2, piperazine), 2.84 (s, 3 H, NCH_3), 3.70 (s, 2 H, NCH_2), 5.88 (s, 5 H, Cp), 6.57 (d, ^3J = 7 Hz, 1 H, pyridone), 6.92 (d, ^3J = 7 Hz, 1 H, pyridone).

VIII.II.3.19 [(C_5HMe_4)Rh(L2)Cl]Cl

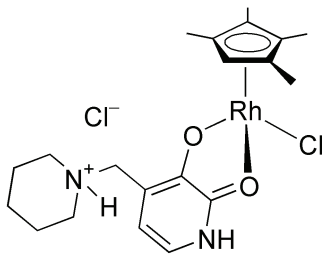

^{1}H NMR (400 MHz, D_2O): δ (ppm) = 1.30–2.05 (m, 6 H, CH_2, piperidine), 1.67 (s, 6 H, $(CH_3)_4C_5H$), 1.74 (s, 6 H, $(CH_3)_4C_5H$), 3.01 (m_c, 2 H, CH_2, piperidine), 3.51 (m_c, 2 H, CH_2, piperidine), 4.20 (s, 2 H, NCH_2), 5.34 (s, 1 H, C_5HMe_4), 6.48 (d, ^3J = 7 Hz, 1 H, pyridone), 6.85 (d, ^3J = 7 Hz, 1 H, pyridone).

VIII.II.3.20 [(C_5HMe_4)Rh(L5)Cl]Cl

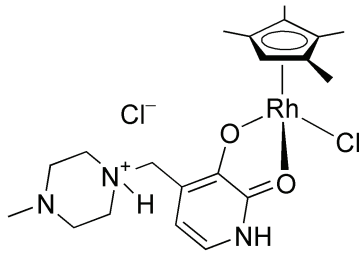

^{1}H NMR (400 MHz, D_2O): δ (ppm) = 1.66 (s, 6 H, $(CH_3)_4C_5H$), 1.72 (s, 6 H, $(CH_3)_4C_5H$), 2.45–3.65 (m, 8 H, CH_2, piperazine), 2.81 (s, 3 H, NCH_3), 3.74 (s, 2 H, NCH_2), 5.31 (s, 1 H, C_5HMe_4), 6.51 (d, ^3J = 7 Hz, 1 H, pyridone), 6.84 (d, ^3J = 6 Hz, 1 H, pyridone).

VIII.II.3.21 [Cp*Rh(L2)Cl]Cl

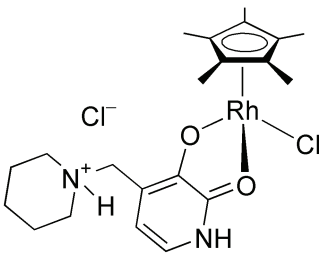

^{1}H NMR (400 MHz, D_2O): δ (ppm) = 1.35–2.05 (m, 6 H, CH_2, piperidine), 1.67 (s, 15 H, Cp*), 3.00 (m_c, 2 H, NCH_2, piperidine), 3.50 (m, br, 2 H, NCH_2, piperidine), 4.18 (s, 2 H, NCH_2), 6.45 (d, ^3J = 7 Hz, 1 H, pyridone), 6.81 (d, ^3J = 7 Hz, 1 H, pyridone).

VIII.II.3.22 [Cp*Rh(L5)Cl]Cl

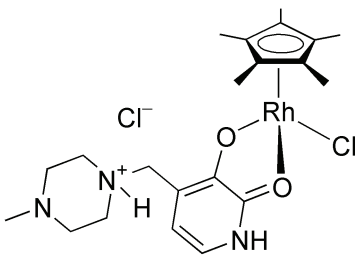

^{1}H NMR (400 MHz, D_2O): δ (ppm) = 1.66 (s, 15 H, Cp*), 2.35–3.60 (m, br, 8 H, CH_2, piperazine), 2.79 (s, 3 H, NCH_3), 3.72 (s, 2 H, NCH_2), 6.49 (d, ^3J = 7 Hz, 1 H, pyridone), 6.82 (d, ^3J = 7 Hz, 1 H, pyridone).

VIII.II.3.23 [(C_5HMe_4)Ir(L2)Cl]Cl

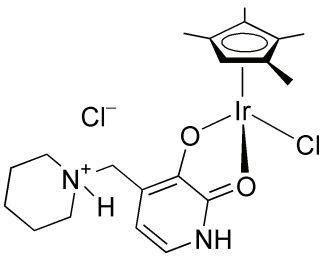

^{1}H NMR (400 MHz, D_2O): δ (ppm) = 1.30–2.05 (m, 6 H, CH_2, piperidine), 1.63 (s, 6 H, (CH_3)$_4C_5H$), 1.72 (s, 6 H, (CH_3)$_4C_5H$), 3.00 (m_c, 2 H, CH_2, piperidine), 3.51 (m_c, 2 H, CH_2, piperidine), 4.21 (s, 2 H, NCH_2), 5.48 (s, 1 H, C_5HMe_4), 6.50 (d, ^3J = 7 Hz, 1 H, pyridone), 6.89 (d, ^3J = 7 Hz, 1 H, pyridone).

VIII.II.3.24 [(C_5HMe_4)Ir(L5)Cl]Cl

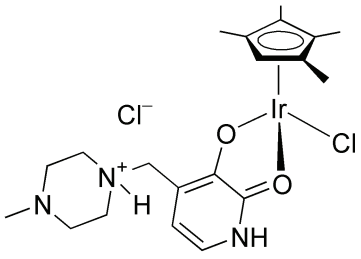

^{1}H NMR (400 MHz, D_2O): δ (ppm) = 1.62 (s, 6 H, (CH_3)$_4C_5H$), 1.72 (s, 6 H, (CH_3)$_4C_5H$), 2.45–3.65 (m, 8 H, CH_2, piperazine), 2.83 (s, 3 H, NCH_3), 3.78 (s, 2 H, NCH_2), 5.46 (s, 1 H, C_5HMe_4), 6.52 (d, ^3J = 7 Hz, 1 H, pyridone), 6.89 (d, ^3J = 7 Hz, 1 H, pyridone).

VIII.II.3.25 [Cp*Ir(L2)Cl]Cl

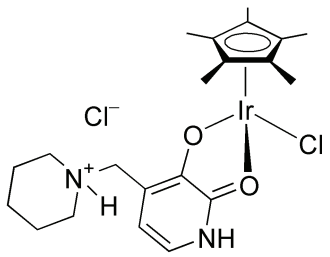

^{1}H NMR (400 MHz, D_2O): δ (ppm) = 1.35–2.05 (m, 6 H, CH_2, piperidine), 1.68 (s, 15 H, Cp*), 3.02 (m_c, 2 H, NCH_2, piperidine), 3.52 (m, br, 2 H, NCH_2, piperidine), 4.23 (s, 2 H, NCH_2), 6.49 (d, ^3J = 7 Hz, 1 H, pyridone), 6.89 (d, ^3J = 6 Hz, 1 H, pyridone).

VIII.II.3.26 [Cp*Ir(L5)Cl]Cl

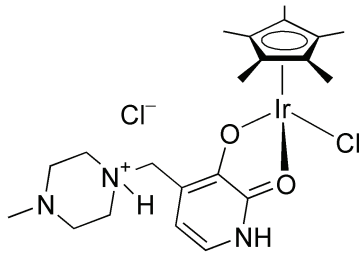

^{1}H NMR (400 MHz, D_2O): δ (ppm) = 1.62 (s, 15 H, Cp*), 2.45–3.65 (m, br, 8 H, CH_2, piperazine), 2.81 (s, 3 H, NCH_3), 3.77 (s, 2 H, NCH_2), 6.50 (d, ^3J = 7 Hz, 1 H, pyridone), 6.86 (d, ^3J = 7 Hz, 1 H, pyridone).

VIII.II.4 Trimeric Complexes and their LiCl Adducts in Water

Trimeric metallamacrocycles composed of halfsandwich complexes [(π-ligand)MCl_2]$_2$ and ligands **L2**, **L3**, **L4** and **L5** and their LiCl adducts are described. All complexes were characterized by ^{1}H NMR spectroscopy. The ^{1}H NMR spectra were calibrated to the internal HDO signal. Trimerisation could be induced by mixing [(π-ligand)MCl_2]$_2$ and ligand in phosphate buffer solution[z] (100 mM, pH 7.0) or by using a CsOH solution in D_2O as base. In both cases, the ^{1}H NMR signals of the π-ligand were identical. The NCH_2 signals which are more sensitive to the pH did vary slightly in some cases and the piperidine, morpholine and methylpiperazine CH_2 signals were broader when using CsOH solution than in phosphate buffer solution.

General procedure for the formation of trimeric complexes in PBS: A mixture of half-sandwich complex [(π-ligand)MCl_2]$_2$ (37.5 µmol) and ligand (75.0 µmol) were stirred in phosphate buffer solution (5.00 mL, 100 mM) until a clear solution of trimer (5.0 mM) was obtained. Trimerisation was found to be pH dependant and did vary for different metal fragments.[z]

General procedure for the formation of trimeric complexes in water: A mixture of half-sandwich complex [(π-ligand)MCl_2]$_2$ (37.5 µmol) and ligand (75.0 µmol) were stirred in

z. For complexes with a basic pK_a, a higher pH is necessary for trimerisation, e.g. for the mixture of [Cp*$RhCl_2$]$_2$ and **L2** no trimerisation was observed at pH 7.0.

water (4.50 mL) until a clear solution of the monomer (16.7 mM) was obtained. A CsOH solution in water (0.15 M) was added to the monomer solution. If not specified otherwise, 1.0 equiv. of CsOH (based on the mmol of ligand, 0.5 mL, 75 µmol) was used to form the trimeric complex in quantitative yield. Due to their low solubility, the trimeric macrocycles with **5** and **6** as metal fragments were not investigated.

VIII.II.4.1 $[(C_6H_6)Ru(L2–H^+)]_3^{3+}$

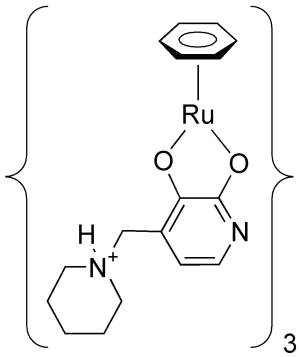

$[(C_6H_6)Ru(L2–H^+)]_3^{3+}$: ^{1}H NMR (400 MHz, D_2O): δ (ppm) = 1.45–1.85 (m, br, 18 H, CH_2, piperidine), 2.88 (m, br, 12 H, NCH_2, piperidine), 3.79 (d, ^2J = 13 Hz, 3 H, NCH_2), 4.01 (d, ^2J = 13 Hz, 3 H, NCH_2), 5.78 (s, 18 H, C_6H_6), 5.82 (d, ^3J = 7 Hz, 3 H, pyridone), 6.77 (d, ^3J = 7 Hz, 3 H, pyridone).

$[(C_6H_6)Ru(L2–H^+)]_3^{3+}$ × LiCl: ^{1}H NMR (400 MHz, D_2O): δ (ppm) = 1.45–1.85 (m, br, 18 H, CH_2, piperidine), 2.83 (m, br, 12 H, NCH_2, piperidine), 3.91 (d, ^2J = 13 Hz, 3 H, NCH_2), 4.03 (d, ^2J = 13 Hz, 3 H, NCH_2), 5.90 (s, 18 H, C_6H_6), 6.08 (d, ^3J = 6 Hz, 3 H, pyridone), 6.92 (d, ^3J = 6 Hz, 3 H, pyridone).

^{7}Li NMR (156 MHz, D_2O): δ (ppm) = − 0.35.

VIII.II.4.2 $[(C_6H_6)Ru(L5–H^+)]_3^{3+}$

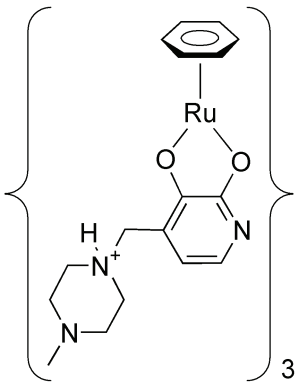

$[(C_6H_6)Ru(L5–H^+)]_3^{3+}$: ^{1}H NMR (400 MHz, D_2O): δ (ppm) = 2.45–3.45 (m, br, 24 H, CH_2, piperazine), 2.60 (s, 9 H, NCH_3), 3.33 (d, ^2J = 13 Hz, 3 H, NCH_2), 3.60 (d, ^2J = 13 Hz, 3 H, NCH_2), 5.73 (s, 18 H, C_6H_6), 5.78 (d, ^3J = 6 Hz, 3 H, pyridone), 6.69 (d, ^3J = 6 Hz, 3 H, pyridone).

$[(C_6H_6)Ru(L5–H^+)]_3^{3+}$ × LiCl: ^{1}H NMR (400 MHz, D_2O): δ (ppm) = 2.50 (m, br, 6 H, CH_2, piperazine), 2.64 (s, 9 H, NCH_3), 2.80–3.30 (m, br, 18 H, CH_2, piperazine), 3.37 (d, ^2J = 13 Hz, 3 H, NCH_2), 3.60 (d, ^2J = 14 Hz, 3 H, NCH_2), 5.85 (s, 18 H, C_6H_6), 6.03 (d, ^3J = 6 Hz, 3 H, pyridone), 6.69 (d, ^3J = 6 Hz, 3 H, pyridone).

^{7}Li NMR (156 MHz, D_2O): δ (ppm) = − 0.36.

VIII.II.4.3 $[(C_6H_5Me)Ru(L2–H^+)]_3^{3+}$

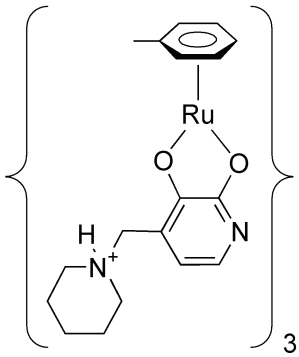

$[(C_6H_5Me)Ru(L2–H^+)]_3^{3+}$: ^{1}H NMR (400 MHz, D_2O): δ (ppm) = 1.35–1.95 (m, br, 18 H, CH_2, piperidine), 2.00 (s, 9 H, $CH_3C_6H_5$), 2.60–3.60 (m, br, 12 H, NCH_2, piperidine), 3.83 (d, ^2J = 13 Hz, 3 H, NCH_2), 4.03 (d, ^2J = 13 Hz, 3 H, NCH_2), 5.24 (d, ^3J = 6 Hz, 3 H, C_6H_5Me), 5.49 (t, ^3J = 6 Hz, 3 H, C_6H_5Me), 5.56 (d, ^3J = 6 Hz, 3 H, C_6H_5Me), 5.83 (m, 6 H,C_6H_5Me and pyridone), 6.08 (t, ^3J = 6 Hz, 3 H, C_6H_5Me), 6.75 (d, ^3J = 6 Hz, 3 H, pyridone).

$[(C_6H_5Me)Ru(L2–H^+)]_3^{3+}$ × LiCl: ^{1}H NMR (400 MHz, D_2O): δ (ppm) = 1.35–1.95 (m, br, 18 H, CH_2, piperidine), 1.88 (s, 9 H, $CH_3C_6H_5$), 2.60–3.60 (m, br, 12 H, NCH_2, piperidine), 3.97 (d, ^2J = 13 Hz, 3 H, NCH_2), 4.10 (d, ^2J = 13 Hz, 3 H, NCH_2), 5.26 (d, ^3J = 6 Hz, 3 H, C_6H_5Me), 5.68 (m, 6 H, C_6H_5Me), 6.11 (m, 6 H, C_6H_5Me and pyridone), 6.23 (t, ^3J = 6 Hz, 3 H, C_6H_5Me), 6.92 (d, ^3J = 6 Hz, 3 H, pyridone).

^{7}Li NMR (156 MHz, D_2O): δ (ppm) = − 0.37.

VIII.II.4.4 $[(C_6H_5Me)Ru(L5–H^+)]_3^{3+}$

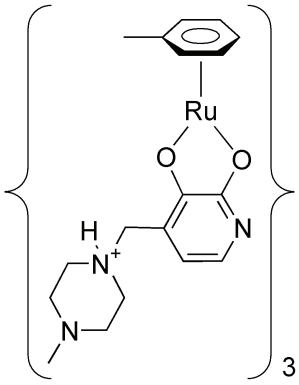

$[(C_6H_5Me)Ru(L5–H^+)]_3^{3+}$: ^{1}H NMR (400 MHz, D_2O): δ (ppm) = 1.93 (s, 9 H, $CH_3C_6H_5$), 2.50–3.35 (m, 24 H, CH_2, piperazine), 2.64 (s, 9 H, NCH_3), 3.39 (d, ^2J = 13 Hz, 3 H, NCH_2), 3.65 (d, ^2J = 10 Hz, 3 H, NCH_2), 5.15 (d, ^3J = 6 Hz, 3 H, C_6H_5Me), 5.44 (t, ^3J = 6 Hz, 3 H, C_6H_5Me), 5.54 (d, ^3J = 6 Hz, 3 H, C_6H_5Me), 5.81 (m, 6 H, C_6H_5Me and pyridone), 6.12 (t, ^3J = 6 Hz, 3 H, C_6H_5Me), 6.68 (d, ^3J = 7 Hz, 3 H, pyridone).

$[(C_6H_5Me)Ru(L5–H^+)]_3^{3+}$ × LiCl: ^{1}H NMR (400 MHz, D_2O): δ (ppm) =1.78 (s, 9 H, $CH_3C_6H_5$), 2.35–3.55 (m, 24 H, CH_2, piperazine), 2.72 (s, 9 H, NCH_3), 3.42 (d, ^2J = 13 Hz, 3 H, NCH_2), 3.65 (d, ^2J = 13 Hz, 3 H, NCH_2), 5.15 (d, ^3J = 6 Hz, 3 H, C_6H_5Me), 5.61 (t, ^3J = 6 Hz, 3 H, C_6H_5Me), 5.66 (d, ^3J = 6 Hz, 3 H, C_6H_5Me), 6.06 (m, 6 H, C_6H_5Me and pyridone), 6.29 (t, ^3J = 6 Hz, 3 H, C_6H_5Me), 6.82 (d, ^3J = 6 Hz, 3 H, pyridone).

^{7}Li NMR (156 MHz, D_2O): δ (ppm) = − 0.37.

VIII.II.4.5 [(cymene)Ru(L2–H$^+$)]$_3^{3+}$

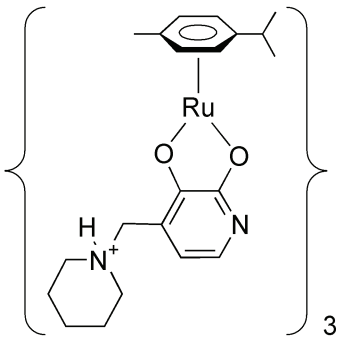

[(cymene)Ru(L2–H$^+$)]$_3^{3+}$: ^{1}H NMR (400 MHz, D_2O): δ (ppm) = 1.26 (d, ^3J = 7 Hz, 9 H, CH(CH_3)$_2$), 1.28 (d, ^3J = 7 Hz, 9 H, CH(CH_3)$_2$), 1.40–2.05 (m, br, 18 H, CH_2, piperidine), 1.84 (s, 9 H, CH_3C$_6$H$_4$^{i}Pr), 2.81 (sept, ^3J = 7 Hz, 3 H, CH(CH$_3$)$_2$), 2.98 (m, br, 12 H, NCH_2, piperidine), 3.77 (d, ^2J = 13 Hz, 3 H, NCH_2), 4.07 (d, ^2J = 13 Hz, 3 H, NCH_2), 5.27 (d, ^3J = 6 Hz, 3 H, MeC$_6$H$_4$^{i}Pr), 5.52 (d, ^3J = 6 Hz, 3 H, MeC$_6$H$_4$^{i}Pr), 5.80 (d, ^3J = 5 Hz, 3 H, MeC$_6$H$_4$^{i}Pr), 5.81 (d, ^3J = 6 Hz, 3 H, pyridone), 6.04 (d, ^3J = 6 Hz, 3 H, MeC$_6$H$_4$^{i}Pr), 6.69 (d, ^3J = 6 Hz, 3 H, pyridone).

[(cymene)Ru(L2–H$^+$)]$_3^{3+}$ × LiCl: ^{1}H NMR (400 MHz, D_2O): δ (ppm) = 1.24 (d, ^3J = 7 Hz, 9 H, CH(CH_3)$_2$), 1.27 (d, ^3J = ^3J = 7 Hz, 9 H, CH(CH_3)$_2$), 1.35–2.10 (m, br, 18 H, CH_2, piperidine), 1.78 (s, 9 H, CH_3C$_6$H$_4$^{i}Pr), 2.79 (sept, ^3J = 7 Hz, 3 H, CH(CH$_3$)$_2$), 2.99 (m, br, 12 H, NCH_2, piperidine), 3.90 (d, ^2J = 13 Hz, 3 H, NCH_2), 4.12 (d, ^2J = 13 Hz, 3 H, NCH_2), 5.29 (d, ^3J = 5 Hz, 3 H, MeC$_6$H$_4$^{i}Pr), 5.73 (d, ^3J = 6 Hz, 3 H, MeC$_6$H$_4$^{i}Pr), 6.03 (d, ^3J = 6 Hz, 3 H, MeC$_6$H$_4$^{i}Pr), 6.09 (d, ^3J = 6 Hz, 3 H, pyridone), 6.19 (d, ^3J = 5 Hz, 3 H, MeC$_6$H$_4$^{i}Pr), 6.86 (d, ^3J = 6 Hz, 3 H, pyridone).

^{7}Li NMR (156 MHz, D_2O): δ (ppm) = – 0.40.

VIII.II.4.6 [(cymene)Ru(L3–H$^+$)]$_3^{3+}$

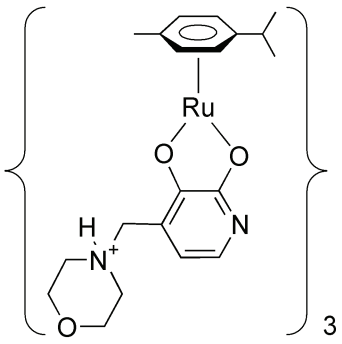

[(cymene)Ru(L3–H$^+$)]$_3^{3+}$ (1.0 equiv. CsOH): ^{1}H NMR (400 MHz, D_2O): δ (ppm) = 1.26 (d, ^3J = 7 Hz, 9 H, CH(CH_3)$_2$), 1.29 (d, ^3J = 7 Hz, 9 H, CH(CH_3)$_2$), 1.83 (s, 9 H, CH_3C$_6$H$_4$^{i}Pr), 2.81 (sept, ^3J = 7 Hz, 3 H, CH(CH$_3$)$_2$), 3.03 (m, br, 12 H, NCH_2, morpholine), 3.76 (d, ^2J = 13 Hz, 3 H, NCH_2), 3.85 (m, br, 12 H, OCH_2, morpholine), 4.11 (d, ^2J = 13 Hz, 3 H, NCH_2), 5.27 (d, ^3J = 6 Hz, 3 H, MeC$_6$H$_4$^{i}Pr), 5.51 (d, ^3J = 6 Hz, 3 H, MeC$_6$H$_4$^{i}Pr), 5.80 (d, ^3J = 7 Hz, 3 H, pyridone), 5.82 (d, ^3J = 7 Hz, 3 H, MeC$_6$H$_4$^{i}Pr), 6.05 (d, ^3J = 6 Hz, 3 H, MeC$_6$H$_4$^{i}Pr), 6.70 (d, ^3J = 6 Hz, 3 H, pyridone).

[(cymene)Ru(L3–H$^+$)]$_3^{3+}$ × LiCl: ^{1}H NMR (400 MHz, D_2O): δ (ppm) = 1.24 (d, ^3J = 7 Hz, 9 H, CH(CH_3)$_2$), 1.27 (d, ^3J = 7 Hz, 9 H, CH(CH_3)$_2$), 1.77 (s, 9 H, CH_3C$_6$H$_4$^{i}Pr), 2.79 (sept, ^3J = 7 Hz, 3 H, CH(CH$_3$)$_2$), 3.03 (m, br, 12 H, NCH_2, morpholine), 3.85 (m, br, 15 H, OCH_2, morpholine and NCH_2), 4.13 (d, ^2J = 15 Hz, 3 H, NCH_2), 5.28 (d, ^3J = 7 Hz, 3 H, MeC$_6$H$_4$^{i}Pr), 5.72 (d, ^3J = 6 Hz, 3 H, MeC$_6$H$_4$^{i}Pr), 6.04

(d, ^3J = 6 Hz, 3 H, $MeC_6H_4{}^iPr$), 6.09 (d, ^3J = 6 Hz, 3 H, pyridone), 6.19 (d, ^3J = 5 Hz, 3 H, $MeC_6H_4{}^iPr$), 6.86 (d, ^3J = 6 Hz, 3 H, pyridone).

^{7}Li NMR (156 MHz, D_2O): δ (ppm) = − 0.40.

VIII.II.4.7 [(cymene)Ru(L4–H$^+$)]$_3^{3+}$

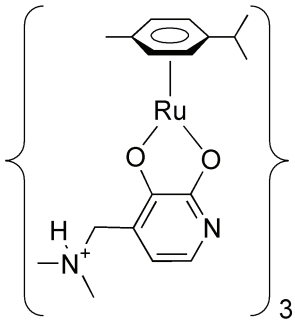

[(cymene)Ru(L4–H$^+$)]$_3^{3+}$: ^{1}H NMR (400 MHz, D_2O): δ (ppm) = 1.26 (d, ^3J = 7 Hz, 9 H, $CH(CH_3)_2$), 1.28 (d, ^3J = 8 Hz, 9 H, $CH(CH_3)_2$), 1.82 (s, 9 H, $CH_3C_6H_4{}^iPr$), 2.69 (s, 18 H, NMe_2), 2.82 (sept, ^3J = 7 Hz, 3 H, $CH(CH_3)_2$), 3.86 (d, ^2J = 13 Hz, 3 H, NCH_2), 4.18 (d, ^2J = 13 Hz, 3 H, NCH_2), 5.26 (d, ^3J = 6 Hz, 3 H, $MeC_6H_4{}^iPr$), 5.51 (d, ^3J = 6 Hz, 3 H, $MeC_6H_4{}^iPr$), 5.79 (d, ^3J = 7 Hz, 3 H, pyridone), 5.81 (d, ^3J = 6 Hz, 3 H, $MeC_6H_4{}^iPr$), 6.05 (d, ^3J = 6 Hz, 3 H, $MeC_6H_4{}^iPr$), 6.72 (d, ^3J = 6 Hz, 3 H, pyridone).

[(cymene)Ru(L4–H$^+$)]$_3^{3+}$ × LiCl: ^{1}H NMR (400 MHz, D_2O): δ (ppm) = 1.23 (d, ^3J = 7 Hz, 9 H, $CH(CH_3)_2$), 1.27 (d, ^3J = 7 Hz, 9 H, $CH(CH_3)_2$), 1.78 (s, 9 H, $CH_3C_6H_4{}^iPr$), 2.70 (s, 18 H, NMe_2), 2.79 (sept, ^3J = 7 Hz, 3 H, $CH(CH_3)_2$), 3.97 (d, ^2J = 13 Hz, 3 H, NCH_2), 4.14 (d, ^2J = 13 Hz, 3 H, NCH_2), 5.29 (d, ^3J = 5 Hz, 3 H, $MeC_6H_4{}^iPr$), 5.72 (d, ^3J = 6 Hz, 3 H, $MeC_6H_4{}^iPr$), 6.05 (d, ^3J = 6 Hz, 6 H, $MeC_6H_4{}^iPr$ and pyridone), 6.17 (d, ^3J = 5 Hz, 3 H, $MeC_6H_4{}^iPr$), 6.89 (d, ^3J = 6 Hz, 3 H, pyridone).

^{7}Li NMR (156 MHz, D_2O): δ (ppm) = − 0.40.

VIII.II.4.8 [(cymene)Ru(L5–2 H$^+$)]$_3$

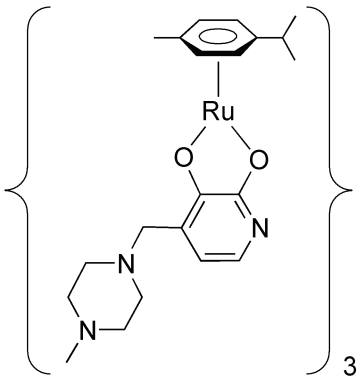

The complex **[(cymene)Ru(L5–2 H$^+$)]$_3$** is special in so far, as it was soluble even if completely deprotonated. Starting from a monomer solution, the trimerisation was complete after addition of 1.25 equiv. of CsOH. The binding constant towards Li^+ increases with further deprotonation. This behaviour is in agreement with the fact that three positive charges (the protonated amine groups) close to the binding site decreases the affinity towards cations. Whereas the pyridone and all cymene (CH_3, ^iPr, as well as the aromatic $MeC_6H_4{}^iPr$) peaks undergo no further shift when increasing the amount of CsOH, the NCH_2 and NCH_3 peaks of the ligand are more susceptible to the pH. For both peaks, an high field shift (towards lower ppm) is observed. In general, the complex obtained from

the self-assembly of **3** and **L5** in MeOH in the presence of Cs_2CO_3 was used for any kind of experiment. Its ^{1}H NMR spectrum is *identical* to the spectrum obtained after addition of 2.0 equiv. of CsOH. The ^{1}H NMR spectrum given beneath is the spectrum obtained by dissolving the synthesised complex in water. The same complex was used for the binding study.

[(Cymene)Ru(L5–2 H$^+$)]$_3$: ^{1}H NMR (400 MHz, D_2O): δ (ppm) = 1.22 (d, ^3J = 7 Hz, 9 H, CH(CH_3)$_2$), 1.28 (d, ^3J = 7 Hz, 9 H, CH(CH_3)$_2$), 1.77 (s, 9 H, CH_3C$_6$H$_4$^{i}Pr), 1.85–2.95 (m, br, 24 H, CH_2, piperazine), 2.18 (s, 9 H, NCH_3), 2.76 (sept, ^3J = 7 Hz, 3 H, CH(CH$_3$)$_2$), 3.20 (d, ^2J = 13 Hz, 3 H, NCH_2), 3.37 (d, ^2J = 13 Hz, 3 H, NCH_2), 5.22 (d, ^3J = 6 Hz, 3 H, MeC$_6$H$_4$^{i}Pr), 5.41 (d, ^3J = 6 Hz, 3 H, MeC$_6$H$_4$^{i}Pr), 5.71 (d, ^3J = 6 Hz, 3 H, MeC$_6$H$_4$^{i}Pr), 5.74 (d, ^3J = 7 Hz, 3 H, pyridone), 5.98 (d, ^3J = 6 Hz, 3 H, MeC$_6$H$_4$^{i}Pr), 6.62 (d, ^3J = 7 Hz, 3 H, pyridone).

[(Cymene)Ru(L5–2 H$^+$)]$_3$ × LiCl: ^{1}H NMR (400 MHz, D_2O): δ (ppm) = 1.23 (d, ^3J = 7 Hz, 9 H, CH(CH_3)$_2$), 1.25 (d, ^3J = 7 Hz, 9 H, CH(CH_3)$_2$), 1.73 (s, 9 H, CH_3C$_6$H$_4$^{i}Pr), 1.80–2.95 (m, br, 24 H, CH_2, piperazine), 2.21 (s, 9 H, NCH_3), 2.75 (sept, ^3J = 7 Hz, 3 H, CH(CH$_3$)$_2$), 3.29 (d, ^2J = 13 Hz, 3 H, NCH_2), 3.45 (d, ^2J = 13 Hz, 3 H, NCH_2), 5.23 (m, br, 3 H, MeC$_6$H$_4$^{i}Pr), 5.66 (d, ^3J = 6 Hz, 3 H, MeC$_6$H$_4$^{i}Pr), 5.97 (d, ^3J = 6 Hz, 3 H, MeC$_6$H$_4$^{i}Pr), 6.00 (d, ^3J = 6 Hz, 3 H, pyridone), 6.13 (m, br, 3 H, MeC$_6$H$_4$^{i}Pr), 6.77 (d, ^3J = 6 Hz, 3 H, pyridone).

^{7}Li NMR (156 MHz, D_2O): δ (ppm) = – 0.43.

[(Cymene)Ru(L5–2 H$^+$)]$_3$ × Na$^+$: ^{1}H NMR (400 MHz, D_2O): δ (ppm) = 1.27 (d, ^3J = 7 Hz, 9 H, CH(CH_3)$_2$), 1.30 (d, ^3J = 7 Hz, 9 H, CH(CH_3)$_2$), 1.81 (s, 9 H, CH_3C$_6$H$_4$^{i}Pr), 1.90–2.90 (m, br, 24 H, CH_2, piperazine), 2.23 (s, 9 H, NCH_3), 2.79 (sept, ^3J = 7 Hz, 3 H, CH(CH$_3$)$_2$), 3.30(d, ^2J = 13 Hz, 3 H, NCH_2), 3.46 (d, ^2J = 14 Hz, 3 H, NCH_2), 5.37 (d, ^3J = 6 Hz, 3 H, MeC$_6$H$_4$^{i}Pr), 5.62 (d, ^3J = 6 Hz, 3 H, MeC$_6$H$_4$^{i}Pr), 5.95 (m, 6 H, MeC$_6$H$_4$^{i}Pr), 6.12 (d, ^3J = 6 Hz, 3 H, pyridone), 6.75 (d, ^3J = 6 Hz, 3 H, MeC$_6$H$_4$^{i}Pr), 6.77 (d, ^3J = 6 Hz, 3 H, pyridone).

VIII.II.4.9 $[(C_6H_5CO_2Et)Ru(L2–H^+)]_3^{3+}$

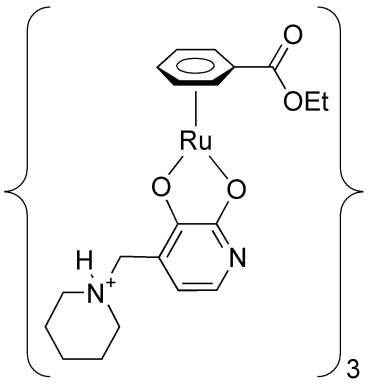

$[(C_6H_5CO_2Et)Ru(L2–H^+)]_3^3$: ^{1}H NMR (400 MHz, D_2O): δ (ppm) = 1.23 (t, ^3J = 7 Hz, 9 H, $CO_2CH_2CH_3$), 1.35–2.05 (m, br, 18 H, CH_2, piperidine), 2.55–3.55 (m, 12 H, NCH_2, piperidine), 3.85 (d, ^2J = 13 Hz, 3 H, NCH_2), 4.02 (d, ^2J = 13 Hz, 3 H, NCH_2), 4.26 (q, ^3J = 7 Hz, 6 H, $CO_2CH_2CH_3$), 5.84 (d, ^3J = 7 Hz, 3 H, $C_5H_5CO_2Et$), 5.98 (m, 6 H, $C_5H_5CO_2Et$), 6.16 (t, ^3J = 6 Hz, 3 H, $C_5H_5CO_2Et$), 6.56 (m, 6 H, $C_5H_5CO_2Et$ and pyridone), 6.77 (d, ^3J = 6 Hz, 3 H, pyridone).

$[(C_6H_5CO_2Et)Ru(L2–H^+)]_3^3 \times LiCl$: ^{1}H NMR (400 MHz, D_2O): δ (ppm) = 1.25 (t, ^3J = 7 Hz, 9 H, $CO_2CH_2CH_3$), 1.35–2.05 (m, br, 18 H, CH_2, piperidine), 2.60–3.60 (m, 12 H, NCH_2, piperidine), 3.97 (d, ^2J = 13 Hz, 3 H, NCH_2), 4.12 (d, ^2J = 13 Hz, 3 H, NCH_2), 4.30 (q, ^3J = 7, Hz, 6 H, $CO_2CH_2CH_3$), 6.10–6.30 (m, 12 H, $C_5H_5CO_2Et$), 6.72 (d, ^3J = 6 Hz, 3 H, $C_5H_5CO_2Et$ or pyridone), 6.77 (d, ^3J = 6 Hz, 3 H, $C_5H_5CO_2Et$ or pyridone), 6.87 (d, ^3J = 5 Hz, 3 H, pyridone).

^{7}Li NMR (156 MHz, D_2O): δ (ppm) = − 0.45.

VIII.II.4.10 $[(C_6H_5CO_2Et)Ru(L5–H^+)]_3^{3+}$

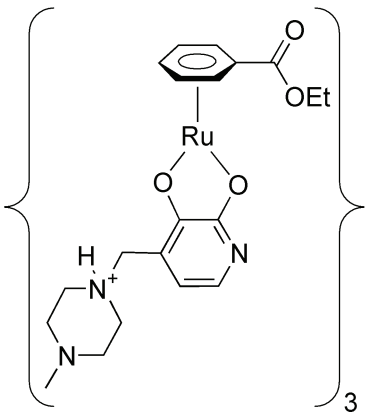

$[(C_6H_5CO_2Et)Ru(L5–H^+)]_3^{3+}$: ^{1}H NMR (400 MHz, D_2O): δ (ppm) = 1.22 (t, ^3J = 7 Hz, 9 H, $CO_2CH_2CH_3$), 2.35–3.45 (m, br, 24 H, CH_2, piperazine), 2.64 (s, 9 H, NCH_3), 3.35 (d, ^2J = 13 Hz, 3 H, NCH_2), 3.57 (d, ^2J = 13 Hz, 3 H, NCH_2), 4.22 (q, ^3J = 7, Hz, 6 H, $CO_2CH_2CH_3$), 5.79 (d, ^3J = 6 Hz, 3 H, $C_5H_5CO_2Et$), 5.95 (m, 6 H, $C_5H_5CO_2Et$), 6.11 (t, ^3J = 6 Hz, 3 H, $C_5H_5CO_2Et$), 6.51 (m, 6 H, $C_5H_5CO_2Et$ and pyridone), 6.73 (d, ^3J = 6 Hz, 3 H, pyridone).

$[(C_6H_5CO_2Et)Ru(L5–H^+)]_3^{3+} \times LiCl$: ^{1}H NMR (400 MHz, D_2O): δ (ppm) = 1.22 (t, ^3J = 7 Hz, 9 H, $CO_2CH_2CH_3$), 2.35–3.45 (m, br, 24 H, CH_2, piperazine), 2.64 (s, 9 H, NCH_3), 3.35 (d, ^2J = 13 Hz, 3 H, NCH_2), 3.57 (d, ^2J = 13 Hz, 3 H, NCH_2), 4.22 (q, ^3J = 7 Hz, 6 H, $CO_2CH_2CH_3$), 5.79 (d, ^3J = 6 Hz, 3 H, $C_5H_5CO_2Et$), 5.95 (m, 6 H, $C_5H_5CO_2Et$), 6.11 (t, ^3J = 6 Hz, 3 H, $C_5H_5CO_2Et$), 6.51 (m, 6 H, $C_5H_5CO_2Et$ and pyridone), 6.73 (d, ^3J = 6 Hz, 3 H, pyridone).

^{7}Li NMR (156 MHz, D_2O): δ (ppm) = − 0.46.

VIII.II.4.11 $[CpRh(L2–H^+)]_3^{3+}$

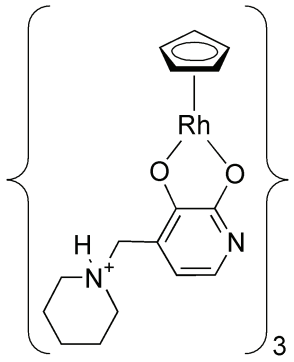

$[CpRh(L2–H^+)]_3^{3+}$: ^1H NMR (400 MHz, D_2O): δ (ppm) = 1.45–1.85 (m, br, 18 H, CH_2, piperidine), 2.95 (m, br, 12 H, NCH_2, piperidine), 3.92 (d, ^2J = 13 Hz, 3 H, NCH_2), 4.07 (d, ^2J = 13 Hz, 3 H, NCH_2), 5.77 (s, 15 H, Cp), 5.98 (d, ^3J = 6 Hz, 3 H, pyridone), 6.92 (d, ^3J = 6 Hz, 3 H, pyridone).

$[CpRh(L2\text{-}H^+)]_3^{3+}$ × LiCl: ^1H NMR (400 MHz, D_2O): δ (ppm) = 1.35–1.90 (m, br, 18 H, CH_2, piperidine), 2.92 (m, br, 12 H, NCH_2, piperidine), 4.04 (d, ^2J = 13 Hz, 3 H, NCH_2), 4.10 (d, ^2J = 13 Hz, 3 H, NCH_2), 5.90 (s, 15 H, Cp), 6.23 (d, ^3J = 6 Hz, 3 H, pyridone), 7.05 (d, ^3J = 6 Hz, 3 H, pyridone).

^7Li NMR (156 MHz, D_2O): δ (ppm) = − 0.05.

VIII.II.4.12 $[CpRh(L5–H^+)]_3^{3+}$

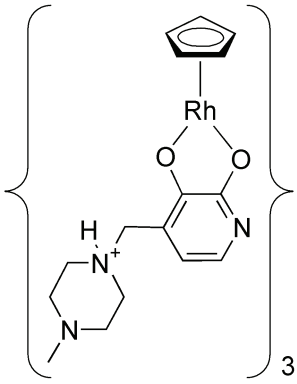

$[(Cp)Rh(L5–H^+)]_3^{3+}$: ^1H NMR (400 MHz, D_2O): δ (ppm) = 2.45–3.30 (m, br, 24 H, CH_2, piperazine), 2.65 (s, 9 H, NCH_3), 3.41 (d, ^2J = 13 Hz, 3 H, NCH_2), 3.62 (d, ^2J = 13 Hz, 3 H, NCH_2), 5.72 (s, 15 H, Cp), 5.94 (d, ^3J = 6 Hz, 3 H, pyridone), 6.85 (d, ^3J = 6 Hz, 3 H, pyridone).

$[(Cp)Rh(L5\text{-}H^+)]_3^{3+}$ × LiCl: ^1H NMR (400 MHz, D_2O): δ (ppm) = 2.45–3.30 (m, br, 24 H, CH_2, piperazine), 2.69 (s, 9 H, NCH_3), 3.45 (d, ^2J = 13 Hz, 3 H, NCH_2), 3.61 (d, ^2J = 13 Hz, 3 H, NCH_2), 5.84 (s, 15 H, Cp), 6.18 (d, ^3J = 6 Hz, 3 H, pyridone), 6.97 (d, ^3J = 6 Hz, 3 H, pyridone).

^7Li NMR (156 MHz, D_2O): δ (ppm) = − 0.08.

VIII.II.4.13 $[(C_5HMe_4)Rh(L2–H^+)]_3^{3+}$

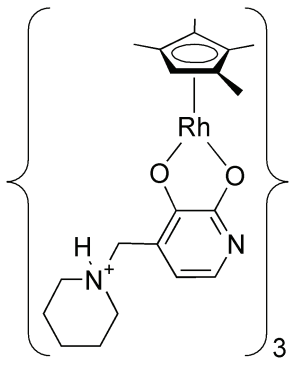

$[(C_5HMe_4)Rh(L2–H^+)]_3^{3+}$: ^1H NMR (400 MHz, D_2O): δ (ppm) = 1.35–2.00 (m, br, 18 H, CH_2, piperidine), 1.45 (s, 9 H, CH_3), 1.59 (s, 9 H, CH_3), 1.70 (s, 9 H, CH_3), 1.86 (s, 9 H, CH_3), 2.70–3.55 (m, br, 12 H, NCH_2, piperidine), 3.86 (d, ^2J = 13 Hz, 3 H, NCH_2), 4.09 (d, ^2J = 13 Hz, 3 H, NCH_2), 5.29 (s, 3 H, C_5Me_4H), 5.87 (d, ^3J = 6 Hz, 3 H, pyridone), 6.75 (d, ^3J = 6 Hz, 3 H, pyridone).

$[(C_5HMe_4)Rh(L2–H^+)]_3^{3+}$ × LiCl: ^1H NMR (400 MHz, D_2O): δ (ppm) = 1.25–2.10 (m, br, 18 H, CH_2, piperidine),

1.35 (s, 9 H, CH_3), 1.52 (s, 9 H, CH_3), 1.73 (s, 9 H, CH_3), 1.88 (s, 9 H, CH_3), 2.60–3.60 (m, br, 12 H, NCH_2, piperidine), 4.00 (d, ^2J = 13 Hz, 3 H, NCH_2), 4.15 (d, ^2J = 13 Hz, 3 H, NCH_2), 5.64 (s, 3 H, C_5Me_4H), 6.15 (d, ^3J = 6 Hz, 3 H, pyridone), 6.85 (d, ^3J = 6 Hz, 3 H, pyridone).

^{7}Li NMR (156 MHz, D_2O): δ (ppm) = 0.08.

VIII.II.4.14 [(C$_5$HMe$_4$)Rh(L5–2 H$^+$)]$_3$

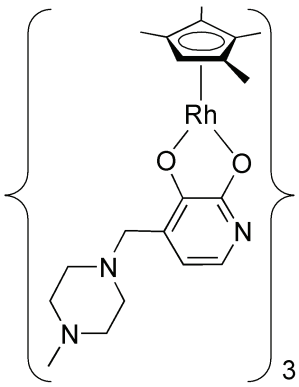

Similar to complex **[(cymene)Ru(L5–2 H$^+$)]$_3$**, the complex **[(C$_5$HMe$_4$)Rh(L5–H$^+$)]$_3^{3+}$** was soluble in water even after complete deprotonation of the amine groups. However, the difference lies in the fact the 2.0 eqiv. of CsOH were *necessary* to ensure complete trimerisation. The complex obtained from the self-assembly of **8** and **L5** in MeOH in the presence of Cs_2CO_3 was used for any kind of experiment.

[(C$_5$HMe$_4$)Rh(L5–2 H$^+$)]$_3$: ^{1}H NMR (400 MHz, D_2O): δ (ppm) = 1.47 (s, 9 H, CH_3), 1.60 (s, 9 H, CH_3), 1.74 (s, 9 H, CH_3), 1.88 (s, 9 H, CH_3), 2.05–3.10 (m, br, 24 H, CH_2, piperazine), 2.24 (s, 9 H, NCH_3, piperazine), 3.35 (d, ^2J = 13 Hz, 3 H, NCH_2), 3.44 (d, ^2J = 13 Hz, 3 H, NCH_2), 5.31 (s, 3 H, C_5Me_4H), 5.83 (d, ^3J = 6 Hz, 3 H, pyridone), 6.79 (d, ^3J = 7 Hz, 3 H, pyridone).

[(C$_5$HMe$_4$)Rh(L5–2 H$^+$)]$_3$ × LiCl: ^{1}H NMR (400 MHz, D_2O): δ (ppm) = 1.32 (s, 9 H, CH_3), 1.47 (s, 9 H, CH_3), 1.76 (s, 9 H, CH_3), 1.91 (s, 9 H, CH_3), 2.05–3.05 (m, br, 24 H, CH_2, piperazine), 2.21 (s, 9 H, NCH_3, piperazine), 3.41 (d, ^2J = 14 Hz, 3 H, NCH_2), 3.49 (d, ^2J = 14 Hz, 3 H, NCH_2), 5.63 (s, 3 H, C_5Me_4H), 6.07 (d, ^3J = 6 Hz, 3 H, pyridone), 6.86 (d, ^3J = 6 Hz, 3 H, pyridone).

^{7}Li NMR (156 MHz, D_2O): δ (ppm) = 0.03.

[(C$_5$HMe$_4$)Rh(L5–2 H$^+$)]$_3$ × Na$^+$: ^{1}H NMR (400 MHz, D_2O): δ (ppm) = 1.38 (s, 9 H, CH_3), 1.52 (s, 9 H, CH_3), 1.71 (s, 9 H, CH_3), 1.85 (s, 9 H, CH_3), 1.90–3.05 (m, br, 24 H, CH_2, piperazine), 2.21 (s, 9 H, NCH_3, piperazine), 3.38 (d, ^2J = 13 Hz, 3 H, NCH_2), 3.45 (d, ^2J = 14 Hz, 3 H, NCH_2), 5.39 (s, 3 H, C_5Me_4H), 6.98 (d, ^3J = 6 Hz, 3 H, pyridone), 6.82 (d, ^3J = 6 Hz, 3 H, pyridone).

VIII.II.4.15 $[Cp^*Rh(L2–H^+)]_3^{3+}$

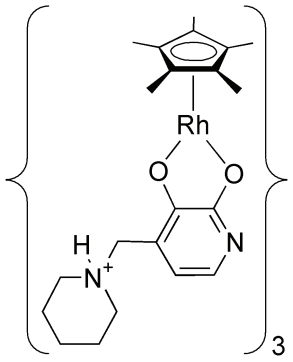

$[Cp^*Rh(L2–H^+)]_3^{3+}$: ^{1}H NMR (400 MHz, D_2O): δ (ppm) = ^{1}H NMR (400 MHz, D_2O): δ (ppm) = 1.40–1.90 (m, br, 18 H, CH_2, piperidine), 1.72 (s, 45 H, Cp*), 2.80–3.35 (m, br, 12 H, CH_2, piperidine), 3.85 (d, ^2J = 13 Hz, 3 H, NCH_2), 4.00 (d, ^2J = 13 Hz, 3 H, NCH_2), 5.76 (d, ^3J = 7 Hz, 3 H, pyridone), 6.70 (d, ^3J = 7 Hz, 3 H, pyridone).

$[Cp^*Rh(L2–H^+)]_3^{3+}$ × LiCl: ^{1}H NMR (400 MHz, D_2O): δ (ppm) = 1.35–1.95 (m, br, 18 H, CH_2, piperidine), 1.70 (s, 45 H, Cp*), 2.75–3.25 (m, br, 12 H, CH_2, piperidine), 3.92 (d, ^2J = 14 Hz, 3 H, NCH_2), 4.01 (d, ^2J = 13 Hz, 3 H, NCH_2), 6.19 (d, ^3J = 6 Hz, 3 H, pyridone), 685 (d, ^3J = 6 Hz, 3 H, pyridone).

^{7}Li NMR (156 MHz, D_2O): δ (ppm) = 0.07.

VIII.II.4.16 $[Cp^*Rh(L5–H^+)]_3^{3+}$

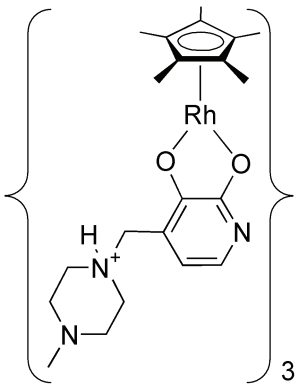

More than 1.0 equiv of CsOH was necessary to induce complete trimerisation in water. Unfortunately, the complex precipitated when adding more than 1.0 equiv. of CsOH, rendering the investiagation of its binding properties impossible. However, the synthesis of the deprotonated complex **$[Cp^*Rh(L5–2\ H^+)]_3$** starting from **9** and **L5** in MeOH in the presence of Cs_2CO_3 was achieved. The detailed synthesis and characterisation of the complex is described in the next section.

VIII.II.4.17 $[(C_5HMe_4)Ir(L2–H^+)]_3^{3+}$

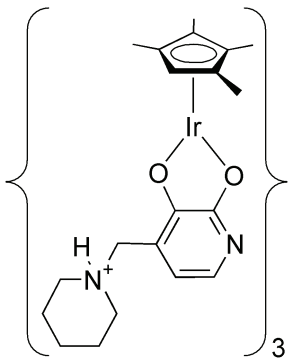

$[(C_5HMe_4)Ir(L2–H^+)]_3^{3+}$: ^{1}H NMR (400 MHz, D_2O): δ (ppm) = ^{1}H NMR (400 MHz, D_2O): δ (ppm) = 1.35–2.05 (m, br, 18 H, CH_2, piperidine), 1.50 (s, 9 H, CH_3), 1.53 (s, 9 H, CH_3), 1.65 (s, 9 H, CH_3), 1.81 (s, 9 H, CH_3), 2.70–3.50 (m, br, 12 H, NCH_2, piperidine), 3.92 (d, ^2J = 13 Hz, 3 H, NCH_2), 4.16 (d, ^2J = 13 Hz, 3 H, NCH_2), 5.40 (s, 3 H, C_5HMe_4), 5.89 (d, ^3J = 7 Hz, 3 H, pyridone), 6.83 (d, ^3J = 7 Hz, 3 H, pyridone).

$[(C_5HMe_4)Ir(L2–H^+)]_3^{3+}$ × LiCl: ^{1}H NMR (400 MHz, D_2O): δ (ppm) = 1.35 (s, 9 H, CH_3), 1.40 (s, 9 H, CH_3), 1.45–1.95 (m, br, 18 H, CH_2, piperidine), 1.69 (s, 9 H, CH_3), 1.85 (s, 9 H, CH_3), 3.03 (m, br, 12 H, NCH_2, piperidine), 4.00

(d, ^2J = 13 Hz, 3 H, NCH_2), 4.19 (d, ^2J = 13 Hz, 3 H, NCH_2), 5.77 (s, 3 H, C_5HMe_4), 6.18 (d, ^3J = 6 Hz, 3 H, pyridone), 6.91 (d, ^3J = 6 Hz, 3 H, pyridone).

^{7}Li NMR (156 MHz, D_2O): δ (ppm) = − 0.55.

VIII.II.4.18 $[(C_5HMe_4)Ir(L5–H^+)]_3^{3+}$

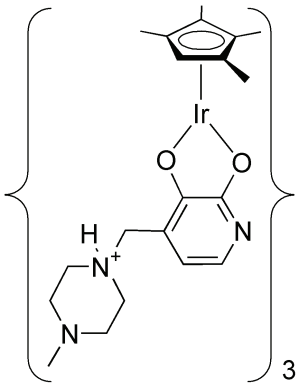

$[(C_5HMe_4)Ir(L5–H^+)]_3^{3+}$: ^{1}H NMR (400 MHz, D_2O): δ (ppm) = 1.48 (s, 9 H, CH_3), 1.52 (s, 9 H, CH_3), 1.66 (s, 9 H, CH_3), 1.79 (s, 9 H, CH_3), 2.45–3.40 (m, br, 24 H, CH_2, piperazine), 2.59 (s, 9 H, NCH_3), 3.54 (d, ^2J = 13 Hz, 3 H, NCH_2), 3.85 (d, ^2J = 13 Hz, 3 H, NCH_2), 5.37 (s, 3 H, C_5HMe_4), 5.85 (d, ^3J = 6 Hz, 3 H, pyridone), 6.81 (d, ^3J = 7 Hz, 3 H, pyridone).

$[(C_5HMe_4)Ir(L5–H^+)]_3^{3+}$ × LiCl: ^{1}H NMR (400 MHz, D_2O): δ (ppm) = 1.33 (s, 9 H, CH_3), 1.38 (s, 9 H, CH_3), 1.70 (s, 9 H, CH_3), 1.85 (s, 9 H, CH_3), 2.45–3.45 (m, br, 24 H, CH_2, piperazine), 2.66 (s, 9 H, NCH_3), 3.54 (d, ^2J = 13 Hz, 3 H, NCH_2), 3.84 (d, ^2J = 13 Hz, 3 H, NCH_2), 5.74 (s, 3 H, C_5HMe_4), 6.11 (d, ^3J = 6 Hz, 3 H, pyridone), 6.90 (d, ^3J = 6 Hz, 3 H, pyridone).

^{7}Li NMR (156 MHz, D_2O): δ (ppm) = − 0.60.

VIII.II.4.19 $[Cp^*Ir(L2–H^+)]_3^{3+}$

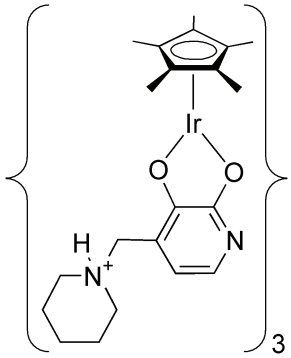

$[Cp^*Ir(L2–H^+)]_3^{3+}$: ^{1}H NMR (400 MHz, D_2O): δ (ppm) = ^{1}H NMR (400 MHz, D_2O): δ (ppm) = 1.45–1.95 (m, br, 18 H, CH_2, piperidine), 1.67 (s, 45 H, Cp*), 3.04 (m, br, 12 H, NCH_2, piperidine), 3.90 (d, ^2J = 13 Hz, 3 H, NCH_2), 4.09 (d, ^2J = 13 Hz, 3 H, NCH_2), 5.81 (d, ^3J = 7 Hz, 3 H, pyridone), 6.78 (d, ^3J = 7 Hz, 3 H, pyridone).

$[Cp^*Ir(L2–H^+)]_3^{3+}$ × LiCl: ^{1}H NMR (400 MHz, D_2O): δ (ppm) = 1.35–2.05 (m, br, 18 H, CH_2, piperidine), 1.64 (s, 45 H, Cp*), 3.03 (m, br, 12 H, NCH_2, piperidine), 3.96 (d, ^2J = 13 Hz, 3 H, NCH_2), 4.17 (d, ^2J = 13 Hz, 3 H, NCH_2), 6.22 (d, ^3J = 6 Hz, 3 H, pyridone), 6.91 (d, ^3J = 6 Hz, 3 H, pyridone).

The binding affinity towards Li^+ was so low, that a ^{7}Li NMR spectrum in reasonable quality could not be obtained.

VIII.II.4.20 $[Cp^*Ir(L5–H^+)]_3^{3+}$

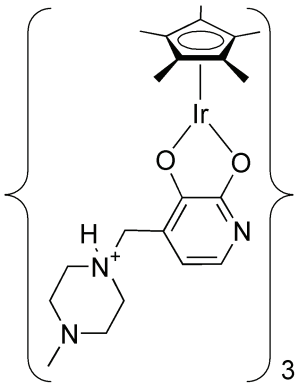

$[Cp^*Ir(L5–H^+)]_3^{3+}$: ^{1}H NMR (400 MHz, D_2O): δ (ppm) = 1.65 (s, 45 H, Cp*), 2.35–3.45 (m, br, 24 H, CH_2, piperazine), 2.58 (s, 9 H, NCH_3), 3.56 (d, ^2J = 13 Hz, 3 H, NCH_2), 3.87 (d, ^2J = 11 Hz, 3 H, NCH_2), 5.76 (d, ^3J = 7 Hz, 3 H, pyridone), 6.75 (d, ^3J = 6 Hz, 3 H, pyridone).

$[Cp^*Ir(L5–H^+)]_3^{3+}$ × LiCl: Although the complex did form, the quality of the obtained ^{1}H NMR spectrum was not sufficient to present any data. Especially the NCH_2 peaks were so broad, that no fine structure was visible. In addition, the pyridone and Cp* peaks indicated that a third species beside **$[Cp^*Ir(L5–H^+)]_3^{3+}$** and its LiCl adduct was present.

VIII.II.5 Neutral 12-Metallacrown-3 Complexes

General synthesis for trimeric metallamacrocycles: A suspension of halfsandwich complex [(π-ligand)$MCl_2]_2$ (0.50 mmol), ligand (**L1**, **L2**, **L3**, **L4** or **L5**) (1.00 mmol) and Cs_2CO_3 (815 mg, 2.50 mmol) was stirred for 2 h in degassed methanol (20 mL) at room temperature. After evaporation of the solvent under reduced pressure, the product was extracted with dichloromethane (40 mL). Twice the volume of hexane (80 mL) was added and the solution was concentrated to 10 mL. In general, most of the trimeric metallamacrocycles precipitated. The precipitate was filtered and dried in vacuo. The average yield is about 60 %.

General method for the synthesis of LiCl adducts: A double Schlenk with integrated fritte and equipped with teflon stoppers was used in order to avoid any contamination of the product with grease. $CHCl_3$ was dried using by chromatography and MeOH was distilled over Mg. A mixture of the trimeric metallamacrocycle (0.50 mmol) and an 100fold excess of LiCl (10 mL, 50 mmol, 0.5 M solution in dry MeOH) were stirred at room temperature. After removal of the solvant under reduced pressure, the LiCl adducts were extracted with $CHCl_3$.

VIII.II.5.a Trimers Obtained from [(π-ligand)$MCl_2]_2$ and Ligand L1

The trimers **$[(C_6H_6)Ru(L1–2\ H^+)]_3$**, **$[(C_6Me_6)Ru(L1–2\ H^+)]_3$**, **$[Cp^*Rh(L1–2\ H^+)]_3$** and their corresponding LiCl adducts were synthesised according to literature procedures.[124]

VIII.II.5.1 $[(C_6H_6)Ru(L1–2\ H^+)]_3$[124]

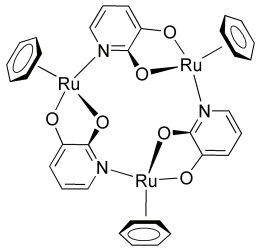

The synthetic procedure described in the literature used water as solvent. Unfortunately, the complex seems to be very air sensitive in the presence of water. A green-brown instead of an orange product indicated that the synthesis failed. Alternatively, the complex can be self-assembled in MeOH. Representative synthetic procedure: A suspension of **1** (250 mg, 0.50 mmol) and **L1** (115 mg, 1.00 mmol) and Cs_2CO_3 (815 mg, 2.5 mmol) was stirred in degassed MeOH (20 mL) for 2 h at room temperature. The reaction mixture became a clear orange solution. After evaporation of the solvent under reduced pressure, the product was extracted with CH_2Cl_2 (100 mL). Hexane (100 mL) was added and the volume reduced to about 25 mL. The product precipitated, was filtered off and dried in vacuo. The trimer was obtained as an orange powder in 69 % yield (200 mg, 0.23 mmol).

^{1}H NMR (400 MHz, $CDCl_3$): δ (ppm) = 5.56 (s, 18 H, C_6H_6), 5.72 (dd, ^3J = 7 Hz, ^3J = 6 Hz, 3 H, pyridone), 6.22 (dd, ^3J = 7 Hz, ^4J = 2 Hz, 3 H, pyridone), 6.72 (dd, ^3J = 6 Hz, ^4J = 2 Hz, 3 H, pyridone).

^{13}C NMR (101 MHz, $CDCl_3$): δ (ppm) = 81.92 (C_6H_6), 110.79, 115.82, 133.06. 156.11, 170.87 (pyridone).

^{1}H NMR (400 MHz, MeOD): δ (ppm) = 5.58 (s, 18 H, C_6H_6), 5.67 (dd, ^3J = 7 Hz, ^3J = 6 Hz, 3 H, pyridone), 6.11 (dd, ^3J = 7 Hz, ^4J = 2 Hz, 3 H, pyridone), 6.65 (dd, ^3J = 6 Hz, ^4J = 2 Hz, 3 H, pyridone).

^{13}C NMR (101 MHz, MeOD): δ (ppm) = 83.00 (C_6H_6), 110.51, 116.05, 134.19. 156.05, 172.30 (pyridone).

VIII.II.5.2 $[(C_6H_5Me)Ru(L1–2\ H^+)]_3$

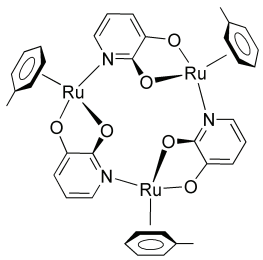

A suspension of **2** (264 mg, 0.50 mmol) and **L1** (115 mg, 1.00 mmol) and Cs_2CO_3 (815 mg, 2.5 mmol) was stirred in degassed MeOH (20 mL) for 2 h at room temperature. The reaction mixture became a clear orange solution. After evaporation of the solvent under reduced pressure, the product was extracted with CH_2Cl_2 (40 mL). Hexane (50 mL) was added and the volume reduced to about 15 mL. The product precipitated, was filtered off and dried in vacuo. The trimer was obtained as an orange powder in 75 % yield (228 mg, 0.25 mmol). Crystals were obtained from $CHCl_3$ layered with pentane.

^{1}H NMR (400 MHz, $CDCl_3$): δ (ppm) = 2.20 (s, 9 H, $CH_3C_6H_5$), 5.16 (d, ^3J = 6 Hz, 3 H, C_6H_5Me), 5.21 (t, ^3J = 5 Hz, 3 H, C_6H_5Me), 5.25 (d, ^3J = 6 Hz, 3 H, C_6H_5Me),

5.56 (t, ^3J = 6 Hz, 3 H, C_6H_5Me), 5.69 (t, ^3J = 6 Hz, 3 H, C_6H_5Me), 5.71 (dd, ^3J = 7 Hz, ^3J = 6 Hz, 3 H, pyridone), 6.18 (dd, ^3J = 7 Hz, ^4J = 1 Hz, 3 H, pyridone), 6.67 (dd, ^3J = 6 Hz, ^4J = 2 Hz, 3 H, pyridone).

^{13}C NMR (101 MHz, $CDCl_3$): δ (ppm) = 18.98 (CH_3), 75.60, 77.53, 79.19, 85.22, 85.62, 98.16 (C_6H_5), 110.489, 115.19, 132.522, 156.62, 171.00 (pyridone).

VIII.II.5.3 [(C$_6$H$_5$Me)Ru(L1–2 H$^+$)]$_3$ × LiCl

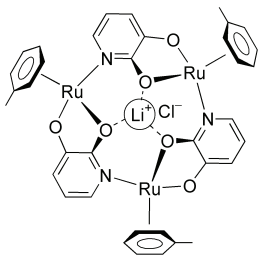

[(C$_6$H$_5$Me)Ru(L1–2 H$^+$)]$_3$ (45 mg, 50 µmol) was stirred in a LiCl solution in MeOH (10 mL, 0.5 M) for 5 min at room temperature using a double Schlenk with integrated fritte. After evaporation of the solvent under reduced pressure, the LiCl adduct was extracted with $CHCl_3$ (20 mL). The orange solution was concentrated to dryness and the product dried in vacuo. An orange powder was obtained in 40 % yield (19 mg, 20 µmol). Crystals suited for single crystal X-ray analysis were obtained by slow diffusion of Et_2O into $CHCl_3$.

^{1}H NMR (400 MHz, $CDCl_3$): δ (ppm) = 1.91 (s, 9 H, CH_3C$_6$H$_5$), 5.10 (d, ^3J = 6 Hz, 3 H, C_6H_5Me), 5.58 (t, ^3J = 5 Hz, 3 H, C_6H_5Me), 5.89 (d, ^3J = 6 Hz, 3 H, C_6H_5Me), 5.93 (dd, ^3J = 8 Hz, ^3J = 6 Hz, 3 H, pyridone), 6.11 (t, ^3J = 6 Hz, 3 H, C_6H_5Me), 6.38 (dd, ^3J = 7 Hz, ^4J = 1 Hz, 3 H, pyridone), 6.53 (t, ^3J = 6 Hz, 3 H, C_6H_5Me), 6.76 (dd, ^3J = 6 Hz, ^4J = 1 Hz, 3 H, pyridone).

^{13}C NMR (101 MHz, $CDCl_3$): δ (ppm) = 18.72 (CH_3), 75.21, 75.56, 78.61, 87.46, 81.81, 100.95 (C_6H_5), 113.11, 117.88, 133.00, 156.06, 167.90 (pyridone).

^{7}Li NMR (156 MHz, $CDCl_3$): δ (ppm) = – 0.10.

VIII.II.5.4 [(C$_6$H$_3$^{i}Pr$_3$)Ru(L1–2 H$^+$)]$_3$

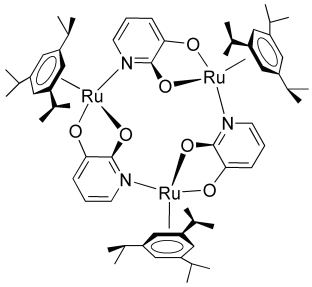

A suspension of **5** (300 mg, 0.40 mmol), 3-hydroxy-2-pyridone (88 mg, 0.80 mmol) and Cs_2CO_3 (650 mg, 2.00 mmol) in degassed MeOH (20 mL) was stirred for 2 h at room temperature. After evaporation of the solvent under reduced pressure, the product was extracted with CH_2Cl_2 (40 mL). Evaporation of the solvent under reduced pressure gave an orange powder. The product was recrystallised from hot hexane. Red crystals suited for single crystal X-ray analysis in 69 % yield (239 mg, 0.18 mmol) were obtained.

^{1}H NMR (400 MHz, $CDCl_3$): δ (ppm) = 1.24 (d, ^3J = 7 Hz, 27 H, CH(CH_3)$_2$), 1.35 (d, ^3J = 7 Hz, 27 H, CH(CH_3)$_2$), 3.09 (sept, ^3J = 7 Hz, 9 H, CH(CH$_3$)$_2$), 4.84 (s, 9 H,

$C_6H_3{}^iPr_3$), 5.53 (t, ^3J = 7 Hz, 3 H, pyridone), 5.96 (dd, ^3J = 7 Hz, ^4J = 2 Hz, 3 H, pyridone), 6.61 (dd, ^3J = 6 Hz, ^4J = 2 Hz, 3 H, pyridone).

^{13}C NMR (101 MHz, $CDCl_3$): δ (ppm) = 21.85, 23.74 (CH_3), 30.84 ($CH(CH_3)_2$), 68.45 ($C_6H_3{}^iPr_3$), 108.85, 109.21, 113.63, 133.23, 157.91, 172.34 ($C_6H_3{}^iPr_3$ & pyridone).

^{1}H NMR (400 MHz, MeOD): δ (ppm) = 1.27 (d, ^3J = 7 Hz, 27 H, $CH(CH_3)_2$), 1.38 (d, ^3J = 7 Hz, 27 H, $CH(CH_3)_2$), 3.14 (sept, ^3J = 7 Hz, 9 H, $CH(CH_3)_2$), 5.00 (s, 9 H, $C_6H_3{}^iPr_3$), 5.54 (t, ^3J = 7 Hz, 3 H, pyridone), 6.00 (dd, ^3J = 7 Hz, ^4J = 2 Hz, 3 H, pyridone), 6.69 (dd, ^3J = 6 Hz, ^4J = 2 Hz, 3 H, pyridone).

^{13}C NMR (101 MHz, MeOD): δ (ppm) = 22.26, 23.99 (CH_3), 32.02 ($CH(CH_3)_2$), 69.57 ($C_6H_3{}^iPr_3$), 109.96, 110.69, 115.52, 135.36, 157.76, 173.43 ($C_6H_3{}^iPr_3$ & pyridone).

Elemental analysis (%) calcd (found) for $C_{60}H_{81}N_3O_6Ru_3 \times 0.5\ C_6H_{14} \times H_2O$: C 58.00 (58.13), H 6.95 (6.92), N 3.22 (3.24).

VIII.II.5.5 $[(C_6H_3{}^iPr_3)Ru(L1–2\ H^+)]_3 \times LiCl$

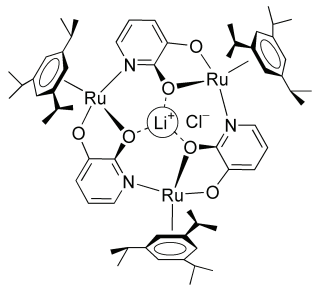

$[(C_6H_3{}^iPr_3)Ru(L1–2\ H^+)]_3$ (62 mg, 50 µmol) was stirred in a LiCl solution in MeOH (10 mL, 0.5 M) for 1 h at room temperature using a double Schlenk with integrated fritte. After evaporation of the solvent under reduced pressure, the LiCl adduct was extracted with dry $CHCl_3$ (20 mL). The orange solution was concentrated to dryness and the product dried in vacuo. An orange powder was obtained in 22 % yield (14 mg, 11 µmol). Crystals suited for single crystal X-ray analysis were obtained by recrystallisation from hot hexane.

^{1}H NMR (400 MHz, $CDCl_3$): δ (ppm) = 1.13 (d, ^3J = 6 Hz, 27 H, $CH(CH_3)_2$), 1.27 (d, ^3J = 7 Hz, 27 H, $CH(CH_3)_2$), 3.53 (sept, br, ^3J = 6 Hz, 9 H, $CH(CH_3)_2$), 5.57 (s, 9 H, $C_6H_3{}^iPr_3$), 5.71 (t, ^3J = 7 Hz, 3 H, pyridone), 6.14 (dd, ^3J = 7 Hz, ^4J = 1 Hz, 3 H, pyridone), 6.63 (dd, ^3J = 6 Hz, ^4J = 1 Hz, 3 H, pyridone).

^{13}C NMR (101 MHz, $CDCl_3$): δ (ppm) = 22.60, 23.43 (CH_3), 30.00 ($CH(CH_3)_2$), 70.38 ($C_6H_3{}^iPr_3$), 109.10, 111.72, 116.57, 133.20, 157.50, 170.15 ($C_6H_3{}^iPr_3$ & pyridone).

^{7}Li NMR (156 MHz, $CDCl_3$): δ (ppm) = − 0.18.

VIII.II.5.6 $[(C_6Me_6)Ru(L1–2\ H^+)]_3$[124]

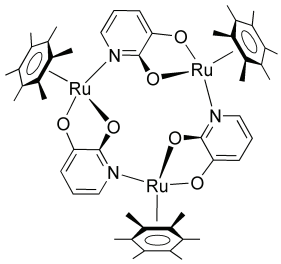

Alternatively to the synthesis described in the literature, the complex can be isolated by extraction with dichloromethane. Representative synthetic procedure: A suspension of **6** (334 mg, 0.50 mmol) and **L1** (115 mg, 1.00 mmol) and Cs_2CO_3 (815 mg, 2.5 mmol) was stirred in degassed MeOH (20 mL) for 2 h at room temperature. The reaction mixture became a clear orange solution. After evaporation of the solvent under reduced pressure, the product was extracted with CH_2Cl_2 (40 mL). Hexane (40 mL) was added and the volume reduced to about 15 mL. The product precipitated, was filtered off and dried in vacuo. The trimer was obtained as an orange powder in 76 % yield (289 mg, 0.26 mmol).

^{1}H NMR (400 MHz, $CDCl_3$): δ (ppm) = 2.10 (s, 18 H, C_6Me_6), 5.53 (d, ^3J = 7 Hz, 3 H, pyridone), 5.96 (d, ^3J = 9 Hz, 3 H, pyridone), 6.34 (dd, ^3J = 6 Hz, 3 H, pyridone).

^{1}H NMR (400 MHz, MeOD): δ (ppm) = 2.19 (s, 18 H, C_6Me_6), 5.53 (d, ^3J = 7 Hz, 3 H, pyridone), 6.02 (d, ^3J = 7 Hz, 3 H, pyridone), 6.44 (dd, ^3J = 6 Hz, 3 H, pyridone).

^{13}C NMR (101 MHz, MeOD): δ (ppm) = 16.73 (CH_3), 90.46 (C_6Me_6), 110.15, 114.51, 134.04, 157.94, 173.16 (pyridone).

VIII.II.5.7 $[(C_6Me_6)Ru(L1–2\ H^+)]_3 \times LiCl$[124]

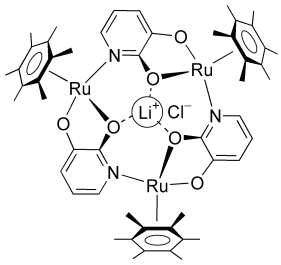

$[(C_6Me_6)Ru(L1–2\ H^+)]_3$ (49 mg, 44 µmol) was stirred in a LiCl solution in MeOH (9 mL, 0.5 M) for 1 h at room temperature using a double Schlenk with integrated fritte. After evaporation of the solvent under reduced pressure, the LiCl adduct was extracted with dry $CHCl_3$ (20 mL). The orange solution was concentrated to dryness and the product dried in vacuo. A red powder was obtained in 51 % yield (26 mg, 23 µmol). Remark: The solubility of the trimer is rather low. The reaction mixture is best described as suspension instead of a solution.

^{1}H NMR (400 MHz, $CDCl_3$): δ (ppm) = 2.16 (s, 18 H, C_6Me_6), 5.91 (dd, ^3J = 7 Hz, ^3J = 6 Hz, 3 H, pyridone), 6.32 (dd, ^3J = 8 Hz, ^4J = 2 Hz, 3 H, pyridone), 6.37 (dd, ^3J = 6 Hz, ^4J = 2 Hz, 3 H, pyridone).

^{13}C NMR (101 MHz, $CDCl_3$): δ (ppm) = 16.39 (CH_3), 90.21 (C_6Me_6), 114.41, 118.18, 131.89, 156.71, 167.48 (pyridone).

^{7}Li NMR (156 MHz, D_2O): δ (ppm) = – 0.58 (br).

VIII.II.5.8 $[(C_5HMe_4)Rh(L1–2\ H^+)]_3$

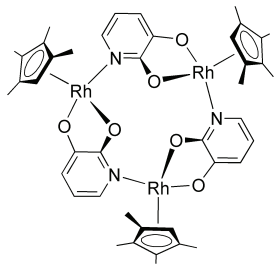

A suspension of **8** (300 mg, 0.40 mmol), 3-hydroxy-2-pyridone (88 mg, 0.80 mmol) and Cs_2CO_3 (650 mg, 2.00 mmol) in degassed MeOH (20 mL) was stirred for 2 h at room temperature. After evaporation of the solvent under reduced pressure, the product was extracted with CH_2Cl_3 (40 mL). The solvent was evaporated to dryness and the product dried in vacuo. A red-brown powder in 64 % yield (173 mg, 0.17 mmol) were obtained. Crystals were obtained from Et_2O.

^{1}H NMR (400 MHz, $CDCl_3$): δ (ppm) = 1.48 (s, 9 H, CH_3), 1.58 (s, 9 H, CH_3), 1.74 (s, 9 H, CH_3), 1.89 (s, 9 H, CH_3), 5.12 (s, 3 H, C_5HMe_4), 5.79 (dd, ^3J = 7 Hz, ^3J = 6 Hz, 3 H, pyridone), 6.21 (dd, ^3J = 7 Hz, ^4J = 2 Hz, 3 H, pyridone), 6.73 (dd, ^3J = 6 Hz, ^4J = 2 Hz, 3 H, pyridone).

VIII.II.5.9 $[(C_5HMe_4)Rh(L1–2\ H^+)]_3 \times LiCl$

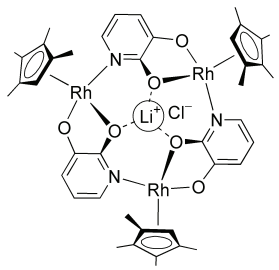

Crystals were obtained by vapour diffusion of pentane into a solution of the complex in toluene.

^{1}H NMR (400 MHz, $CDCl_3$): δ (ppm) = 1.33 (s, 9 H, $(CH_3)_4C_5H$), 1.47 (s, 9 H, $(CH_3)_4C_5H$), 1.75 (s, 9 H, $(CH_3)_4C_5H$), 2.05 (s, 9 H, $(CH_3)_4C_5H$), 5.99 (dd, ^3J = 7 Hz, ^3J = 6 Hz, 3 H, pyridone), 6.40 (dd, ^3J = 7 Hz, ^4J = 2 Hz, 3 H, pyridone), 6.78 (dd, ^3J = 6 Hz, ^4J = 1 Hz, 3 H, pyridone), 6.90 (s, 3 H, C_5HMe_4).

VIII.II.5.10 $[Cp^*Ru(L1–2\ H^+)]_3$[124]

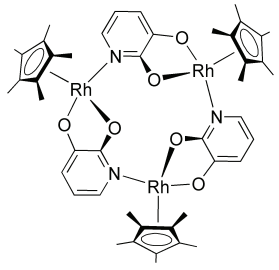

Representative synthetic procedure: A suspension of **9** (309 mg, 0.50 mmol), 3-hydroxy-2-pyridone (115 mg, 1.00 mmol) and Cs_2CO_3 (815 mg, 2.50 mmol) in degassed MeOH (20 mL) was stirred for 2 h at room temperature. After evaporation of the solvent under reduced pressure, the product was extracted with CH_2Cl_2 (40 mL). Hexane (40 mL) was added and the volume reduced to about 15 mL. The product precipitated, was filtered off and dried in vacuo. The trimer was obtained as an red-brown powder in 89 % yield (309 mg, 0.30 mmol).

^{1}H NMR (400 MHz, $CDCl_3$): δ (ppm) = 1.73 (s, 15 H, Cp*), 5.72 (t, ^3J = 7 Hz, 3 H, pyridone), 6.14 (dd, ^3J = 7 Hz, ^4J = 2 Hz, 3 H, pyridone), 6.71 (dd, ^3J = 6 Hz, ^4J = 1 Hz, 3 H, pyridone).

VIII.II.5.11 $[Cp^*Ru(L1–2\ H^+)]_3 \times LiCl$[124]

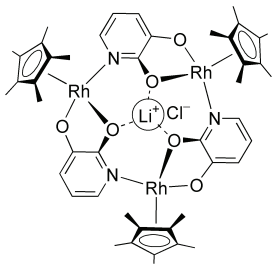

$[Cp^*Ru(L1–2\ H^+)]_3$ (52 mg, 50 µmol) was stirred in a LiCl solution in MeOH (10 mL, 0.5 M) for 1 h at room temperature using a double Schlenk with integrated fritte. After evaporation of the solvent under reduced pressure, the LiCl adduct was extracted with dry $CHCl_3$ (20 mL). The solution was concentrated to dryness and the product dried in vacuo. An red-brown powder was obtained in 35 % yield (19 mg, 18 µmol).

^{1}H NMR (400 MHz, $CDCl_3$): δ (ppm) = 1.74 (s, 15 H, Cp*), 6.02 (dd, ^3J = 8 Hz, ^3J = 6 Hz, 3 H, pyridone), 6.40 (dd, ^3J = 8 Hz, ^4J = 2 Hz, 3 H, pyridone), 6.74 (dd, ^3J = 6 Hz, ^4J = 1 Hz, 3 H, pyridone).

^{7}Li NMR (156 MHz, D_2O): δ (ppm) = 009.

VIII.II.5.b Mixed-Metal Complexes

VIII.II.5.1 $[\{(C_6H_6)Ru(L1–2\ H^+)\}_2\{(C_6H_3{}^iPr_3)Ru(L1–2\ H^+)\}]$

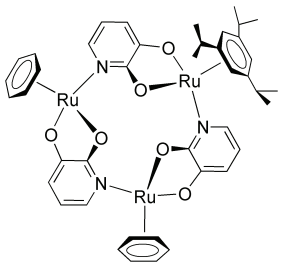

A suspension of **5** (62 mg, 0.10 mmol, 1.0 equiv.), **1** (110 mg, 0.22 mmol, 2.2 equiv.), 3-hydroxy-2-pyridone (69 mg, 0.60 mmol) and Cs_2CO_3 (489 mg, 1.50 mmol) in degassed MeOH (20 mL) was stirred over night at 45 °C. After evaporation of the solvent under reduced pressure, the product was extracted with CH_2Cl_2 (30 mL). A small amount of precipitate was observed after addition of hexane (60 mL), which was removed by filtration. The clear solution was concentrated to 15 mL, the resulting precipitate filtered off and dried in vacuo. The mixed trimer was obtained as an orange powder in 64 % yield (126 mg, 0.13 mmol) and 96 % purity.

^{1}H NMR (400 MHz, $CDCl_3$): δ (ppm) = 1.40 (d, ^3J = 7 Hz, 9 H, $CH(CH_3)_2$), 1.44 (d, ^3J = 7 Hz, 9 H, $CH(CH_3)_2$), 2.81 (sept, br, ^3J = 7 Hz, 3 H, $CH(CH_3)_2$), 4.97 (s, 3 H, $C_6H_3{}^iPr_3$), 5.44 (s, 6 H, C_6H_6), 5.45 (s, 6 H, C_6H_6), 5.62–5.69 (m, 3 H, pyridone), 6.08 (dd, ^3J = 7 Hz, ^4J = 2 Hz, 1 H, pyridone), 6.12 (dd, ^3J = 7 Hz, ^4J = 2 Hz, 1 H, pyridone), 6.16 (dd, ^3J = 7 Hz, ^4J = 1 Hz, 1 H, pyridone), 6.60 (dd, ^3J = 6 Hz, ^4J = 1 Hz, 1 H, pyridone), 6.63 (dd, ^3J = 6 Hz, ^4J = 2 Hz, 1 H, pyridone), 6.67 (dd, ^3J = 6 Hz, ^4J = 1 Hz, 1 H, pyridone).

^{13}C NMR (101 MHz, $CDCl_3$): δ (ppm) = 22.60, 23.28 (CH_3), 31.51 (CH), 71.09 (C_6H_3), 81.60, 81.66 (C_6H_6), 107.10 (C_6H_3), 109.99, 110.24, 110.30, 114.82, 115.09, 115.33, 132.11, 132.81, 133.11, 156.05, 156.28, 157.43, 171.06, 171.07, 171.62 (pyridone).

VIII.II.5.2 [{(C_6H_6)Ru(L1–2 H^+)}$_2${(C_6Me_6)Ru(L1–2 H^+)}]

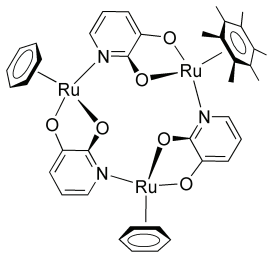

A suspension of **6** (67 mg, 0.10 mmol, 1.0 equiv.), **1** (110 mg, 0.22 mmol, 2.2 equiv.), 3-hydroxy-2-pyridone (69 mg, 0.60 mmol) and Cs_2CO_3 (489 mg, 1.50 mmol) in degassed MeOH (20 mL) was stirred over night at 45 °C. After evaporation of the solvent under reduced pressure, the product was extracted with CH_2Cl_2 (30 mL). A small amount of precipitate was observed after addition of hexane (60 mL), which was removed by filtration. The clear solution was concentrated to 15 mL, the resulting precipitate filtered off and dried in vacuo. The mixed trimer was obtained as an orange powder in 60 % yield (113 mg, 0.12 mmol) and 92 % purity. The complex was crystallised from $CHCl_3$/pentane.

^{1}H NMR (400 MHz, $CDCl_3$): δ (ppm) = 2.16 (s, 18 H, C_6Me_6), 5.46 (s, 6 H, C_6H_6), 5.48 (s, 6 H, C_6H_6), 5.60 (dd, ^3J = 7 Hz, ^3J = 6 Hz, 1 H, pyridone), 5.67 (t, ^3J = 7 Hz, 1 H, pyridone), 5.71 (dd, ^3J = 7 Hz, ^3J = 6 Hz, 1 H, pyridone), 6.03 (dd, ^3J = 7 Hz, ^4J = 1 Hz, 1 H, pyridone), 6.16 (dd, ^3J = 7 Hz, ^4J = 1 Hz, 1 H, pyridone), 6.17 (dd, ^3J = 7 Hz, ^4J = 2 Hz, 1 H, pyridone), 6.47 (dd, ^3J = 6 Hz, ^4J = 2 Hz, 1 H, pyridone), 6.60 (dd, ^3J = 6 Hz, ^4J = 2 Hz, 1 H, pyridone), 6.60 (dd, ^3J = 6 Hz, ^4J = 2 Hz, 1 H, pyridone).

^{13}C NMR (101 MHz, $CDCl_3$): δ (ppm) = 15.71 (CH_3), 81.47, 81.62 (C_6H_6), 89.11 (C_6Me_6), 109.51, 110.14, 110.53, 113.38, 114.73, 115.05, 131.36, 132.23, 132.21, 156.10, 156.13, 158.39, 170.28, 171.19, 171.76 (pyridone).

VIII.II.5.3 [{(C_6H_6)Ru(L1–2 H^+)}$_2${Cp*Rh(L1–2 H^+)}]

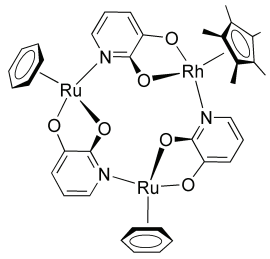

A suspension of **9** (62 mg, 0.10 mmol, 1.0 equiv.), **1** (150 mg, 0.30 mmol, 3.0 equiv.), 3-hydroxy-2-pyridone (69 mg, 0.60 mmol) and Cs_2CO_3 (489 mg, 1.50 mmol) in degassed MeOH (20 mL) was stirred over night at 45 °C. After evaporation of the solvent under reduced pressure, the product was extracted with CH_2Cl_2 (30 mL). A small amount of precipitate was observed after addition of hexane (60 mL), which was removed by filtration. The clear solution was concentrated to 15 mL, the resulting precipitate filtered off and dried in vacuo. The mixed trimer was obtained as brown-red powder in 62 % yield (114 mg, 0.12 mmol) and 83 % purity. The complex was crystallised from benzene/pentane.

^{1}H NMR (400 MHz, $CDCl_3$): δ (ppm) = 1.77 (s, 18 H, Cp*), 5.45 (s, 6 H, C_6H_6), 5.46 (s, 6 H, C_6H_6), 5.65 (t, ^3J = 7 Hz, 1 H, pyridone), 5.69 (t, ^3J = 7 Hz, 1 H, pyridone), 5.79 (t, ^3J = 7 Hz, 1 H, pyridone), 6.10 (dd, ^3J = 7 Hz, ^4J = 1 Hz, 1 H, pyridone), 6.19 (dd, ^3J = 7 Hz, ^4J = 1 Hz, 1 H, pyridone), 6.23 (dd, ^3J = 7 Hz, ^4J = 1 Hz, 1 H, pyridone), 6.62

(dd, ^3J = 6 Hz, ^4J = 1 Hz, 1 H, pyridone), 6.64 (dd, ^3J = 6 Hz, ^4J = 1 Hz, 1 H, pyridone), 6.73 (dd, ^3J = 6 Hz, ^4J = 1 Hz, 1 H, pyridone).

^{13}C NMR (101 MHz, $CDCl_3$): δ (ppm) = 14.26 (CH_3), 81.57, 81.77 (C_6H_6), 90.32 (d, ^1J(C,Rh) = 8 Hz, C, Cp*), 109.72, 110.24, 110.96, 113.99, 115.12, 115.21, 131.76, 131.84, 132.38, 156.25, 156.63, 157.93, 169.95, 171.22, 171.88 (pyridone).

VIII.II.5.c Trimers obtained from [(π-ligand)MCl_2]$_2$ and Ligands L2–L5

VIII.II.5.1 [(cymene)Ru(L2–2 H^+)]$_3$

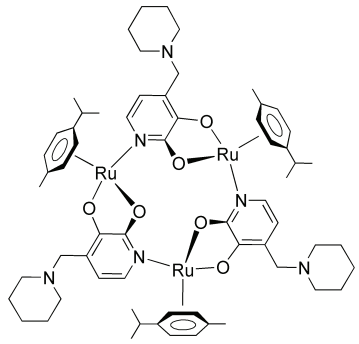

^{1}H NMR (400 MHz, $CDCl_3$): δ (ppm) = 1.26 (d, ^3J = 7 Hz, 9 H, $CH(CH_3)_2$), 1.34 (d, ^3J = 7 Hz, 9 H, $CH(CH_3)_2$), 1.41 (m, br, 18 H, CH_2, piperidine), 2.05 (s, 9 H, $CH_3C_6H_4{}^i$Pr), 2.16 (m, br, 12 H, NCH_2, piperidine), 2.74 (sept, ^3J = 7 Hz, 3 H, $CH(CH_3)_2$), 3.23 (d, ^2J = 14 Hz, 3 H, NCH_2), 3.33 (d, ^2J = 14 Hz, 3 H, NCH_2), 5.09 (d, ^3J = 6 Hz, 3 H, $MeC_6H_4{}^i$Pr), 5.22 (d, ^3J = 5 Hz, 3 H, $MeC_6H_4{}^i$Pr), 5.33 (d, ^3J = 5 Hz, 3 H, $MeC_6H_4{}^i$Pr), 5.58 (d, ^3J = 6 Hz, 3 H, $MeC_6H_4{}^i$Pr), 5.69 (d, ^3J = 6 Hz, 3 H, pyridone), 6.50 (d, ^3J = 6 Hz, 3 H, pyridone).

VIII.II.5.2 [(cymene)Ru(L3–2 H^+)]$_3$

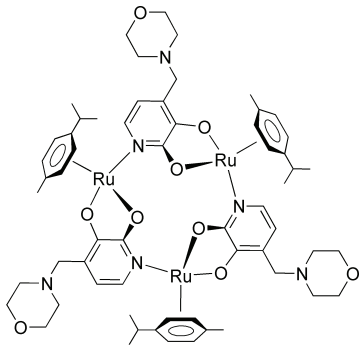

A suspension of complex **3** (306 mg, 0.50 mmol), ligand **L3** (210 mg, 1.00 mmol) and Cs_2CO_3 (815 mg, 2.50 mmol) in degassed methanol (20 mL) was stirred for 2 h at room temperature. After evaporation of the solvent under reduced pressure, the product was extracted with dichloromethane (40 mL). Twice the volume of hexane (80 mL) was added and the solution was concentrated to 10 mL. The precipitate was filtered and dried in vacuo. The product was obtained as an orange powder in 62 %yield (305 mg, 0.21 mmol). Orange crystals were obtained either by slow diffusion of pentane into a solution of **[(cymene)Ru(L3–2 H^+)]$_3$** in benzene.

^{1}H NMR (400 MHz, $CDCl_3$): δ (ppm) = 1.28 (d, ^3J = 7 Hz, 9 H, $CH(CH_3)_2$), 1.37 (d, ^3J = 7 Hz, 9 H, $CH(CH_3)_2$), 2.12 (s, 9 H, $CH_3C_6H_4{}^i$Pr), 2.22 (m, br, 12 H, CH_2, morpholine), 2.75 (sept, ^3J = 7 z, 3 H, $CH(CH_3)_2$), 3.35 (d, ^2J = 14 Hz, 3 H, NCH_2), 3.33 (d,

^2J = 14 Hz, 3 H, NCH_2), 2.55 (m, br, 12 H, CH_2, morpholine), 5.08 (d, ^3J = 6 Hz, 3 H, $MeC_6H_4{}^iPr$), 5.20 (d, ^3J = 6 Hz, 3 H, $MeC_6H_4{}^iPr$), 5.29 (d, ^3J = 6 Hz, 3 H, $MeC_6H_4{}^iPr$), 5.52 (d, ^3J = 6 Hz, 3 H, $MeC_6H_4{}^iPr$), 5.68 (d, ^3J = 6 Hz, 3 H, pyridone), 6.49 (d, ^3J = 6 Hz, 3 H, pyridone).

^{13}C NMR (101 MHz, $CDCl_3$): δ (ppm) = 18.60, 22.93, 23.20 (CH_3, $MeC_6H_4{}^iPr$), 31.37 (CH, $CH(CH_3)_2$), 54.08, 55.71, 67.28 (NCH_2, OCH_2, morpholine), 77.36, 79.93, 81.49, 82.03 (CH, $MeC_6H_4{}^iPr$), 95.80, 98.07 (C, $MeC_6H_4{}^iPr$), 110.25, 123.11, 131.22, 155.32, 170.83 (pyridone).

Elemental analysis (%) calcd (found) for $C_{60}H_{78}N_6O_9Ru_3$: C 54.16 (54.45), H 5.91 (5.98), N 6.32 (6.24).

VIII.II.5.3 [(cymene)Ru(L4–2 H$^+$)]$_3$

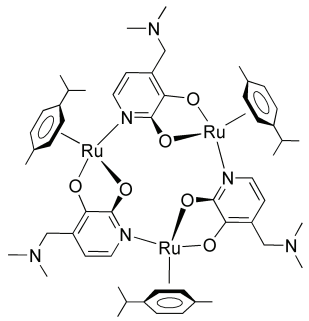

^{1}H NMR (400 MHz, $CDCl_3$): δ (ppm) = 1.26 (d, ^3J = 7 Hz, 9 H, $CH(CH_3)_2$), 1.34 (d, ^3J = 7 Hz, 9 H, $CH(CH_3)_2$), 1.93 (s, 9 H, $CH_3C_6H_4{}^iPr$), 1.99 (s, 18 H, $N(CH_3)_2$), 2.78 (sept, ^3J = 7 Hz, 3 H, $CH(CH_3)_2$), 3.09 (d, ^2J = 13 Hz, 3 H, NCH_2), 3.35 (d, ^2J = 13 Hz, 3 H, NCH_2), 5.05 (d, ^3J = 6 Hz, 3 H, $MeC_6H_4{}^iPr$), 5.28 (d, ^3J = 6 Hz, 3 H, $MeC_6H_4{}^iPr$), 5.45 (d, ^3J = 6 Hz, 3 H, $MeC_6H_4{}^iPr$), 5.75 (d, ^3J = 6 Hz, 3 H, pyridone), 5.58 (d, ^3J = 6 Hz, 3 H, $MeC_6H_4{}^iPr$), 6.56 (d, ^3J = 6 Hz, 3 H, pyridone).

VIII.II.5.4 [(cymene)Ru(L5–2 H$^+$)]$_3$

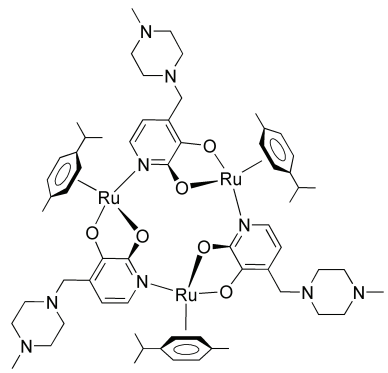

A suspension of complex **3** (612 mg, 1.00 mmol), ligand **L5** (447 mg, 2.00 mmol) and Cs_2CO_3 (1.60 g, 5.00 mmol) in degassed methanol (40 mL) was stirred for 2 h at room temperature. After evaporation of the solvent under reduced pressure the product was extracted with hot hexane (1 × 300 mL and 3 × 125 mL). The solution was concentrated (15 mL) and cooled down to − 18 °C for 1 h. The precipitate was filtered and dried in vauco. The product was obtained as an orange powder in 54 % yield (502 mg, 0.36 mmol). Red crystals were obtained by slow diffusion of pentane into a solution of **[(cymene)Ru(L5–2 H$^+$)]$_3$** in benzene.

^{1}H NMR (400 MHz, $CDCl_3$): δ (ppm) = 1.26 (d, ^3J = 7 Hz, 9 H, $CH(CH_3)_2$), 1.34 (d, ^3J = 7 Hz, 9 H, $CH(CH_3)_2$), 2.09 (s, 9 H, $CH_3C_6H_4{}^iPr$), 2.22 (s, 9 H, NCH_3, piperazine),

1.75–2.65 (m, br, 24 H, NCH_2, piperazine), 2.73 (sept, ^3J = 7 Hz, 3 H, $CH(CH_3)_2$), 3.28 (d, ^2J = 13 Hz, 3 H, NCH_2), 3.33 (d, ^2J = 13 Hz, 3 H, NCH_2), 5.09 (d, ^3J = 5 Hz, 3 H, $MeC_6H_4{}^i Pr$), 5.21 (d, ^3J = 6 Hz, 3 H, $MeC_6H_4{}^i Pr$), 5.30 (d, ^3J = 6 Hz, 3 H, $MeC_6H_4{}^i Pr$), 5.56 (d, ^3J = 5 Hz, 3 H, $MeC_6H_4{}^i Pr$), 5.69 (d, ^3J = 6 Hz, 3 H, pyridone), 6.49 (d, ^3J = 6 Hz, 3 H, pyridone).

^{13}C NMR (101 MHz, $CDCl_3$): δ (ppm) = 18.86, 22.87, 23.19 (CH_3, $MeC_6H_4{}^i Pr$), 31.26 (CH, $CH(CH_3)_2$), 46.27 (NCH_3), 53.48, 55.27, 55.54 (NCH_2, piperazine), 77.32, 79.89, 81.53, 82.15 (CH, $MeC_6H_4{}^i Pr$), 95.97, 98.01 (C, $MeC_6H_4{}^i Pr$), 110.35, 123.96, 131.20, 154.99, 170.67 (pyridone).

Elemental analysis (%) calcd (found) for $C_{63}H_{87}N_9O_6Ru_3 \times H_2O$: C 54.53 (54.48), H 6.46 (6.79), N 9.08 (9.22).

VIII.II.5.5 $[(C_6H_3{}^i Pr_3)Ru(L2–2\ H^+)]_3$

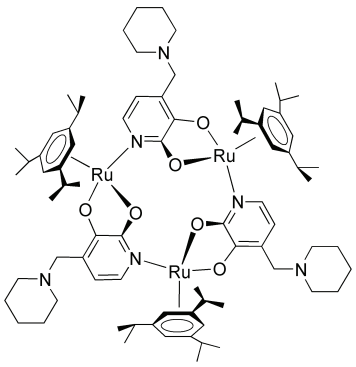

^1H NMR (400 MHz, $CDCl_3$): δ (ppm) = 1.19 (d, ^3J = 7 Hz, 27 H, $CH(CH_3)_2$), 1.37 (d, ^3J = 7 Hz, 27 H, $CH(CH_3)_2$), 1.90 (m, br, 18 H, CH_2, piperidine), 2.30 (m, br, 12 H, CH_2, piperidine), 2.85 (d, ^2J = 13 Hz, 3 H, NCH_2), 3.10 (sept, ^3J = 7 Hz, 3 H, $CH(CH_3)_2$), 3.47 (d, ^2J = 12 Hz, 3 H, NCH_2), 4.77 (s, 9 H, $C_6H_3{}^i Pr_3$), 5.46 (d, ^3J = 6 Hz, 3 H, pyridone), 6.44 (d, ^3J = 6 Hz, 3 H, pyridone).

VIII.II.5.6 $[(C_6H_3{}^i Pr_3)Ru(L3–2\ H^+)]_3$

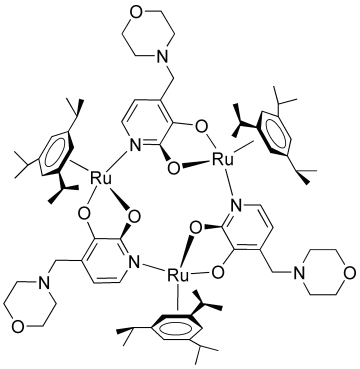

^1H NMR (400 MHz, $CDCl_3$): δ (ppm) = 1.20 (d, ^3J = 7 Hz, 27 H, $CH(CH_3)_2$), 1.37 (d, ^3J = 7 Hz, 27 H, $CH(CH_3)_2$), 2.32 (m, br, 12 H, CH_2, morpholine), 3.01 (d, ^2J = 13 Hz, 3 H, NCH_2), 3.07 (sept, ^3J = 7 Hz, 3 H, $CH(CH_3)_2$), 3.39 (d, ^2J = 13 Hz, 3 H, NCH_2), 3.63 (m, br, 12 H, CH_2, morpholine), 4.77 (s, 9 H, $C_6H_3{}^i Pr_3$), 5.49 (d, ^3J = 6 Hz, 3 H, pyridone), 6.47 (d, ^3J = 6 Hz, 3 H, pyridone).

VIII.II.5.7 $[(C_6H_3{}^{i}Pr_3)Ru(L4–2\ H^+)]_3$

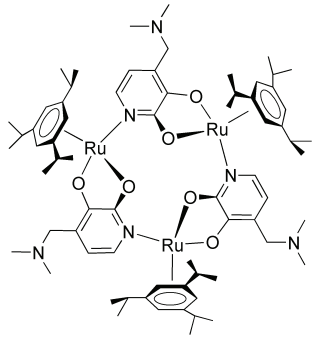

^{1}H NMR (400 MHz, $CDCl_3$): δ (ppm) = 1.20 (d, ^3J = 7 Hz, 27 H, $CH(CH_3)_2$), 1.36 (d, ^3J = 7 Hz, 27 H, $CH(CH_3)_2$), 2.10 (s, 18 H, $N(CH_3)_2$), 2.88 (d, ^2J = 12 Hz, 3 H, NCH_2), 3.08 (sept, ^3J = 7 Hz, 3 H, $CH(CH_3)_2$), 3.37 (d, ^2J = 12 Hz, 3 H, NCH_2), 4.77 (s, 9 H, $C_6H_3{}^{i}Pr_3$), 5.48 (d, ^3J = 6 Hz, 3 H, pyridone), 6.47 (d, ^3J = 6 Hz, 3 H, pyridone).

VIII.II.5.8 $[(C_6H_3{}^{i}Pr_3)Ru(L5–2\ H^+)]_3$

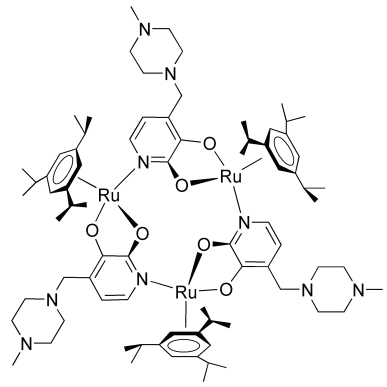

^{1}H NMR (400 MHz, $CDCl_3$): δ (ppm) = 1.19 (d, ^3J = 7 Hz, 27 H, $CH(CH_3)_2$), 1.35 (d, ^3J = 7 Hz, 27 H, $CH(CH_3)_2$), 2.25 (s, 9 H, NCH_3), 2.35 (m, br, 24 H, CH_2, piperazine), 2.96 (d, ^2J = 12 Hz, 3 H, NCH_2), 3.08 (sept, ^3J = 7 Hz, 3 H, $CH(CH_3)_2$), 3.39 (d, ^2J = 12 Hz, 3 H, NCH_2), 4.77 (s, 9 H, $C_6H_3{}^{i}Pr_3$), 5.49 (d, ^3J = 6 Hz, 3 H, pyridone), 6.46 (d, ^3J = 6 Hz, 3 H, pyridone).

VIII.II.5.9 $[(C_6Me_6)Ru(L2–2\ H^+)]_3$

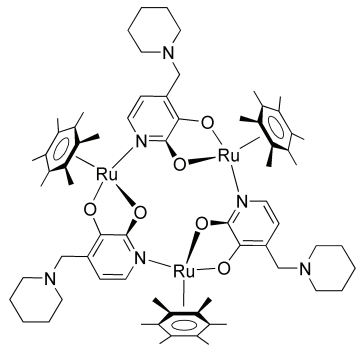

^{1}H NMR (400 MHz, $CDCl_3$): δ (ppm) = 1.85–2.45 (m, br, 30 H, CH_2, piperidine), 2.10 (s, 54 H, C_6Me_6), 3.06 (d, ^2J = 13 Hz, 3 H, NCH_2), 3.48 (d, ^2J = 12 Hz, 3 H, NCH_2), 5.50 (m, br, 3 H, pyridone), 6.16 (d, ^3J = 6 Hz, 3 H, pyridone).

VIII.II.5.10 $[(C_6Me_6)Ru(L3–2\ H^+)]_3$

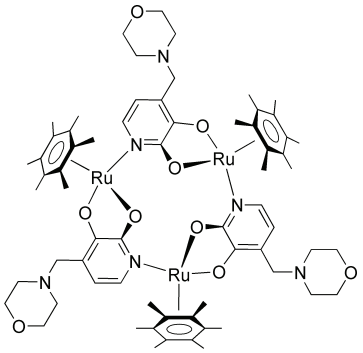

^{1}H NMR (400 MHz, $CDCl_3$): δ (ppm) = 2.10 (s, 54 H, C_6Me_6), 2.41 (m, br, 12 H, CH_2, morpholine), 3.13 (d, ^2J = 13 Hz, 3 H, NCH_2), 3.47 (d, ^2J = 13 Hz, 3 H, NCH_2), 3.65 (m, br, 12 H, CH_2, morpholine), 5.50 (m, br, 3 H, pyridone), 6.17 (d, ^3J = 6 Hz, 3 H, pyridone).

VIII.II.5.11 $[(C_6Me_6)Ru(L4–2\ H^+)]_3$

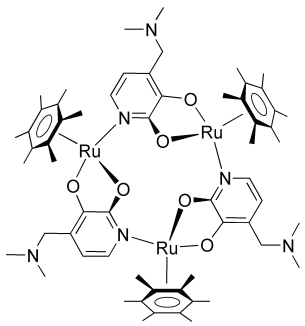

^{1}H NMR (400 MHz, $CDCl_3$): δ (ppm) = 2.10 (s, 54 H, C_6Me_6), 2.18 (s, 18 H, $N(CH_3)_2$), 3.03 (d, br, ^2J = 10 Hz, 3 H, NCH_2), 3.43 (d, br, ^2J = 10 Hz, 3 H, NCH_2), 5.51 (m, br, 3 H, pyridone), 6.17 (d, ^3J = 6 Hz, 3 H, pyridone).

VIII.II.5.12 $[(C_6Me_6)Ru(L5–2\ H^+)]_3$

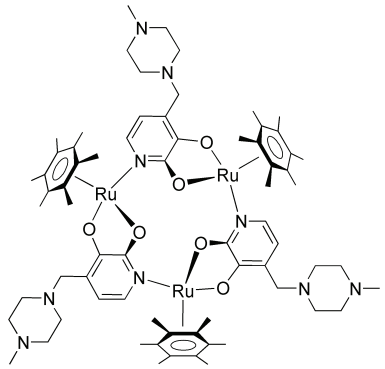

^{1}H NMR (400 MHz, $CDCl_3$): δ (ppm) = 2.09 (s, 54 H, C_6Me_6), 2.26 (s, 9 H, NCH_3), 2.15–2.65 (m, br, 24 H, piperazine), 3.10 (d, ^2J = 13 Hz, 3 H, NCH_2), 3.46 (d, ^2J = 12 Hz, 3 H, NCH_2), 5.49 (d, ^3J = 6 Hz, 3 H, pyridone), 6.16 (d, ^3J = 6 Hz, 3 H, pyridone).

VIII.II.5.13 $[(C_5HMe_4)Rh(L5–2\ H^+)]_3$

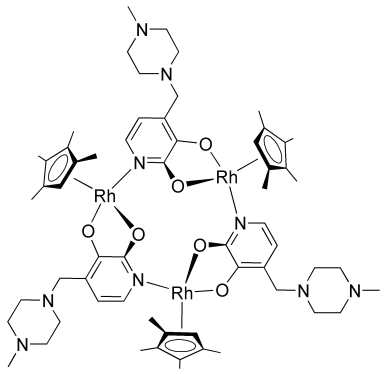

A suspension of complex **8** (295 mg, 0.50 mmol), ligand **L5** (223 mg, 1.00 mmol) and Cs_2CO_3 (815 mg, 2.50 mmol) in degassed methanol (30 mL) was stirred for 2 h at room temperature. After evaporation of the solvent under reduced pressure, the product was extracted with dichloromethane (40 mL). Addition of hexane (60 mL) and concentration of the solvent gave a red-brown powder which was dried in vacuo. The product was obtained in 64 % yield (348 mg, 0.21 mmol). Red crystals were obtained from water.

^{1}H NMR (400 MHz, $CDCl_3$): δ (ppm) = 1.44 (s, 9 H, CH_3), 1.53 (s, 9 H, CH_3), 1.67 (s, 9 H, CH_3), 1.86 (s, 9 H, CH_3), 2.00–2.75 (m, br, 24 H, CH_2, piperazine), 2.25 (s, 9 H, NCH_3, piperazine), 3.24 (d, ^2J = 13 Hz, 3 H, NCH_2), 3.43 (d, ^2J = 13 Hz, 3 H, NCH_2), 5.04 (s, 3 H, C_5HMe_4), 5.75 (d, ^3J = 6 Hz, 3 H, pyridone), 6.57 (d, ^3J = 6 Hz, 3 H, pyridone).

^{13}C NMR (101 MHz, $CDCl_3$): δ (ppm) = 11.21, 11.43, 13.20, 13.37 (CH_3, C_5HMe_4), 49.07 (NCH_3), 56.20, 58.30, 58.63 (NCH_2, piperazine), 76.80 (d, ^1J(C,Rh) = 8 Hz, CH, C_5HMe_4), 97.34 (d, ^1J(C,Rh) = 6 Hz, C, C_5HMe_4), 102.68 (d, ^1J(C,Rh) = 6 Hz, C, C_5HMe_4), 115.40, 125.34, 132.54, 159.38, 172.85 (pyridone).

Elemental analysis (%) calcd (found) for $C_{60}H_{84}N_9O_6Rh_3 \times 2\ H_2O \times 3\ CH_2Cl_2$: C 46.51 (46.46), H 5.82 (5.97), N 7.75 (7.71).

During the NMR experiments with receptor **$[(C_5HMe_4)Rh(L5–2\ H^+)]_3$**, it was observed that the ^{1}H NMR signals of the methyl groups of the π-ligand gradually lost intensity. A likely explanation for this observation is a selective H/D exchange. An exchange of this kind has been observed for aqueous solutions of Cp*Rh[377] as well as Cp*Ru[378] complexes. A more detailed analysis revealed that the H/D exchange is slightly inhibited if the receptor is bound to a Li^+ guest: in the presence of two equivalents of LiCl, 7 % of the methyl protons were exchanged after 24 hours whereas without lithium ions 20 % were exchanged.

VIII.II.5.14 [Cp*Rh(L2–2 H^+)]$_3$

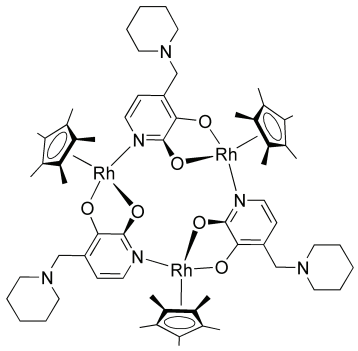

The complex was obtained as a dark red powder in 75 % yield (255 mg, 0.25 mmol).

^{1}H NMR (400 MHz, $CDCl_3$): δ (ppm) = 1.25–1.55 (m, br, 18 H, CH_2, piperidine), 1.70 (s, 45 H, Cp*), 2.29 (m, br, 12 H, CH_2, piperidine), 3.28 (d, ^2J = 13 Hz, 3 H, NCH_2), 3.34 (d, ^2J = 13 Hz, 3 H, NCH_2), 5.67 (m, br, 3 H, pyridone), 6.56 (d, ^3J = 6 Hz, 3 H, pyridone).

VIII.II.5.15 [Cp*Rh(L3–2 H^+)]$_3$

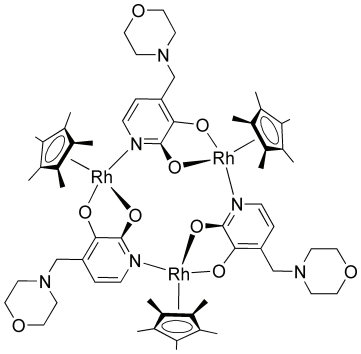

The complex was obtained as a dark red powder in 75 % yield (318 mg, 0.24 mmol).

^{1}H NMR (400 MHz, $CDCl_3$): δ (ppm) = 1.70 (s, 45 H, Cp*), 2.35 (m, br, 12 H, CH_2, morpholine), 3.27 (d, ^2J = 12 Hz, 3 H, NCH_2), 3.35 (d, ^2J = 13 Hz, 3 H, NCH_2), 3.63 (m, br, 12 H, CH_2, morpholine), 5.65 (d, ^3J = 6 Hz, 3 H, pyridone), 6.55 (d, ^3J = 6 Hz, 3 H, pyridone).

VIII.II.5.16 [Cp*Rh(L4–2 H^+)]$_3$

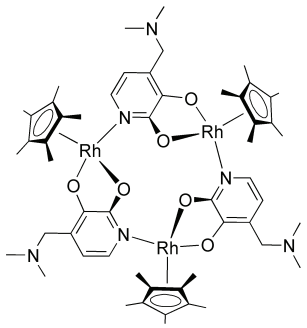

^{1}H NMR (400 MHz, $CDCl_3$): δ (ppm) = 1.69 (s, 45 H, Cp*), 2.10 (s, 18 H, $N(CH_3)_2$), 3.19 (d, ^2J = 13 Hz, 3 H, NCH_2), 3.36 (d, ^2J = 12 Hz, 3 H, NCH_2), 5.66 (d, ^3J = 6 Hz, 3 H, pyridone), 6.56 (d, ^3J = 6 Hz, 3 H, pyridone).

VIII.II.5.17 [Cp*Rh(L5–2 H$^+$)]$_3$

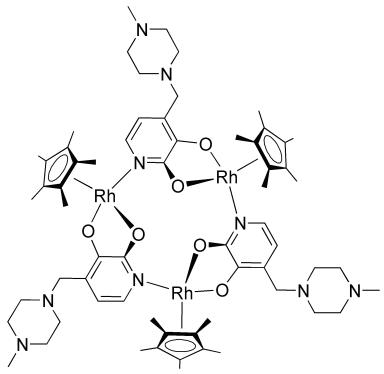

A suspension of complex **9** (309 mg, 0.50 mmol), ligand **L5** (223 mg, 1.00 mmol) and Cs_2CO_3 (815 mg, 2.50 mmol) in degassed methanol (40 mL) was stirred for 2 h at room temperature. After evaporation of the solvent under reduced pressure the product was extracted with dichloromethane (40 mL). The solvent was removed to dryness under reduced pressure and the red-brown powder dried in vacuo. The product was obtained in 55 % yield (325 mg, 0.18 mmol). Crystals were obtained by slow diffusion of pentane into a solution of **[Cp*Rh(L5–2 H$^+$)]$_3$** in benzene.

^{1}H NMR (400 MHz, $CDCl_3$): δ (ppm) = 1.68 (s, 45 H, CH_3, Cp*), 2.05–2.75 (m, br, 24 H, NCH_2, piperazine), 2.25 (s, 9 H, NCH_3, piperazine), 3.27 (d, ^2J = 13 Hz, 3 H, NCH_2), 3.37 (d, ^2J = 13 Hz, 3 H, NCH_2), 5.66 (d, ^3J = 6 Hz, 3 H, pyridone), 6.54 (d, ^3J = 6 Hz, 3 H, pyridone).

^{13}C NMR (101 MHz, $CDCl_3$): δ (ppm) = 9.31 (CH_3, Cp*), 46.30 (NCH_3), 53.43, 55.56, 55.92 (NCH_2, piperazine), 89.83 (d, ^1J(C,Rh) = 8 Hz, C, Cp*), 111.45, 121.36, 130.11, 157.24, 170.53 (pyridone).

Elemental analysis (%) calcd (found) for $C_{63}H_{87}N_9O_6Ru_3 \times 1.5\ CH_2Cl_2$: C 51.46 (51.26), H 6.23 (6.24), N 8.37 (8.31).

VIII.II.5.18 [Cp*Ir(L2–2 H$^+$)]$_3$

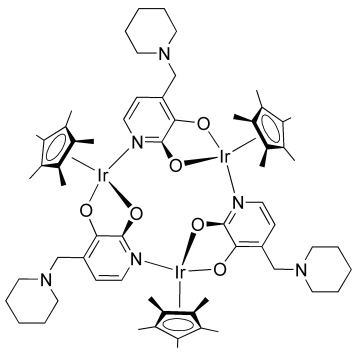

^{1}H NMR (400 MHz, $CDCl_3$): δ (ppm) = 1.25–1.55 (m, br, 18 H, CH_2, piperidine), 1.66 (s, 45 H, Cp*), 2.31 (m, br, 12 H, CH_2, piperidine), 3.25 (d, ^2J = 13 Hz, 3 H, NCH_2), 3.40 (d, ^2J = 13 Hz, 3 H, NCH_2), 5.67 (d, ^3J = 6 Hz, 3 H, pyridone), 6.60 (d, ^3J = 6 Hz, 3 H, pyridone).

VIII.II.5.19 [Cp*Ir(L3–2 H$^+$)]$_3$

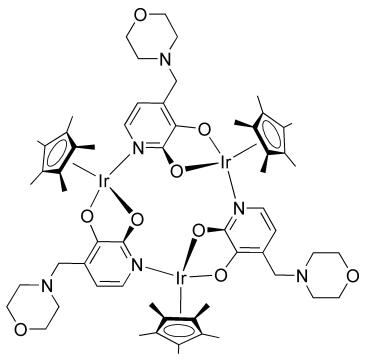

A suspension of complex **11** (398 mg, 0.50 mmol), ligand **L3** (210 mg, 1.00 mmol) and Cs_2CO_3 (815 mg, 2.50 mmol) in degassed methanol (40 mL) was stirred for 2 h at room temperature. After evaporation of the solvent under reduced pressure the product was extracted with dichloromethane (40 mL). Evaporation of the solvent gave an orange powder, which was dried in vacuo. The product was obtained in 59 % yield (321 mg, 0.20 mmol). Crystals were obtained by slow diffusion of pentane into a solution of **[Cp*Ir(L3–2 H$^+$)]$_3$** in dichloromethane.

^{1}H NMR (400 MHz, $CDCl_3$): δ (ppm) = 1.65 (s, 45 H, CH_3, Cp*), 2.35 (m, br, 12 H, CH_2, morpholine), 3.34 (d, ^2J = 3 Hz, 3 H, NCH_2), 3.39 (d, ^2J = 13 Hz, 3 H, NCH_2), 3.63 (m, br, 12 H, CH_2, morpholine), 5.67 (d, ^3J = 6 Hz, 3 H, pyridone), 6.59 (d, ^3J = 6 Hz, 3 H, pyridone).

^{13}C NMR (101 MHz, $CDCl_3$): δ (ppm) = 9.54 (CH_3, Cp*), 54.02, 56.07, 67.38 (CH_2, morpholine), 80.94 (C, Cp*), 111.59, 122.10, 130.51, 158.24, 172.55 (pyridone).

Elemental analysis (%) calcd (found) for $C_{60}H_{81}N_6O_9Ir_3 \times 2\ H_2O$: C 43.86 (43.55), H 5.21 (5.14), N 5.12 (4.74).

VIII.II.5.20 [Cp*Ir(L4–2 H$^+$)]$_3$

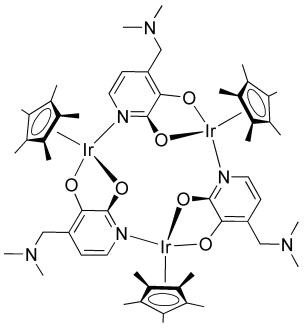

^{1}H NMR (400 MHz, $CDCl_3$): δ (ppm) = 1.66 (s, 45 H, Cp*), 2.12 (s, 18 H, $N(CH_3)_2$), 3.16 (d, ^2J = 13 Hz, 3 H, NCH_2), 3.40 (d, ^2J = 12 Hz, 3 H, NCH_2), 5.68 (d, ^3J = 6 Hz, 3 H, pyridone), 6.61 (d, ^3J = 6 Hz, 3 H, pyridone).

VIII.II.5.21 $[Cp^*Ir(L5–2\ H^+)]_3$

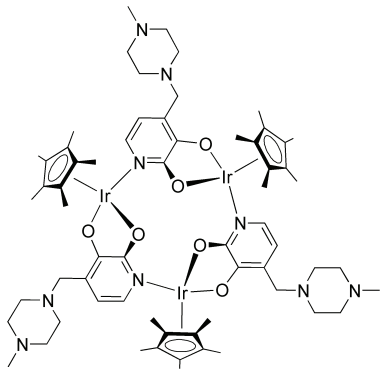

The complex could be obtained as yellow powder in 96 % yield (329 mg, 0.32 mmol).

^{1}H NMR (400 MHz, $CDCl_3$): δ (ppm) = 1.64 (s, 45 H, Cp*), 2.25–2.65 (m, br, 24 H, piperazine), 2.25 (s, 9 H, NCH_3), 3.32 (d, ^2J = 13 Hz, 3 H, NCH_2), 3.41 (d, ^2J = 13 Hz, 3 H, NCH_2), 5.68 (d, ^3J = 6 Hz, 3 H, pyridone), 6.58 (d, ^3J = 6 Hz, 3 H, pyridone).

VIII.II.6 Expanded Triple-Stranded Helicates

Complexes from the self-assembly of **1**, **2** and **8** and the ligands bearing two dihydroxypyridine units **L13**, **L14** and **L15** are presented. They were crystallised from a monomer solution in the presence of NEt_3. The solubilized complexes were sensitive towards acid and $CDCl_3$ used for the NMR spectra was stored over basic Al_2O_3 in order to remove any traces of acid.

General procedure for the synthesis of expanded trinuclear helicates by crystallisation from water: A mixture of halfandwich complex $[(\pi\text{-ligand})MCl_2]_2$ (30 µmol) and the ligand (30.0 µmol) was stirred in water (10 mL) until a clear solution of the dinuclear monomeric complex (3.0 mM) was obtained. NEt_3 was added by either layering it carefully over the aqueous solution or by vapor diffusion. Both methods gave similar yields. Non-crystalline precipitate was separated from the crystals by repeated addition of water and decantation. The crystals were filtered isolated and dried in air. The ligands can be used either without further purification or after purification by HPLC as TFA salts. In the latter case, the yields of the complexes are higher. The purity of the complexes determined by ^{1}H NMR spectroscopy was similar for both methods. If ligands were used without further purification, the crystals had to be separated from a fluffy precipitate by repeated addition of water and decantation.

VIII.II.6.1 $[\{(C_6H_6)Ru\}_2(L13–4\ H^+)]_3$

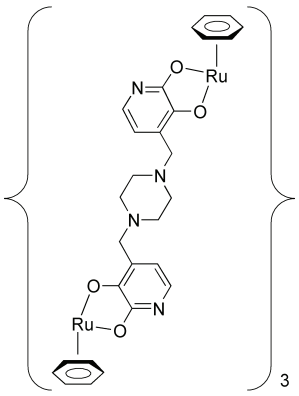

A suspension of halfsandwich complex **1** (15.0 mg, 30.0 µmol) and the TFA salt of ligand **L13** (16.8 mg, 30.0 mmol) was stirred in water (10 mL) until a clear solution of monomer (3 mM) was obtained. The solution was carefully layered with NEt_3. Orange crystals in 52 % yield (14.5 mg, 5.21 µmol) were obtained. Vapour diffusion of NEt_3 into a monomer solution in water showed slightly better yields (16.0 mg, 5.75 µmol, 58 %).

^{1}H NMR (400 MHz, C_2DCl_2): δ (ppm) = 1.42 (m, br, 6 H, NCH_2), 1.85 (m, br, 6 H, NCH_2), 2.27 (m, br, 6 H, NCH_2), 2.59 (m, br, 6 H, NCH_2), 3.12 (d, ^2J = 16 Hz, 6 H, NCH_2), 3.21 (d, ^2J = 16 Hz, 6 H, NCH_2), 5.59 (s, 36 H, C_6H_6), 5.67 (d, ^3J = 6 Hz, pyridone), 6.56 (d, ^3J = 6 Hz, pyridone).

^{1}H NMR (400 MHz, $CDCl_3$): δ (ppm) = 1.47 (m, br, 6 H, NCH_2), 1.88 (m, br, 6 H, NCH_2), 2.47 (m, br, 6 H, NCH_2), 2.69 (m, br, 6 H, NCH_2), 3.24 (d, ^2J = 17 Hz, 6 H, NCH_2), 3.40 (d, ^2J = 17 Hz, 6 H, NCH_2), 5.52 (s, 36 H, C_6H_6), 5.77 (d, ^3J = 6 Hz, pyridone), 6.65 (d, ^3J = 6 Hz, pyridone).

VIII.II.6.2 $[\{(C_6H_5Me)Ru\}_2(L13–4\ H^+)]_3$

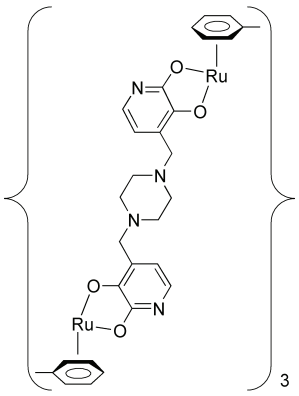

A suspension of complex **2** (15.9 mg, 30.0 µmol) and the TFA salt of ligand **L13** (16.8 mg, 30.0 mmol) was stirred in water (10 mL) until a clear solution of monomer (3 mM) was obtained. The solution was carefully layered with NEt_3. Orange crystals in 60 % yield (14.4 mg, 6.01 µmol) were obtained. Vapour diffusion of NEt_3 into a monomer solution in water showed similar yields (13.0 mg, 5.42 µmol, 54 %).

^{1}H NMR (400 MHz, C_2DCl_2): δ (ppm) = 1.40 (m, br, 6 H, NCH_2), 1.85 (m, br, 6 H, NCH_2), 2.24 (s, 18 H, CH_3), 2.35 (m, br, 6 H, NCH_2), 2.60 (m, br, 6 H, NCH_2), 3.13 (d, ^2J = 17 Hz, 6 H, NCH_2), 3.20 (d, ^2J = 16 Hz, 6 H, NCH_2), 5.16 (m, 18 H, C_6H_5Me), 5.39 (t, ^3J = 6 Hz, C_6H_5Me), 5.57 (t, ^3J = 5 Hz, C_6H_5Me), 5.64 (d, ^3J = 6 Hz, pyridone), 6.51 (d, ^3J = 6 Hz, pyridone).

^{1}H NMR (400 MHz, $CDCl_3$): δ (ppm) = 1.50 (m, br, 6 H, NCH_2), 1.95 (m, br, 6 H, NCH_2), 2.12 (s, 18 H, CH_3), 2.47 (m, br, 6 H, NCH_2), 2.68 (m, br, 6 H, NCH_2), 3.25 (d, ^2J = 17 Hz, 6 H, NCH_2), 3.39 (d, ^2J = 17 Hz, 6 H, NCH_2), 5.13 (d, ^3J = 6 Hz, C_6H_5Me), 5.19 (d, ^3J = 6 Hz, C_6H_5Me), 5.21 (t, ^3J = 6 Hz, C_6H_5Me), 5.54 (t, ^3J = 5 Hz, C_6H_5Me), 5.75 (t, ^3J = 6 Hz, C_6H_5Me), 5.75 (d, ^3J = 6 Hz, pyridone), 6.61 (d, ^3J = 6 Hz, pyridone).

^{13}C NMR (101 MHz, $CDCl_3$): δ (ppm) = 18.83 (Me), 52.00, 55.50 (br, NCH_2, piperazine), 56.36 (NCH_2), 75.65, 76.84, 79.08, 85.28, 85.71, 98.28 (C_6H_5), 108.06, 126.31, 131.76, 153.52, 169.72 (pyridone).

Elemental analysis (%) calcd (found) for $C_{90}H_{96}N_{12}O_{12}Ru_6 \times 14\ H_2O$: C 45.11 (45.23), H 5.22, (4.98), N 7.01 (7.29).

VIII.II.6.3 [{(C_6H_5Me)Ru}$_2$(L14–4 H$^+$)]$_3$

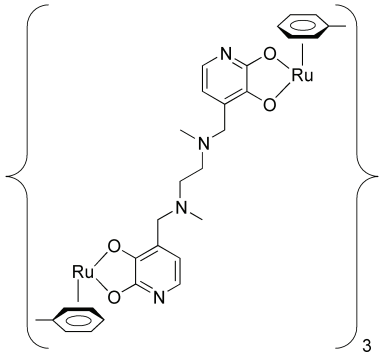

A suspension of complex **2** (39.6 mg, 75.0 µmol) and the unpurified ligand **L14** (25.1 mg, 75.0 mmol) was stirred in water (20 mL) until a clear solution of monomer (7.5 mM) was obtained. The solution was evenly distributed on two test tubes which were placed in a Schlenk containing NEt_3. Red crystals in 38 % yield (450 mg, 19.0 µmol) were obtained. Slow diffusion of NEt_3 into a monomer solution in water showed similar yields (48.8 mg, 20.6 µmol, 41 %).

^{1}H NMR (400 MHz, $CDCl_3$): δ (ppm) = 1.83 (s, 18 H, CH_3), 2.14 (s, 18 H, NCH_3), 3.32 (d, ^2J = 15 Hz, 6 H, NCH_2), 3.49 (d, ^2J = 15 Hz, 6 H, NCH_2), 5.12 (d, ^3J = 6 Hz, C_6H_5Me), 5.14 (d, ^3J = 6 Hz, C_6H_5Me), 5.24 (t, ^3J = 6 Hz, C_6H_5Me), 5.57 (t, ^3J = 5 Hz, C_6H_5Me), 5.69 (t, ^3J = 6 Hz, C_6H_5Me), 5.85 (d, ^3J = 6 Hz, pyridone), 6.55 (d, ^3J = 6 Hz, pyridone).

^{13}C NMR (101 MHz, $CDCl_3$): δ (ppm) = 18.79 (Me), 42.90 (NMe), 55.78, 56.16 (NCH_2), 75.57, 77.09, 78.733, 85.45, 85.84, 98.24 (C_6H_5), 109.95, 126.40, 131,66, 154.11, 170.02 (pyridone).

Elemental analysis (%) calcd (found) for $C_{90}H_{102}N_{12}O_{12}Ru_6 \times 12\ H_2O$: C 45.68 (45.45), H 5.37 (5.05), N 7.10 (7.15).

VIII.II.6.4 $[\{(C_5HMe_4)Rh\}_2(L15–4\ H^+)]_3$

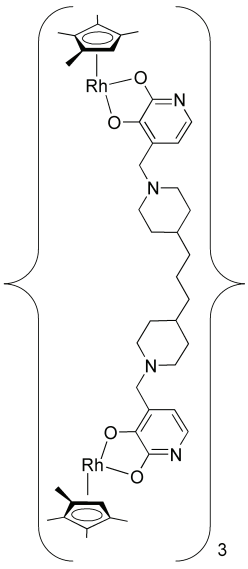

A mixture of half-sandwich complex $[(C_5HMe_4)RhCl_2]_2$ (17.7 mg, 30.0 µmol) and the TFA salt of ligand **L15** (20.5 mg, 30.0 µmol) was stirred in water (10 mL) until a clear solution of monomer (3.0 mM) was obtained. The solution was carefully layered with NEt_3. Red-brown crystals in 30 % yield (9.4 mg, 2.97 µmol) were obtained. Vapour diffusion of NEt_3 into a monomer solution in water showed slightly better yields (11.8 mg, 3.72 µmol, 37 %).

^{1}H NMR (400 MHz, $CDCl_3$): δ (ppm) = 0.84 (m, br, 6 H, CH_2), 1.12 (m, br, 24 H, CH_2), 1.35–1.95 (m, br, 30 H, CH & CH_2), 1.50 (s, 18 H, CH_3), 1.56 (s, 18 H, CH_3), 1.67 (s, 18 H, CH_3), 1.86 (s, 18 H, CH_3), 2.38 (m_c, 6 H, CH_2), 2.67 (m_c, 6 H, CH_2), 3.03 (d, ^2J = 14 Hz, 6 H, NCH_2), 3.74 (d, ^2J = 14 Hz, 6 H, NCH_2), 5.09 (s, 6 H, C_5HMe_4), 5.77 (d, ^3J = 6 Hz, pyridone), 6.68 (d, ^3J = 6 Hz, pyridone).

^{13}C NMR (101 MHz, $CDCl_3$): δ (ppm) = 8.39, 8.68, 10.41, 10.75 (Me), 23.99, 32.65, 33.76, 35.64, 37.69 (CH, CH_2), 53.71, 54.09, 56.29 (NCH_2), 74.38, 81.78, 93.73, 96.98, 100.66 (C_5HMe_4), 111.98, 123.67, 130.68, 155.85, 169.79 (pyridone). The fine structure of the C_5HMe_4 peaks was not resolved enough to determine the ^1J(Rh,C) coupling constants.

Elemental analysis (%) calcd (found) for $C_{129}H_{174}N_{12}O_{12}Rh_6 \times 15\ H_2O$: C 52.12 (52.08), H 6.92 (6.73), N 5.65 (5.83).

VIII.III Measurements

VIII.III.1 Kinetic Measurements

VIII.III.1.a Metal Fragment Exchange Kinetics

Metal fragment exchange between **[(cymene)Ru(L2–H$^+$)]$_3$** and **[(C$_6$H$_3$^{i}Pr$_3$)Ru(L2–H$^+$)]$_3$**: **[(cymene)Ru(L2–H$^+$)]$_3$** (3.1 mg, 3.03 µmol) and **[(C$_6$H$_3$^{i}Pr$_3$)Ru(L2–H$^+$)]$_3$** (3.7 mg, 3.01 µmol) were dissolved in MeOD (0.6 mL). After heating the mixture to 40 °C, ^{1}H NMR measurements were started immediately. The concentration of the symmetric and mixed receptors was determined by integration of suited ^{1}H NMR signals. he total concentration of trimers was 10.1 mM.

Metal fragment exchange between **[(C$_6$H$_6$)Ru(L2–H$^+$)]$_3$** and **[(C$_6$H$_3$^{i}Pr$_3$)Ru(L2–H$^+$)]$_3$**: **[(C$_6$H$_6$)Ru(L2–H$^+$)]$_3$** (2.5 mg, 2.9 µmol) and **[(C$_6$H$_3$^{i}Pr$_3$)Ru(L2–H$^+$)]$_3$** (1.7 mg, 1.4 µmol) were dissolved in MeOD (0.7 mL). After heating the mixture to 40 °C, ^{1}H NMR measurements were started immediately. The concentration of the symmetric and mixed complexes was determined by integration of suited ^{1}H NMR signals. The total concentration of trimers was 6.08 mM.

VIII.III.1.b Li^+ Complexation Kinetics

A solution of LiCl in D_2O (12µL, 0.5 M, 2.0 equiv.) was added to a solution of complex **[(cymene)Ru(L5–2 H$^+$)]$_3$** or **[(cymene)Ru(L2–H$^+$)]$_3$** in D_2O (0.6 mL, 5.0 mM) in an NMR tube (final concentratios: [receptor] = 4.9 mM, [Li^+] = 9.8 mM). The mixture was shaken vigorously and the ^{1}H NMR measurements were started immediately. The concentration of the free receptor and its Li^+ adduct was determined by integration of suited ^{1}H NMR signals.

VIII.III.2 Binding Constants K_a

General procedure for the determination of the binding constant K_a: In a typical experiment, a mixture of the halfsandwich complex [(π-ligand)MCl_2]$_2$ (37.5 µmol) and the respective ligand (75.0 µmol) was stirred in water (4.25 mL) until a clear solution was obtained. CsOH solution (250 µL, 0.3 M) was added to induce the assembly process. The solution was divided in five equal parts (900 µL, 5.56 mM) and stock solutions of various alkali metal salts were added: LiCl (100 µL, 0.10 M, 2.0 equiv.), Na_2SO_4 (125 µL, 2.0 M, 100 equiv.), KOAc (125 µL, 4.0 M, 100 equiv.), CsOAc (125 µL, 4.0 M, 100 equiv.). The mixtures were equilibrated for 24 hours at room temperature. The binding constants K_a were determined by integration of suited ^{1}H NMR signals of

the free and complexed receptor. In most cases, several baseline-separated signals were available and averaged values were employed. The concentration of the receptor in such an experiment was 5.0 mM and the concentration of Li^+ 10.0 mM (2.0 equiv.). For experiments with lower receptor concentration (1.00 mM for **[(C$_5$HMe$_4$)Rh(L5–2 H$^+$)]$_3$** and **[(cymene)Ru(L5–2 H$^+$)]$_3$**) or higher Li^+ concentrations, the amounts were varied accordingly. No binding was observed for potassium or cesium acetate.

The binding constant was calculated as follows. Assumed was the reaction in equilibrium of one molecule trimer (Δ) with one cation Li^+ to give one [ΔLi^+] complex. The association constant K_a is:

$$K_a = \frac{[\Delta Li^+]}{[\Delta] \cdot [Li^+]} \qquad \text{Eq. VIII.1}$$

The total trimer concentration $[\Delta]_{tot}$ and the total Li^+ concentration $[Li^+]_{tot}$ are the sum of the trimer concentration [Δ] or the Li^+ concentration in equilibrium [Li^+], respectively and the concentration of the complexed receptor [ΔLi^+]:

$$[\Delta]_{tot} = [\Delta] + [\Delta Li^+] \qquad \text{Eq. VIII.2}$$

$$[Li^+]_{tot} = [Li^+] + [\Delta Li^+] \qquad \text{Eq. VIII.3}$$

Experimentally, the ratio I of the free and the complexed receptor is accessible:

$$I = \frac{[\Delta Li^+]}{[\Delta]} \qquad \text{Eq. VIII.4}$$

The equilibrium constant can thus be expressed as:

$$K_a = I \cdot \frac{1}{[Li^+]} \qquad \text{Eq. VIII.5}$$

The Li^+ concentration in equilibrium [Li^+] can be calculated by using the ratio of the free and the complexed receptor I and the total trimer and Li^+ concentrations. First, the total trimer concentration $[\Delta]_{tot}$ is divided by the trimer concentration in equilibrium [Δ]:

$$\frac{[\Delta]_{tot}}{[\Delta]} = \frac{[\Delta]}{[\Delta]} + \frac{[\Delta Li^+]}{[\Delta]} \qquad \text{Eq. VIII.6}$$

$$\frac{[\Delta Li^+]}{[\Delta]} = I = \frac{[\Delta]_{tot}}{[\Delta]} - 1 \qquad \text{Eq. VIII.7}$$

Thus, the trimer concentration in equilibrium [Δ] can be expressed as:

$$[\Delta] = \frac{[\Delta]_{tot}}{1 + I} \qquad \text{Eq. VIII.8}$$

This expression is combined with the expression of the total trimer concentration $[\Delta]_{tot}$:

$$[\Delta]_{tot} = \frac{[\Delta]_{tot}}{1+I} + [\Delta Li^+] \qquad \text{Eq. VIII.9}$$

The bound receptor concentration $[\Delta Li^+]$ can now be expressed as a function of the ratio of free and complexed receptor I:

$$[\Delta Li^+] = [\Delta]_{tot} - \frac{[\Delta]_{tot}}{1+I} \qquad \text{Eq. VIII.10}$$

Combined with the expression of the total Li^+ concentration $[Li^+]_{tot}$, the Li^+ concentration in equilibrium $[Li^+]$ is now available:

$$[Li^+] = [Li^+]_{tot} - \left([\Delta]_{tot} - \frac{[\Delta]_{tot}}{1+I}\right) \qquad \text{Eq. VIII.11}$$

$$[Li^+] = [Li^+]_{tot} - [\Delta]_{tot} + \frac{[\Delta]_{tot}}{1+I} \qquad \text{Eq. VIII.12}$$

Finally, the binding constant K_a can be calculated as a function of the ratio of the free and complexed receptor I:

$$K_a = I \cdot \frac{1}{[Li^+]_{tot} - [\Delta]_{tot} + \frac{[\Delta]_{tot}}{1+I}} \qquad \text{Eq. VIII.13}$$

VIII.III.3 Colorimetric Test for Lithium Ions

A stock solution of receptor **[(cymene)Ru(L5–2 H^+)]$_3$** (5.0 mM) was prepared by adding CsOH solution (3.12 mL, 96.0 mM) to a solution of complex **3** (45.9 mg, 75.0 µmol) and ligand **L5** (31.2 mg, 150 µmol) in water (6.88 mL). The nine different samples shown in Figure IV.20 were made by mixing the trimer stock solution (5.0 mM) and a LiCl solution (10.0 mM) with water in the right amounts to obtain the given concentrations. The total volume of each sample amounts to 2.0 mL. After equilibration for 3 h, a solution of $FeCl_3$ in water was added (0.1 M, final Fe_3^+ conc.: 1.7, 3.3 and 5.0 mM). The color changes occurred instantly.

VIII.III.4 Titrations

VIII.III.4.a Potentiometric Titrations

General procedure for the potentiometric titration of monomeric complexes with CsOH: A mixture of the halfsandwich complex $[(\pi\text{-ligand})MCl_2]_2$ (75.0 µmol) and the respective ligand (150 µmol) was stirred in water (10 mL) until a clear solution was obtained. The pH was measured after adding a CsOH stock solution in steps of 0.05 equiv. (78 µL, 96 mM). The reaction mixture was allowed to equilibrate for five minutes after each addition of base. The concentration of the monomeric complex at the beginning of the titration was 15.0 mM. All titration curves are given in chapter IX.V of the Appendix.

General procedure for the potentiometric titration of trimeric complexes with HCl: A solution of the trimeric complex (5.0 mM) was generated in situ: A mixture of the halfsandwich complex $[(\pi\text{-ligand})MCl_2]_2$ (75.0 µmol) and the respective ligand (150 µmol) was stirred in water ($v(H_2O)$ = 10 mL − x mL CsOH solution) until a clear solution was obtained. The trimeric macrocycle formed after addition of 1.0 equiv.[aa] of CsOH (1.56 mL, 96 mM). In case of **[(cymene)Ru(L5–2 H$^+$)]$_3$** and **[(C$_5$HMe$_4$)Rh(L5–2 H$^+$)]$_3$**, 2.0 equiv.[aa] of CsOH were added (3.12 mL). HCl was added in steps of 0.05 equiv.[aa] (76 µL, 0.1 M Titrisol) and the pH measured five minutes after addition. All titration curves with HCl are given in chapter IX.V of the Appendix.

Titrations of **[(cymene)Ru(L5–2 H$^+$)]$_3$** in the presence of LiCl were performed in a similar manner. The LiCl adduct of the complex was generated in situ by mixing $[(cymene)RuCl_2]_2$ (45.9 mg, 75.0 µmol) and ligand **L5** (33.5 mg, 150 µmol) in water ($v(H_2O)$ = 6.88 mL − x mL LiCl solution) until a clear solution was obtained. Then, CsOH solution (3.12 mL, 96 mM, 2.0 equiv.[aa]) and various amounts of a Li^+ stock solution (0.25 equiv.: 125 µL, 0.50 equiv.: 250 µL, 0.75 equiv.: 325 µL, 1.00 equiv.: 500 µL, [LiCl] = 0.1 M; 20 equiv.: 2.0 mL, [LiCl] = 0.5 M). The reaction mixture was equilibrated for three hours. Then, HCl solution was added in steps of 0.05 equiv.[aa] (76µL, 0.1 M Titrisol) and the pH was measured after 500s. The concentration of the **[(cymene)Ru(L5–2 H$^+$)]$_3$ × Li$^+$** complex at the beginning was 5.0 mM. The titration curves in the presence of the different amounts of LiCl are given in chapter IX.V of the Appendix.

The calibration of curve of the pH as a function of the LiCl concentration (Figure IV.19 on page 107) was obtained as follows: A mixture of $[(cymene)RuCl_2]_2$ (206.7 mg, 337.5 µmol) and ligand **L5** (150.7 mg, 675 µmol) was stirred in water (26.44 mL) until a clear orange solution was obtained. After addition of CsOH (14.06 mL, 96 mM, 2.0 equiv.[aa]), a stock solution of the free receptor **[(cymene)Ru(L5–**

aa. Equivalents with respect to the ligand / metal fragments.

2 H^+)]$_3$ (5.56 mM) was obtained. Various amounts of a LiCl stock solution (0.0–2.0 equiv., 0.1 M, 0.1 equiv: 15 µL) were added to samples of 2.7 mL. The sample volume was then completed to 3.0 mL in order to obtain a receptor concentration of 5.0 mM. The reaction mixture was equilibrated for three hours. After addition of 4.5 equiv.[ab] of HCl (150 µL, 0.1 M), the solutions were allowed to equilibrate for five minutes before measuring the pH.

VIII.III.4.b ^{1}H NMR Titrations

A mixture of the halfsandwich complex [(π-ligand)$MCl_2]_2$ (37.5 µmol) and the respective ligand (75 µmol) was stirred in D_2O (4.5 mL) until a clear solution of the corresponding monomer (16.7) was obtained. Incremental amounts of 0.25 equiv. of CsOH in D_2O (25 µL, 0.15 M, 0.25 equiv.) were added to 900 µL monomer solution; the sample solution was completed to 1.0 mL. In case of the mixture of [(cymene)$RuCl_2]_2$ or [$(C_5HMe_4)RhCl_2]_2$ with ligand **L5**, a 0.3 M CsOH solution (12.5µL, 0.3 M, 0.25 equiv.) was employed. The solution was stirred for two minutes before measuring the ^{1}H NMR spectra.

VIII.III.5 Measurement of the ^{7}Li/^{6}Li Isotopic ratio

The ^{7}Li/^{6}Li isotopic ratios were measured by isotope selective laser graphite furnace atomic absorption spectroscopy in cooperation with Dr. H. D. Wizemann from the University of Hohenheim, Germany. The method will be decribed only briefly and for more details it is referred to the literature.[379–381]

The instrumentation used two diode lasers as radiation sources for the simultaneous isotope selective excitation. The LiCl adduct of the corresponding 12-metallacrown-3 complex (7.2 µmol) was solubilized in MeOH (0.5 mL) and diluted with HNO_3 solution (0.1 M, 500 mL). Special care had to be taken not to contaminate the sample with traces of lithium. The concentration of the macrocycle in solution was 14.4 µM which correponds to a lithium concentration of 100 ng/mL. A small sample volume (10–50 µL) was then given into the sealed graphite furnace. After drying and ashing steps the furnace was evacuated to a noble gas pressure of a few hPa and then heated up to approximately 1500–2000 K where free analyte isotopes are generated. In order to suppress the contribution of light radiated by the hot surface of the tube wall or other ambient radiation, the radiation of each diode laser was modulated either by use of a chopper or by sinusoidal wavelength modulation. Wavelength modulation provides a better signal-to-noise ratio and is preferred for small absorbances. The entire transmitted laser intensity was recorded by a photodiode and finally processed by one lock-in amplifier for each laser beam (i.e. for each

ab. Equivalents with respect to the receptor concentration.

isotope). This lock-in amplifier is referenced to the respective modulation frequency or a higher harmonic thereof. For each atomization cycle a transient signal of a few seconds duration was obtained for each isotope.

To avoid lithium carbide formation, the lithium solutions were atomized from a tantalum foil which was placed on the bottom of the graphite tube. For this configuration, the atomization temperature was determined out of the line width to be 1900 K. We measured the Li isotope signals simultaneously by use of two laser diodes. The laser diode used for ^{7}Li detection had to be tuned to match the ^{7}Li D2 (670.962 nm) resonance transition while the other laser diode used for ^{6}Li detection had to be tuned to ^{6}Li D1 (670.994 nm).[379] The two laser beams were collimated and merged by a mirror and a beam splitter. The absorption of ^{6}Li was expected to be only about a few percent of the absorption of ^{7}Li because the isotope abundance of the samples should be in the range of the natural abundance (^{7}Li/^{6}Li = 12.18)[382] and the transition probability of D1 amounts to only one half of the D2 transition probability. Thus, for ^{6}Li detection 2f-wavelength modulation[380] (3.8 kHz) was applied while the light used for ^{7}Li excitation was modulated by a chopper (10 kHz). The introduction of 10 µL of aqueous solutions with a Li content of 100 ng/mL provided approximately 25% ^{7}Li absorption. A part of the emission of each laser was directed through a hot pipe oven which contained a constant amount of Li vapor. This provided permanent signals suitable to control the frequency stability of the diode lasers.

For the determination of the ^{7}Li enrichment, the ^{7}Li/^{6}Li signal intensity ratio measured for the LiCl solution was compared with the corresponding ratio found for the Li bound in the corresponding metallamacrocyle. For each macrocycle, the investigation encompassed ten cycles of the following measurement sequence: LiCl solution, blank solution, 12-metallacrown-3 LiCl adduct solution. The measurements of the blank solution was carried out in order to verify the absence of memory effects. When the solution of the macrocycle and the LiCl solution contained the same quantity of Li, it was found that the signals obtained by introduction of solutions of the metallamacrocycles were reduced to approximately 2/3 compared with the signal of the LiCl solution. This observation is referred to a matrix effect.[383] Since both isotopes are affected by a matrix effect in the same way, it will have no influence on the measured isotope signal ratio. The ^{7}Li/^{6}Li peak height ratio as well as the ratio for the peak area was determined for the simultaneously measured ^{7}Li and ^{6}Li signals. The ratio obtained for area evaluation was always a little bit larger than the peak height ratio. This is caused by the faster diffusion of ^{6}Li out of the region of interaction due to its lower mass.[379] The standard deviation of the ^{7}Li/^{6}Li ratio mean value for ten measurements was below 1.5%.

According to the usual definition of isotope enrichment[384] the enrichment of the ^{7}Li isotope in the macrocycle is given by Equation V.7 of chapter V.III.

Chapter IX
Appendix

IX.I Abbreviatons

br	broad
CL	Combinatorial Library
COT	Cyclooctatriene
d	dublett
DCC	Dynamic Combinatorial Chemistry
DCL	Dynamic Combinatorial Library
DDQ	2,3-Dichloro-5,6-dicyano-1,4-benzoquinone
e.g.	exempli gratia
EM	Effective Molarity
equiv.	equivalent
ESI	Electrospray Ionisation
et al.	et altera (and others)
HOMO	Highest Occupied Molecular Orbital
ICP	Inductively Coupled Plasma
i.e.	id est
LUMO	Lowest Unoccupied Molecular Orbital
lsac	Lower Self-Assembly Concentration
MeOH	Methanol
PBS	Phosphate Buffer Solution
q	quartuplett
s	singulett
sept	septuplett
t	triplett
PCT	Photoinduced Electron Transfer
PET	Photoinduced Charge Transfer
ppm	parts per million
δ	Chemical shift (ppm)

IX.II List of Complexes

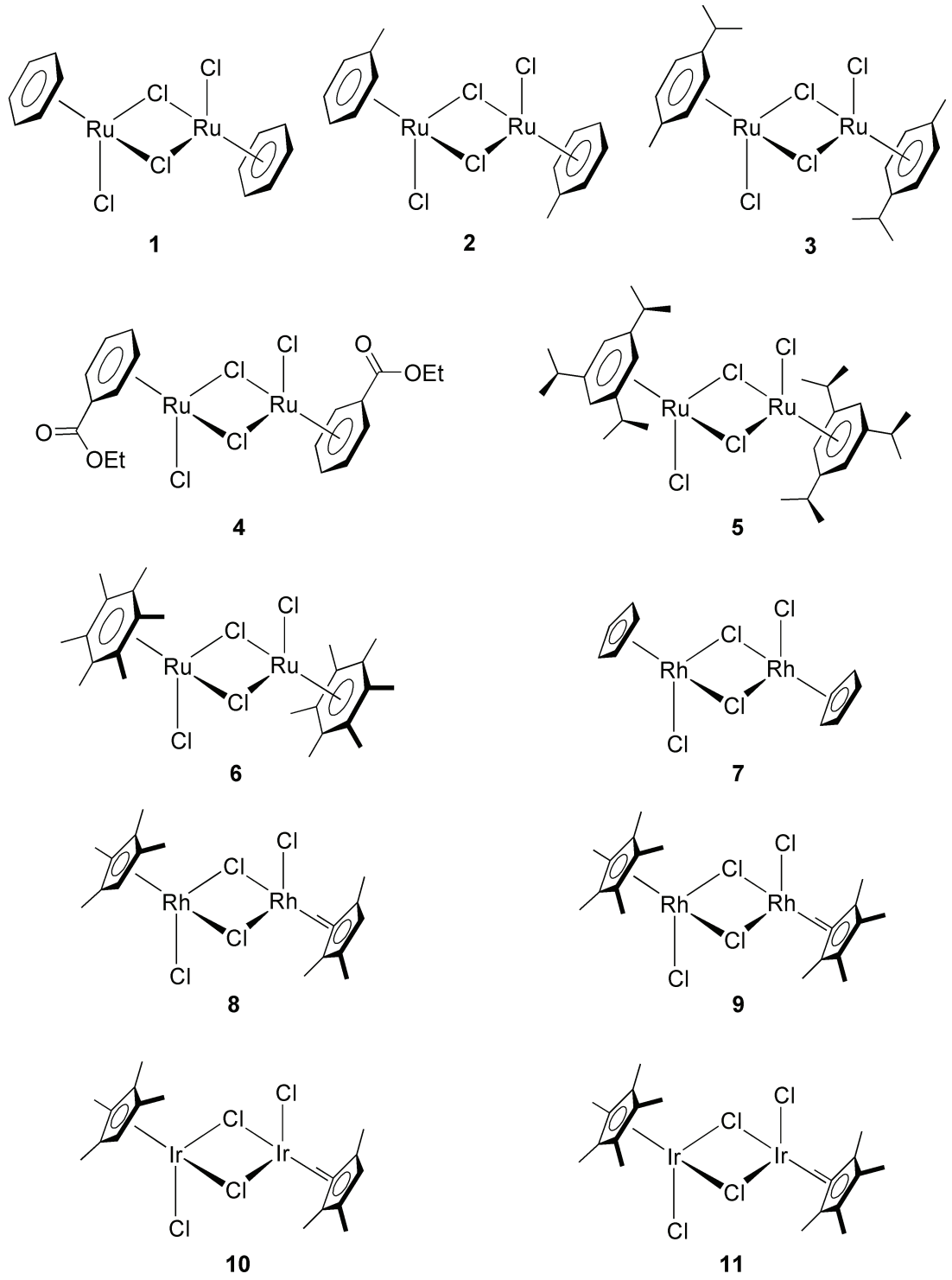

Figure IX.1 Halfsandwich Complexes [(π-ligand)$MCl_2]_2$.

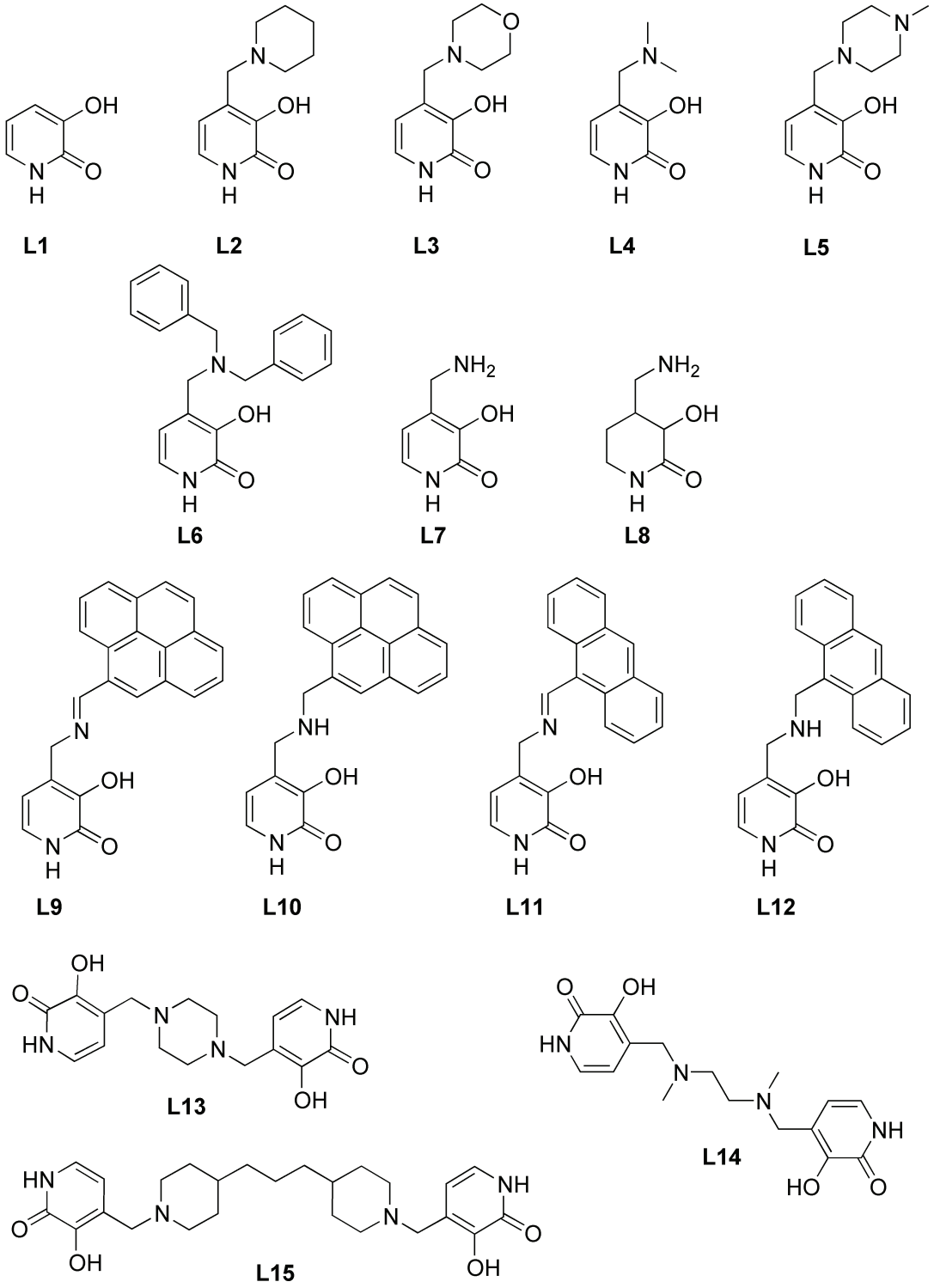

Figure IX.2 Bridging ligands based on the structural 3-hydroxy-2-pyridone motif.

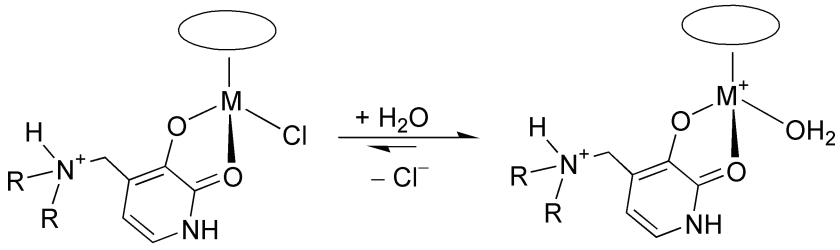

Figure IX.3 General structure of monomers formed by [(π-ligand)MCl_2]$_2$ and 2.0 equiv. of the ligands **L2**, **L3**, **L4** or **L5**.

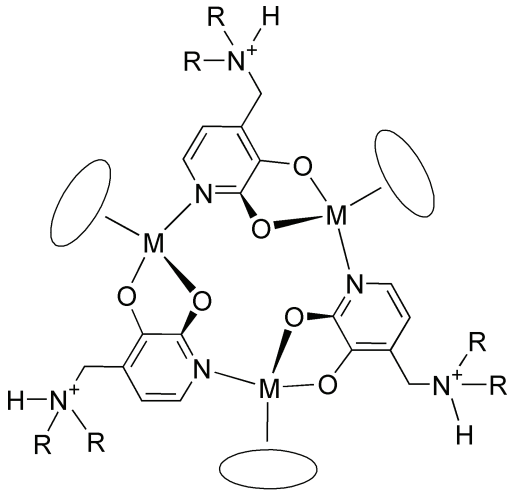

Figure IX.4 General structure of water soluble trinuclear 12-metallacrown-3 complexes formed by self-assembly of [(π-ligand)MCl_2]$_2$, 2.0 equiv. of the ligands **L2**, **L3**, **L4** or **L5** and 1.0 equiv. CsOH.

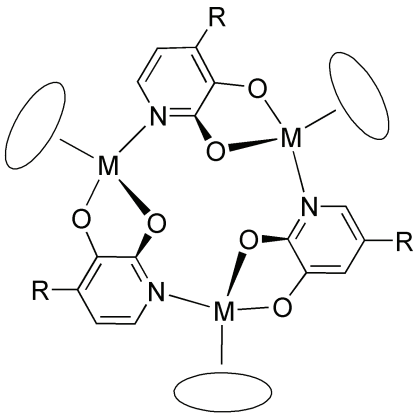

Figure IX.5 General structure of trinuclear 12-metallacrown-3 complexes formed by self-assembly of [(π-ligand)MCl_2]$_2$ and 2.0 equiv. of the ligands **L1**, **L2**, **L3**, **L4** or **L5** in MeOH in the presence of and Cs_2CO_3. Use of the ligands **L6**, **L7**, **L10** or **L12** are expected to assemble into similar structures.

IX.III Available ^{1}H NMR Data

Table IX.1: Available ^{1}H NMR data of monomeric complexes [(π-ligand)M(H_2O)]$^{2+}$ in D_2O composed of the respective metal fragment and ligand.[a]

Metal Fragment	L2	L3	L4	L5
(C_6H_6)Ru	✓	n.d.	n.d.	✓
(C_6H_5Me)Ru	✓	n.d.	n.d.	✓
(cymene)Ru	✓[b]	✓[b]	✓[b]	✓
($C_6H_5CO_2Et$)Ru	✓	n.d.	n.d.	✓
($C_6H_3{}^iPr_3$)Ru	✓[b]	n.d.	n.d.	✓
(C_6Me_6)Ru	✓[c]	✓[c]	✓[c]	✓
CpRh	✓	n.d.	n.d.	✓
(C_5HMe_4)Rh	✓	n.d.	n.d.	✓
Cp*Rh	✓	n.d.	n.d.	✓
(C_5HMe_4)Ir	✓	n.d.	n.d.	✓
Cp*Ir	✓	n.d.	n.d.	✓

a. n.d.: not determined
b. Crystals (not suited for single crystal X-ray analysis) were obtained from $CHCl_3$ or CH_2Cl_2 and pentane or Et_2O.
c. Crystals suited for single crystal X-ray analysis were obtained from $CHCl_3$ or CH_2Cl_2 and pentane or Et_2O.

Table IX.2: Available ^{1}H NMR data of trimeric complexes [(π-ligand)M(ligand–H^+)]$_3$ and their LiCl adducts[a] in D_2O, obtained from [(π-ligand)MCl_2]$_2$, ligands **L2**, **L3**, **L4** or **L5** and 1.0 equiv. CsOH.[b]

Metal Fragment	L2	L3	L4	L5
(C_6H_6)Ru	✓[c]	n.d.	n.d.	✓
(C_6H_5Me)Ru	✓[c]	n.d.	n.d.	✓
(cymene)Ru	✓[c]	✓[c]	✓[c]	✓[c,d]
($C_6H_5CO_2Et$)Ru	✓[c]	n.d.	n.d.	✓
($C_6H_3{}^iPr_3$)Ru	No ^{1}H NMR data available due to the low solublity of the resulting complexes in water.			
(C_6Me_6)Ru				
CpRh	✓	n.d.	n.d.	✓
(C_5HMe_4)Rh	✓	n.d.	n.d.	✓[d]
Cp*Rh	✓[e]	n.d.	n.d.	✓
(C_5HMe_4)Ir	✓	n.d.	n.d.	✓
Cp*Ir	✓[c]	n.d.	n.d.	✓

a. For LiCl adducts, also ^{7}Li NMR data is available.
b. n.d.: not determined
c. Trimerisation was observed also in phosphate buffer solution (100 mM, pH 7.0).
d. 2.0 equiv. of CsOH were used.
e. Trimerisation in phosphate buffer solution (100 mM, pH 7.0) was not observed.

Table IX.3: Available ^{1}H NMR data of trimeric complexes [(π-ligand)M(ligand–2 H^+)]$_3$ in $CDCl_3$ synthesised from [(π-ligand)MCl_2]$_2$ and ligands **L1**, **L2**, **L3**, **L4** or **L5** in the presence of Cs_2CO_3.[a]

Metal Fragment	**L1**	**L2**	**L3**	**L4**	**L5**
$(C_6H_6)Ru$	Ref. [124][b,c]	n.d.	n.d.	n.d.	n.d.
$(C_6H_5Me)Ru$	✓[b,c]	n.d.	n.d.	n.d.	n.d.
(cymene)Ru	Ref. [126][b,c,d]	✓[b]	✓[b]	✓	✓[b]
$(C_6H_5CO_2Et)Ru$	Ref. [165][b,c,d]	n.d.	n.d.	n.d.	n.d.
$(C_6H_3{}^iPr_3)Ru$	✓[b,c]	✓	✓	✓	✓
$(C_6Me_6)Ru$	Ref. [124][b]	✓	✓	✓	✓
CpRh	n.d.	✓	n.d.	n.d.	✓
$(C_5HMe_4)Rh$	✓[b,c]	n.d.	n.d.	n.d.	n.d.[b]
Cp*Rh	Ref. [124][b,c]	✓	✓	✓	✓[b]
$(C_5HMe_4)Ir$	n.d.	n.d.	n.d.	n.d.	n.d.
Cp*Ir	Ref. [166]	✓	✓[b]	✓	✓

a. n.d.: not determined
b. Crystals suited for single crystal X-ray analysis were obtained.
c. The LiCl adduct was crystallised too.
d. The NaCl adduct was crystallised too.

IX.IV Physical Properties

IX.IV.1 Water Solubility of 12-Metallacrown-3 Complexes

Table IX.4: Equivalents of CsOH[a] after which precipitation of mixtures containing the respective metal fragment and ligand occured.[b]

Metal Fragment	L2	L3	L4	L5
$(C_6H_6)Ru$	1.85	soluble	soluble	soluble
$(C_6H_5Me)Ru$	1.85	soluble	soluble	soluble
(cymene)Ru	1.25	1.55	1.65	soluble
$(C_6H_5CO_2Et)Ru$	1.50	n.d.	n.d.	soluble
CpRh	soluble	soluble	soluble	soluble
$(C_5HMe_4)Rh$	1.55	soluble	soluble	soluble
Cp*Rh	1.40	n.d.	n.d.	1.50
$(C_5HMe_4)Ir$	1.25	n.d.	n.d.	1.60
Cp*Ir	1.15	1.25	1.50	1.30

a. Equivalents with respect to the ligand.
b. n.d.: not determined; soluble means that no precipitation was observed after addition of 2.0 equiv. of CsOH

IX.IV.2 Li^+ Binding Constants in Water

Table IX.5: Binding constants K_a for the complexation of Li^+ of trimeric 12-metallacrown-3 complexes $[(\pi\text{-ligand})M(\text{ligand}{-}H^+)]_3$ in M^{-1}[a].

Metal Fragment	L2	L3	L4	L5
$(C_6H_6)Ru$	$7.5 \pm 0.6 \times 10^2$	n.d.	n.d.	$4.0 \pm 0.6 \times 10^3$
$(C_6H_5Me)Ru$	$1.2 \pm 0.6 \times 10^3$	n.d.	n.d.	$5.4 \pm 0.5 \times 10^3$
(cymene)Ru	$2.1 \pm 0.6 \times 10^3$	$2.3 \pm 0.6 \times 10^3$	$2.4 \pm 0.6 \times 10^3$	$5.8 \pm 1.0 \times 10^4$ [b]
$(C_6H_5CO_2Et)Ru$	$2.8 \pm 0.6 \times 10^1$	n.d.	n.d.	n.d.[c]
CpRh	$2.9 \pm 0.5 \times 10^2$	n.d.	n.d.	$2.7 \pm 0.6 \times 10^3$
$(C_5HMe_4)Rh$	$1.3 \pm 0.2 \times 10^4$	n.d.	n.d.	$5.6 \pm 2.1 \times 10^4$ [b]
Cp*Rh	$1.3 \pm 0.4 \times 10^1$	n.d.	n.d.	n.d.[d]
$(C_5HMe_4)Ir$	$2.6 \pm 0.5 \times 10^2$	n.d.	n.d.	$1.2 \pm 0.6 \times 10^3$
Cp*Ir	$9.0 \pm 2.0 \times 10^{-2}$	n.d.	n.d.	$< 5 \times 10^{-2}$

a. Binding constants were determined by ^1H NMR spectroscopy at receptor concentrations of 5.0 mM. The trimeric complexes were generated in situ from mixtures of $[(\pi\text{-ligand})MCl_2]_2$, 2.0 equiv. of the corresponding ligand and 1.0 equiv. of CsOH.
b. 2.0 equiv. of CsOH were employed.
c. The integrals of the free and complexed receptors were not suited to determine a binding constant.
d. The complex precipitated before trimerisation was complete.

IX.IV.3 pK_a of Water Soluble 12-Metallarown-3 Complexes

Table IX.6: pka_1[a] of complexes containing the corresponding metal fragment and ligand.[b]

Metal Fragment	**L2**	**L3**	**L4**	**L5**
—	10.8	n.d.	10.3	9.5
$(C_6H_6)Ru$	5.7	n.d.	n.d.	n.d.
$(C_6H_5Me)Ru$	5.4	n.d.	n.d.	n.d.
(cymene)Ru	5.5	5.4	5.4	6.1
$(C_6H_5CO_2Et)Ru$	4.4	n.d.	n.d.	n.d.
CpRh	5.3	n.d.	n.d.	n.d.
$(C_5HMe_4)Rh$	6.9	n.d.	n.d.	7.1
Cp*Rh	7.6	n.d.	n.d.	n.d.
$(C_5HMe_4)Ir$	4.9	n.d.	n.d.	n.d.
Cp*Ir	5.3	5.2	5.3	5.9

a. pH after addition of 0.5 equiv. CsOH.
b. n.d.: not determined.

Table IX.7: pka_2[a] of complexes containing the corresponding metal fragment and ligand.[b]

Metal Fragment	**L2**	**L3**	**L4**	**L5**
—	11.8	n.d.	11.7	11.6
$(C_6H_6)Ru$	9.4	n.d.	n.d.	n.d.
$(C_6H_5Me)Ru$	9.2	n.d.	n.d.	n.d.
(cymene)Ru	9.1	7.1	9.1	8.1
$(C_6H_5CO_2Et)Ru$	9.1	n.d.	n.d.	n.d.
CpRh	9.4	n.d.	n.d.	n.d.
$(C_5HMe_4)Rh$	9.7	n.d.	n.d.	8.4
Cp*Rh	9.9	n.d.	n.d.	n.d.
$(C_5HMe_4)Ir$	8.5	n.d.	n.d.	n.d.
Cp*Ir	8.9	6.6	8.7	7.4

a. pH after addition of 1.5 equiv. CsOH.
b. n.d.: not determined

IX.IV.4 pH of Monomeric and Trimeric Complexes

Table IX.8: pH[a] of monomeric complexes $[(\pi\text{-ligand})M(H_2O)]^{2+}$ composed of the corresponding metal fragment and ligand.[b]

Metal Fragment	**L2**	**L3**	**L4**	**L5**
—	8.6	7.7	8.3	8.5
$(C_6H_6)Ru$	4.8	n.d.	n.d.	n.d.
$(C_6H_5Me)Ru$	4.4	n.d.	n.d.	n.d.
(cymene)Ru	4.2	3.4	3.3	4.7
$(C_6H_5CO_2Et)Ru$	3.5	n.d.	n.d.	n.d.
CpRh	4.4	n.d.	n.d.	n.d.
$(C_5HMe_4)Rh$	5.1	n.d.	n.d.	5.0
Cp*Rh	5.5	n.d.	n.d.	n.d.
$(C_5HMe_4)Ir$	3.9	n.d.	n.d.	n.d.
Cp*Ir	4.2	4.1	4.1	4.8

a. pH before addiotion of CsOH.
b. n.d.: not determined.

Table IX.9: pH[a] of trimeric complexes $[(\pi\text{-ligand})M(\text{ligand}{-}H^+)]_3$ composed of the corresponding metal fragment and ligand.[b]

Metal Fragment	**L2**	**L3**	**L4**	**L5**
—	11.4	n.d.	11.2	10.8
$(C_6H_6)Ru$	7.9	n.d.	n.d.	n.d.
$(C_6H_5Me)Ru$	6.9	n.d.	n.d.	n.d.
(cymene)Ru	7.5	6.1	6.7	7.1[c]
$(C_6H_5CO_2Et)Ru$	7.3	n.d.	n.d.	n.d.
CpRh	7.9	n.d.	n.d.	n.d.
$(C_5HMe_4)Rh$	7.8	n.d.	n.d.	7.7[c]
Cp*Rh	8.7	n.d.	n.d.	n.d.
$(C_5HMe_4)Ir$	n.d.	n.d.	n.d.	n.d.
Cp*Ir	7.9	6.1	7.1	7.1

a. pH after addition of 1.0 equiv. CsOH.
b. n.d.: not determined
c. Trimerisation was not complete.

IX.V pH Triggered Assembly

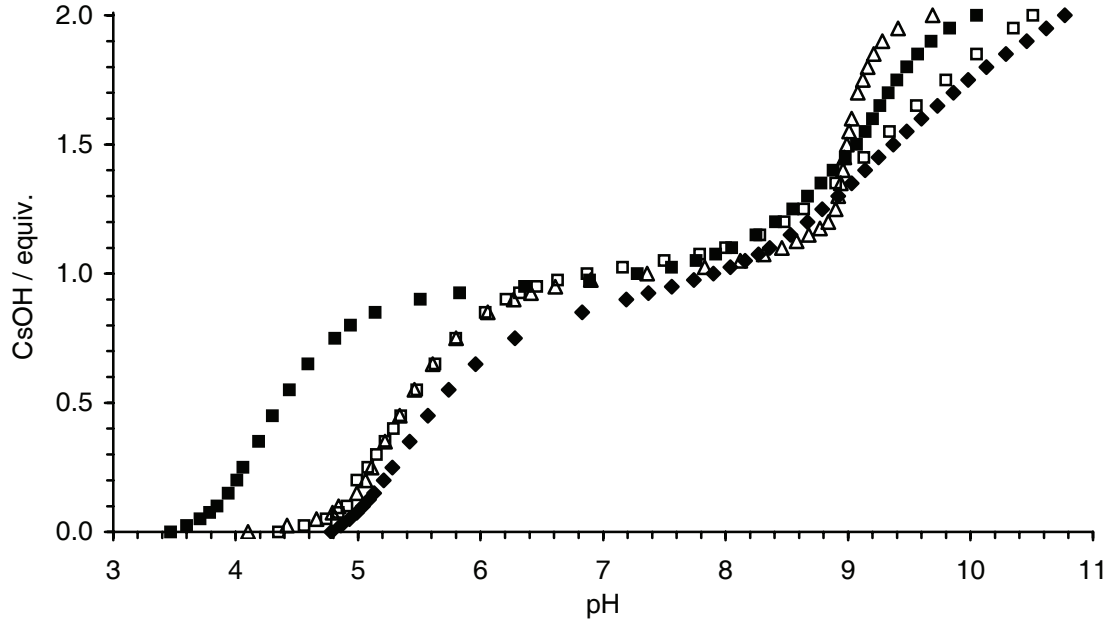

Figure IX.6 The pH of solutions containing the ligand **L2** (15.0 mM) and the complexes **1** (◆), **2** (□), **3** (Δ) and **4** (■) ([Ru] = 15.0 mM) after addition of increasing amounts of CsOH (0.0–2.0 equiv. with respect to the ligand).

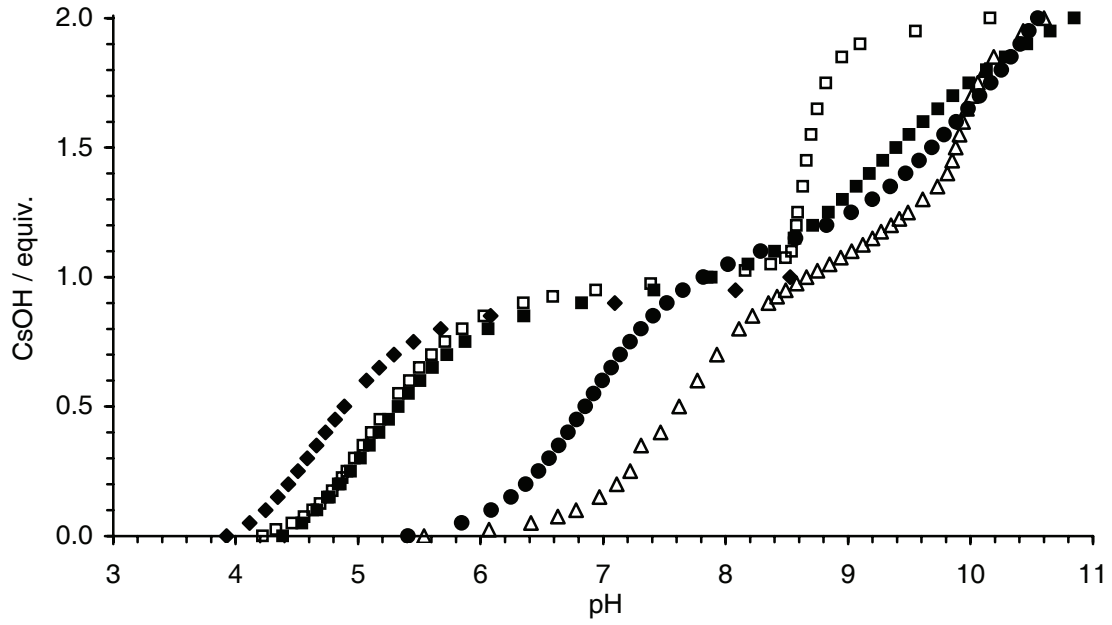

Figure IX.7 The pH of solutions containing the ligand **L2** (15.0 mM) and the complexes **7** (■), **8** (●), **9** (Δ), **10** (◆) and **11** (□) ([Rh] = [Ir] = 15.0 mM) after addition of increasing amounts of CsOH (0.0–2.0 equiv. with respect to the ligand).

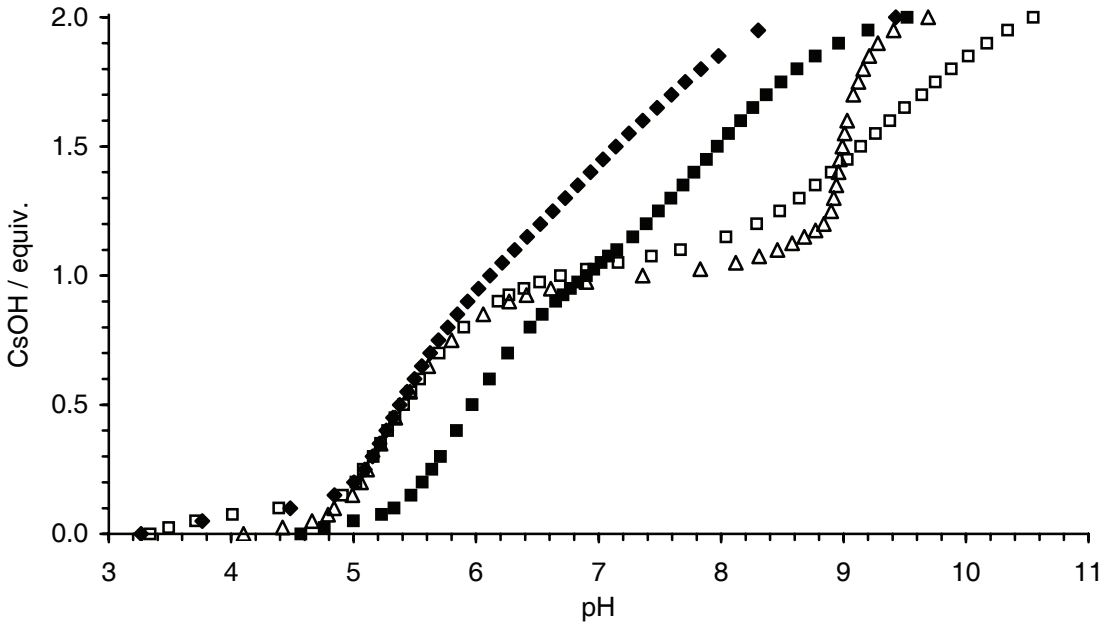

Figure IX.8 The pH of solutions containing the complex **3** ([Ru] = 15.0 mM) and the ligands **L2** (Δ), **L3** (◆), **L4** (□) and **L5** (■) (15.0 mM) after addition of increasing amounts of CsOH (0.0–2.0 equiv. with respect to the ligand).

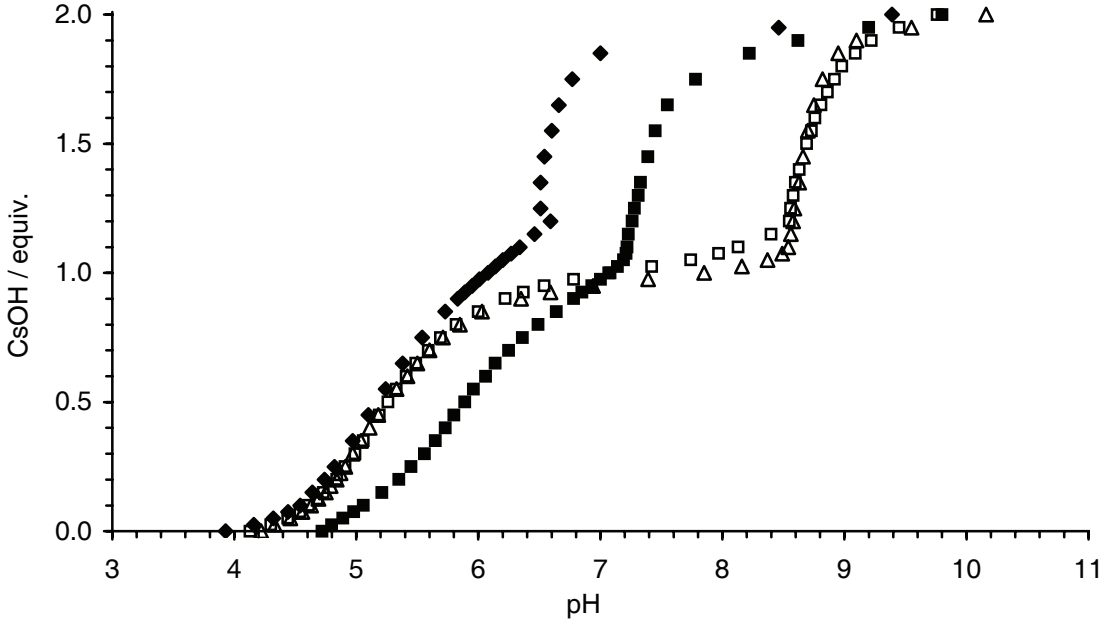

Figure IX.9 The pH of solutions containing the complex **11** ([Ir] = 15.0 mM) and the ligands **L2** (Δ), **L3** (◆), **L4** (□) and **L5** (■) (15.0 mM) after addition of increasing amounts of CsOH (0.0–2.0 equiv. with respect to the ligand).

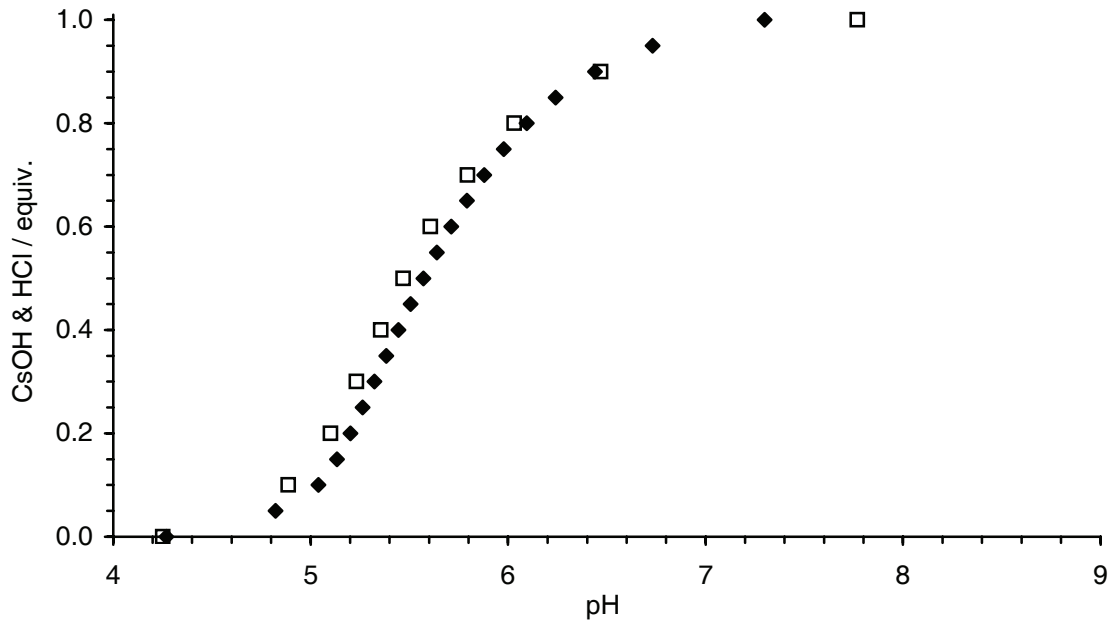

Figure IX.10 The pH of solutions containing the complex **3** ([Ru] = 15.0 mM) and the ligand **L2** (15.0 mM) after addition of increasing amounts of CsOH (◆), and subsequent addition of HCl (□) (0.0–1.0 equiv. with respect to the ligand).

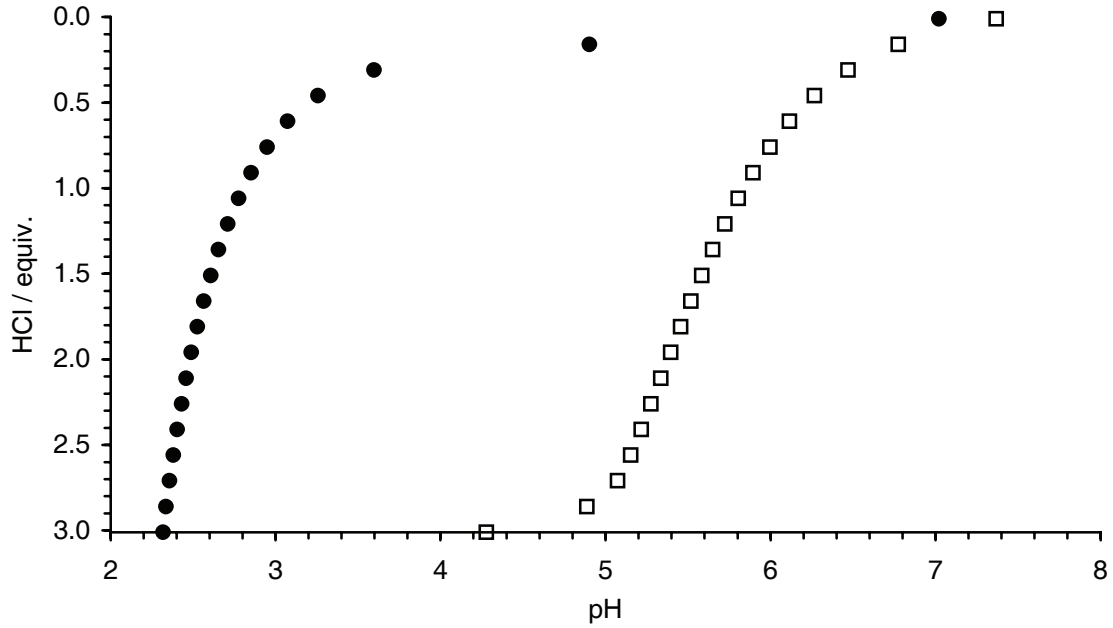

Figure IX.11 pH of solutions containing receptor **[(cymene)Ru(L2**−**1 H^+)]$_3$** (5.0 mM) after addition of increasing amounts of HCl (0.0–3.0 equiv. with respect to the receptor). The titrations were performed in the presence of 20 equiv. $LiNO_3$ (●) and without $LiNO_3$ (□).

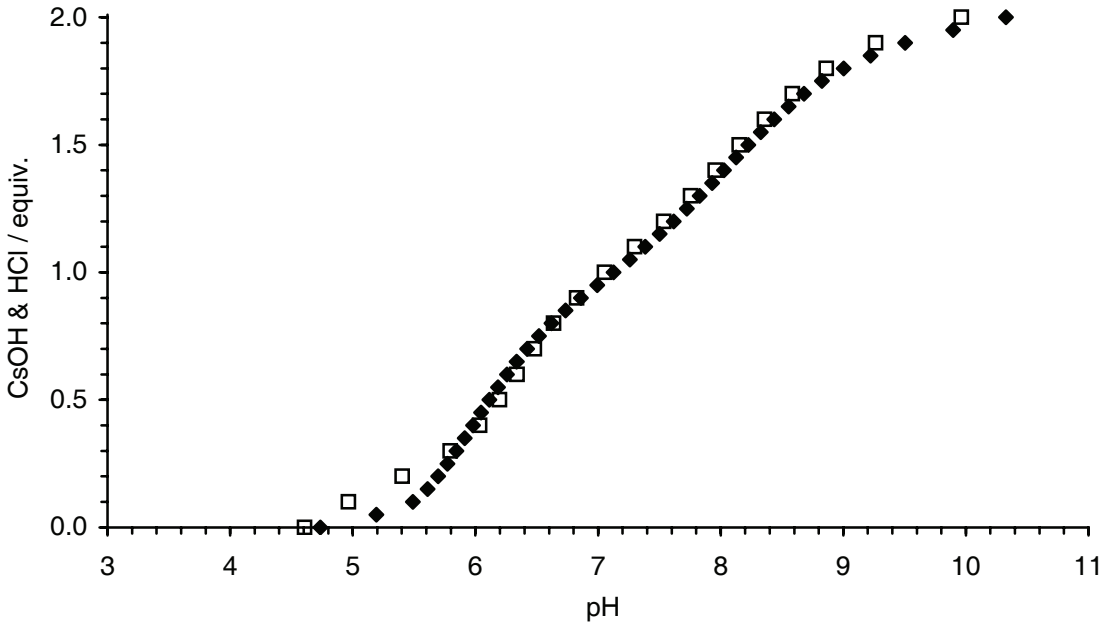

Figure IX.12 The pH of solutions containing the complex **3** ([Ru] = 15.0 mM) and the ligand **L5** (15 mM) after addition of increasing amounts of CsOH (◆), and subsequent addition of HCl (□) (0.0–2.0 equiv. with respect to the ligand).

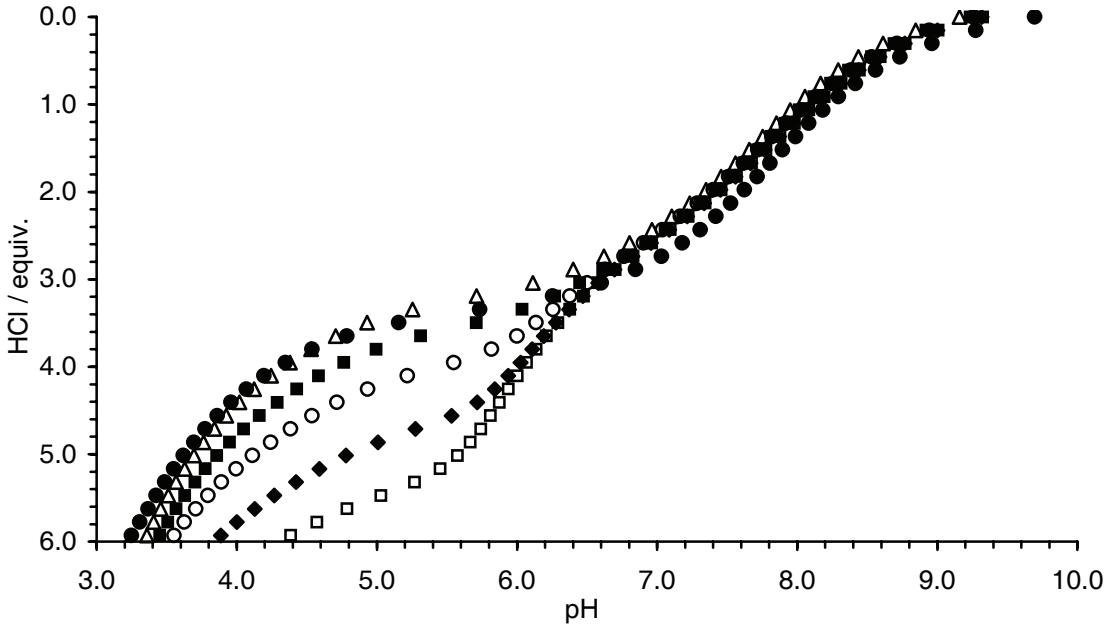

Figure IX.13 pH of solutions containing receptor **[(cymene)Ru(L5**–**2 H$^+$)]$_3$** (5.0 mM) after addition of increasing amounts of HCl (0.0–3.0 equiv. with respect to the receptor). The titrations were performed in the presence of 20 equiv. $LiNO_3$ (●), 1.00 equiv. $LiNO_3$ (Δ), 0.75 equiv. $LiNO_3$ (■), 0.50 equiv. $LiNO_3$ (❍), 0.25 equiv. $LiNO_3$ (◆) and without $LiNO_3$ (□).

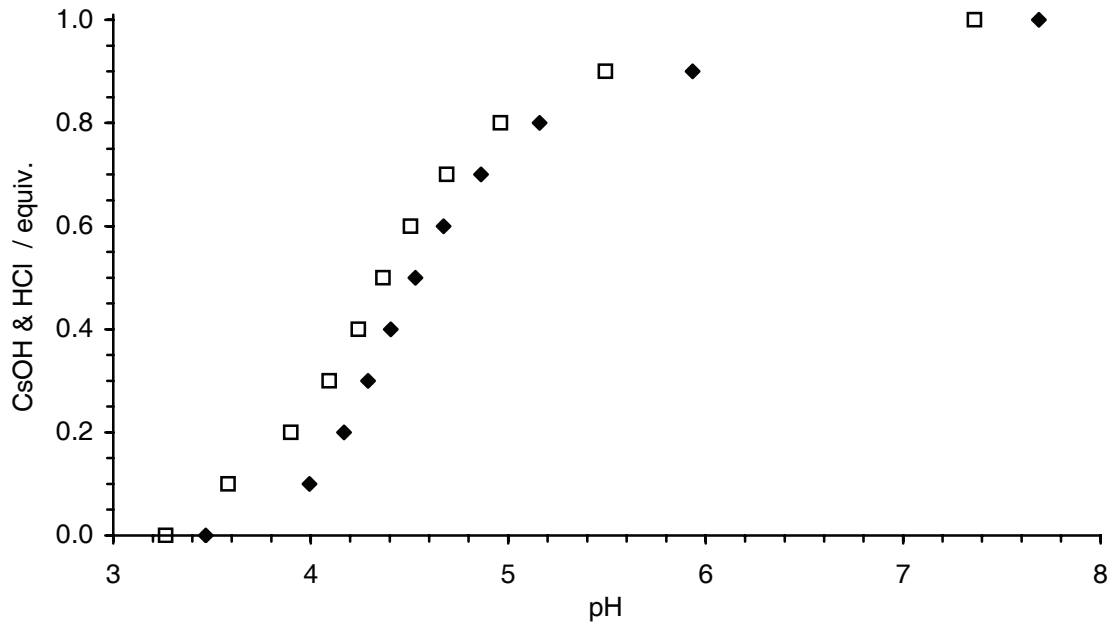

Figure IX.14 The pH of solutions containing the complex **4** ([Ru] = 15.0 mM) and the ligand **L2** (15 mM) after addition of increasing amounts of CsOH (◆), and subsequent addition of HCl (□) (0.0–1.0 equiv. with respect to the ligand).

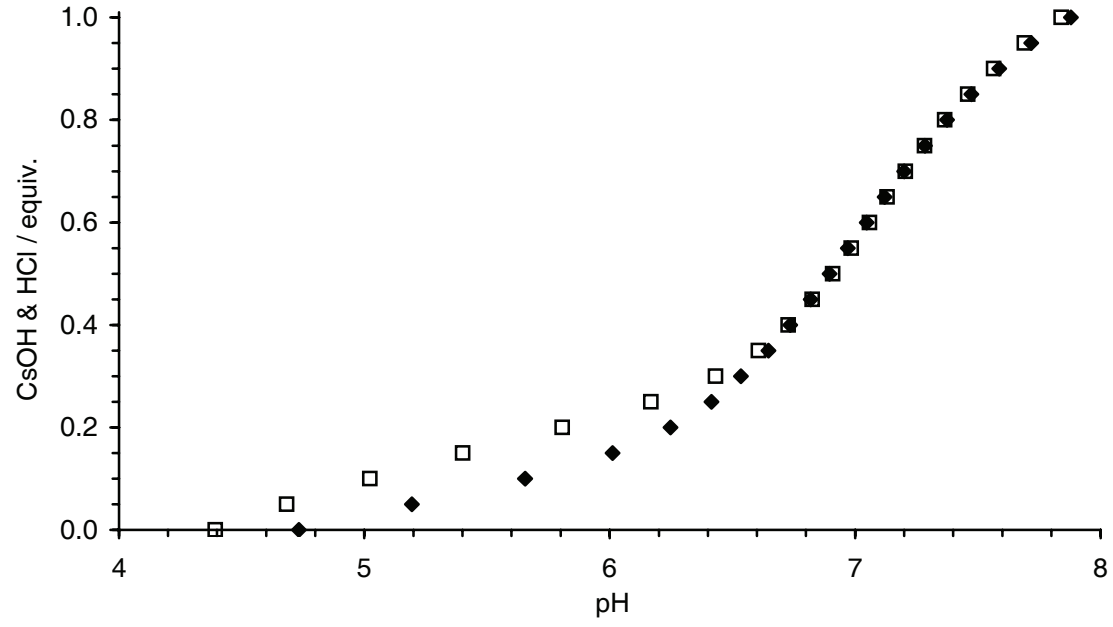

Figure IX.15 The pH of solutions containing the complex **8** ([Rh] = 15.0 mM) and the ligand **L2** (15 mM) after addition of increasing amounts of CsOH (◆), and subsequent addition of HCl (□) (0.0–1.0 equiv. with respect to the ligand).

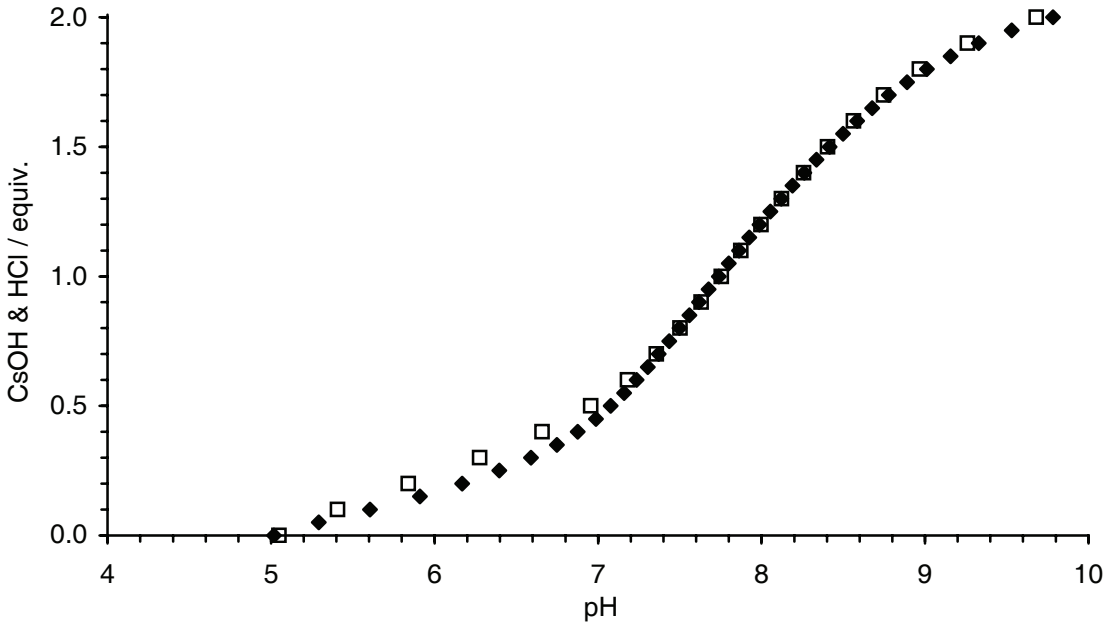

Figure IX.16 The pH of solutions containing the complex **8** ([Rh] = 15.0 mM) and the ligand **L5** (15 mM) after addition of increasing amounts of CsOH (◆), and subsequent addition of HCl (□) (0.0–2.0 equiv. with respect to the ligand).

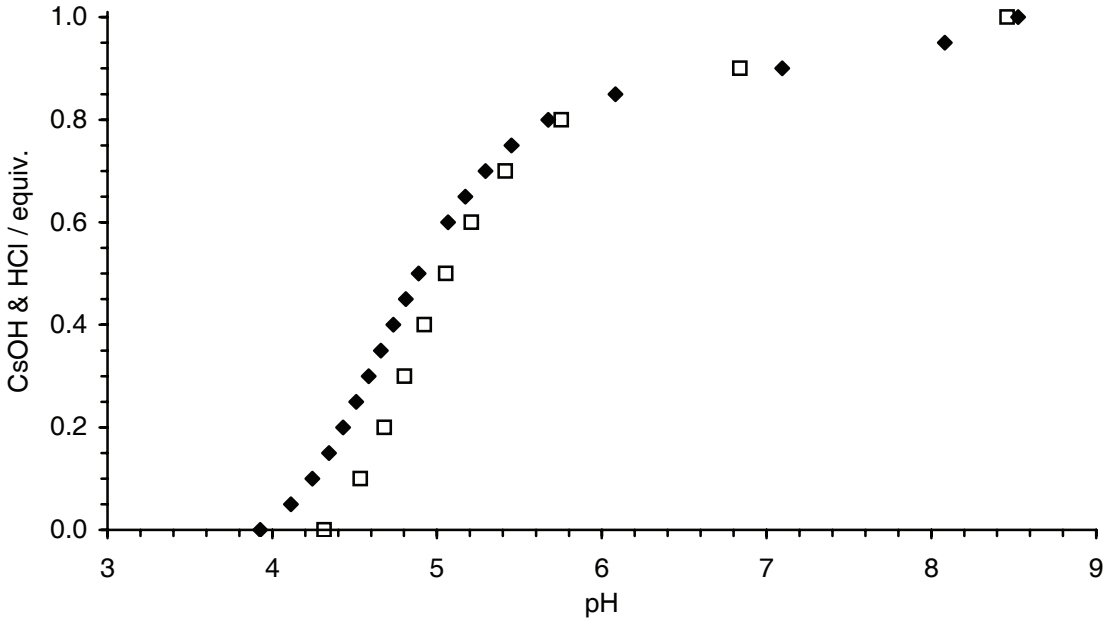

Figure IX.17 The pH of solutions containing the complex **10** ([Ir] = 15.0 mM) and the ligand **L2** (15 mM) after addition of increasing amounts of CsOH (◆), and subsequent addition of HCl (□) (0.0–1.0 equiv. with respect to the ligand).

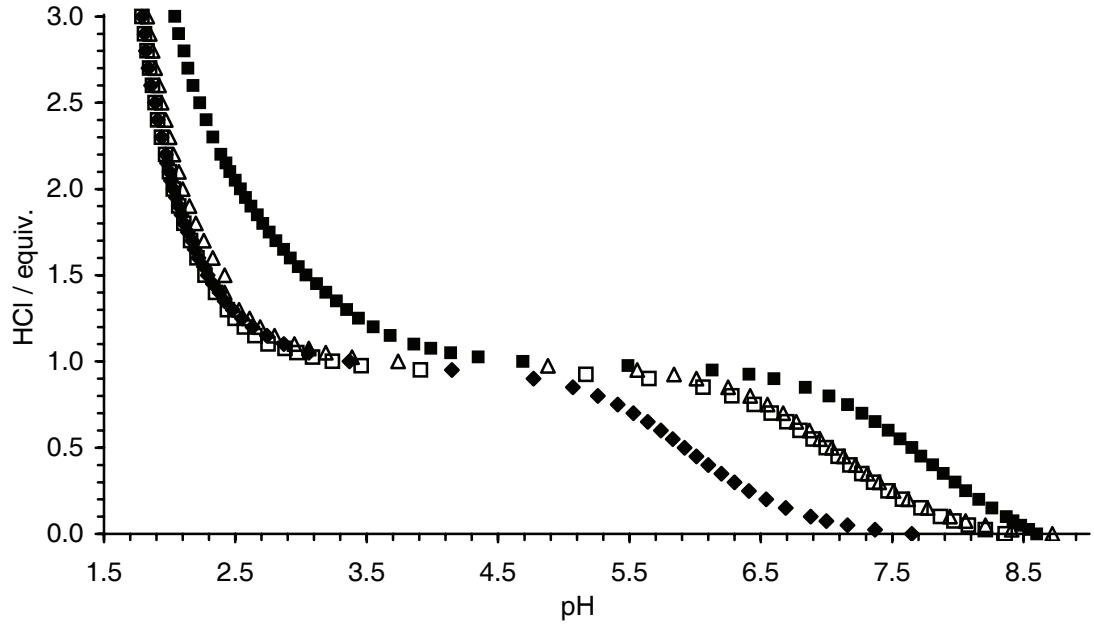

Figure IX.18 pH of solutions containing the ligands **L2** (Δ), **L3** (◆), **L4** (□) and **L5** (■) (15.0 mM) after addition of increasing amounts of HCl (0.0–3.0 equiv.).

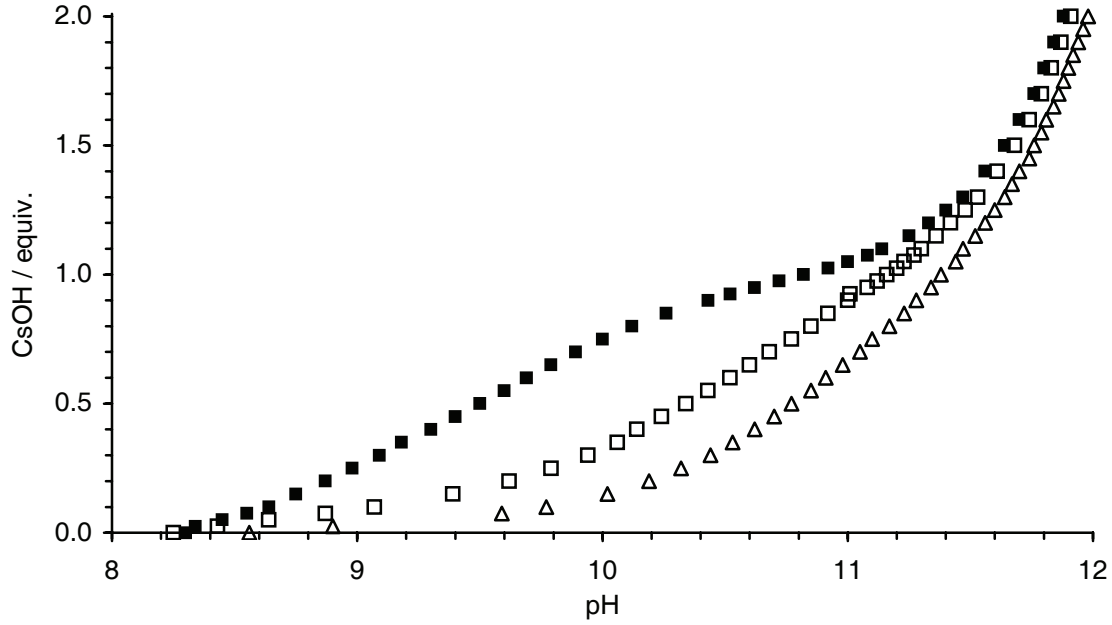

Figure IX.19 pH of solutions containing the ligands **L2** (Δ), **L4** (□) and **L5** (■) (15.0 mM) after addition of increasing amounts of CsOH (0.0–2.0 equiv.).

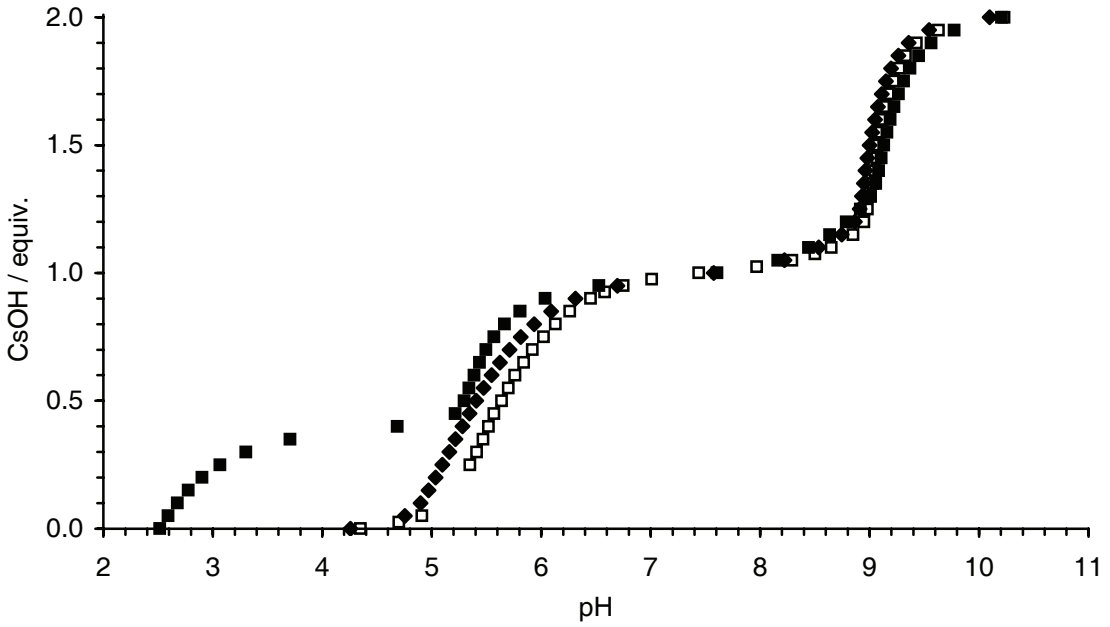

Figure IX.20 The pH of solutions containing the complex **3** ([Ru] = 15.0 mM) and the ligand **L2** (15 mM) in the presence of different salts (100 mM): no salt (◆), CsCl (□), and $LiNO_3$ (■) after addition of increasing amounts of CsOH (0.0–2.0 equiv. with respect to the ligand).

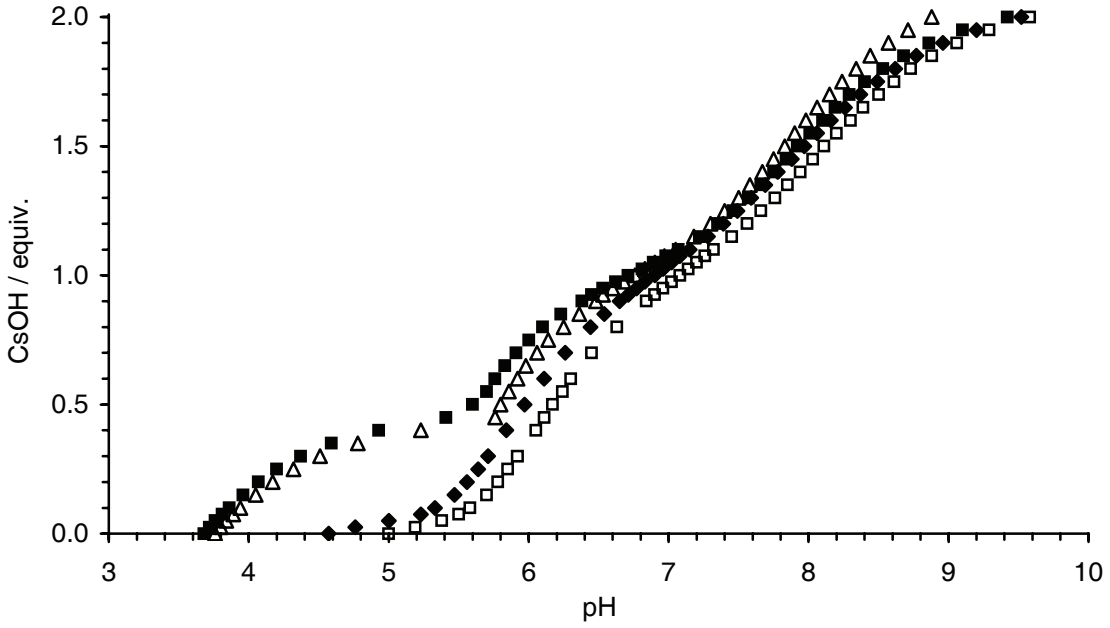

Figure IX.21 The pH of solutions containing the complex **3** ([Ru] = 15.0 mM) and the ligand **L5** (15 mM) in the presence of different salts (100 mM): no salt (◆), CsCl (□), LiCl (△) and $LiNO_3$ (■) after addition of increasing amounts of CsOH (0.0–2.0 equiv. with respect to the ligand).

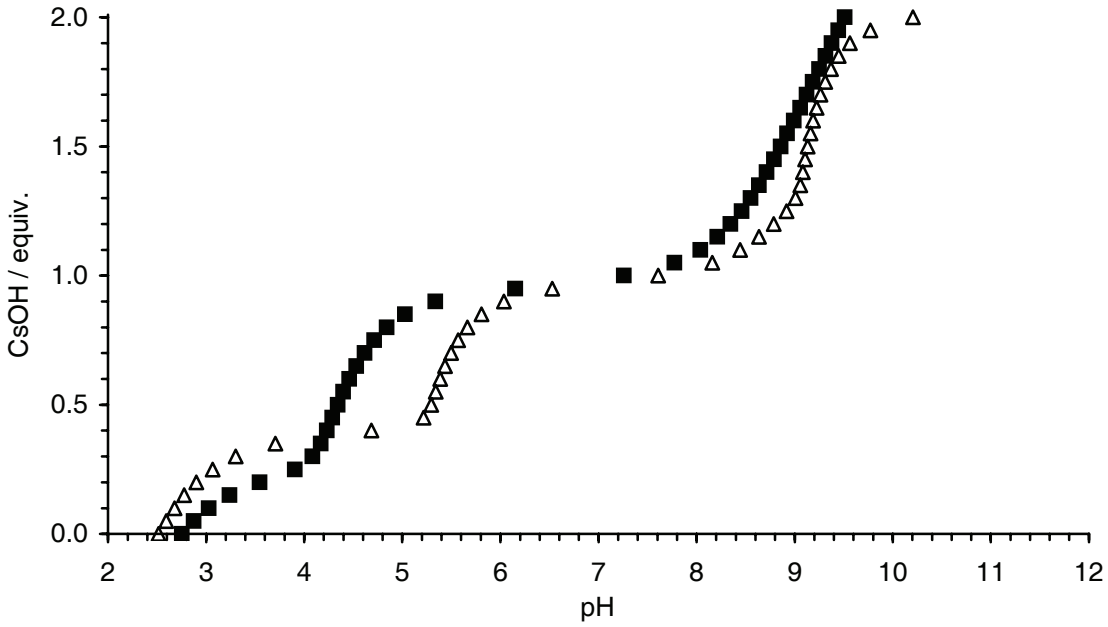

Figure IX.22 The pH of solutions containing the ligand **L2** (15.0 mM) and the complexes **3** (Δ) and **4** (■) ([Ru] = 15.0 mM) in the presence of $LiNO_3$ (100 mM) after addition of increasing amounts of CsOH (0.0–2.0 equiv. with respect to the ligand).

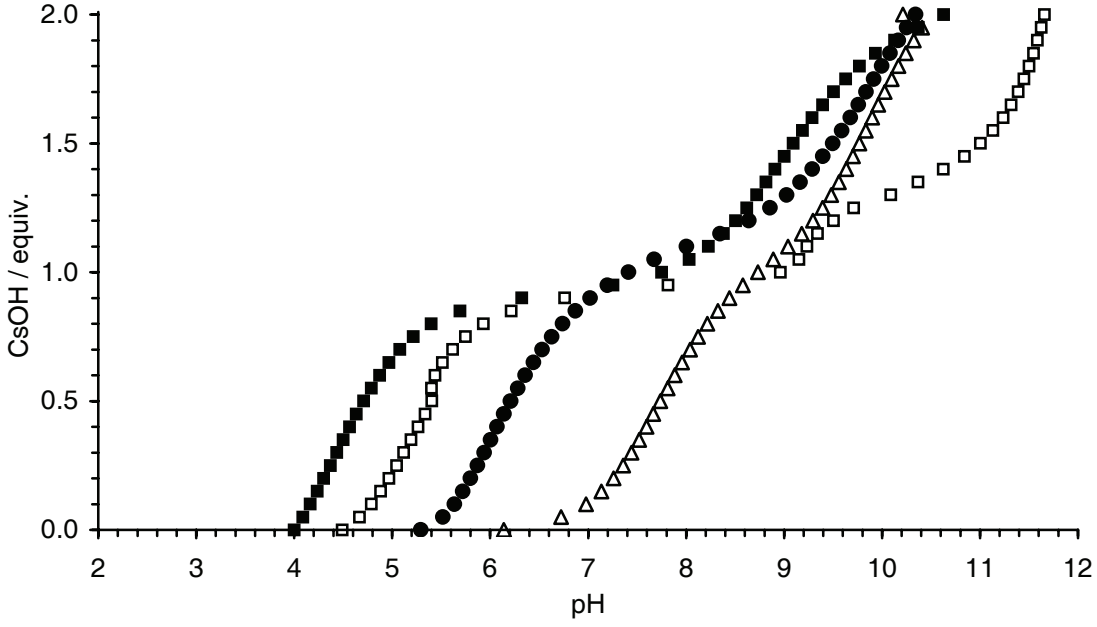

Figure IX.23 The pH of solutions containing the ligand **L2** (15.0 mM) and the complexes **7** (■), **8** (●), **9** (Δ), and **11** (□) ([Rh] = [Ir] = 15.0 mM) in the presence of $LiNO_3$ (100 mM) after addition of increasing amounts of CsOH (0.0–2.0 equiv. with respect to the ligand).

IX.VI Crystallographic Data

Table IX.10: Selected bond lengths (Å) and angles (°)[a] for 12-metallacrown-3 complexes of 3-hydroxy-2-pyridone ligands with diverse metal fragments.

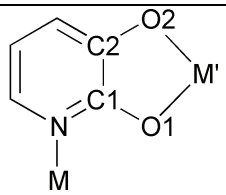

Complex	M–N	M–O1	M–O2	O1–M–O2	M–O–C1–C2	M–N–C1–C2	O–O'	M–M'
$[(C_6H_6)Ru(L1–2\ H^+)]_3$[126]	2.13	2.08	2.07	79.66	8.2	5.2	3.04	5.32
$[(C_6H_6)Ru(L1–2\ H^+)]_3 \times LiCl$[126]	2.14	2.11	2.05	79.44	8.4	8.1	2.98	5.38
$[(C_6H_6)Ru(L1–2\ H^+)]_3 \times NaBr$[126]	2.14	2.11	2.06	79.1	10.8	5.7	3.11	5.39
$[(C_6H_5Me)Ru(L1–2\ H^+)]_3$	2.14	2.09	2.08	79.5	4.5	7.4	3.04	5.37
$[(C_6H_5Me)Ru(L1–2\ H^+)]_3 \times LiCl$	2.14	2.12	2.08	79.5	8.7	5.8	2.96	5.40
$[(cymene)Ru(L1–2\ H^+)]_3$[126]	2.13	2.08	2.05	79.41	11.1	7.6	3.09	5.38
$[(cymene)Ru(L1–2\ H^+)]_3 \times LiCl$[126]	2.14	2.10	2.06	79.51	8.8	9.2	2.97	5.36
$[(cymene)Ru(L1–2\ H^+)] \times NaCl$[126]	2.14	2.09	2.04	79.29	11.6	7.8	3.11	5.36
$[(cymene)Ru(L1–2\ H^+)]_3 \times NaI$[126]	2.15	2.10	2.05	79.2	12.3	8.5	3.14	5.42
$[(C_6H_5CO_2Et)Ru(L1–2\ H^+)]_3$[165]	2.12	2.06	2.05	80.3	10.5	7.9	3.00	5.28
$[(C_6H_5CO_2Et)Ru(L1–2\ H^+)]_3 \times LiCl$[165]	2.13	2.08	2.05	80.0	8.3	6.1	2.93	5.33
$[(C_6H_3{}^iPr_3)Ru(L1–2\ H^+)]_3$	2.14	2.09	2.06	79.5	13.5	8.7	3.15	5.39
$[(C_6H_3{}^iPr_3)Ru(L1–2\ H^+)]_3 \times LiCl$	2.14	212	2.03	79.5	11.7	11.8	3.07	5.48
$[(C_6Me_6)Ru(L1–2\ H^+)]_3$[124]	2.14	2.12	2.05	78.6	15.1	9.8	3.21	5.46
$[(C_5HMe_4)Rh(L1–2\ H^+)]_3$	2.14	2.11	2.10	80.4	13.9	9.6	3.10	5.33
$[(C_5HMe_4)Rh(L1–2\ H^+)]_3 \times LiCl$	2.13	2.08	2.13	79.5	11.4	10.9	2.99	5.34
$[Cp^*Rh(L1–2\ H^+)]_3$[124]	2.13	2.09	2.06	80.1	11.2	5.8	3.10	5.35
$[Cp^*Rh(L1–2\ H^+)]_3 \times LiCl$[124]	2.12	2.14	2.06	79.2	10.8	9.1	3.07	5.47
$[Cp^*Ir(L1–2\ H^+)]_3$[166]	2.13	2.11	2.07	79.2	10.3	7.7	3.05	5.37
$[(C_6H_6Ru)_2(C_6Me_6Ru)(L1–2\ H^+)_3]$	2.13	2.07	2.07	80.0	11.5	8.6	3.03	5.26
$[(C_6H_6Ru)_2(Cp^*Rh)(L1–2\ H^+)_3]$	2.11	2.08	2.08	79.6	11.9	8.1	3.04	5.26
$[(cymene)Ru(L2–2\ H^+)]_3$	2.14	2.08	2.07	79.6	11.7	7.0	3.10	5.43
$[(cymene)Ru(L3–2\ H^+)]_3$	2.14	2.09	2.06	79.1	13.4	9.7	3.13	5.37
$[(cymene)Ru(L5–2\ H^+)]_3$	2.14	2.08	2.05	79.5	12.8	8.7	3.10	5.34
$[(C_5HMe_4)Rh(L5–2\ H^+)]_3$	2.12	2.08	2.09	78.0	9.9	16.2	3.15	5.32
$[Cp^*Rh(L5–2\ H^+)]_3$	2.13	2.09	2.05	80.1	12.4	7.4	3.11	5.35
$[Cp^*Ir(L3–2\ H^+)]_3$	2.13	2.12	2.09	78.6	8.8	5.8	3.04	5.37

a. Averaged values are given, except for **$[Cp^*Rh(L5–2\ H^+)]_3$**, **$[Cp^*Ir(L3–2\ H^+)]_3$** and **$[(C_5HMe_4)Rh(L5–2\ H^+)]_3$** which display a C_3 axis.

Table IX.11: Selected bond lengths (Å) and angles (°) for monomeric complexes .

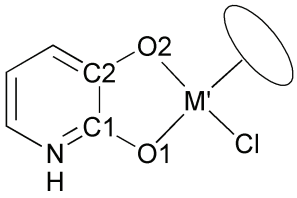

Complex	M–Cl	M–O1	M–O2	O1–M–O2	O1–M–Cl1	M–O1–C1–C2	N2–Cl2	N1-Cl2
[(C_6Me_6)Ru(L2)Cl]Cl	2.42	2.15	2.09	78.6	83.3	14.23	3.08	3.14
[(C_6Me_6)Ru(L3)Cl]Cl	2.43	2.17	2.07	78.4	84.5	11.24	3.07	3.17
[(C_6Me_6)Ru(L4)Cl]Cl	2.43	2.14	2.08	78.3	85.2	13.79	3.02	3.14
[Cp*Rh(L2–H^+)Cl]	2.42	2.14	2.13	78.3	86.9	7.52	—	—

Table IX.12: Crystallographic data of monomeric complexes **[(C_6Me_6)Ru(L2)Cl]Cl** and **[(C_6Me_6)Ru(L3)Cl]Cl**.

	[(C_6Me_6)Ru(L2)Cl]Cl × 0.5 CH_2Cl_2	**[(C_6Me_6)Ru(L3)Cl]Cl × 0.5 $CHCl_3$**
	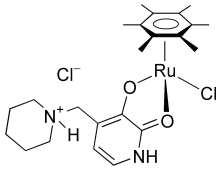	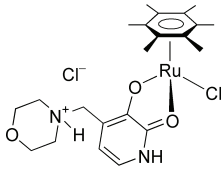
Empirical formula	$C_{23.5}H_{35}Cl_3N_2O_2Ru$	$C_{22.5}H_{32.5}Cl_{3.5}N_2O_3Ru$
Mol. weight / g mol^{-1}	584.96	604.15
Crystal size / mm^3	0.22 × 0.14 x 0.09	0.18 x 0.16 x 0.09
Crystal system	monoclinic	monoclinic
Space group	$P2_1/n$	$P2_1/c$
a / Å	8.7505(8)	9.3253(6)
b / Å	21.6323(15)	16.161(5)
c / Å	13.6254(8)	17.709(6)
α / °	90	90
β / °	95.697(6)	94.734(14)
γ / °	90	90
Volume / $Å^3$	2566.5(3)3	2659.7(12)3
Z	4	4
Density / g cm^{-3}	1.514	1.509
Temperature / K	140(2)	140(2)
Absorption Coeff. / mm^{-1}	0.946	0.967
Θ range / °	3.00 to 25.03	2.85 to 25.02
Index ranges	$-9 \rightarrow h \rightarrow 9$, $-25 \rightarrow k \rightarrow 25$, $-16 \rightarrow l \rightarrow 16$	$-10 \rightarrow h \rightarrow 10$, $-19 \rightarrow k \rightarrow 19$, $-21 \rightarrow l \rightarrow 21$
Reflections collected	14809	16307
Independent reflections	4266 (R_{int} = 0.0382)	4434 (R_{int} = 0.0439)
Absorption corrrection	semi-empirical	semi-empirical
Max. & min. transmission	0.9486 and 0.7834	0.9471 and 0.8191
Data / restraints / param.	4266 / 0 / 289	4434 / 0 / 308
Goodness-of-fit on F^2	1.066	1.188
Final *R* indices [I > 2 σ (I)]	*R*1 = 0.0422, *wR*2 = 0.1157	*R*1 = 0.0527, *wR*2 = 0.1481
R indices (all data)	*R*1 = 0.0536, *wR*2 = 0.1223	*R*1 = 0.0679, *wR*2 = 0.1659
Larg. diff. peak/hole / $eÅ^{-3}$	1.653 and −1.261	0.823 and −0.875

Table IX.13: Crystallographic data of monomeric complexes **[(C_6Me_6)Ru(L4)Cl]Cl** and **[Cp*Rh(L3–H^+)Cl]**.

	[(C_6Me_6)Ru(L4)Cl]Cl × 0.5 $CHCl_3$	**[Cp*Rh(L3–H^+)Cl]**
	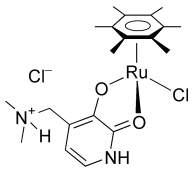	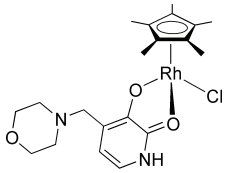
Empirical formula	$C_{20.5}H_{30.5}Cl_{3.5}N_2O_2Ru$	$C_{20}H_{28}ClN_2O_3Rh$
Mol. weight / g mol^{-1}	562.11	482.8
Crystal size / mm^3	0.19 × 0.15 × 0.09	0.23 × 0.12 × 0.07
Crystal system	monoclinic	monoclinic
Space group	$P2_1/c$	$P2_1/c$
a / Å	8.8640(10)	7.4799(5)
b / Å	18.626(6)	22.9529(14)
c / Å	14.885(5)	12.0712(6)
α / °	90	90
β / °	100.814(19)	93.000(5)
γ / °	90	90
Volume / $Å^3$	2413.9(12)	2069.6(2)
Z	4	4
Density / g cm^{-3}	1.547	1.550
Temperature / K	140(2)	140(2)
Absorption Coeff. / mm^{-1}	1.056	0.976
Θ range / °	2.99 to 25.02	3.15 to 25.02
Index ranges	$-9 \rightarrow h \rightarrow 10$, $-22 \rightarrow k \rightarrow 22$, $-15 \rightarrow l \rightarrow 17$	$-8 \rightarrow h \rightarrow 8$, $-27 \rightarrow k \rightarrow 27$, $-12 \rightarrow l \rightarrow 12$
Reflections collected	14850	12027
Independent reflections	4033 (R_{int} = 0.0434)	3421 (R_{int} = 0.0325)
Absorption corrrection	semi-empirical	semi-empirical
Max. & min. transmission	0.8949 and 0.8213	1.0371 and 0.7320
Data / restraints / param.	4033 / 0 / 281	3421 / 0 / 245
Goodness-of-fit on F^2	1.213	1.072
Final *R* indices [I > 2 σ (I)]	*R*1 = 0.0451, *wR*2 = 0.1221	*R*1 = 0.0282, *wR*2 = 0.0676
R indices (all data)	*R*1 = 0.0625, *wR*2 = 0.1339	*R*1 = 0.0331, *wR*2 = 0.0698
Larg. diff. peak/hole / e$Å^{-3}$	0.584 and –0.641	0.657 and –0.845

Table IX.14: Crystallographic data of the trinuclear complexes **$[(C_6H_5Me)Ru(L1{-}2\,H^+)]_3$** and **$[(C_6H_5Me)Ru(L1{-}2\,H^+)]_3 \times LiCl$**.

	$[C_6H_5MeRu(L1{-}2\,H^+)]_3 \times CHCl_3 \times 2\,H_2O$	**$[C_6H_5MeRu(L1{-}2\,H^+)]_3 \times LiCl \times CHCl_3 \times H_2O$**
	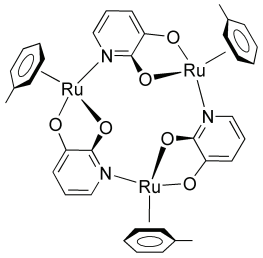	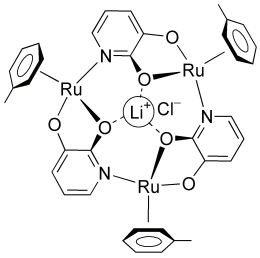
Empirical formula	$C_{37}H_{38}Cl_3N_3O_8Ru_3$	$C_{37}H_{36}Cl_4LiN_3O_7Ru_3$
Mol. weight / g mol^{-1}	1062.26	1086.64
Crystal size / mm^3	0.52 x 0.27 x 0.19	0.24 x 0.14 x 0.13
Crystal system	monoclinic	monoclinic
Space group	$P2_1/n$	$P2_1/n$
a / Å	15.512(3)	15.580(3)
b / Å	13.6976(10)	14.1083(14)
c / Å	17.9333(18)	17.736(2)
α / °	90	90
β / °	102.723(10)	102.820(10)
γ / °	9	90
Volume / Å^3	3717.0(8)	3801.5(9)
Z	4	4
Density / g cm^{-3}	1.898	1.899
Temperature / K	100(2)	100(2)
Absorption Coeff. / mm^{-1}	1.477	1.512
Θ range / °	3.07 to 25.03	3.04 to 25.03
Index ranges	$-18 \rightarrow h \rightarrow 18$, $-16 \rightarrow k \rightarrow 16$, $-21 \rightarrow l \rightarrow 21$	$16 \rightarrow h \rightarrow 18$, $-16 \rightarrow k \rightarrow 16$, $-21 \rightarrow l \rightarrow 18$
Reflections collected	73189	29632
Independent reflections	6563 (R_{int} = 0.0901)	6591 (R_{int} = 0.1100)
Absorption corrrection	semi-empirical	semi-empirical
Max. & min. transmission	1.0000 and 0.6795	1.0000 and 0.7079
Data / restraints / param.	6563 / 6 / 499	6591 / 3 / 502
Goodness-of-fit on F^2	1.141	1.127
Final *R* indices [I > 2 σ (I)]	*R*1 = 0.0392, *wR*2 = 0.0736	*R*1 = 0.0567, *wR*2 = 0.0757
R indices (all data)	*R*1 = 0.0623, *wR*2 = 0.0838	*R*1 = 0.1136, *wR*2 = 0.0919
Larg. diff. peak/hole / eÅ^{-3}	0.790 and −0.649	1.133 and −0.915

Table IX.15: Crystallographic data of the trinuclear complexes **[($C_6H_3{}^iPr_3$)Ru(L1–2 H^+)]$_3$** and **[($C_6H_3{}^iPr_3$)Ru(L1–2 H^+)]$_3$ × LiCl**.

	[($C_6H_3{}^iPr_3$)Ru(L1–2 H^+)]$_3$ × 0.5 C_6H_{14} × H_2O	**[($C_6H_3{}^iPr_3$)Ru(L1–2 H^+)]$_3$ × LiCl × 2 C_6H_{14}**
	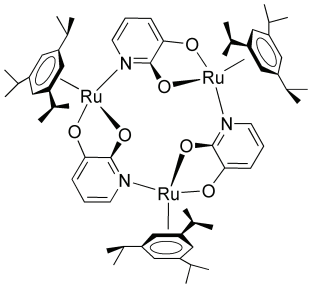	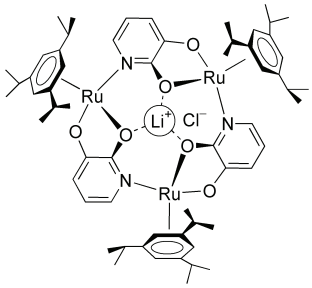
Empirical formula	$C_{63}H_{90}N_3O_7Ru_3$	$C_{72}H_{109}ClLiN_3O_6Ru_3$
Mol. weight / g mol^{-1}	1304.59	1458.22
Crystal size / mm^3	0.50 × 0.36 × 0.26	0.33 x 0.17 x 0.13
Crystal system	monoclinic	orthorhombic
Space group	$P2_1/n$	$P2_12_12_1$
a / Å	13.4120(6)	13.2934(6)
b / Å	24.4988(13)	16.9892(11)
c / Å	18.6820(8)	32.829(2)
α / °	90	90
β / °	100.255(4)	90
γ / °	90	90
Volume / Å^3	6040.4(5)	7414.3(7)
Z	4	4
Density / g cm^{-3}	1.435	1.306
Temperature / K	140(2)	140(2)
Absorption Coeff. / mm^{-1}	0.794	0.688
Θ range / °	3.34 to 25.03	2.70 to 25.03
Index ranges	$-15 \rightarrow h \rightarrow 15$, $-29 \rightarrow k \rightarrow 29$, $-18 \rightarrow l \rightarrow 22$	$-15 \rightarrow h \rightarrow 15$, $-20 \rightarrow k \rightarrow 20$, $-39 \rightarrow l \rightarrow 35$
Reflections collected	35584	45721
Independent reflections	10064 (R_{int} = 0.0439)	13029 (R_{int} = 0.1970)
Absorption corrrection	empirical	none
Max. & min. transmission	0.9020 and 0.6630	0
Data / restraints / param.	10064 / 11 / 709	13029 / 607 / 733
Goodness-of-fit on F^2	0.961	0.751
Final *R* indices [I > 2 σ (I)]	*R*1 = 0.0339, *wR*2 = 0.0674	*R*1 = 0.0671, *wR*2 = 0.0984
R indices (all data)	*R*1 = 0.0584, *wR*2 = 0.0746	*R*1 = 0.1858, *wR*2 = 0.1361
Larg. diff. peak/hole / eÅ^{-3}	0.890 and –0.640	0.742 and –0.557

Table IX.16: Crystallographic data of the trinuclear complexes **$[(C_5HMe_4)Rh(L1–2\ H^+)]_3$** and **$[(C_5HMe_4)Rh(L1–2\ H^+)]_3 \times LiCl$**.

	$[(C_5HMe_4)Rh(L1–2\ H^+)]_3 \times Et_2O$	**$[(C_5HMe_4)Rh(L1–2\ H^+)]_3 \times LiCl \times 2\ H_2O$**
	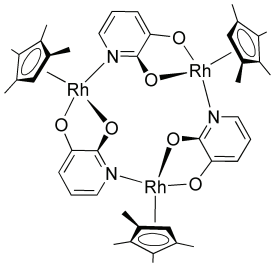	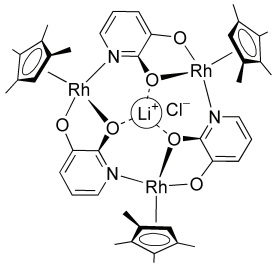
Empirical formula	$C_{46}H_{58}N_3O_7Rh_3$	$C_{42}H_{52}ClLiN_3O_8Rh_3$
Mol. weight / g mol^{-1}	1073.68	1077.99
Crystal size / mm^3	0.23 × 0.12 × 0.09	0.32 x 0.21 x 0.16
Crystal system	triclinic	monoclinic
Space group	$P\bar{1}$	$P2_1/c$
a / Å	9.2098(15)	17.405(3)
b / Å	11.7685(15)	12.8191(13)
c / Å	23.039(3)	20.414(3)
α / °	75.250(11)	90
β / °	85.279(17)	109.714(10)
γ / °	74.286(12)	90
Volume / Å^3	2324.3(6)	4287.8(9)
Z	2	4
Density / g cm^{-3}	1.534	1.670
Temperature / K	140(2)	100(2)
Absorption Coeff. / mm^{-1}	1.103	1.258
Θ range / °	3.31 to 25.03	3.11 to 25.01
Index ranges	$-10 \rightarrow h \rightarrow 9$, $-14 \rightarrow k \rightarrow 14$, $-27 \rightarrow l \rightarrow 27$	$-20 \rightarrow h \rightarrow 20$, $-15 \rightarrow k \rightarrow 15$, $-24 \rightarrow l \rightarrow 24$
Reflections collected	13419	58639
Independent reflections	7120 (R_{int} = 0.0693)	7519 (R_{int} = 0.1339)
Absorption corrrection	none	semi-empirical
Max. & min. transmission		1.0000 and 0.5761
Data / restraints / param.	7120 / 0 / 533	7519 / 6 / 534
Goodness-of-fit on F^2	1.205	1.121
Final *R* indices [I > 2 σ (I)]	*R*1 = 0.0920, *wR*2 = 0.2593	*R*1 = 0.0663, *wR*2 = 0.1161
R indices (all data)	*R*1 = 0.0991, *wR*2 = 0.2798	*R*1 = 0.1243, *wR*2 = 0.1407
Larg. diff. peak/hole / eÅ^{-3}	1.971 and –3.117	2.178 and –1.821

Table IX.17: Crystallographic data of the mixed trinuclear complexes **[($C_6H_6Ru)_2(C_6Me_6Ru)(L1–2\ H^+)_3$]** and **[$(C_6H_6Ru)_2(Cp^*Rh)(L1–2\ H^+)_3$]**.

	[$(C_6H_6Ru)_2(C_6Me_6Ru)(L1–2\ H^+)_3$] × 2 $CHCl_3$	**[$(C_6H_6Ru)_2(Cp^*Rh)(L1–2\ H^+)_3$] × MeOH × C_7H_8 × H_2O**
	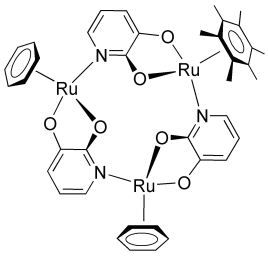	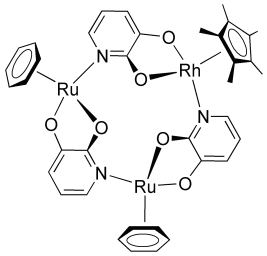
Empirical formula	$C_{41}H_{41}Cl_6N_3O_6Ru_3$	$C_{45}H_{50}N_3O_8RhRu_2$
Mol. weight / g mol^{-1}	1187.68	1065.93
Crystal size / mm^3	0.20 × 0.12 × 0.09	0.17 × 0.17 × 0.13
Crystal system	triclinic	monoclinic
Space group	$P\bar{1}$	$P2_1/n$
a / Å	9.2537(14)	13.273(5)
b / Å	12.040(3)	18.718(5)
c / Å	20.007(5)	18.668(4)
α / °	85.44(2)	90
β / °	80.731(16)	110.09(3)
γ / °	88.110(16)	90
Volume / $Å^3$	2192.5(8)	4356(2)
Z	2	4
Density / g cm^{-3}	1.799	1.625
Temperature / K	140(2)	140(2)
Absorption Coeff. / mm^{-1}	1.436	1.115
Θ range / °	3.09 to 25.03	2.73 to 25.03
Index ranges	$-10 \rightarrow h \rightarrow 10$, $-14 \rightarrow k \rightarrow 14$, $-23 \rightarrow l \rightarrow 23$	$-15 \rightarrow h \rightarrow 15$, $-22 \rightarrow k \rightarrow 22$, $-21 \rightarrow l \rightarrow 22$
Reflections collected	14091	26761
Independent reflections	7271 (R_{int} = 0.0439)	7694 (R_{int} = 0.0626)
Absorption corrrection	semi-empirical	semi-empirical
Max. & min. transmission	0.9528 and 0.7704	0.8564 and 0.7350
Data / restraints / param.	7271 / 0 / 533	7694 / 3 / 492
Goodness-of-fit on F^2	1.08	0.998
Final *R* indices [$I > 2\sigma(I)$]	*R*1 = 0.0638, *wR*2 = 0.1757	*R*1 = 0.0688, *wR*2 = 0.1885
R indices (all data)	*R*1 = 0.0769, *wR*2 = 0.1941	*R*1 = 0.1118, *wR*2 = 0.2197
Larg. diff. peak/hole / $eÅ^{-3}$	1.152 and −1.076	0.946 and −0.957

Table IX.18: Crystallographic data of the trinuclear complexes **[(cymene)Ru(L3–2 H^+)]$_3$** and **[(cymene)Ru(L5–2 H^+)]$_3$**.

	[(cymene)Ru(L3–2 H^+)]$_3$ × 3 H_2O	**[(cymene)Ru(L5–2 H^+)]$_3$ × 2 C_6H_6 × H_2O**
	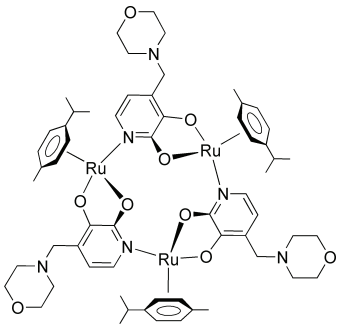	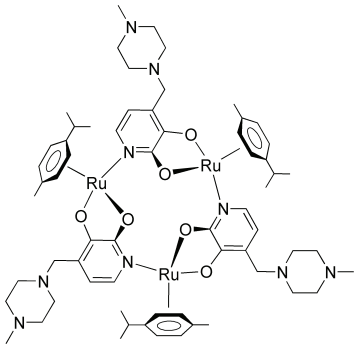
Empirical formula	$C_{60}H_{84}N_6O_{12}Ru_3$	$C_{75}H_{101}N_9O_7Ru_3$
Mol. weight / g mol^{-1}	1384.54	1543.86
Crystal size / mm^3	0.25 × 0.19 × 0.13	0.16 × 0.15 × 0.15
Crystal system	monoclinic	triclinic
Space group	$P2_1/n$	$P\bar{1}$
a / Å	13.0075(9)	15.289(3)
b / Å	24.6431(14)	15.347(3)
c / Å	18.6453(9)	16.3869(11)
α / °	90	103.747(11)
β / °	90.045(5)	97.591(11)
γ / °	90	95.256(16)
Volume / Å^3	5976.7(6)	3672.0(10)
Z	4	2
Density / g cm^{-3}	1.539	1.396
Temperature / K	140(2)	293(2)
Absorption Coeff. / mm^{-1}	0.815	0.667
Θ range / °	2.71 to 25.03	2.83 to 25.03
Index ranges	$-15 \rightarrow h \rightarrow 15$, $-29 \rightarrow k \rightarrow 29$, $-21 \rightarrow l \rightarrow 18$	$-18 \rightarrow h \rightarrow 18$, $-18 \rightarrow k \rightarrow 17$, $-18 \rightarrow l \rightarrow 18$
Reflections collected	34821	23883
Independent reflections	10178 (R_{int} = 0.0433)	12170 (R_{int} = 0.0343)
Absorption corrrection	semi-empirical	semi-empirical
Max. & min. transmission	0.9680 and 0.8113	0.9480 and 0.8733
Data / restraints / param.	10178 / 0 / 740	12170 / 0 / 848
Goodness-of-fit on F^2	1.071	1.104
Final *R* indices [I > 2 σ (I)]	*R*1 = 0.0479, *wR*2 = 0.1180	*R*1 = 0.0655, *wR*2 = 0.1783
R indices (all data)	*R*1 = 0.0659, *wR*2 = 0.1276	*R*1 = 0.0825, *wR*2 = 0.2039
Larg. diff. peak/hole / eÅ^{-3}	1.650 and −1.391	1.957 and −1.086

Table IX.19: Crystallographic data of the trinuclear complexes **$[(C_5HMe_4)Rh(L5–2\ H^+)]_3$** and **$[Cp^*Rh(L5–2\ H^+)]_3$**.

	$[(C_5HMe_4)Rh(L5–2\ H^+)]_3 \times 12\ H_2O$	**$[Cp^*Rh(L5–2\ H^+)]_3 \times 4.5\ C_6H_6$**
	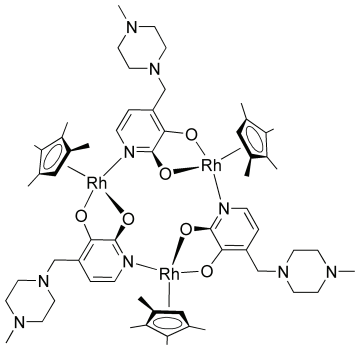	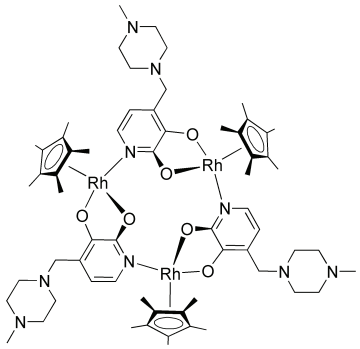
Empirical formula	$C_{60}H_{108}N_9O_{18}Rh_3$	$C_{90}H_{117}N_9O_6Rh_3$
Mol. weight / g mol^{-1}	1552.28	1729.66
Crystal size / mm^3	0.32 × 0.20 × 0.15	0.26 × 0.26 × 0.26
Crystal system	rhombohedral	cubic
Space group	$R\bar{3}c$	$I23$
a / Å	20.5761(11)	26.0844(7)
b / Å	20.5761(11)	26.0844(7)
c / Å	145.280(11)	26.0844(7)
α / °	90	90
β / °	90	90
γ / °	120	90
Volume / Å^3	53268(6)	17747.7(8)
Z	24	8
Density / g cm^{-3}	1.161	1.295
Temperature / K	140(2)	140(2)
Absorption Coeff. / mm^{-1}	0.608	0.606
Θ range / °	2.60 to 25.03	2.92 to 25.02
Index ranges	$-24 \rightarrow h \rightarrow 24$, $-24 \rightarrow k \rightarrow 24$, $-172 \rightarrow l \rightarrow 172$	$-29 \rightarrow h \rightarrow 29$, $-31 \rightarrow k \rightarrow 31$, $-31 \rightarrow l \rightarrow 30$
Reflections collected	100131	55759
Independent reflections	10477 (R_{int} = 0.1864)	5230 (R_{int} = 0.0526)
Absorption corrrection	none	none
Max. & min. transmission		
Data / restraints / param.	10477 / 0 / 503	5230 / 0 / 325
Goodness-of-fit on F^2	1.062	1.11
Final R indices [I > 2 σ (I)]	$R1$ = 0.1104, $wR2$ = 0.2884	$R1$ = 0.0265, $wR2$ = 0.0648
R indices (all data)	$R1$ = 0.1644, $wR2$ = 0.3183	$R1$ = 0.0290, $wR2$ = 0.0656
Larg. diff. peak/hole / eÅ^{-3}	1.420 and –1.083	0.362 and –0.414

Table IX.20: Crystallographic data of the trinuclear complex **[Cp*Ir(L3–2 H$^+$)]$_3$** and the dimeric halfsandwich complex **[(C$_5$HMe$_4$)IrCl$_2$]$_2$** (**10**).

	[Cp*Ir(L3–2 H$^+$)]$_3$	**[(C$_5$HMe$_4$)IrCl$_2$]$_2$**
	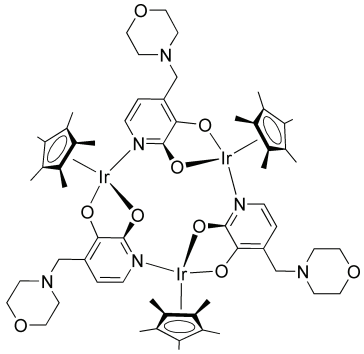	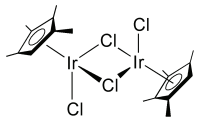
Empirical formula	$C_{60}H_{81}Ir_3N_6O_9$	$C_{18}H_{26}Cl_4Ir_2$
Mol. weight / g mol^{-1}	1606.91	768.59
Crystal size / mm^3	0.19 × 0.19 × 0.14	0.17 × 0.16 × 0.08
Crystal system	rhombohedral	monoclinic
Space group	*R*3	$P2_1/c$
a / Å	18.832(4)	15.6001(11)
b / Å	18.832(4)	8.1663(6)
c / Å	13.812(5)	16.7110(12)
α / °	90	90
β / °	90	101.477(6)
γ / °	120	90
Volume / Å^3	4242.3(19)	2086.3(3)
Z	3	4
Density / g cm^{-3}	1.887	2.447
Temperature / K	140(2)	140(2)
Absorption Coeff. / mm^{-1}	7.104	13.255
Θ range / °	2.90 to 25.02	2.98 to 25.03
Index ranges	$-22 \rightarrow h \rightarrow 19$, $-22 \rightarrow k \rightarrow 22$, $-16 \rightarrow l \rightarrow 16$	$-18 \rightarrow h \rightarrow 18$, $-8 \rightarrow k \rightarrow 9$, $-19 \rightarrow l \rightarrow 19$
Reflections collected	8956	11408
Independent reflections	3304 (R_{int} = 0.0498)	3621 (R_{int} = 0.0648)
Absorption corrrection	semi-empirical	semi-empirical
Max. & min. transmission	0.4041 and 0.3390	0.2723 and 0.1103
Data / restraints / param.	3304 / 1 / 235	3621 / 0 / 217
Goodness-of-fit on F^2	1.013	0.997
Final *R* indices [I > 2 σ (I)]	*R*1 = 0.0314, *wR*2 = 0.0537	*R*1 = 0.0372, *wR*2 = 0.0887
R indices (all data)	*R*1 = 0.0388, *wR*2 = 0.0566	*R*1 = 0.0478, *wR*2 = 0.0936
Larg. diff. peak/hole / eÅ^{-3}	3.388 and −1.077	2.089 and −1.835

Table IX.21: Crystallographic data of the hexanuclear complexes **[{(C_6H_6)Ru}$_2$(L13–4 H$^+$)]$_3$** and **[{(C_6H_5Me)Ru}$_2$(L13–4 H$^+$)]$_3$**.

	[{(C_6H_6)Ru}$_2$(L13–4 H$^+$)]$_3$ × 39.25 H_2O	**[{(C_6H_5Me)Ru}$_2$(L13–4 H$^+$)]$_3$ × 14 H_2O**
	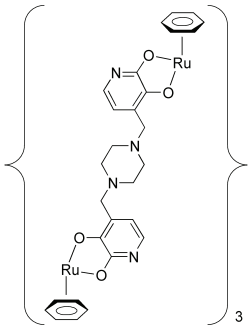	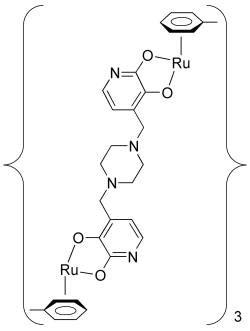
Empirical formula	$C_{84}H_{162.50}N_{12}O_{51.25}Ru_6$	$C_{90}H_{124}N_{12}O_{26}Ru_6$
Mol. weight / g mol^{-1}	2767.18	2396.43
Crystal size / mm^3	0.34 x 0.30 x 0.26	0.24 × 0.21 × 0.18
Crystal system	triclinic	orthorhombic
Space group	$P\bar{1}$	$Pna2_1$
a / Å	16.2163(17)	21.3799(7)
b / Å	18.3321(19)	24.3158(14)
c / Å	22.563(5)	18.4091(10)
α / °	101.528(11)	90
β / °	93.817(11)	90
γ / °	115.455(10)	90
Volume / Å^3	5845.3(15)	9570.3(8)
Z	2	4
Density / g cm^{-3}	1.572	1.663
Temperature / K	100(2)	140(2)
Absorption Coeff. / mm^{-1}	0.849	1.004
Θ range / °	2.92 to 25.03	2.91 to 25.03
Index ranges	$-19 \rightarrow h \rightarrow 19$, $-21 \rightarrow k \rightarrow 21$, $-26 \rightarrow l \rightarrow 26$	$-22 \rightarrow h \rightarrow 22$, $-28 \rightarrow k \rightarrow 28$, $-21 \rightarrow l \rightarrow 21$
Reflections collected	101158	57579
Independent reflections	20469 (R_{int} = 0.0694)	16075 (R_{int} = 0.0778)
Absorption corrrection	Semi-empirical from equivalents (SADABS)	none
Max. & min. transmission	1.0000 and 0.6742	0
Data / restraints / param.	20469 / 0 / 1375	16075 / 697 / 1208
Goodness-of-fit on F^2	1.063	0.794
Final *R* indices [I > 2 σ (I)]	*R*1 = 0.0581, *wR*2 = 0.1358	*R*1 = 0.0416, *wR*2 = 0.0683
R indices (all data)	*R*1 = 0.0890, *wR*2 = 0.1580	*R*1 = 0.0699, *wR*2 = 0.0744
Larg. diff. peak/hole / eÅ^{-3}	1.859 and –1.789	1.116 and –0.981

Table IX.22: Crystallographic data of the hexanuclear complexes **[{(C_6H_5Me)Ru}$_2$(L14–4 H^+)]$_3$** and **[{(C_5HMe_4)Rh}$_2$(L15–4 H^+)]$_3$**.

	[{C_6H_5Me)Ru}$_2$(L14–4 H^+)]$_3$ × 26 H_2O	**[{(C_5HMe_4)Rh}$_2$(L15–4 H^+)]$_3$ × 3 NEt_3 × 5 H_2O**
	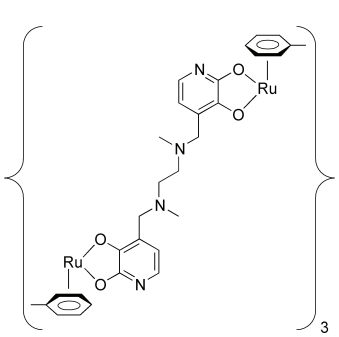	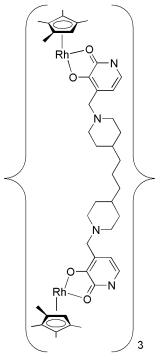
Empirical formula	$C_{90}H_{154}N_{12}O_{38}Ru_6$	$C_{147}H_{229}N_{15}O_{17}Rh_6$
Mol. weight / g mol^{-1}	2618.67	3095.91
Crystal size / mm^3	0.32 × 0.24 × 0.15	0.26 × 0.26 × 0.26
Crystal system	monoclinic	cubic
Space group	*I*2/*a*	$P2_13$
a / Å	24.471(5)	25.758(2)
b / Å	14.566(3)	25.758(2)
c / Å	31.674(6)	25.758(2)
α / °	90	90
β / °	91.08(3)	90
γ / °	90	90
Volume / Å^3	11288(4)	17091(2)
Z	4	4
Density / g cm^{-3}	1.541	1.203
Temperature / K	100(2)	140(2)
Absorption Coeff. / mm^{-1}	0.866	0.623
Θ range / °	2.93 to 25.03	2.85 to 25.02
Index ranges	$-28 \rightarrow h \rightarrow 29$, $-16 \rightarrow k \rightarrow 17$, $-37 \rightarrow l \rightarrow 37$	$-30 \rightarrow h \rightarrow 30$, $-29 \rightarrow k \rightarrow 30$, $-30 \rightarrow l \rightarrow 30$
Reflections collected	41808	107235
Independent reflections	9830 (R_{int} = 0.0673)	10065 (R_{int} = 0.1578)
Absorption corrrection	semi-empirical	none
Max. & min. transmission	1.0000 and 0.8729	0
Data / restraints / param.	9830 / 120 / 727	10065 / 7 / 506
Goodness-of-fit on F^2	1.091	1.166
Final *R* indices [I > 2 σ (I)]	*R*1 = 0.0868, *wR*2 = 0.1933	*R*1 = 0.1346, *wR*2 = 0.3297
R indices (all data)	*R*1 = 0.1567, *wR*2 = 0.2397	*R*1 = 0.1697, *wR*2 = 0.3625
Larg. diff. peak/hole / eÅ^{-3}	1.959 and −1.419	4.403 and −1.350

Chapter X
Bibliography

[1] L. R. MacGillivray, J. L. Atwood, *Angew. Chem., Int. Ed.* **1999**, *38*, 1019–1034.

[2] C. Branden, J. Tooze, *Introduction into Protein Structure*, Garland, New York, **1991**.

[3] G. Maier, S. Pfriem, U. Schafer, R. Matusch, *Angew. Chem., Int. Ed.* **1978**, *17*, 520–521.

[4] P. E. Eaton, T. W. Cole, *J. Am. Chem. Soc.* **1964**, *86*, 3157–3158.

[5] E. B. Fleischer, *J. Am. Chem. Soc.* **1964**, *86*, 3889–3890.

[6] L. A. Paquette, R. J. Ternansky, D. W. Balogh, *J. Am. Chem. Soc.* **1982**, *104*, 4502–4503.

[7] R. J. Ternansky, D. W. Balogh, L. A. Paquette, *J. Am. Chem. Soc.* **1982**, *104*, 4503–4504.

[8] V. Prelog, R. Seiwerth, *Chem. Ber.* **1941**, *74*, 1769–1772.

[9] H. Stetter, O. E. Bander, W. Neumann, *Chem. Ber.* **1956**, *89*, 1922–1926.

[10] R. C. Fort, P. V. Schleyer, *Chem. Rev.* **1964**, *64*, 277–300.

[11] H. W. Kroto, J. R. Heath, S. C. Obrien, R. F. Curl, R. E. Smalley, *Nature* **1985**, *318*, 162–163.

[12] W. Kratschmer, L. D. Lamb, K. Fostiropoulos, D. R. Huffman, *Nature* **1990**, *347*, 354–358.

[13] W. E. Billups, M. A. Ciufolini, *Buckminsterfullerenes*, VCH, New York, **1993**.

[14] M. Fujita, J. Yazaki, K. Ogura, *J. Am. Chem. Soc.* **1990**, *112*, 5645–5647.

[15] M. Fujita, O. Sasaki, T. Mitsuhashi, T. Fujita, J. Yazaki, K. Yamaguchi, K. Ogura, *Chem. Commun.* **1996**, 1535–1536.

[16] M. Fujita, M. Tominaga, A. Hori, B. Therrien, *Acc. Chem. Res.* **2005**, *38*, 369–378.

[17] P. M. Stricklen, E. J. Volcko, J. G. Verkade, *J. Am. Chem. Soc.* **1983**, *105*, 2494–2495.

[18] A. W. Maverick, F. E. Klavetter, *Inorg. Chem.* **1984**, *23*, 4129–4130.

[19] A. W. Maverick, S. C. Buckingham, Q. Yao, J. R. Bradbury, G. G. Stanley, *J. Am. Chem. Soc.* **1986**, *108*, 7430–7431.

[20] S. R. Seidel, P. J. Stang, *Acc. Chem. Res.* **2002**, *35*, 972–983.

[21] J.-M. Lehn, *Comprehensive Supramolecular Chemistry*, Pergamon Press, Oxford, U.K., **1996**.

[22] P. J. Stang, B. Olenyuk, *Acc. Chem. Res.* **1997**, *30*, 502–518.

[23] B. Olenyuk, A. Fechtenkötter, P. J. Stang, *J. Chem. Soc., Dalton Trans.* **1998**, 1707–1728.

[24] D. L. Caulder, K. N. Raymond, *Acc. Chem. Res.* **1999**, *32*, 975–982.

[25] D. L. Caulder, K. N. Raymond, *J. Chem. Soc., Dalton Trans.* **1999**, 1185–1200.

[26] D. L. Caulder, C. Brückner, R. E. Powers, S. König, T. N. Parac, J. A. Leary, K. N. Raymond, *J. Am. Chem. Soc.* **2001**, *123*, 8923–8938.

[27] B. J. Holliday, C. A. Mirkin, *Angew. Chem., Int. Ed.* **2001**, *40*, 2022–2043.

[28] N. C. Gianneschi, M. S. Masar III, C. A. Mirkin, *Acc. Chem. Res.* **2005**, *38*, 825–837.

[29] F. Würthner, C. C. You, C. R. Saha–Möller, *Chem. Soc. Rev.* **2004**, *33*, 133–146.

[30] D. Fiedler, D. H. Leung, R. G. Bergman, K. N. Raymond, *Acc. Chem. Res.* **2005**, *38*, 349–358.

[31] A. Lützen, *Angew. Chem., Int. Ed.* **2005**, *44*, 1000–1002.

[32] C. H. M. Amijs, G. P. M. van Klink, G. van Koten, *Dalton Trans.* **2006**, 308–327.

[33] C. M. Drain, J.-M. Lehn, *J. Chem. Soc., Chem. Commun.* **1994**, 2313–2315.

[34] P. J. Stang, J. Fan, B. Olenyuk, *Chem. Commun.* **1997**, 1453–1454.

[35] S. Leininger, B. Olenyuk, P. J. Stang, *Chem. Rev.* **2000**, *100*, 853–907.

[36] G. Ercolani, L. Mandolini, P. Mencarelli, S. Roelens, *J. Am. Chem. Soc.* **1993**, *115*, 3901–3908.

[37] G. Ercolani, *J. Phys. Chem. B* **1998**, *102*, 5699–5703.

[38] A. Sautter, D. G. Schmid, G. Jung, F. Würthner, *J. Am. Chem. Soc.* **2001**, *123*, 5424–5430.

[39] J. A. R. Navarro, B. Lippert, *Coord. Chem. Rev.* **2001**, *222*, 219–250.

[40] M. Fujita, K. Umemoto, M. Yoshizawa, N. Fujita, T. Kusukawa, K. Biradha, *Chem. Commun.* **2001**, 509–518.

[41] W. Y. Sun, M. Yoshizawa, T. Kusukawa, M. Fujita, *Curr. Opin. Chem. Biol.* **2002**, *6*, 757–764.

[42] M. Fujita, K. Ogura, *Coord. Chem. Rev.* **1996**, *148*, 249–264.

[43] M. Fujita, *Chem. Soc. Rev.* **1998**, *27*, 417–425.

[44] G. F. Swiegers, T. J. Malefetse, *Chem. Rev.* **2000**, *100*, 3483–3537.

[45] R. W. Saalfrank, R. Burak, S. Reihs, N. Löw, F. Hampel, H. D. Stachel, J. Lentmaier, K. Peters, E. M. Peters, H. G. von Schnering, *Angew. Chem., Int. Ed.* **1995**, *34*, 993–995.

[46] R. W. Saalfrank, I. Bernt, *Curr. Opin. Solid. St. M.* **1998**, *3*, 407–413.

[47] P. N. W. Baxter, J.-M. Lehn, G. Baum, D. Fenske, *Chem. Eur. J.* **1999**, *5*, 102–112.

[48] P. N. W. Baxter, J.-M. Lehn, B. O. Kneisel, G. Baum, D. Fenske, *Chem. Eur. J.* **1999**, *5*, 113–120.

[49] J. R. Farrell, C. A. Mirkin, I. A. Guzei, L. M. Liable–Sands, A. L. Rheingold, *Angew. Chem., Int. Ed.* **1998**, *37*, 465–467.

[50] P. J. Steel, *Acc. Chem. Res.* **2005**, *38*, 243–250.

[51] A. Bader, E. Lindner, *Coord. Chem. Rev.* **1991**, *108*, 27–110.

[52] C. S. Slone, D. A. Weinberger, C. A. Mirkin, in *Progress in Inorganic Chemistry, Vol. 48* (Ed.: K. Karlin), Wiley, New York, **1999**, pp. 233–350.

[53] J. R. Farrell, A. H. Eisenberg, C. A. Mirkin, I. A. Guzei, L. M. Liable–Sands, C. D. Incarvito, A. L. Rheingold, C. L. Stern, *Organometallics* **1999**, *18*, 4856–4868.

[54] F. A. Cotton, G. Wilkinson, C. A. Murillo, M. Bochmann, *Advanced Inorganic Chemistry*, 6th ed., John Wiley & Sons, New York, **1999**.

[55] R. W. Saalfrank, A. Stark, K. Peters, H. G. von Schnering, *Angew. Chem., Int. Ed.* **1988**, *27*, 851–853.

[56] R. W. Saalfrank, A. Stark, M. Bremer, H. U. Hummel, *Angew. Chem., Int. Ed.* **1990**, *29*, 311–314.

[57] R. W. Saalfrank, B. Horner, D. Stalke, J. Salbeck, *Angew. Chem., Int. Ed.* **1993**, *32*, 1179–1182.

[58] R. W. Saalfrank, R. Burak, A. Breit, D. Stalke, R. Herbstirmer, J. Daub, M. Porsch, E. Bill, M. Muther, A. X. Trautwein, *Angew. Chem., Int. Ed.* **1994**, *33*, 1621–1623.

[59] C. Piguet, G. Bernardinelli, G. Hopfgartner, *Chem. Rev.* **1997**, *97*, 2005–2062.

[60] J. S. Fleming, K. L. V. Mann, C. A. Carraz, E. Psillakis, J. C. Jeffery, J. A. McCleverty, M. D. Ward, *Angew. Chem., Int. Ed.* **1998**, *37*, 1279–1281.

[61] M. Albrecht, I. Janser, R. Fröhlich, *Chem. Commun.* **2005**, 157–165.

[62] R. V. Slone, K. D. Benkstein, S. Bélanger, J. T. Hupp, I. A. Guzei, A. L. Rheingold, *Coord. Chem. Rev.* **1998**, *171*, 221–243.

[63] J. A. R. Navarro, B. Lippert, *Coord. Chem. Rev.* **1999**, *186*, 653–667.

[64] C. J. Jones, *Chem. Soc. Rev.* **1998**, *27*, 289–299.

[65] K. Nakabayashi, M. Kawano, M. Yoshizawa, S.-i. Ohkoshi, M. Fujita, *J. Am. Chem. Soc.* **2004**, *126*, 16694–16695.

[66] K. Nakabayashi, M. Kawano, M. Fujita, *Angew. Chem., Int. Ed.* **2005**, *44*, 5322–5325.

[67] M. Yoshizawa, K. Ono, K. Kumazawa, T. Kato, M. Fujita, *J. Am. Chem. Soc.* **2005**, *127*, 10800–10801.

[68] S. Tashiro, M. Tominaga, Y. Yamaguchi, K. Kato, M. Fujita, *Angew. Chem., Int. Ed.* **2006**, *45*, 241–244.

[69] P. J. Stang, D. H. Cao, K. C. Chen, G. M. Gray, D. C. Muddiman, R. D. Smith, *J. Am. Chem. Soc.* **1997**, *119*, 5163–5168.

[70] P. J. Stang, B. Olenyuk, J. Fan, A. M. Arif, *Organometallics* **1996**, *15*, 904–908.

[71] S. M. ALQaisi, K. J. Galat, M. H. Chai, D. G. Ray, P. L. Rinaldi, C. A. Tessier, W. J. Youngs, *J. Am. Chem. Soc.* **1998**, *120*, 12149–12150.

[72] F. Würthner, A. Sautter, *Chem. Commun.* **2000**, 445–446.

[73] F. Würthner, A. Sautter, D. Schmid, P. J. A. Weber, *Chem. Eur. J.* **2001**, *7*, 894–902.

[74] C. C. You, F. Würthner, *J. Am. Chem. Soc.* **2003**, *125*, 9716–9725.

[75] S. M. Contakes, K. K. Klausmeyer, R. M. Milberg, S. R. Wilson, T. B. Rauchfuss, *Organometallics* **1998**, *17*, 3633–3635.

[76] K. K. Klausmeyer, T. B. Rauchfuss, S. R. Wilson, *Angew. Chem., Int. Ed.* **1998**, *37*, 1694–1696.

[77] S. Roche, C. Haslam, H. Adams, S. L. Heath, J. A. Thomas, *Chem. Commun.* **1998**, 1681–1682.

[78] K. K. Klausmeyer, S. R. Wilson, T. B. Rauchfuss, *J. Am. Chem. Soc.* **1999**, *121*, 2705–2711.

[79] S. C. Johannessen, R. G. Brisbois, *J. Am. Chem. Soc.* **2001**, *123*, 3818–3819.

[80] M. Fujita, D. Oguro, M. Miyazawa, H. Oka, K. Yamaguchi, K. Ogura, *Nature* **1995**, *378*, 469–471.

[81] N. Takeda, K. Umemoto, K. Yamaguchi, M. Fujita, *Nature* **1999**, *398*, 794–796.

[82] B. Olenyuk, J. A. Whiteford, A. Fechtenkötter, P. J. Stang, *Nature* **1999**, *398*, 796–799.

[83] T. Kusukawa, M. Fujita, *Angew. Chem., Int. Ed.* **1998**, *37*, 3142–3144.

[84] H. Ito, T. Kusukawa, M. Fujita, *Chem. Lett.* **2000**, 598–599.

[85] M. Yoshizawa, T. Kusukawa, M. Fujita, S. Sakamoto, K. Yamaguchi, *J. Am. Chem. Soc.* **2001**, *123*, 10454–10459.

[86] W.-Y. Sun, T. Kusukawa, M. Fujita, *J. Am. Chem. Soc.* **2002**, *124*, 11570–11571.

[87] M. Yoshizawa, Y. Takeyama, T. Kusukawa, M. Fujita, *Angew. Chem., Int. Ed.* **2002**, *41*, 1347–1349.

[88] T. Kusukawa, T. Nakai, T. Okano, M. Fujita, *Chem. Lett.* **2003**, *32*, 284–285.

[89] M. Yoshizawa, M. Tamura, M. Fujita, *J. Am. Chem. Soc.* **2004**, *126*, 6846–6847.

[90] H. Hosoi, S. Yamaguchi, T. Tahara, *Chem. Lett.* **2005**, *34*, 618–619.

[91] S. Karthikeyan, V. Ramamurthy, *Tetrahedron Lett.* **2005**, *46*, 4495–4498.

[92] S. M. Contakes, M. L. Kuhlman, M. Ramesh, S. R. Wilson, T. B. Rauchfuss, *Proc. Natl. Acad. Sci. USA* **2002**, *99*, 4889–4893.

[93] S. C. N. Hsu, M. Ramesh, J. H. Espenson, T. B. Rauchfuss, *Angew. Chem., Int. Ed.* **2003**, *42*, 2663–2666.

[94] M. L. Kuhlman, T. B. Rauchfuss, *J. Am. Chem. Soc.* **2003**, *125*, 10084–10092.

[95] Y. Tanabe, S. Kuwata, Y. Ishii, *J. Am. Chem. Soc.* **2002**, *124*, 6528–6529.

[96] H. Kajitani, Y. Tanabe, S. Kuwata, M. Iwasaki, Y. Ishii, *Organometallics* **2005**, *24*, 2251–2254.

[97] H. Suzuki, N. Tajima, K. Tatsumi, Y. Yamamoto, *Chem. Commun.* **2000**, 1801–1802.

[98] Y. Yamamoto, H. Nakamura, J.-F. Ma, *J. Organomet. Chem.* **2001**, *640*, 10–20.

[99] Y. Yamamotoa, H. Suzuki, N. Tajima, K. Tatsumi, *Chem. Eur. J.* **2002**, *8*, 372–379.

[100] H. Amouri, M. N. Rager, F. Cagnol, J. Vaissermann, *Angew. Chem., Int. Ed.* **2001**, *40*, 3636–3638.

[101] J. Q. Wang, C. X. Ren, G. X. Jin, *Organometallics* **2006**, *25*, 74–81.

[102] Q. F. Zhang, R. D. Adams, W. H. Leung, *Inorg. Chim. Acta* **2006**, *359*, 978–983.

[103] M. L. Kuhlman, H. J. Yao, T. B. Rauchfuss, *Chem. Commun.* **2004**, 1370–1371.

[104] E. Baralt, S. J. Smith, J. Hurwitz, I. T. Horvath, R. H. Fish, *J. Am. Chem. Soc.* **1992**, *114*, 5187–5196.

[105] H. Chen, S. Ogo, R. H. Fish, *J. Am. Chem. Soc.* **1996**, *118*, 4993–5001.

[106] R. Bakhtiar, H. Chen, S. Ogo, R. H. Fish, *Chem. Commun.* **1997**, 2135–2136.

[107] S. Ogo, S. Nakamura, H. Chen, K. Isobe, Y. Watanabe, R. H. Fish, *J. Org. Chem.* **1998**, *63*, 7151–7156.

[108] R. H. Fish, *Coord. Chem. Rev.* **1999**, *186*, 569–584.

[109] S. Ogo, O. Buriez, J. B. Kerr, R. H. Fish, *J. Organomet. Chem.* **1999**, *589*, 66–74.

[110] R. H. Fish, G. Jaouen, *Organometallics* **2003**, *22*, 2166–2177.

[111] S. Korn, W. S. Sheldrick, *Inorg. Chim. Acta* **1997**, *254*, 85–91.

[112] S. Korn, W. S. Sheldrick, *J. Chem. Soc., Dalton Trans.* **1997**, 2191–2199.

[113] P. Annen, S. Schildberg, W. S. Sheldrick, *Inorg. Chim. Acta* **2000**, *307*, 115–124.

[114] K. Yamanari, R. Ito, S. Yamamoto, A. Fuyuhiro, *Chem. Commun.* **2001**, 1414–1415.

[115] K. Yamanari, R. Ito, S. Yamamoto, T. Konno, A. Fuyuhiro, M. Kobayashi, R. Arakawa, *Dalton Trans.* **2003**, 380–386.

[116] N. Shan, S. J. Vickers, H. Adams, M. D. Ward, J. A. Thomas, *Angew. Chem., Int. Ed.* **2004**, *43*, 3938–3941.

[117] R. Kramer, K. Polborn, C. Robl, W. Beck, *Inorg. Chim. Acta* **1992**, *200*, 415–420.

[118] S. Ogo, H. Chen, M. M. Olmstead, R. H. Fish, *Organometallics* **1996**, *15*, 2009–2013.

[119] K. Sunkel, W. Hoffmüller, W. Beck, *Z. Naturforsch. B.* **1998**, *53*, 1365–1368.

[120] D. Carmona, F. J. Lahoz, R. Atencio, L. A. Oro, M. P. Lamata, F. Viguri, E. San Jose, C. Vega, J. Reyes, F. Joo, A. Katho, *Chem. Eur. J.* **1999**, *5*, 1544–1564.

[121] A. Katho, D. Carmona, F. Viguri, C. D. Remacha, J. Kovacs, F. Joo, L. A. Oro, *J. Organomet. Chem.* **2000**, *594*, 299–306.

[122] D. Carmona, M. P. Lamata, F. Viguri, I. Dobrinovich, F. J. Lahoz, L. A. Oro, *Adv. Synth. Catal.* **2002**, *344*, 499–502.

[123] H. Chen, M. M. Olmstead, D. P. Smith, M. F. Maestre, R. H. Fish, *Angew. Chem., Int. Ed.* **1995**, *34*, 1514–1517.

[124] H. Piotrowski, G. Hilt, A. Schulz, P. Mayer, K. Polborn, K. Severin, *Chem. Eur. J.* **2001**, *7*, 3196–3208.

[125] M.-L. Lehaire, R. Scopelliti, L. Herdeis, K. Polborn, P. Mayer, K. Severin, *Inorg. Chem.* **2004**, *43*, 1609–1617.

[126] H. Piotrowski, K. Polborn, G. Hilt, K. Severin, *J. Am. Chem. Soc.* **2001**, *123*, 2699–2700.

[127] K. Severin, *Coord. Chem. Rev.* **2003**, *245*, 3–10.

[128] M.-L. Lehaire, A. Schulz, R. Scopelliti, K. Severin, *Inorg. Chem.* **2003**, *42*, 3576–3581.

[129] L. Mimassi, C. Guyard–Duhayon, M. N. Rager, H. Amouri, *Inorg. Chem.* **2004**, *43*, 6644–6649.

[130] K. Yamanari, R. Ito, S. Yamamoto, T. Konno, A. Fuyuhiro, K. Fujioka, R. Arakawa, *Inorg. Chem.* **2002**, *41*, 6824–6830.

[131] K. Yamanari, R. Yamamoto, R. Ito, Y. Kushi, A. Fuyuhiro, N. Kubota, T. Fukuo, R. Arakawa, *Angew. Chem., Int. Ed.* **2001**, *40*, 2268–2271.

[132] K. Yamanari, I. Fukuda, S. Yamamoto, Y. Kushi, A. Fuyuhiro, N. Kubota, T. Fukuo, R. Arakawa, *J. Chem. Soc., Dalton Trans.* **2000**, 2131–2136.

[133] K. Haas, H. Nöth, W. Beck, *Z. Naturforsch. B.* **1999**, *54*, 989–992.

[134] M. S. Lah, M. L. Kirk, W. Hatfield, V. L. Pecoraro, *J. Chem. Soc., Chem. Commun.* **1989**, 1606–1608.

[135] M. S. Lah, V. L. Pecoraro, *J. Am. Chem. Soc.* **1989**, *111*, 7258–7259.

[136] V. L. Pecoraro, *Inorg. Chim. Acta* **1989**, *155*, 171–173.

[137] V. L. Pecoraro, A. J. Stemmler, B. R. Gibney, J. J. Bodwin, H. Wang, J. W. Kampf, A. Barwinski, in *Progress in Inorganic Chemistry, Vol. 45*, **1997**, pp. 83–177.

[138] J. J. Bodwin, A. D. Cutland, R. G. Malkani, V. L. Pecoraro, *Coord. Chem. Rev.* **2001**, *216*, 489–512.

[139] B. R. Gibney, A. J. Stemmler, S. Pilotek, J. W. Kampf, V. L. Pecoraro, *Inorg. Chem.* **1993**, *32*, 6008–6015.

[140] R. M. Izatt, J. S. Bradshaw, S. A. Nielsen, J. D. Lamb, J. J. Christensen, *Chem. Rev.* **1985**, *85*, 271–339.

[141] D. P. Kessissoglou, J. Kampf, V. L. Pecoraro, *Polyhedron* **1994**, *13*, 1379–1391.

[142] B. R. Gibney, D. P. Kessissoglou, J. W. Kampf, V. L. Pecoraro, *Inorg. Chem.* **1994**, *33*, 4840–4849.

[143] B. R. Gibney, H. Wang, J. W. Kampf, V. L. Pecoraro, *Inorg. Chem.* **1996**, *35*, 6184–6193.

[144] A. J. Stemmler, A. Barwinski, M. J. Baldwin, V. Young, V. L. Pecoraro, *J. Am. Chem. Soc.* **1996**, *118*, 11962–11963.

[145] A. J. Stemmler, J. W. Kampf, V. L. Pecoraro, *Angew. Chem., Int. Ed.* **1996**, *35*, 2841–2843.

[146] A. J. Stemmler, J. W. Kampf, M. L. Kirk, B. H. Atasi, V. L. Pecoraro, *Inorg. Chem.* **1999**, *38*, 2807–2817.

[147] S. K. Mandal, V. G. Young, Jr., L. Que, *Inorg. Chem.* **2000**, *39*, 1831–1833.

[148] A. D. Cutland, J. A. Halfen, J. W. Kampf, V. L. Pecoraro, *J. Am. Chem. Soc.* **2001**, *123*, 6211–6212.

[149] C. Dendrinou–Samara, G. Psomas, L. Iordanidis, V. Tangoulis, D. P. Kessissoglou, *Chem. Eur. J.* **2001**, *7*, 5041–5051.

[150] G. Psomas, A. J. Stemmler, C. Dendrinou–Samara, J. J. Bodwin, M. Schneider, M. Alexiou, J. W. Kampf, D. P. Kessissoglou, V. L. Pecoraro, *Inorg. Chem.* **2001**, *40*, 1562–1570.

[151] Y. Bai, D.-b. Dang, C.-y. Duan, Y. Song, Q.-j. Meng, *Inorg. Chem.* **2005**, *44*, 5972–5974.

[152] R. W. Saalfrank, N. Löw, F. Hampel, H.-D. Stachel, *Angew. Chem., Int. Ed.* **1996**, *35*, 2209–2210.

[153] R. W. Saalfrank, N. Löw, S. Kareth, V. Seitz, F. Hampel, D. Stalke, M. Teichert, *Angew. Chem., Int. Ed.* **1998**, *37*, 172–175.

[154] G. Psomas, C. Dendrinou–Samara, M. Alexiou, A. Tsohos, C. P. Raptopoulou, A. Terzis, D. P. Kessissoglou, *Inorg. Chem.* **1998**, *37*, 6556–6557.

[155] A. D. Cutland, R. G. Malkani, J. W. Kampf, V. L. Pecoraro, *Angew. Chem., Int. Ed.* **2000**, *39*, 2689–2691.

[156] F.-F. Jian, K. Jiao, Y. Li, P.-S. Zhao, L.-D. Lu, *Angew. Chem., Int. Ed.* **2003**, *42*, 5722–5724.

[157] H. Rauter, E. C. Hillgeris, A. Erxleben, B. Lippert, *J. Am. Chem. Soc.* **1994**, *116*, 616–624.

[158] M. S. Lah, B. R. Gibney, D. L. Tierney, J. E. Penner–Hahn, V. L. Pecoraro, *J. Am. Chem. Soc.* **1993**, *115*, 5857–5858.

[159] A. J. Stemmler, J. W. Kampf, V. L. Pecoraro, *Inorg. Chem.* **1995**, *34*, 2271–2272.

[160] M. Alexiou, C. Dendrinou–Samara, C. P. Raptopoulou, A. Terzis, D. P. Kessissoglou, *Inorg. Chem.* **2002**, *41*, 4732–4738.

[161] M. Alexiou, E. Katsoulakou, C. Dendrinou–Samara, C. P. Raptopoulou, V. Psycharis, E. Manessi–Zoupa, S. P. Perlepes, D. P. Kessissoglou, *Eur. J. Inorg. Chem.* **2005**, 1964–1978.

[162] T. C. Stamatatos, S. Dionyssopoulou, G. Efthymiou, P. Kyritsis, C. P. Raptopoulou, A. Terzis, R. Vicente, A. Escuer, S. P. Perlepes, *Inorg. Chem.* **2005**, *44*, 3374–3376.

[163] C. Papatriantafyllopoulou, C. P. Raptopoulou, A. Terzis, E. Manessi–Zoupa, S. P. Perlepes, *Z. Naturforsch. B.* **2006**, *61*, 37–46.

[164] T. Habereder, M. Warchhold, H. Nöth, K. Severin, *Angew. Chem., Int. Ed.* **1999**, *38*, 3225–3228.

[165] H. Piotrowski, K. Severin, *Proc. Natl. Acad. Sci. USA* **2002**, *99*, 4997–5000.

[166] M.-L. Lehaire, R. Scopelliti, H. Piotrowski, K. Severin, *Angew. Chem., Int. Ed.* **2002**, *41*, 1419–1422.

[167] I. Fernandez, E. Martinez–Viviente, P. S. Pregosin, *Inorg. Chem.* **2005**, *44*, 5509–5513.

[168] M.-L. Lehaire, R. Scopelliti, K. Severin, *Inorg. Chem.* **2002**, *41*, 5466–5474.

[169] M.-L. Lehaire, R. Scopelliti, K. Severin, *Chem. Commun.* **2002**, 2766–2767.

[170] G. W. Gokel, W. M. Leevy, M. E. Weber, *Chem. Rev.* **2004**, *104*, 2723–2750.

[171] B. G. Cox, H. Schneider, J. Stroka, *J. Am. Chem. Soc.* **1978**, *100*, 4746–4749.

[172] B. G. Cox, J. Garciarosas, H. Schneider, *J. Am. Chem. Soc.* **1981**, *103*, 1054–1059.

[173] G. W. Liesegang, M. M. Farrow, F. A. Vazquez, N. Purdie, E. M. Eyring, *J. Am. Chem. Soc.* **1977**, *99*, 3240–3243.

[174] R. M. Izatt, K. Pawlak, J. S. Bradshaw, R. L. Bruening, *Chem. Rev.* **1991**, *91*, 1721–2085.

[175] G. W. Gokel, D. M. Goli, C. Minganti, L. Echegoyen, *J. Am. Chem. Soc.* **1983**, *105*, 6786–6788.

[176] F. A. Cotton, G. Wilkinson, C. A. Murillo, M. Bochmann, 6th ed., John Wiley & Sons, New York, **1999**, p. 102.

[177] S. J. Rowan, S. J. Cantrill, G. R. L. Cousins, J. K. M. Sanders, J. F. Stoddart, *Angew. Chem., Int. Ed.* **2002**, *41*, 898–952.

[178] R. Hoss, F. Vögtle, *Angew. Chem., Int. Ed.* **1994**, *33*, 375–384.

[179] S. Otto, R. L. E. Furlan, J. K. M. Sanders, *Curr. Opin. Chem. Biol.* **2002**, *6*, 321–327.

[180] A. Ganesan, *Angew. Chem., Int. Ed.* **1998**, *37*, 2828–2831.

[181] J.-M. Lehn, *Chem. Eur. J.* **1999**, *5*, 2455–2463.

[182] C. Karan, B. L. Miller, *Drug Discov. Today* **2000**, *5*, 67–75.

[183] S. Otto, R. L. E. Furlan, J. K. M. Sanders, *Drug Discov. Today* **2002**, *7*, 117–125.

[184] J. L. Reymond, *Angew. Chem., Int. Ed.* **2004**, *43*, 5577–5579.

[185] J. D. Cheeseman, A. D. Corbett, J. L. Gleason, R. J. Kazlauskas, *Chem. Eur. J.* **2005**, *11*, 1708–1716.

[186] P. T. Corbett, J. Leclaire, L. Vial, K. R. West, J.-L. Wietor, J. K. M. Sanders, S. Otto, *Chem. Rev.* **2006**, *ASAP Article*.

[187] M. Freemantle, *C. & En.* **2002**, *September*, 31–33.

[188] P. A. Brady, R. P. Bonar–Law, S. J. Rowan, C. J. Suckling, J. K. M. Sanders, *Chem. Commun.* **1996**, 319–320.

[189] S. J. Rowan, P. A. Brady, J. K. M. Sanders, *Angew. Chem., Int. Ed.* **1996**, *35*, 2143–2145.

[190] S. J. Rowan, D. G. Hamilton, P. A. Brady, J. K. M. Sanders, *J. Am. Chem. Soc.* **1997**, *119*, 2578–2579.

[191] S. J. Rowan, J. K. M. Sanders, *Chem. Commun.* **1997**, 1407–1408.

[192] B. Hasenknopf, J.-M. Lehn, B. O. Kneisel, G. Baum, D. Fenske, *Angew. Chem., Int. Ed.* **1996**, *35*, 1838–1840.

[193] B. Hasenknopf, J.-M. Lehn, N. Boumediene, A. DupontGervais, A. VanDorsselaer, B. Kneisel, D. Fenske, *J. Am. Chem. Soc.* **1997**, *119*, 10956–10962.

[194] I. Huc, J.-M. Lehn, *Proc. Natl. Acad. Sci. USA* **1997**, *94*, 2106–2110.

[195] T. Hayashi, T. Asai, H. Hokazono, H. Ogoshi, *J. Am. Chem. Soc.* **1993**, *115*, 12210–12211.

[196] B. A. Katz, J. Finermoore, R. Mortezaei, D. H. Rich, R. M. Stroud, *Biochemistry* **1995**, *34*, 8264–8280.

[197] P. G. Swann, R. A. Casanova, A. Desai, M. M. Frauenhoff, M. Urbancic, U. Slomczynska, A. J. Hopfinger, G. C. LeBreton, D. L. Venton, *Biopolymers* **1996**, *40*, 617–625.

[198] A. V. Eliseev, M. I. Nelen, *J. Am. Chem. Soc.* **1997**, *119*, 1147–1148.

[199] B. Klekota, M. H. Hammond, B. L. Miller, *Tetrahedron Lett.* **1997**, *38*, 8639–8642.

[200] S. Sakai, Y. Shigemasa, T. Sasaki, *Tetrahedron Lett.* **1997**, *38*, 8145–8148.

[201] R. T. S. Lam, A. Belenguer, S. L. Roberts, C. Naumann, T. Jarrosson, S. Otto, J. K. M. Sanders, *Science* **2005**, *308*, 667–669.

[202] P. A. Brady, J. K. M. Sanders, *J. Chem. Soc., Perk. Trans. 1* **1997**, 3237–3253.

[203] M. Albrecht, O. Blau, R. Fröhlich, *Chem. Eur. J.* **1999**, *5*, 48–56.

[204] R. L. E. Furlan, Y. F. Ng, S. Otto, J. K. M. Sanders, *J. Am. Chem. Soc.* **2001**, *123*, 8876–8877.

[205] S. L. Roberts, R. L. E. Furlan, S. Otto, J. K. M. Sanders, *Org. Biomol. Chem.* **2003**, *1*, 1625–1633.

[206] O. Storm, U. Luning, *Chem. Eur. J.* **2002**, *8*, 793–798.

[207] G. R. L. Cousins, R. L. E. Furlan, Y. F. Ng, J. E. Redman, J. K. M. Sanders, *Angew. Chem., Int. Ed.* **2001**, *40*, 423–428.

[208] R. L. E. Furlan, Y. F. Ng, G. R. L. Cousins, J. E. Redman, J. K. M. Sanders, *Tetrahedron* **2002**, *58*, 771–778.

[209] S. Otto, R. L. E. Furlan, J. K. M. Sanders, *Science* **2002**, *297*, 590–593.

[210] S. L. Roberts, R. L. E. Furlan, G. R. L. Cousins, J. K. M. Sanders, *Chem. Commun.* **2002**, 938–939.

[211] S. Otto, S. Kubik, *J. Am. Chem. Soc.* **2003**, *125*, 7804–7805.

[212] M. C. Calama, P. Timmerman, D. N. Reinhoudt, *Angew. Chem., Int. Ed.* **2000**, *39*, 755–758.

[213] G. Kaiser, J. K. M. Sanders, *Chem. Commun.* **2000**, 1763–1764.

[214] E. Stulz, Y. F. Ng, S. M. Scott, J. K. M. Sanders, *Chem. Commun.* **2002**, 524–525.

[215] R. L. E. Furlan, G. R. L. Cousins, J. K. M. Sanders, *Chem. Commun.* **2000**, 1761–1762.

[216] I. Huc, M. J. Krische, D. P. Funeriu, J.-M. Lehn, *Eur. J. Inorg. Chem.* **1999**, 1415–1420.

[217] S. Hiraoka, M. Fujita, *J. Am. Chem. Soc.* **1999**, *121*, 10239–10240.

[218] Y. Kubota, S. Sakamoto, K. Yamaguchi, M. Fujita, *Proc. Natl. Acad. Sci. USA* **2002**, *99*, 4854–4856.

[219] M. Yoshizawa, M. Nagao, K. Umemoto, K. Biradha, M. Fujita, S. Sakamoto, K. Yamaguchi, *Chem. Commun.* **2003**, 1808–1809.

[220] Y. Yamanoi, Y. Sakamoto, T. Kusukawa, M. Fujita, S. Sakamoto, K. Yamaguchi, *J. Am. Chem. Soc.* **2001**, *123*, 980–981.

[221] B. Klekota, B. L. Miller, *Tetrahedron* **1999**, *55*, 11687–11697.

[222] C. Karan, B. L. Miller, *J. Am. Chem. Soc.* **2001**, *123*, 7455–7456.

[223] H. Hioki, W. C. Still, *J. Org. Chem.* **1998**, *63*, 904–905.

[224] Y. Krishnan–Ghosh, S. Balasubramanian, *Angew. Chem., Int. Ed.* **2003**, *42*, 2171–2173.

[225] O. Ramström, J.-M. Lehn, *ChemBioChem* **2000**, *1*, 41–48.

[226] M. Hochgürtel, R. Biesinger, H. Kroth, D. Piecha, M. W. Hofmann, S. Krause, O. Schaaf, C. Nicolau, A. V. Eliseev, *J. Med. Chem.* **2003**, *46*, 356–358.

[227] M. S. Congreve, D. J. Davis, L. Devine, C. Granata, M. O'Reilly, P. G. Wyatt, H. Jhoti, *Angew. Chem., Int. Ed.* **2003**, *42*, 4479–4482.

[228] B. Brisig, J. K. M. Sanders, S. Otto, *Angew. Chem., Int. Ed.* **2003**, *42*, 1270–1273.

[229] O. Ramström, J.-M. Lehn, *Nat. Rev. Drug Discov.* **2002**, *1*, 26–36.

[230] S. Otto, *J. Mater. Chem.* **2005**, *15*, 3357–3361.

[231] Y. G. Ma, S. V. Kolotuchin, S. C. Zimmerman, *J. Am. Chem. Soc.* **2002**, *124*, 13757–13769.

[232] S. Otto, R. L. E. Furlan, J. K. M. Sanders, *J. Am. Chem. Soc.* **2000**, *122*, 12063–12064.

[233] P. Mendes, *Comput. Appl. Biosci.* **1993**, *9*, 563–571.

[234] P. Mendes, *Trends Biochem. Sci.* **1997**, *22*, 361–363.

[235] A. V. Eliseev, M. I. Nelen, *Chem. Eur. J.* **1998**, *4*, 825–834.

[236] M. A. Case, G. L. McLendon, *J. Am. Chem. Soc.* **2000**, *122*, 8089–8090.

[237] M. Hochgürtel, H. Kroth, D. Piecha, M. W. Hofmann, C. Nicolau, S. Krause, O. Schaaf, G. Sonnenmoser, A. V. Eliseev, *Proc. Natl. Acad. Sci. USA* **2002**, *99*, 3382–3387.

[238] H. J. Cooper, M. A. Case, G. L. McLendon, A. G. Marshall, *J. Am. Chem. Soc.* **2003**, *125*, 5331–5339.

[239] K. Severin, *Chem. Eur. J.* **2004**, *10*, 2565–2580.

[240] P. T. Corbett, J. K. M. Sanders, S. Otto, *J. Am. Chem. Soc.* **2005**, *127*, 9390–9392.

[241] I. Saur, K. Severin, *Chem. Commun.* **2005**, 1471–1473.

[242] P. T. Corbett, S. Otto, J. K. M. Sanders, *Chem. Eur. J.* **2004**, *10*, 3139–3143.

[243] I. Saur, R. Scopelliti, K. Severin, *Chem. Eur. J.* **2006**, *12*, 1058–1066.

[244] B. de Bruin, P. Hauwert, J. N. H. Reek, *Angew. Chem., Int. Ed.* **2006**, *45*, 2660–2663.

[245] P. Thanasekaran, R. T. Liao, Y. H. Liu, T. Rajendran, S. Rajagopal, K. L. Lu, *Coord. Chem. Rev.* **2005**, *249*, 1085–1110.

[246] S. J. Lee, J. T. Hupp, *Coord. Chem. Rev.* **2006**, *250*, 1710–1723.

[247] R. V. Slone, D. I. Yoon, R. M. Calhoun, J. T. Hupp, *J. Am. Chem. Soc.* **1995**, *117*, 11813–11814.

[248] P. J. Stang, N. E. Persky, *Chem. Commun.* **1997**, 77–78.

[249] J. A. Whiteford, C. V. Lu, P. J. Stang, *J. Am. Chem. Soc.* **1997**, *119*, 2524–2533.

[250] C. Müller, J. A. Whiteford, P. J. Stang, *J. Am. Chem. Soc.* **1998**, *120*, 9827–9837.

[251] M. M. Ali, F. M. MacDonnell, *J. Am. Chem. Soc.* **2000**, *122*, 11527–11528.

[252] R. D. Sommer, A. L. Rheingold, A. J. Goshe, B. Bosnich, *J. Am. Chem. Soc.* **2001**, *123*, 3940–3952.

[253] N. C. Gianneschi, C. A. Mirkin, L. N. Zakharov, A. L. Rheingold, *Inorg. Chem.* **2002**, *41*, 5326–5328.

[254] H. Oshio, H. Onodera, T. Ito, *Chem. Eur. J.* **2003**, *9*, 3946–3950.

[255] J. K. Bera, J. Bacsa, B. W. Smucker, K. R. Dunbar, *Eur. J. Inorg. Chem.* **2004**, 368–375.

[256] J. Forniés, J. Gómez, E. Lalinde, M. T. Moreno, *Chem. Eur. J.* **2004**, *10*, 888–898.

[257] D. Guo, C.-y. Duan, F. Lu, Y. Hasegawa, Q.-j. Meng, S. Yanagida, *Chem. Commun.* **2004**, 1486–1487.

[258] G. R. Newkome, T. J. Cho, C. N. Moorefield, P. P. Mohapatra, L. A. Godínez, *Chem. Eur. J.* **2004**, *10*, 1493–1500.

[259] M. C. Álvarez–Vergara, M. A. Casado, M. L. Martín, F. J. Lahoz, L. A. Oro, J. J. Pérez–Torrente, *Organometallics* **2005**, *24*, 5929–5936.

[260] G. R. Newkome, P. S. Wang, C. N. Moorefield, T. J. Cho, P. P. Mohapatra, S. N. Li, S.-H. Hwang, O. Lukoyanova, L. Echegoyen, J. A. Palagallo, V. Iancu, S.-W. Hla, *Science* **2006**, *312*, 1782–1785.

[261] J. K. Bera, B. W. Smucker, R. A. Walton, K. R. Dunbar, *Chem. Commun.* **20001**, 2562–2563.

[262] S.-T. Cheng, E. Doxiadi, R. Vilar, A. J. P. White, D. J. Williams, *J. Chem. Soc., Dalton Trans.* **2001**, 2239–2244.

[263] E. Doxiadi, R. Vilar, A. J. P. White, D. J. Williams, *Polyhedron* **2003**, *22*, 2991–2998.

[264] M. A. Galindo, S. Galli, J. A. R. Navarro, M. A. Romero, *Dalton Trans.* **2004**, 2780–2785.

[265] M. Yoshizawa, M. Nagao, K. Kumazawa, M. Fujita, *J. Organomet. Chem.* **2005**, *690*, 5383–5388.

[266] M. Yoshizawa, J. Nakagawa, K. Kumazawa, M. Nagao, M. Kawano, T. Ozeki, M. Fujita, *Angew. Chem. Int. Ed.* **2005**, *44*, 1810–1813.

[267] J. Y. Zhang, P. W. Miller, M. Nieuwenhuyzen, S. L. James, *Chem. Eur. J.* **2006**, *12*, 2448–2453.

[268] D. M. De Freitas, M. M. C. A. Castro, C. F. G. C. Geraldes, *Acc. Chem. Res.* **2006**, *39*, 283–291.

[269] J. F. J. Cade, *Med. J. Australia* **1949**, *2*, 349–352.

[270] I. Daly, *Lancet* **1997**, *349*, 1157–1160.

[271] N. J. Birch, *Chem. Rev.* **1999**, *99*, 2659–2682.

[272] R. S. McIntyre, D. A. Mancini, S. Parikh, S. H. Kennedy, *Can. J. Psychiat.* **2001**, *46*, 322–327.

[273] J. M. Pomerantz, *Drug Benefit Trends* **2004**, *16*, 325–326.

[274] B. De Strooper, J. Woodgett, *Nature* **2003**, *423*, 392–393.

[275] C. J. Phiel, C. A. Wilson, V. M. Y. Lee, P. S. Klein, *Nature* **2003**, *423*, 435–439.

[276] H. R. Pilcher, *Nature* **2003**, *11*, 118–120.

[277] R. A. Bartsch, M. Ramesh, R. O. Bach, T. Shono, K. Kumura, in *Lithium Chemistry* (Eds.: A.-M. Sapse, P. von Ragué Schleyer), John Wiley & Sons, New York, **1995**, pp. 393–476.

[278] G. D. Christian, *J. Pharmaceut. Biomed.* **1996**, *14*, 899–908.

[279] J. E. Gough, P. Christian, C. A. Scotchford, C. D. Rudd, C. J. Jones, *J. Biomed. Mater. Res.* **2002**, *59*, 481–489.

[280] S. Faulkner, R. Kataky, D. Parker, A. Teasdale, *J. Chem. Soc., Perk. Trans. 2* **1995**, 1761–1769.

[281] K. Kobiro, *Coord. Chem. Rev.* **1996**, *148*, 135–149.

[282] F. Bockstahl, E. Graf, M. W. Hosseini, D. Suhr, A. DeCian, J. Fischer, *Tetrahedron Lett.* **1997**, *38*, 7539–7542.

[283] H. Tsukube, S. Shinoda, Y. Mizutani, M. Okano, K. Takagi, K. Hori, *Tetrahedron* **1997**, *53*, 3487–3496.

[284] S. Inokuma, M. Takezawa, H. Satoh, Y. Nakamura, T. Sasaki, J. Nishimura, *J. Org. Chem.* **1998**, *63*, 5791–5796.

[285] L. A. Paquette, J. S. Tae, E. R. Hickey, R. D. Rogers, *Angew. Chem., Int. Ed.* **1999**, *38*, 1409–1411.

[286] Y. Y. Chen, F. F. Yang, S. L. Gong, *Tetrahedron Lett.* **2000**, *41*, 4815–4818.

[287] J. A. Chen, J. L. Lai, G. H. Lee, Y. Wang, J. K. Su, H. C. Yeh, W. Y. Lin, M. K. Leung, *Org. Lett.* **2001**, *3*, 3999–4002.

[288] S. O. Obare, C. J. Murphy, *Inorg. Chem.* **2001**, *40*, 6080–6082.

[289] L. A. Paquette, J. S. Tae, *J. Am. Chem. Soc.* **2001**, *123*, 4974–4984.

[290] T. Gunnlaugsson, B. Bichell, C. Nolan, *Tetrahedron Lett.* **2002**, *43*, 4989–4992.

[291] W. Qin, S. O. Obare, C. J. Murphy, S. M. Angel, *Anal. Chem.* **2002**, *74*, 4757–4762.

[292] G. G. Talanova, V. S. Talanov, H. S. Hwang, B. A. Eliasi, R. A. Bartsch, *J. Chem. Soc., Perk. Trans. 2* **2002**, 1869–1874.

[293] S. Tsuchiya, Y. Nakatani, R. Ibrahim, S. Ogawa, *J. Am. Chem. Soc.* **2002**, *124*, 4936–4937.

[294] T. Gunnlaugsson, B. Bichell, C. Nolan, *Tetrahedron* **2004**, *60*, 5799–5806.

[295] A. J. Smetana, A. I. Popov, *J. Solution Chem.* **1980**, *9*, 183–196.

[296] N. R. Jana, L. Gearheart, S. O. Obare, C. J. Murphy, *Langmuir* **2002**, *18*, 922–927.

[297] B. G. Cox, J. Garciarosas, H. Schneider, *J. Am. Chem. Soc.* **1981**, *103*, 1384–1389.

[298] A. Bencini, A. Bianchi, A. Borselli, M. Ciampolini, E. Garciaespana, P. Dapporto, M. Micheloni, P. Paoli, J. A. Ramirez, B. Valtancoli, *Inorg. Chem.* **1989**, *28*, 4279–4284.

[299] A. Bencini, A. Bianchi, A. Borselli, S. Chimichi, M. Ciampolini, P. Dapporto, M. Micheloni, N. Nardi, P. Paoli, B. Valtancoli, *Inorg. Chem.* **1990**, *29*, 3282–3286.

[300] A. Bencini, A. Bianchi, S. Chimichi, M. Ciampolini, P. Dapporto, E. Garciaespana, M. Micheloni, N. Nardi, P. Paoli, B. Valtancoli, *Inorg. Chem.* **1991**, *30*, 3687–3691.

[301] A. Bencini, V. Fusi, C. Giorgi, M. Micheloni, N. Nardi, B. Valtancoli, *J. Chem. Soc., Perk. Trans. 2* **1996**, 2297–2302.

[302] M. Micheloni, M. Formica, V. Fusi, P. Romani, R. Pontellini, P. Dapporto, P. Paoli, P. Rossi, B. Valtancoli, *Eur. J. Inorg. Chem.* **2000**, 51–57.

[303] P. Dapporto, M. Formica, V. Fusi, L. Giorgi, M. Micheloni, R. Pontellini, P. Paoli, P. Rossi, *Eur. J. Inorg. Chem.* **2001**, 1763–1774.

[304] A. Nakamura, S. Kamiya, *Chem. Pharm. Bull.* **1968**, *16*, 1466–&.

[305] A. G. Osborne, L. Jackson, P. D. Taylor, *Spectrochim. Acta A* **1993**, *49*, 1703–1708.

[306] M. K. Patel, R. Fox, P. D. Taylor, *Tetrahedron* **1996**, *52*, 1835–1840.

[307] W.-K. Chi, Y. S. Ahn, T. H. Park, J. S. Ahn, H. A. Kim, J. Y. Park, *J. Korean Chem. Soc.* **2001**, *45*, 51–60.

[308] L. Carter, D. L. Davies, J. Fawcett, D. R. Russel, *Polyhedron* **1993**, *12*, 1599–1602.

[309] R. Lang, K. Polborn, T. Severin, K. Severin, *Inorg. Chim. Acta* **1999**, *294*, 62–67.

[310] Z. Grote, M.-L. Lehaire, R. Scopelliti, K. Severin, *J. Am. Chem. Soc.* **2003**, *125*, 13638–13639.

[311] J. Dale, J. Eggestad, S. B. Fredriksen, P. Groth, *J. Chem. Soc., Chem. Commun.* **1987**, 1391–1393.

[312] S. B. Fredriksen, J. Dale, *Acta Chem. Scand.* **1992**, *46*, 574–588.

[313] K. Severin, R. Bergs, W. Beck, *Angew. Chem., Int. Ed.* **1998**, *37*, 1635–1654.

[314] A. Buryak, K. Severin, *Angew. Chem., Int. Ed.* **2004**, *43*, 4771–4774.

[315] I. W. McNae, K. Fishburne, A. Habtemariam, T. M. Hunter, M. Melchart, F. Y. Wang, M. D. Walkinshaw, P. J. Sadler, *Chem. Commun.* **2004**, 1786–1787.

[316] B. Valeur, I. Leray, *Coord. Chem. Rev.* **2000**, *205*, 3–40.

[317] L. Fabbrizzi, M. Licchelli, P. Pallavicini, D. Sacchi, A. Taglietti, *Analyst* **1996**, *121*, 1763–1768.

[318] R. Bergonzi, L. Fabbrizzi, M. Licchelli, C. Mangano, *Coord. Chem. Rev.* **1998**, *170*, 31–46.

[319] A. Schepartz, J. P. Mcdevitt, *J. Am. Chem. Soc.* **1989**, *111*, 5976–5977.

[320] D. M. Rudkevich, A. N. Shivanyuk, Z. Brzozka, W. Verboom, D. N. Reinhoudt, *Angew. Chem., Int. Ed.* **1995**, *34*, 2124–2126.

[321] T. Nabeshima, T. Takahashi, T. Hanami, A. Kikuchi, T. Kawabe, Y. Yano, *J. Org. Chem.* **1998**, *63*, 3802–3803.

[322] J. T. Davis, *Angew. Chem., Int. Ed.* **2004**, *43*, 668–698.

[323] S. L. Wiskur, H. Ait–Haddou, J. J. Lavigne, E. V. Anslyn, *Acc. Chem. Res.* **2001**, *34*, 963–972.

[324] L. Fabbrizzi, M. Lichelli, A. Taglietti, *Dalton Trans.* **2003**, 3471–3479.

[325] C. Suksai, T. Tuntulani, *Chem. Soc. Rev.* **2003**, *32*, 192–202.

[326] R. D. Shannon, *Acta Crystallogr., Sect. A* **1976**, *32*, 751–767.

[327] J. Thewlis, *Acta Cryst.* **1955**, *8*, 36–38.

[328] D. N. Knyazev, *Russ. J. Phys. Chem.* **1961**, *35*, 298–301.

[329] K. G. Heumann, *Top. Curr. Chem.* **1985**, *127*, 77–132.

[330] K. Nishizawa, T. Takano, I. Ikeda, M. Okahara, *Separ. Sci. Technol.* **1988**, *23*, 333–345.

[331] Y. Kanzaki, N. Suzuki, R. Chitrakar, T. Ohsaka, M. Abe, *J. Phys. Chem. B* **2002**, *106*, 988–995.

[332] R. Kikuchi, H. Takahashi, T. Oi, M. Hosoe, *J. Mater. Sci.* **2003**, *38*, 515–520.

[333] H. Takahashi, Y. H. Zhang, T. Miyajima, T. Oi, *J. Mater. Chem.* **2006**, *16*, 1462–1469.

[334] D. W. Kim, Y. S. Jeon, T. Y. Eom, M. Y. Suh, C. H. Lee, *J. Radioanal. Nucl. Chem.* **1991**, *150*, 417–426.

[335] D. W. Kim, S. R. Park, S. J. Kim, S. J. Kim, H. J. Kim, *J. Radioanal. Nucl. Chem.* **1998**, *229*, 165–168.

[336] Y. Ban, M. Nomura, Y. Fujii, *J. Nucl. Sci. Technol.* **2002**, *39*, 279–281.

[337] D. W. Kim, *J. Radioanal. Nucl. Chem.* **2002**, *253*, 67–71.

[338] A. A. Palko, J. S. Drury, G. M. Begun, *J. Chem. Phys.* **1976**, *64*, 1828–1837.

[339] H. P. Qi, T. B. Coplen, Q. Z. Wang, Y. H. Wang, *Anal. Chem.* **1997**, *69*, 4076–4078.

[340] *Handbook of Chemistry and Physics*, 66th ed. (Ed.: R. C. Weast), CRC Press, Boca Raton, Florida, **1985–1986**, p. B–108.

[341] A. K. Duhme, Z. Dauter, R. C. Hider, S. Pohl, *Inorg. Chem.* **1996**, *35*, 3059–3061.

[342] A. K. Duhme, *Z. Anorg. Allg. Chem.* **1998**, *624*, 1922–1926.

[343] A. K. Duhme, S. C. Davies, D. L. Hughes, *Inorg. Chem.* **1998**, *37*, 5380–5382.

[344] A. K. Duhme–Klair, G. Vollmer, C. Mars, R. Fröhlich, *Angew. Chem., Int. Ed.* **2000**, *39*, 1626–1628.

[345] M. Albrecht, P. Stortz, *Chem. Soc. Rev.* **2005**, *34*, 496–506.

[346] X. K. Sun, D. W. Johnson, D. L. Caulder, R. E. Powers, K. N. Raymond, E. H. Wong, *Angew. Chem., Int. Ed.* **1999**, *38*, 1303–1307.

[347] S. P. Hajela, A. R. Johnson, J. D. Xu, C. J. Sunderland, S. M. Cohen, D. L. Caulder, K. N. Raymond, *Inorg. Chem.* **2001**, *40*, 3208–3216.

[348] X. K. Sun, D. W. Johnson, D. L. Caulder, K. N. Raymond, E. H. Wong, *J. Am. Chem. Soc.* **2001**, *123*, 2752–2763.

[349] M. Albrecht, S. Mirtschin, M. de Groot, I. Janser, J. Runsink, G. Raabe, M. Kogej, C. A. Schalley, R. Frohlich, *J. Am. Chem. Soc.* **2005**, *127*, 10371–10387.

[350] M. Albrecht, *Chem. Rev.* **2001**, *101*, 3457–3497.

[351] M. Fujita, S. Nagao, K. Ogura, *J. Am. Chem. Soc.* **1995**, *117*, 1649–1650.

[352] E. Lindner, C. Hermann, G. Baum, D. Fenske, *Eur. J. Inorg. Chem.* **1999**, 679–685.

[353] Y. Bretonnière, M. Mazzanti, R. Wietzke, J. Pécaut, *Chem. Commun.* **2000**, 1543–1544.

[354] X. G. Liu, C. L. Stern, C. A. Mirkin, *Organometallics* **2002**, *21*, 1017–1019.

[355] M. V. Ovchinnikov, B. J. Holliday, C. A. Mirkin, L. N. Zakharov, A. L. Rheingold, *Proc. Natl. Acad. Sci. USA* **2002**, *99*, 4927–4931.

[356] M. Albrecht, I. Janser, J. Runsink, G. Raabe, P. Weis, R. Fröhlich, *Angew. Chem., Int. Ed.* **2004**, *43*, 6662–6666.

[357] P. S. Mukherjee, N. Das, P. J. Stang, *J. Org. Chem.* **2004**, *69*, 3526–3529.

[358] A. Hori, T. Sawada, K. Yamashita, M. Fujita, *Angew. Chem., Int. Ed.* **2005**, *44*, 4896–4899.

[359] M. Albrecht, S. Kotila, *Angew. Chem., Int. Ed.* **1995**, *34*, 2134–2137.

[360] Markus Albrecht, *Chem. Eur. J.* **2000**, *6*, 3485–3489.

[361] M. Albrecht, I. Janser, H. Houjou, R. Fröhlich, *Chem. Eur. J.* **2004**, *10*, 2839–2850.

[362] Z. Grote, R. Scopelliti, K. Severin, *J. Am. Chem. Soc.* **2004**, *126*, 16959–16972.

[363] Z. Grote, R. Scopelliti, K. Severin, *Angew. Chem., Int. Ed.* **2003**, *42*, 3821–3825.

[364] Z. Grote, R. Scopelliti, K. Severin, *Eur. J. Inorg. Chem.* **2006**, *submitted*.

[365] Z. Grote, S. Bonazzi, R. Scopelliti, K. Severin, *J. Am. Chem. Soc.* **2006**, *125*, 13638–13639.

[366] Bruker AXS Inc., Madison, WI, **1997**.

[367] G. M. Sheldrick, *SHELXTL*, University of Göttingen, Göttingen, Germany, **1997**.

[368] R. A. Zelonka, M. C. Baird, *Can. J. Chem.* **1972**, *50*, 3063 – 3072.

[369] M. A. Bennett, A. K. Smith, *J. Chem. Soc., Dalton Trans.* **1974**, 233–241.

[370] M. A. Bennett, T. N. Huang, T. W. Matheson, A. K. Smith, *Inorg. Synth.* **1982**, *21*, 74–78.

[371] B. Therrien, T. R. Ward, M. Pilkington, C. Hoffmann, F. Gilardoni, J. Weber, *Organometallics* **1998**, *17*, 330–337.

[372] J. W. Hull, W. L. Gladfelter, *Organometallics* **1984**, *3*, 605–613.

[373] J. W. Kang, K. Moseley, P. M. Maitlis, *J. Am. Chem. Soc.* **1969**, *91*, 5970–&.

[374] R. M. Bellabarba, M. Nieuwenhuyzen, G. C. Saunders, *Inorg. Chim. Acta* **2001**, *323*, 78–88.

[375] C. White, A. Yates, P. M. Maitlis, *Inorg. Synth.* **1992**, *29*, 228–234.

[376] A. Mahr, O. Nürnberg, H. Werner, *Z. Anorg. Allg. Chem.* **2003**, *629*, 91–98.

[377] J. W. Kang, P. M. Maitlis, *J. Organomet. Chem.* **1971**, *30*, 127–&.

[378] A. Svetlanova–Larsen, C. R. Zoch, J. L. Hubbard, *Organometallics* **1996**, *15*, 3076–3087.

[379] H. D. Wizemann, K. Niemax, *Mikrochim. Acta* **1998**, *129*, 209–216.

[380] H. D. Wizemann, *Spectrochim. Acta B* **1999**, *54*, 1267–1278.

[381] C. Vadla, M. Movre, R. Beuc, J. Franzke, H. D. Wizemann, K. Niemax, *Spectrochim. Acta B* **2000**, *55*, 1759–1769.

[382] International Union of Pure and Applied Chemistry: Commission on atomic weights and isotopic abundances, *Pure Appl. Chem.* **1998**, *70*, 217–235.

[383] B. Welz, M. Sperling, *Atomabsorptionsspektrometrie*, 4th ed., Wiley–VCH, Weinheim, **1997**.

[384] International Union of Pure and Applied Chemistry: Commission on atomic weights and isotopic abundances, *Pure Appl. Chem.* **2002**, *74*, 1987–2017.

Curriculum Vitae

Zacharias Immanuel Grote

29 years old – Single – German

Professional Address
EPFL-ISIC-LCS
BCH 3409
CH-1015 Lausanne
+ 41 21 693 93 12
zacharias.grote@epfl.ch

Home Adress

Avenue de France 18bis
CH-1004 Lausanne
+ 41 78 807 62 18

Education and Work Experience

10/2002–11/2006 PhD in Chemistry at the École Polytechnique Fédérale de Lausanne (EPFL), Institut des Sciences et Ingénierie Chimiques; Supervisor: Prof. Kay Severin

"Supramolecular Chemistry of 12-Metallacrown-3 Complexes"

10/2001–09/2002 Graduate Degree in Chemistry at the University Regensburg (D) Diploma Work at the University Bordeaux 1 (F), Laboratoire de Chimie Organique et Organométallique (LCOO); Supervisors: Dario Bassani (U. Bordeaux 1) and Prof. Jörg Daub (U. Regensburg)

"Thienylene-Vinylene Oligomers as Building Blocks for Molecular Electronic Devices"

09/2000–06/2001 Diplôme d'Étude Approfondies (DEA) "Structure Matériaux et Processus Moléculaire" at the University Bordeaux 1 (F), LCOO; Supervisor: Dario Bassani

"Étude Photophysique et Photochimique des Chromophores Thienylènevinylènes"

05/1999–07/2000 Second Cycle of Chemistry at the University Regensburg (D).

05/1997–02/1999 First Cycle of Chemistry at the Technical University Berlin (D).

June 1996 High School Degree (Abitur) at the Albert-Schweitzer Gymnasium, Berlin (D).

Assistantship

2003–2005	Supervision of four 4th year Semester Projects.
2005	Tutorial and Practical Chemistry for Biologists.
2004	Tutorial Chemistry for Medical Students.
2003	Practical Organometallic Chemistry.

Conferences Attended

Oral Presentation at the Fall Meeting of the Swiss Chemical Society (SCS), 2005, Lausanne.

Poster Presentation at the Spring School "Supramolecular Chemistry", 2005, Murten.

Poster Presentation at the SCS Fall Meeting, 2004, Zürich.

Poster Presentation at the Summer School "Frontiers in Catalysis", 2003 Champéry.

Poster Presentation at the SCS Fall Meeting, 2004, Lausanne.

Poster Presentation at the 5th International Symposium on Functional π-Electron Systems, 2002, Ulm, Germany.

Publications

"Controlled Desymmetrization of Metallamacrocycles Using Dynamic Exchange Processes and Steric Constraints."
Zacharias Grote, Rosario Scopelliti and Kay Severin, *Eur. J. Inorg. Chem.* **2006**, accepted.

"Bridged Dihydroxypyridine Ligands for the Synthesis of Expanded Helicates."
Zacharias Grote, Simone Bonazzi, Rosario Scopelliti and Kay Severin, *J. Am. Chem. Soc*. **2006**, *128*, 10382–10383.

"Supramolecular Control of Oligothienylenevinylene-Fullerene Interactions: Evidence for a Ground-State EDA Complex."
Nathan D. McClenaghan, **Zacharias Grote**, Karine Darriet, Michael Zimine, René M. Williams, Luisa De Cola, and Dario M. Bassani *Org. Lett.* **2005**, *7*, 807–810.

"pH Triggered Assembly of Organometallic Receptors for Lithium Ions."
Zacharias Grote, Rosario Scopelliti and Kay Severin, *J. Am. Chem. Soc.* **2004**, *126*, 16959–16972.

"Selective Complexation of Li^+ in Water at Neutral pH Using a Self-Assembled Ionophore."
Zacharias Grote, Marie-Line Lehaire, Rosario Scopelliti and Kay Severin, *J. Am. Chem. Soc.* **2003**, *125*, 13638–13639.

"Adaptive Behaviour of Dynamic Combinatorial Libraries Generated by Assembly of Different Building Blocks."
Zacharias Grote, Rosario Scopelliti and Kay Severin, *Ang. Chem. Int. Ed.* **2003**, *42*, 3821–3825. Ang. Chem. 2003, 115 (32), 3951–3955.